NON-COVALENTLY FUNCTIONALIZED SWNTS AS POTENTIAL DELIVERY AGENTS FOR NOVEL BODIPY-BASED PDT SENSITIZERS
&
THE DESIGN AND SYNTHESIS OF DENDRITIC LIGHT HARVESTERS

A THESIS
SUBMITTED TO THE MATERIALS SCIENCE AND NANOTECHNOLOGY
PROGRAM OF THE INSTITUTE OF ENGINEERING AND SCIENCES
OF BİLKENT UNIVERSITY
IN PARTIAL FULFILLMENT OF THE REQUIREMENTS
FOR THE DEGREE OF
MASTER OF SCIENCE

By
SÜNDÜS ERBAŞ
August 2009

I certify that I have read this thesis and that in my opinion it is fully adequate, in scope and in quality, as a thesis of the degree of Master of Science.

…….

Prof. Dr. Engin U. Akkaya (Principal Advisor)

I certify that I have read this thesis and that in my opinion it is fully adequate, in scope and in quality, as a thesis of the degree of Master of Science.

…….

Assist. Prof. Dr. Mehmet Bayındır

I certify that I have read this thesis and that in my opinion it is fully adequate, in scope and in quality, as a thesis of the degree of Master of Science.

…….

Assist. Prof. Dr. Dönüş Tuncel

Approved for the Institute of Engineering and Science:

…….

Prof. Dr. Mehmet Baray

Director of the Institute of Engineering and Science

ABSTRACT

NON-COVALENTLY FUNCTIONALIZED SWNTS AS POTENTIAL DELIVERY AGENTS FOR NOVEL BODIPY-BASED PDT SENSITIZERS & THE DESIGN AND SYNTHESIS OF DENDRITIC LIGHT HARVESTERS

Sündüs Erbaş
M.S. in Materials Science and Nanotechnology
Supervisor: Prof. Dr. Engin U. Akkaya
August, 2009

Photodynamic therapy (PDT) is a non-invasive method used for the treatment of a number of diseases including certain cancers and some cardiovascular diseases. Photodynamic action depends on absorbance of photosensitizer (PS) in near IR region of the spectrum and subsequent generation of cytotoxic singlet oxygen in the vicinity of the PS. Carbon nanotubes are widely used for biomedical applications due to their inertness, biocompatibility, cellular internalization, facile and multi-modification. We have synthesized and characterized novel water soluble boradiazaindacene (BODIPY)-based PS, non-covalently attached on to the single wall carbon nanotube (SWNT). We have observed that near infrared absorbing photosensitizer preserve its singlet oxygen generation capability upon adsorption on SWNT. We have demonstrated that SWNTs can be used as the delivery vehicle of PS for the use in PDT. In the second part of this research, multichromatic cascade-type light harvesting BODIPY dendrimers were synthesized and highly efficient energy transfer was observed. Successful channeling of energy in a predefined region of the dendrimer was revealed.

Keywords: Boradiazaindacene, photodynamic therapy, photosensitizer, single-wall cabon nanotube, light harvesting, dendrimer

ÖZET

YENİ BODIPY-TEMELLİ FOTODİNAMİK TERAPİ SENSİTİZÖRÜ TAŞIMA AMAÇLI KOVALENT OLMAYAN SWNT TÜREVLENDİRMESİ & DENDRİTİK IŞIK HASADI SİSTEMLERİNİN TASARIM VE SENTEZİ

Sündüs Erbaş
Malzeme Bilimi ve Nanoteknoloji Programı, Yüksek Lisans
Tez Yöneticisi: Prof. Dr. Engin U. Akkaya
Ağustos, 2009

Fotodinamik terapi, kanser ve kalp-damar rahatsızlıklarını da kapsayan birçok hastalığın tedavisinde kullanılan non-invazif bir tedavi yöntemidir. Fotodinamik etki, fotouyarıcının yakın kızılötesi bölgedeki ışığı soğurup mütakiben çevresinde sitotoksik singlet oksijen oluşturması prensibine dayanır. Karbon nanotüpler inert özellikleri, biyouyumlulukları, hücre içine alınabilmelerinin yanında kolay ve çeşitli modifikasyonlara açık olmaları sebebiyle biyomedikal uygulamalarda yaygınca kullanılmaktadır. Bu çalışmada, suda çözünür yeni BODIPY- temelli fotosensitizör tek-duvarlı karbon nanotübe (SWNT) bağlanıp karakterize edilmiştir. Yakın kızılötesi bölgede soğuran bu fotouyarıcının nanotübe bağlanma sonrasında singlet oksijen oluşturma kapasitesini koruduğu gözlenmiştir. Nanotüplerin fotodinamik terapide kullanılmak amacıyla fotouyarıcı taşınmasında kullanılabileceği bu çalışmayla gösterilmiştir. Çalışmanın ikinci kısmında, multikromatik şelale tipi enerji hasadı yapan BODIPY dendrimerleri sentezlenmiş, oldukça verimli enerji aktarımı gözlenmiştir. Enerjinin dendrimerin belirli bölgesine başarılı şekilde yönlendirilebileceği gösterilmiştir.

Anahtar Kelimeler: Boradiazaindasen, fotodinamik terapi, fotosensitizör, tek-duvarlı karbon nanotüp, enerji hasadı, dendrimer

ACKNOWLEDGEMENT

I would like to express my sincere thanks to my supervisor Prof. Dr. Engin U. Akkaya for his guidance, support, and patience during the course of this research. I am also grateful to him for teaching us how to become a good scientist. I will never forget his support throughout my life.

I would like to thank to Merve Kocakuşakoğulları and Aslı Görgülü for their partnership in this research. I owe a special thank to Dr. Ö. Altan Bozdemir for his support and guidance to improve my skills in the field of supramolecular chemistry.

I want to thank to our group members Tugba Özdemir, Ruslan Guliyev, Onur Büyükçakır, Barbaros Reis, Safacan Kölemen, Sencer Selçuk, Serdar Atılgan, Fazlı Sözmen, Bilal Kılıç, Nisa Yeşilgül, Tuğrul Nalbantoğlu, Gülcihan Gülseren, Merve Türkşanlı, Eser İden, Hande Boyacı and rest of the SCL (Supramolecular Chemistry Laboratory) members. It was wonderful to work with them.

I would like to express my special thanks to Dr. Aykutlu Dana for his generous help for taking AFM images.

I would like to thank to TÜBİTAK (The Scientific and Technological Research Council of Turkey) for financial support.

Finally, I want to express my gratitude to Yusuf Çakmak and my family for their love, support, and understanding. I owe them a lot.

LIST OF ABBREVIATIONS

PDT:	Photodynamic Therapy
PS:	Photosensitizer
CNT:	Carbon Nanotube
SWNT:	Single-Wall Carbon Nanotube
MWNT:	Multi-Wall Carbon Nanotube
FRET:	Förster Resonance Energy Transfer
EPR:	Enhanced Permeation and Retention
PET:	Photoinduced Electron Transfer
FDA:	Food and Drug Administration
EU:	European Union
PEG:	Polyethylene Glycol
DMF:	Dimethylformamide
THF:	Tetrahydrofuran
TFA:	Trifluoroacetic Acid
DPBF:	1, 3 Diphenylisobenzofuran
AFM:	Atomic Force Microscopy
TEM:	Transmission Electron Microscopy
LH:	Light Harvesting
BODIPY:	Boradiazaindacene

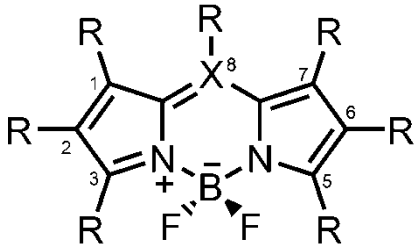

R = H or any other group
X = C or N

TABLE OF CONTENTS

LIST OF FIGURES

LIST OF TABLES

CHAPTER 1

INTRODUCTION

1.1 Photodynamic Therapy

Photodynamic therapy is a relatively young, non-invasive approach to the treatment of certain diseases such as some malignant cancers, actinic keratoses, psoriasis, age-related macular degeneration, oesophageal diseases and some cardiovascular diseases.[1] In this therapy, light-sensitive drugs (or photosensitizers) are introduced topically, intravenously or orally.[1] After certain time of administration, usually 1 to 3 days, light of certain wavelength is exposed. This delay in light exposure maintains accumulation of photosensitizer (PS) in the region of interest up to 28:1 ratio of concentrations for tumor to normal tissue for some photosensitizers due to enhanced permeation and retention in tumor.[2] Intracellular localization on the other hand, depends on hydrophobicity and charge of PS. Hydrophobic ones tend to localize in the membrane and cationic PDT agents are mainly accumulate in mitochondria.[3]

Activation of photosensitizer using suitable light leads to formation of reactive oxygen species including singlet oxygen (O_2^1) from molecular oxygen which attack to nearby molecules such as lipids, proteins or DNA, depending on the location of the photosensitizer and give oxidative damage to the corresponding biological structures.[4,5] This in turn, results in cellular response such as initiation of apoptosis or necrosis, shut down of vascular supply which results in hypoxia or activation of immune system.[6-8] The light used for PDT can come from either a laser or other sources such as light-emitting diodes (LEDs) and should be preferably red or near IR in color since light of this color penetrates through tissues better.[9]

1.1.1 History of Photodynamic Therapy

Use of sun light for the treatment of certain diseases is not a recent finding, rather it was realized by Herodotes more than two thousand years ago and use of photoactive molecules for the treatment of vitiligo were described in holly book of India, *Atharava-veda*.[10] The story of photodynamic therapy in scientific literature however, begins with Oscar Raab's observation on toxic effects of acridine red molecule on certain bacteria in the presence of intense light.[10-12] By doing control experiments, he proposed and demonstrated that presence of fluorophore is required for the corresponding light-induced toxicity. Scientists Tappeiner and Jesionek used the eosin dye for the treatment of skin cancer, thus, eosin becomes the first photosensitizer used for medical purposes.[13]

Following these discoveries, in 1904, indispensable involvement of oxygen in the photodynamic response is realized by Tappeiner and Jodbauer.[14] However, exact mechanism of oxygen-dependent toxicity of photoactive molecules cannot be resolved until 1979, the year when electron spin resonance technique was used to monitor the generation of singlet oxygen, highly reactive excited state oxygen, by Moan *et al*.[15]

First human trial of PDT was done by Meyer-Betz on himself and extreme apses and pain was observed.[16] On the other hand, first clinical application of PDT was at Roswell Park Cancer Institute in 1978 by Dougherty *et al*.[17] Following this, in 1980 photofrin, a mixture of hematoporphyrin derivatives is approved by FDA as a photosensitizer. From that time on, a number of photosensitizers which are either porphyrin or haematoporphyrin derivative, such as HPPH, ALA, Levulan, Foscan, Metvix are approved by FDA or EU. Great success in treatment of a variety of diseases, mainly different forms of cancer is achieved.

1.1.2 Mechanism of Photodynamic Action

Generation of tremendously reactive oxygen in its lowest lying excited state by means of photoactivation of fluorophore is the crucial step in the mechanism of this therapy. The steps involved in photon induced $^1O_2$ generation are shown with a Jablonski diagram in Figure 1. Excitation of fluorophore via photon of appropriate energy from its ground state to the first excited state is the initiation step (step 1). From this singlet excited state, relaxation to ground state vibrational level of excited electronic state occurs. From here on, there are two possible pathways apart from radiationless relaxation to the ground state: electron can fall back to its electronic ground state which gives fluorescence (step 2) or it can go into an intersystem crossing to triplet excited state (step 4). If the latter pathway is favored, such as the case in the presence of heavy atoms, triplet excited state energy can be transferred to ground state oxygen to generate reactive singlet oxygen, otherwise phosphorescence, delayed fluorescence occurs when electron falls back to ground state of the photosensitizer (step 5).[9,18]

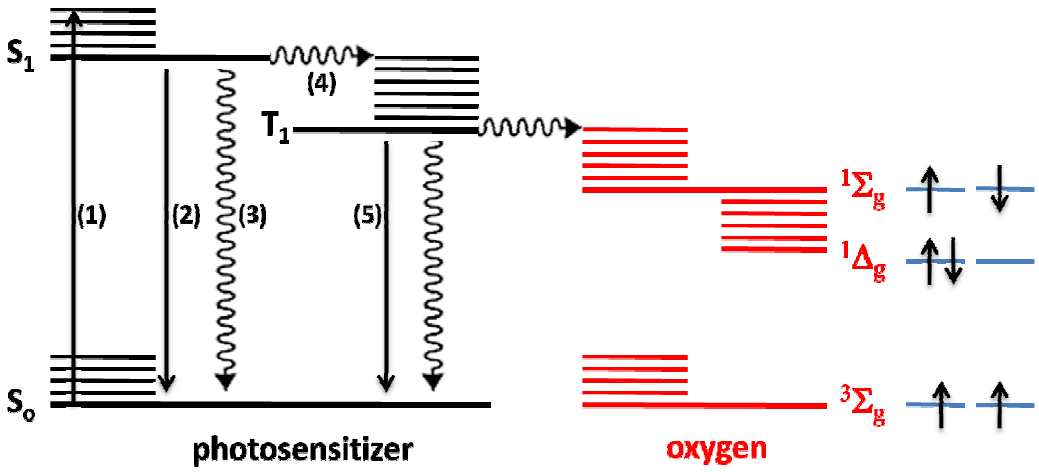

Figure 1. Jablonski diagram of photosensitizer and oxygen

Biological outcome of photodynamic therapy basically relies on the reactivity of photogenerated singlet oxygen which either leads to the formation of other reactive oxygen species or directly gives oxidative damage to cell. Due to the short life time (0.6 μs) hence diffusion distance (0.1 μm) of singlet oxygen, oxidative damage to cellular structures is expected to be initiated in the vicinity of the photosensitizer.[19] For the reasons mentioned above, localization of the photosensitizer determines the targets of reactive oxygen species and mode of cell death.

1.1.2.1 Chemical Response; Oxidative Damage by $^1O_2$

Photosensitizer mediated cytotoxicity results from two different mechanisms. In type-I reaction, excited photosensitizer directly reacts with a substrate, namely a biomolecule and form unstable radicals. These radicals further react with other substrates or molecular oxygen to generate singlet oxygen. In type-II reaction, energy is directly transferred from excited PS to oxygen to produce $^1O_2$. Generally, it is not easy to differentiate between these two modes and both reaction types are known to be involved in photodynamic action simultaneously.[6]

Being a very powerful oxidant, $^1O_2$ reacts immediately with a number of biomolecules giving rise to oxidative stress. Reaction with membrane lipids would be lipid peroxidation that alters membrane structure, integrity and fluidity. Decomposition of these peroxides produce lipid radicals, another cytotoxic danger for the cell. Other reactive oxygen species generated by $^1O_2$ can attack free amino and thiol groups of amino acids and disrupt the folding and proper functioning of proteins.[20] One reason of photoinduced increase in mitochondrial membrane permeability is thought to stem from the oxidation of disulfide histidine amino acids in membrane proteins, leading to formation of more labile membrane, permits the passage of mitochondrial constituents, induce cell death consequently.[21] Formation of different radicals and reactive

compounds in each step leads to the amplification of oxidative stress in the cell.[22] In the structure of DNA, dioxyribose sugar and bases, especially thymines are prone to chemical attack by hydroxyl radicals that are generated by reactions of singlet oxygen.[23] These type of modifications in DNA strand result in mutations; strand breaks. In addition, cross-linking of DNA with proteins or DNA itself is also observed as a genotoxic outcome of PDT.[24] Singlet oxygen also impairs the normal functioning of DNA repair enzyme, thus, each damages on DNA accumulates and triggers cell death immediately after photodynamic action.[25]

1.1.2.2 Biological Response

Two modes of cell death, namely, apoptosis or necrosis can be induced in response to photodynamic therapy, each having different morphological properties.[26] Apart from direct cytotoxic effect, photodynamic therapy results in shutdown of vascular supplements to the tumor tissue. Immunological stimulation against cancerous regions is a long term benefit of this type of therapy as opposed to most of the other types.[27]

Apoptosis is programmed cell death characterized by DNA fragmentation, chromatin condensation and cell shrinkage. Molecular elements responsible for/having role in this phenomenon involve wide range of membrane and cytosolic proteins some of which are receptors or transporters. Mainly, apoptotic signals are introduced in two converging pathways: external signals are introduced to the cell through dead receptors initiated via ligand binding. This recruits some proteins to the receptor, induces the formation of death-inducing signaling complex, and activates certain caspases, cystein aspartic acid proteases such as caspase-8. Internal signals can also trigger caspase activation in response to release of cyctochrome-c and other mitochondrial apoptotic proteins. Formation of active protein complex from caspase-9, cytochrome-c, called apoptosome relays the apoptotic signal to entire

cell in an irreversible way, program cell death is implemented.[19,28,29] Apoptosis in PDT can be triggered due to impairment of ion homeostasis and consequent increase in intracellular Ca^{+2} ion concentration. Drastic rise in Ca^{+2} ion concentration activates phospholipase C, protein kinase C, interferes with arachidonic acid metabolism all in turn lead to apoptosis and inflammatory responses.[24]

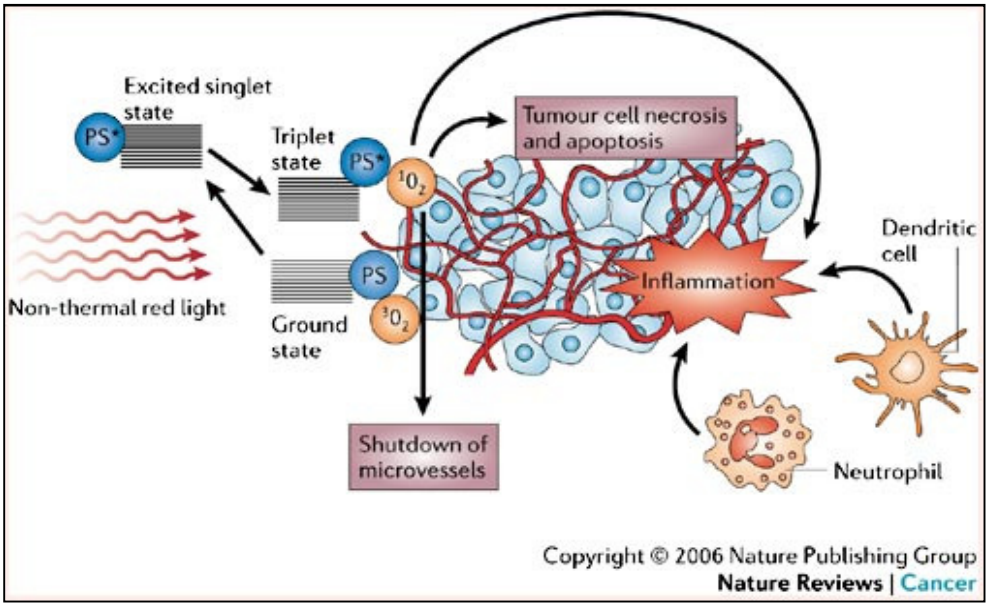

Figure 2. Biological response induced by photodynamic therapy.[19]

Another mode of cell death triggered by photodynamic therapy is necrosis, a more traumatic, unnatural death characterized by swelling of the cell, disruption of intracellular and plasma membranes and subsequent rupture of the cell, release the contents of the cytoplasm to the surrounding tissue. This type of cell death, together with apoptosis is the outcome of cytotoxic effect of photodynamic therapy.[19]

Beside its cytotoxicity to the region of application, PDT has a very distinct property that is not found in traditional chemotherapy or radiotherapy,

immune system stimulation. Oxidative damage to the elements of cell membrane decreases the integrity and phospholipids are liberated. These phospholipids are rapidly metabolized to immune stimulatory molecules such as leukotrienes.[24] When either apoptosis or necrosis takes place after photodynamic action, heat-shock protein-70 (HSP70) is induced.[30] Being a chaperone protein, it interacts with tumor antigens, stimulate anti-tumor response and attract neutrophils to the side of tumor. Korbelik and Sun used this property of photodynamic therapy to develop cancer vaccines, namely, bio-sample that recognize and acts against tumor cells.[31] For this purpose, they inject PDT-applied cell lysates to mice, suffering from cancer. After a short time of administration, obvious regression in tumor size and healing was reported.

1.1.3 Requirements for Photosensitizers

The photosensitizer, which is introduced into the cells before light is shone onto the tissue, must have certain fundamental properties to make it suitably and successfully acting agent. Photodynamic action necessitates intrinsic ability of photosensitizer to generate reactive singlet oxygen species. Thus, specific molecules with appropriate chemical and physical properties are required such that the efficacy of singlet oxygen generation thus photodynamic action should be considerably high.

Spin forbidden transition from triplet ground state of molecular oxygen to singlet excited state is enhanced with increased spin-orbit (SO) coupling since coupling of spin angular momentum with orbital angular momentum mix the singlet and triplet states such that triplet state has certain singlet character. This in turn, makes spin forbidden singlet-triplet transitions possible. Spin-orbit Hamiltonian term is proportional to fourth power of Z, presence of heavy atom increases spin-orbit coupling thus spin forbidden singlet-triplet radiationless transition. SO-Hamiltonian is formulated as below.[32, 33]

$$H_{SO} = \frac{e^2 Z^4}{2a_o m^2 c^2 n^3} \; L.S \qquad (1)$$

where e is electron charge, Z is atomic number, a_o is Bohr's radius, m is mass of electron, c is speed of light, n is principle quantum number, L and S are angular momentum and spin operators respectively.

This phenomenon is studied experimentally in BODIPY dyes and it was verified by O'Shea *et al.* that presence of two bromine atom in the structure of molecule increases the efficacy of the photosensitizer up to thousand folds. Hence, photosensitizers having heavy atoms in their structures exhibit better singlet oxygen generation capability.

Most photosensitizers degrade in the presence of light, so called photobleaching, mainly due to reactive oxygen species generated as a part of PDT action.[35] For this reason, to maintain photodynamic character photosensitizers have to be photostable.

Due to the presence of absorbing molecules in the living organisms, tissue penetration depth of light at different wavelength differs considerably in different regions of the body. Certain aromatic compounds such as amino acids tyrosine, phenylalanine and tryptophan absorb near UV region, different regions of visible light are absorbed by melanin, collagens, nicotinamide, flavins, and haemoglobins. Beyond 1150 nm, light penetration decreases substantially due to absorbance of water. Considering the absorbance of these and other biomolecules, maximum penetration is achieved with light of the range 620-850 nm, so called therapeutic or pharmaceutical window of the body. Thus, design or choice of photosensitizer should be accordingly in order to achieve sufficient intensity of light in the region of therapeutic action, it must absorb light within this given wavelength range strongly so that it can efficiently produce the reactive oxygen species.[3, 9, 37]

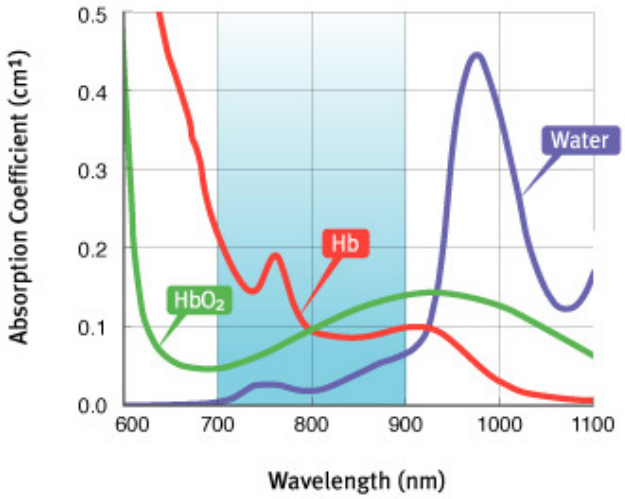

Figure 3. Therapeutic window of the body, absorbance of oxy-hemoglobin (HbO_2), deoxy-hemoglobin (Hb) and water.[36]

Beside its photophysical properties already revealed, the sensitizer has other requirements for biological application such as biocompatibility. It should not have dark toxicity; in other words, has to be ineffective until light is exposed to it. In addition, an important necessity for practical medical use is that it should be water-soluble and there should be no immunological reaction against.

1.1.3 Photosensitizers in Literature

First generation PS are mainly porphyrin derivatives such as photofrin, hematoporphyrin which do not have strong absorption in the therapeutic window of the body.[38] Phthalocyanine related sensitizers and synthetic chlorins are more promising when their absorptions are compared (Figure 4).[38] Xanthanes such as fluorescein, eosin and Rose Bengal are common singlet oxygen generating organic compounds.[39] Perylenediimide dyes have high quantum yield and absorption maxima which can be shifted to longer wavelengths by proper modifications.[39] The only drawback of this dye is its low

solubility in protic solvents. BF_2 chelated tetraaryl azadipyrromethene dyes (aza-BODIPY), as extensively studied by O'Shea *et al*, have sharp absorption in therapeutic window of the body and show highly efficient PDT character.[34, 40] Cyanine dyes, hypericin, squaraines, texaphyrins, fullerenes were also used as sensitizer.[38, 39, 41]

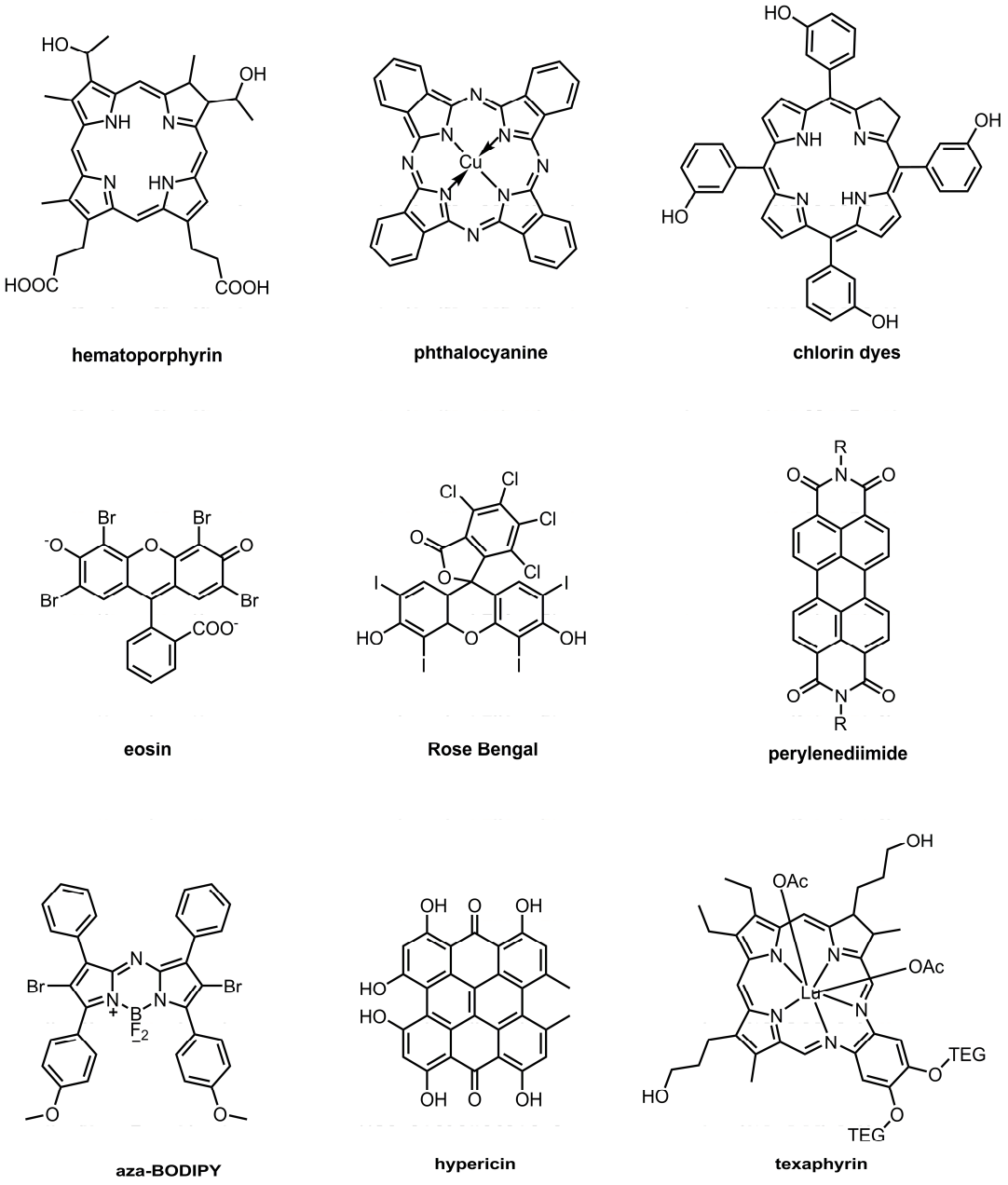

Figure 4. Structures of some photosensitizers in literature.

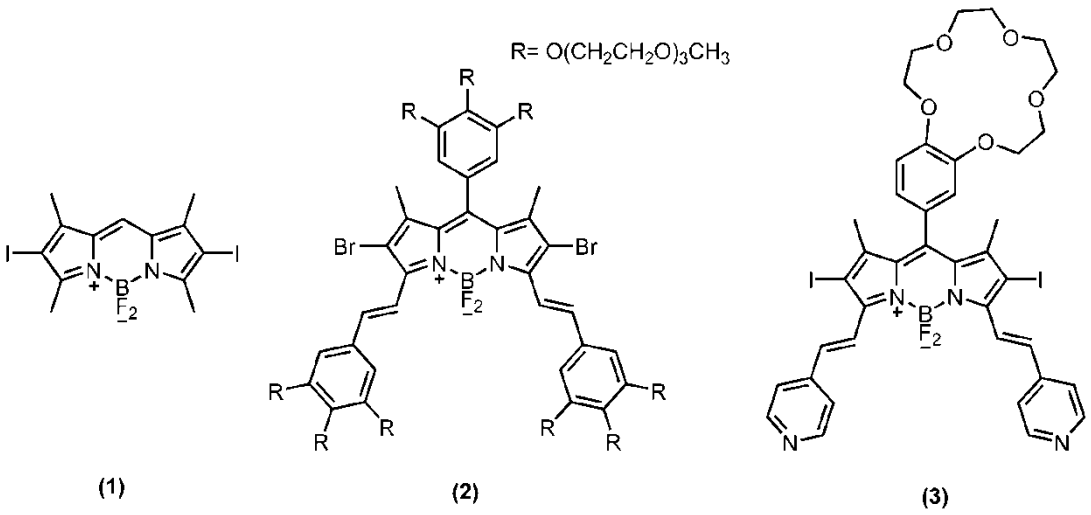

Figure 5. BODIPY- based photosensitizers in literature. Compound **1** is the first BODIPY-based photosensitizrs reported by Nagano *et al.,* compound **2** and **3** were reported by Akkaya *et al.*[42, 43, 44]

Recently, borondipyrromethene (BODIPY) dyes become attractive in this era when their high extinction coefficients and photostabilities are considered.[42, 43, 45] Possibility of multiple and facile chemical modifications on this molecule allow attachment of chemical groups that would enable selective tumor targeting, water solubility together with groups attached to increase photodynamic action (Figure 5).

One impressive example of such BODIPY photosensitizer was synthesized by Akkaya *et al.*[44] This photosensitizer, compound **3** contains chemical groups that detect the acidity and sodium concentration of the medium, namely, singlet oxygen generation property of the molecule is under the control of these two parameters (Figure 5 and Figure 6). Protonation of pyridine groups in acidic media causes a bathochromic shift in the absorbance. When light of 660 nm is introduced, only molecules with protonated pyridine groups are excited and show photodynamic action, provided photo-induced electron transfer (PET) is blocked by Na^+ binding to crown ether moiety. Thus, only in cancer tissues where sodium concentration is high and pH is low, $^1O_2$ generation is

maintained.[46, 47] Nagano *et al*. recently reported a BODIPY derivative that selectively inactivates protein after binding to its hydrophobic cavity.[48]

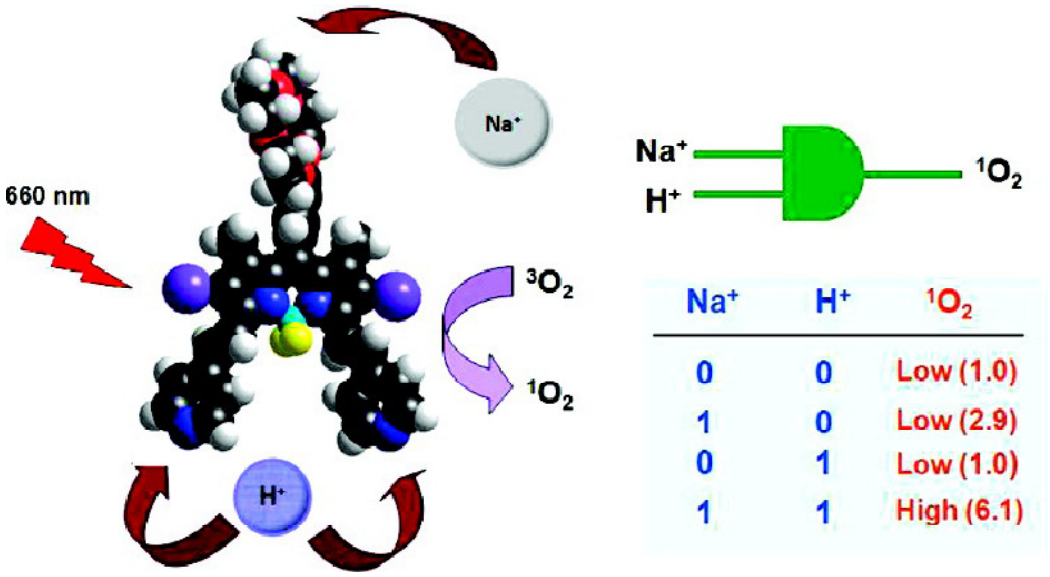

Figure 6. Smart PS seeking for cancer parameters.[44]

Nowadays, PDT with controlled generation of singlet oxygen is becoming more and more important. There are some recent examples in literature that rationally focus on this issue beside the Akkaya's photosensitizer given above. One such example relies on Watson-Crick base pairing of DNA strands in which 5' end of one strand is linked to the photosensitizer whereas 3' end of complementary strand hold a quencher.[49] When there is no quencher-free complementary strand, ability of photosensitizer to generate singlet oxygen is abolished due to the presence of quencher in close proximity to enable Förster resonance energy transfer (FRET, through space) from PS to quencher.[50-52] However, in the presence of a number of target-DNA around, statistically, the chance of pairing with quencher-free DNA increases which in turn increases the singlet oxygen mediated toxicity. This type of dual system where outcome is dependent of hybridization or proximity is called molecular beacon.[53]

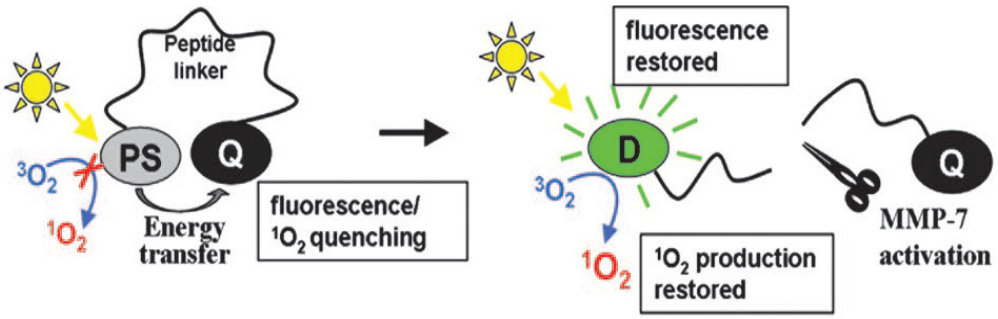

Figure 7. Cancer selective activation of PS through release of quencher by protease MMP7.[54]

One other molecular beacon designed to control photodynamic action is published by Zheng *et al*. and Tung *et al*. separately, and depends on cancer specific expression of proteases (Figure 7).[54, 55] In the case of Zheng's research, photosensitizer is chemically linked to a quencher molecule called Black Hole Quencher 3 through specific peptide spacer. This spacer has special amino acid sequence, the sequence specifically recognized and cleaved by matrix metalloproteinase-7, MMP7. This enzyme is known to be over expressed in certain cancer types such as colon, pancreas and breast cancers, hence, quencher free photosensitizer is ready to generate cytotoxic agents only in these specific tissues.[54, 56]

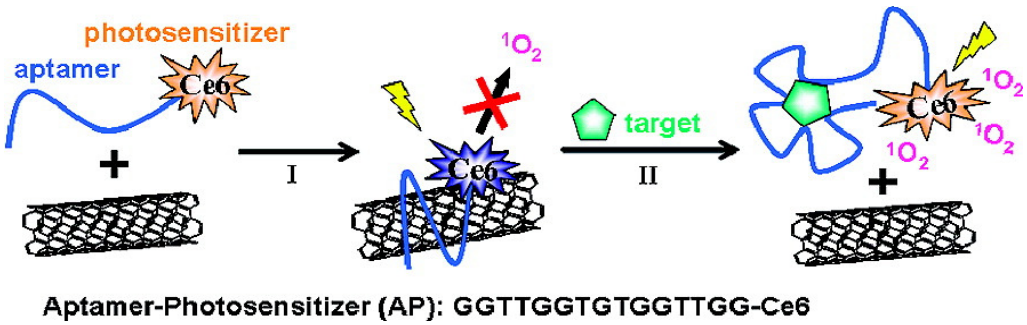

Figure 8. Controlled photodynamic action based on quenching ability of SWNT.[57]

The example shown in Figure 8, based on the quenching of the photosensitizer, chlorine-e6 when it comes close to the surface of single walled carbon nanotube (SWNT).[57] An aptamer attached to the photosensitizer favors this interaction. However, when aptamer preferentially binds to the target, PDT agent detaches from the SWNT, gains its ability to generate singlet oxygen. Thus, the ability to generate singlet oxygen is maintained only in the presence of target molecule.

1.1.5 Clinical Applications

Starting with the first promising medical trial in 1970s photodynamic therapy is widely used in a number of diseases. Most of the photosensitizers approved so far and the diseases they are used for are listed in Table 1. Considering the exigency of conveying light to the region of treatment, dermatologic applications became the first type of trials. In these first treatments, nearly all primary skin cancers such as basal cell carcinomas showed complete response whereas secondary cancers that are formed as a result of breast, colon or endometrium cancers, 80% response were reported.[58]

Age-related macular degeneration is an ophthalmic disease to which PDT is applied. A photosensitizer called Verteporfin is approved as a PDT agent and placebo controlled trials demonstrated that the treatment maintains a stabilized vision afterwards.[59] One other ocular use of PDT was in treatment of choroidal hemangiom, in other words eye cancer. It has been shown in a 10-case study that PDT results in regression of the tumor and reduction in the vascular structures.[60]

Table 1. Some PSs approved so far and the diseases they are used for.[38]

Photosensitizer	**Trade Name**	**Approval**	**λ(nm)**	**Area of Use**
Porfimer sodium	Photofrin	1998 FDA	630	Lung, Barrett's esophagus
ALA-PpIX	Levulan Keratastick	1999 FDA	405 635	Actinic Keratosis
Methyl aminolevulate-PpIX	Metvix	2004 FDA	405 635	Actinic keratosis
Hexyl aminolevulate-PpIX	Hexvix	2005 EU	405	Detection of bladder tumors
BPD-MA	Verteporfin, Visudyne	2000 FDA	689	Choroidal neovascularization
mTHPC	Foscan	2001 EU	652	Head and neck, prostate, pancreas, esophagus, mesothelioma
Motexafin Lutetium	MLu, Lutex, Lutrin	Phase I	732	Prostate, atherosclerosis
Pd-bacteriopheophorbide	Tookad	Phase I	762	Prostate
Taloporfin sodium	LS11	Phase I&II	664	Choroidal neovascularization, liver and colorectal metastasis
Silicon pthalocyanine-4	PC-4	Phase I	672	Skin

In head and neck cancers, those of cancers develop in oral cavity, the pharynx, the nasal cavity and larynx, PDT is preferred as opposed to other conventional radiotherapy and chemotherapy because of higher cure rates and better cosmetic outcome.[61] Photosensitizers, photofrin and foscan are approved to be used in this type of applications. Treating brain tumors with other common surgical methods is challenging due to the risk of giving damage to nearby essentially important structures. That is the reason why PDT is used as a post-surgical follow-up procedure for these types of cancers. In late 1990s, Stummer *et al*. were succeeded in complete removal of tumor in malignant glioma tissue.[62] Complete recovery of visual field, a 46% reduction in tumor size in pituitary adenomas within two years is also reported.[63]

Animal trials and small group patient trials in some cardiovascular diseases such as atherosclerotic plaque, hyperplasia, restenosis and cancers such as gastroenterological, mesothelial and gynecological cancers also give very promising results.[64] It can be said that PDT can be used in the treatment of these diseases as well in the near future.

1.2 Carbon Nanotubes

Carbon nanotubes (CNT) are one dimensional cylinderical allotropes of carbon which are formed by rolling of single or many sheets of graphite with a diameter of a few nanometers. The one with single layer is called single-wall carbon nanotube (SWNT) and those with multiple layers are called multi-wall carbon nanotube (MWNT). First discovered by Iijima *et al.* carbon nanotubes attract enourmous attention as nanomaterial because of their unique electronic, mechanical and structural properties.[65, 66] Because of its high electron conductivity, it is used to develop molecular electronic devices and their use in biomedical area is increasing.[66-68] Carbon nanotubes can be functionalized to modify electronic properties or to make them better delivery system for drugs or related therapeutic agents.

1.2.1 Modifications of Carbon Nanotubes

Although CNTs are very promising for a number of research and application, they suffer from severe solubility problem such that they immediately form bundles and aggregates through strong van der Waals interaction between the side walls.[69] This drawback can be handled via covalent or non-covalent functionalization of CNTs which interfere with bundle formation and increase solubility. In order to preserve electronic properties by maintaining sp^2 hybridization of carbons and for the simplicity of procedure non-covalent modifications are preferred.

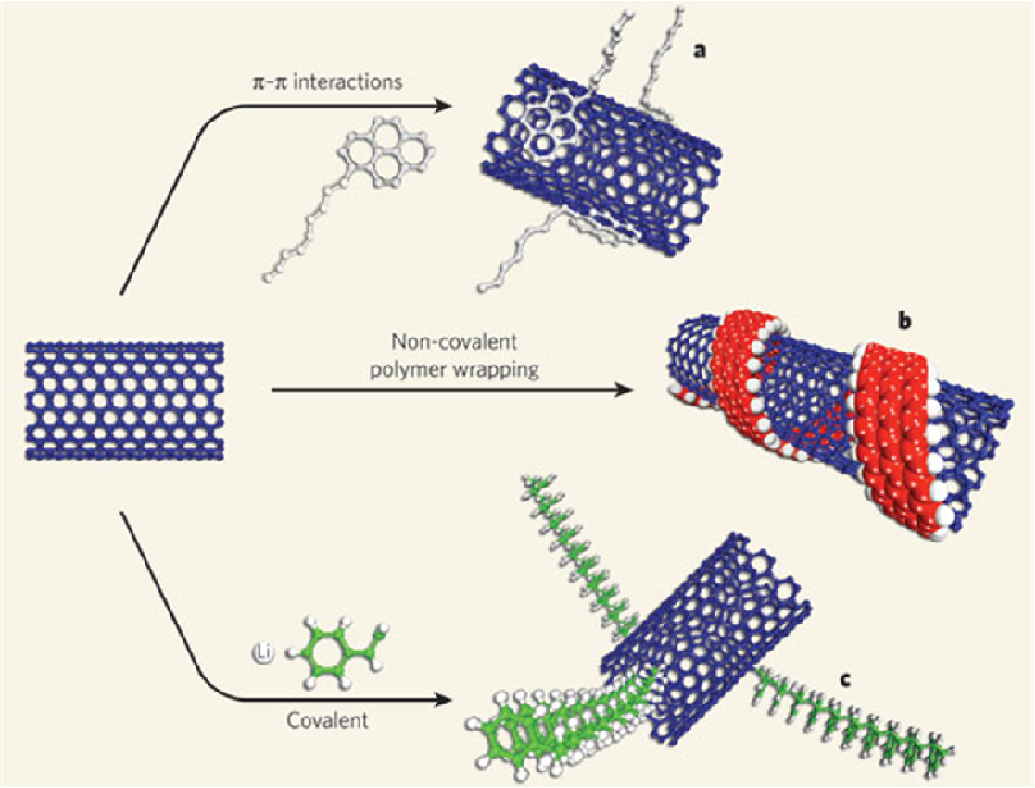

Figure 9. Modifications of carbon nanotubes.[70]

1.2.1.1 Covalent Modifications of Carbon Nanotubes

Covalent modification of carbon nanotubes is quite difficult due to lack of solubility in any kind of solvent. On the other hand, it is possible to oxidize ends of CNTs to carboxylic acid by means of refluxing in concentrated nitric acid.[71-73] This procedure also induces defects on the walls of CNTs which affects their electronic properties but not a concern for most of the biomedical applications.[74] Carboxylic acid bearing CNTs can be further modified using well-known chemical methods to increase their solubility and to functionalize for specific use. Besides, having higher curvature, thus strain, CNTs possess greater reactivity compared to flat graphene sheets.[75] This strain-dependent partial reactivity allows chemical functionalization on the side walls of CNTs through nitrene addition, hydrogenation, arylation, 1, 3-dipolar cycloaddition, fluorination or alkylation.[76-84]

1.2.1.2 Non-covalent Modifications of Carbon Nanotubes

Modification of CNTs without any change in their structure or electromechanical properties are feasible through non-covalent modification which can be done either through hydrophobic interactions of surfactants or through wrapping of polymers, DNA on the walls of CNTs.[85-89] In addition, a number of aromatic compounds adhere on the side walls of CNTs through π-stacking interactions (Figure 9).[70] Among such compounds, interaction of pyrene with CNTs was well studied.[90, 91] The stability against desorption make pyrene-CNT complex very promising for biomedical applications as well as molecular electronics. Interaction of pyrene with CNTs can be easily characterized using quenching of pyrene emission.[92, 93]

Apart from pyrene, other conjugated molecules also bind to the wall of CNTs through π-stacking such as perylene, porphyrin, Congo red dye, trypan

blue dye.[94-96] The main advantage of non-covalent modifications is the lack of requirement of harsh conditions as in the case of most of chemical modifications. Simple sonication is enough for adherence of polymers or aromatic moieties on the walls of CNTs.[85-96]

1.2.2 Biomedical Applications

Carbon nanotubes are appropriate tool for biomedical applications because of their facile internalization into cells.[97] Besides, no significant toxicity was reported although a number of researches were done on this subject.[98-104] CNTs are mainly used as delivery vehicle for proteins, nucleic acids for therapeutic purposes or certain radio-labeled moieties and fluorescent molecules for imaging purposes.[68] Interesting researches where CNTs were used as substrate for neurons, was also done where differently functionalized CNTs induce different branching as the neurons grow.[105] Carbon nanotubes carrying different anticancer drugs and photodynamic therapy reagents are also reported by others.[57, 106, 107]

1.2.2.1 Biodistribution and Cytotoxicity

Biomedical use of carbon nanotubes became more and more popular within last ten years due to its facile preparation as delivery systems. In order to be used as a real delivery system or a biomedical tool for other bioapplications, toxicity, biocompatibility and possible interference with biochemical and cellular functions have to be investigated extensively. For this concern, a number of researches were done either to determine the distribution of CNTs throughout the body, retention, excretion or possible pathological response induced within the organisms.

In an attempt to determine biocompatibility and cytotoxicity Ausman *et al*. prepared different water-dispersible SWNTs and examined the role of degree of functionalization of SWNT for biocompatibility in human dermal fibroblast cell culture.[98] As a consequence, use of solubilized nanotubes rather than naked ones are recommended in order to prevent toxicity. Further, Dumortier, Prato and Bianco *et al*. reported that solubilized carbon nanotubes do not abolish cell viability nor interfere with proper functioning of primary immune cells.[99]

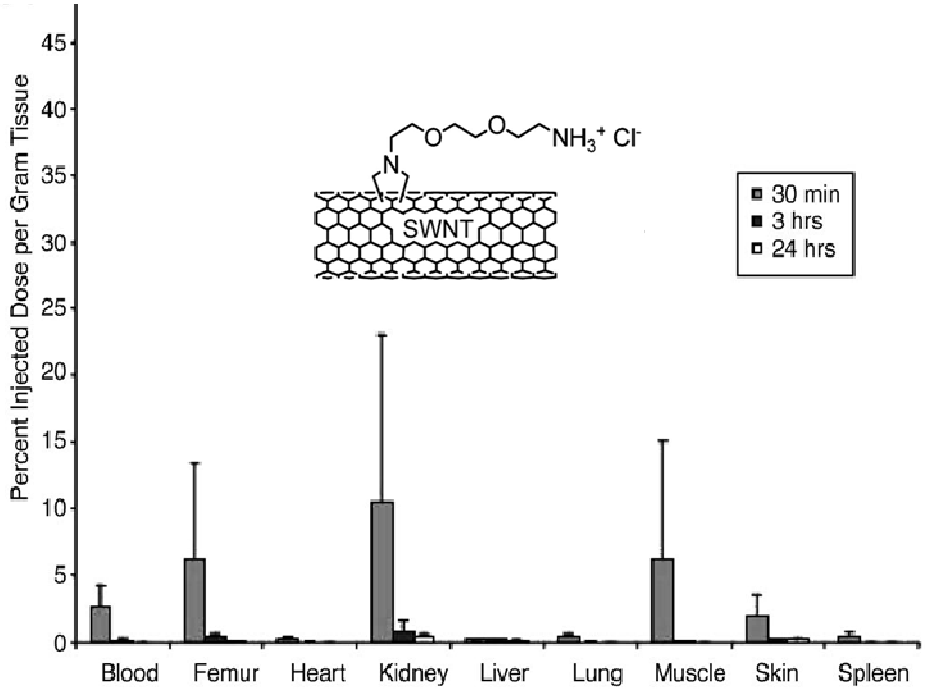

Figure 10. Biodistribution and rapid clearance of carbon nanotubes.[100]

Biodistribution of CNTs and clearance rate from the body of the mice were examined in two different studies and consistent results were obtained.[100, 101] Although CNTs were accumulated in certain parts such as kidney and muscle right after administration, they are cleared rapidly within a few hours and excreted through feces or urine (Figure 10).[100] Circulation half life of CNTs was determined to be 3.5 hours and 5.5 hours for diethylenetriamine pentaacetic acid

and glucoseamine functionalized CNTs respectively. When long term pathologic effects of CNTs are considered, no sufficient experiments are done yet, except from a few pilot researches. In one such research CNTs injected into the abdominal cavity of mice cause asbestos-like symptoms such as inflammation and lesion.[102] Dose dependent inflammation in lung was observed in a 3 months research on rat.[103] However, in a different study mice were observed for much longer time, 4 months after intravenous injection of polyethylene glycol functionalized CNTs and no significant pathogenicity was observed.[104] These works again confirms that CNTs toxicity is associated with its degree of functionalization and highly soluble CNTs are required to avoid possible side effects.

1.2.2.2 SWNT as Delivery System

Considering delivery systems, the most important problem for bio-application is their internalization by cells. They require additional specific functionalization to facilite entrance into the cell. CNTs, on the other hand, are shown to be internalized into mammalian cells mainly through energy dependent mechanism, endocytosis.[97, 108, 109] Moreover, by providing cell specific targeting groups CNTs can more selectively accumulate in certain tissues such as the case in the work of Dai *et al.*[110] In this study, SWNTs carrying RGD amino acids, cancer specific integrin $\alpha\beta$ antagonist, were prepared and the distribution of nanotubes was monitored through positron emitting ^{64}Cu. Biological imaging using fluorophore-CNT conjugates were also done.[111] Antibody conjugated non-covalently modified SWNTs were used as electronic biosensors through which disease specific biomolecules can be detected.[112]

Carbon nanotubes absorb near-infrared light, using this property, thermal destruction of cancer cells were achieved.[113-115] In another research, controlled release and subsequent activation of photosensitizer in the presence of tumor

markers was studied (Figure 8).[57] In this research, SWNT inhibit the singlet oxygen generating capability of the photosensitizer until tumor marker is present. More interestingly, Dai *et al.* non-covalently functionalized SWNTs using hydrophobic interaction of phospholipids with SWNT wall; small interference RNA (siRNA) was attached to phospholipids via disulfide linkage.[116, 117] Reduction of disulfide bond to thiol released siRNA and successful gene silencing was observed.

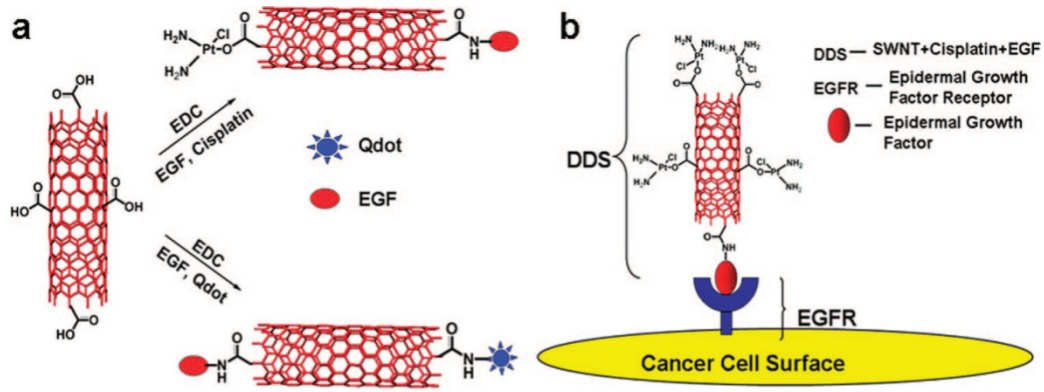

Figure 11. Targeted delivery of cancer drug using SWNT as delivery vehicle.[118]

Three different anticancer drug-loaded CNTs were rationally designed and delivered by two different groups. Dai and Lippard *et al.* tethered Pt (IV) complex on SWNT and release of toxic cis-$[Pt(NH_3)_2Cl_2]$ upon intracellular reduction induced tumor cell death.[106] Low pH in cancer cells facilitate the reduction, thus release of active anticancer complex and there is an obvious increase in cytotoxicity of SWNT-drug conjugate compared to free drug. Same drug was used recently by other research group, where additionally epidermal growth factor (EGF) was attached to SWNTs to maintain cancer targeting (Figure 11).[118] EGF conjugated, drug loaded SWNTs were internalized by cancer cells whereas cells having reduced expression of EGF receptor (EGFR) failed to internalize the SWNTs. In the research of Wong and Ojima *et al.* well-known microtubule destabilizing anticancer drug taxoid was covalently attached

on the surface of the SWNT through disulfide bond.[107] Gluthathione (GSH) mediated reduction of this bond in specific tissue liberates the drug and induces cell death in the vicinity (Figure 12).

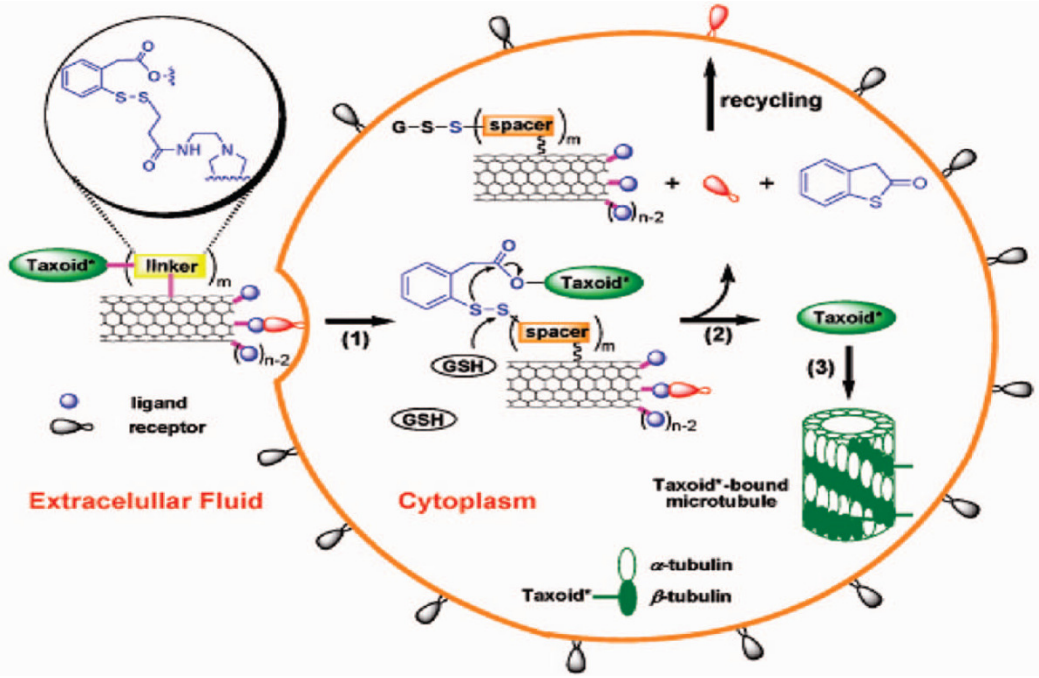

Figure 12. Gluthathione mediated drug delivery using SWNT as a delivery vehicle.[107]

Taking their biocompatibility, non-toxic character into account and considering all the examples given above, SWNTs seem to be very promising delivery system and material for other biomedical applications.

1.3 Light Harvesting and Energy Transfer

1.3.1 Energy Transfer Mechanisms

Energy transfer is the process where energy is transmitted from a chromophore in its excited state to a different chromophore in its ground state.[119] Excitation energy of the former, donor (D) is used to excite the latter, the acceptor (A) to its first singlet excited state. Energy transfer can be characterized using different approaches; comparing relative lifetimes, quantum yields, quenching of the donor emission or increase in acceptor emission would be parameters to follow. Energy transfer is affected from rate of other deactivation pathways of excited system, thus chromophores have to be suitable to compete with these pathways.[119-120] Lifetime of excited state has to be longer than time required for energy transfer. There are two different types of energy transfer mechanisms called Förster and Dexter types, which are theoretically well established and experimentally verified.

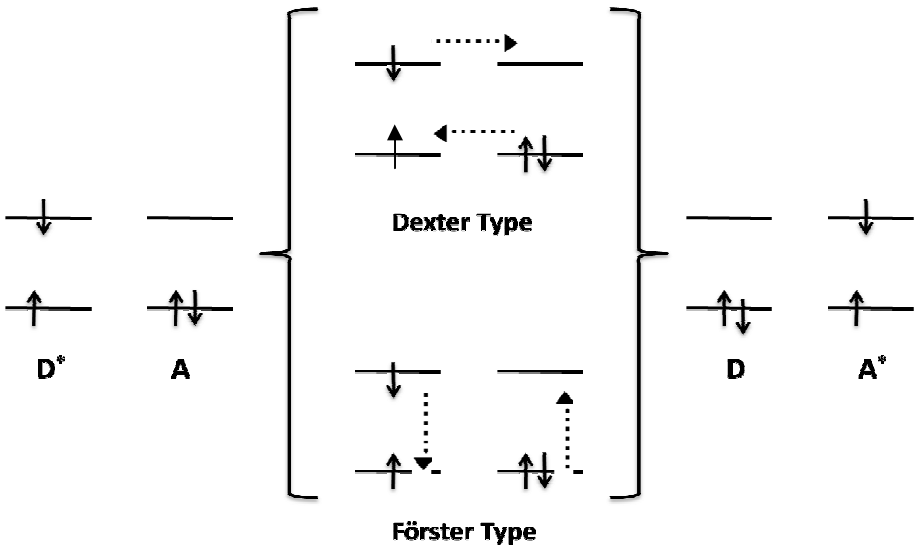

Figure 13. Schematic illustration of Förster and Dexter types of energy transfer.

1.3.1.1 Dexter Type Energy Transfer

Dexter Type, also called "through bond", energy transfer basically relies on orbital interaction of donor and acceptor molecules leading to exchange of electrons from the highest occupied level of the donor to the lowest unoccupied level of the acceptor.[121] Simultaneous exchange of ground state electrons accompanies this process (Figure 13).[119] This dependency on orbital interaction restricts energy transfer to very short distances, usually less than 10 Å.[120] As a consequence, energy transfer rate constant decreases exponentially with increasing donor-acceptor separation as formulated below.

$$\mathbf{k_{ET} = K\ J\ exp(-2R_{DA} / L)} \qquad (2)$$

where K represents orbital interaction, J is the overlap integral between donor emission and acceptor absorbance, R_{DA} is the donor acceptor separation and finally L is the van der Waals radii.[120]

Dexter type energy transfer systems were designed and synthesized with different molecules as shown in Figure 14. These Dexter systems exhibit energy transfer upon excitation at donor's absorbance wavelength in each system. In porphyrin-based system (Figure 14A) central porphyrin was decorated with four terminal pophyrins coordinated to zinc.[122] This difference in the structure allows energy transfer from the terminal porphyrins to the center through ethynyl bridge. In anthracene-BODIPY system as shown in Figure-14B, very fast energy transfer (~200 fs) from anthracene to BODIPY was observed upon excitation at anthracene's absorbance wavelength which would be due to parallel alignment of S_1 - S_o transition dipole moments of donor and acceptor respectively.[45,123]

One interesting example of Dexter type energy transfer in literature would be the one shown in Figure 14C. These ligand-metal based systems provide unidirectional energy transfer in a linear array of system which would be used in the production of molecular wires.[124] In this primitive example, efficient energy transfer from Ru and Os complexes to anthracene was observed.

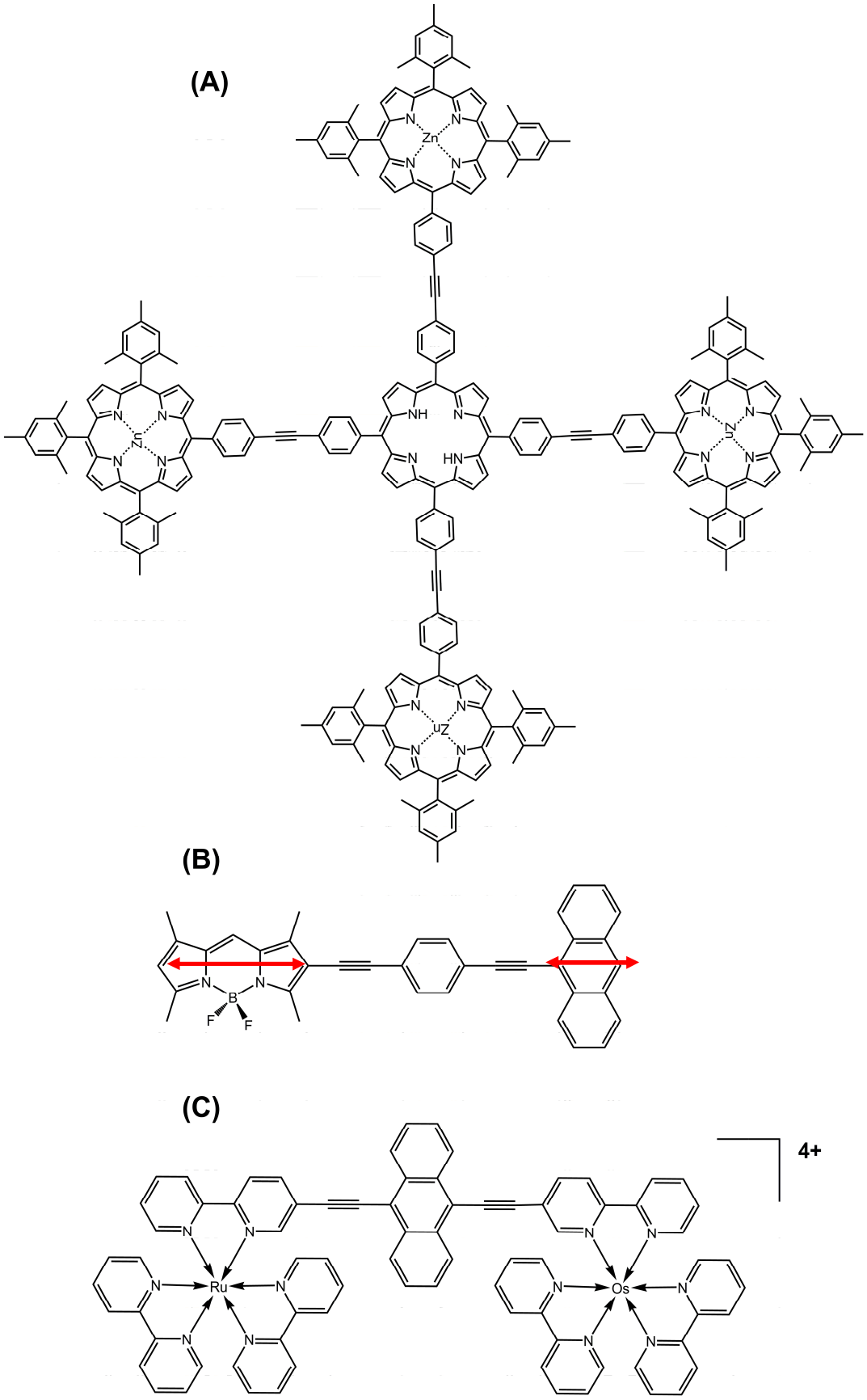

Figure 14. Some Dexter type energy transfer systems in literature.[122-124]

1.3.1.2 Förster Type Energy Transfer

In contrast to Dexter type, Förster resonance energy transfer (FRET) or through space energy transfer does not depend on orbital interaction, hence, larger separation between donor-acceptor still would be allowed to achieve energy transfer. Spectral overlap between donor emission and acceptor absorbance is essentially important together with relative orientation of transition dipoles of donor and acceptor.[50,51,125] Considering the fact that, energy is not transferred through bond, rather through space; other deactivation processes affect the efficiency of energy transfer. Deactivation would be due to intrinsic photophysical properties of chromophores such as internal conversion through vibrational relaxation, quantum yield of donor or as a result of solvent refractive properties.[120] The distance between donor and acceptor at which half of the excited donor energy is transferred to the acceptor is called Förster distance (R_o) and formulated together with energy transfer rate constant (k_{FRET}) as shown below:

$$\mathbf{R_o = 9.78 \times 10^3 [\kappa^2 n^{-4} Q_D J(\lambda)]} \quad (3)$$

$$\mathbf{k_{FRET} = [\ 900\ (\ln 10)\ \kappa^2\ \Phi_D\ J(\lambda)\ ] / [128\ \pi^5\ n^4\ N\ \tau_D\ R^6_{DA}\ ]} \quad (4)$$

where κ represents relative dipole moment orientation of excited donor and ground state acceptor, n is the refractive index of the medium, Q_D is the quantum yield of the donor in the absence of acceptor, $J(\lambda)$ is spectral overlap integral of donor emission and acceptor absorbance, τ_D is excited state lifetime of donor in the absence of the acceptor chromophore and finally R_{DA} is donor-acceptor separation.[120]

1.3.1.2.1 Determination of FRET Efficiency

FRET efficiency can be determined in a number of ways; in general, there are two different approaches, steady state and time-resolved.[126] In one of the steady state approach, decrease in donor fluorescence quantum yield is used. However, in this method one should be careful to avoid so called inner filter effect which refers to reabsorption of the emitted light by the same molecule or other unexpected ones. Self quenching problem can be solved using very dilute solutions.[127-128] In this method, energy transfer efficiency is formulated as shown below:

$$\mathbf{E = 1 - \Phi_{DA} / \Phi_D} \qquad (5)$$

where Φ_{DA} and Φ_D are quantum yield of donor in the presence and absence of acceptor respectively. Excitation spectra or enhancement in fluorescence emission of the acceptor can be used to determine energy transfer in steady state approach. Corresponding equation is given below:

$$\mathbf{E = A_A (\lambda_D) / A_D (\lambda_D) * [I_{AD}(\lambda_A^{em}) / I_A(\lambda_A^{em}) - 1]} \qquad (6)$$

where A_A and A_D refers to absorbance values of acceptor and donor ar the maximum absorbance wavelength of donor. I_{AD} and I_A refer to integrated emission area of acceptor in the presence and absence of donor at λ_A^{em} respectively.

Time resolved approach provides more accurate results since inner filter effect or errors associated with integration are lacking here. This method is based on time-resolved emission of any of acceptor or donor. If the decay of fluorescence is single exponential, FRET rate constant and FRET efficiencies can be defined as shown below:[126, 129]

$$k_{FRET} = 1/\tau_{DA} - 1/\tau_D \quad (7)$$

$$E = \tau_D \, k_{FRET}/(1+\tau_D k_{FRET}) \quad (8)$$

where τ_D and τ_{DA} refer to excited state decay time (lifetime) of donor in the absence and presence of acceptor respectively. More simply, FRET efficiency can be found using following equation:

$$E = 1 - \tau_{DA}/\tau_D \quad (9)$$

1.3.1.2.2 Examples of FRET Systems in Literature

BODIPY dyes are widely used in energy transfer systems some of which are shown in Figures 15 and 16. In the example shown in Figure 15, four BODIPYs were attached covalently to perylene diimide core. In accordance with the increase in BODIPY number on the structure, extinction coefficient of the molecule at BODIPY's maximum absorbance wavelength (526 nm) increases dramatically to 250000 $M^{-1}cm^{-1}$.[130] Energy transfer efficiency was determined to be 99% with a critical Förster radius of 4.7 nm. In the second example shown in Figure 15, enhancement in emission of the core distyryl-BODIPY was observed as the number of terminal BODIPY donors was increased in number, as expected.[131]

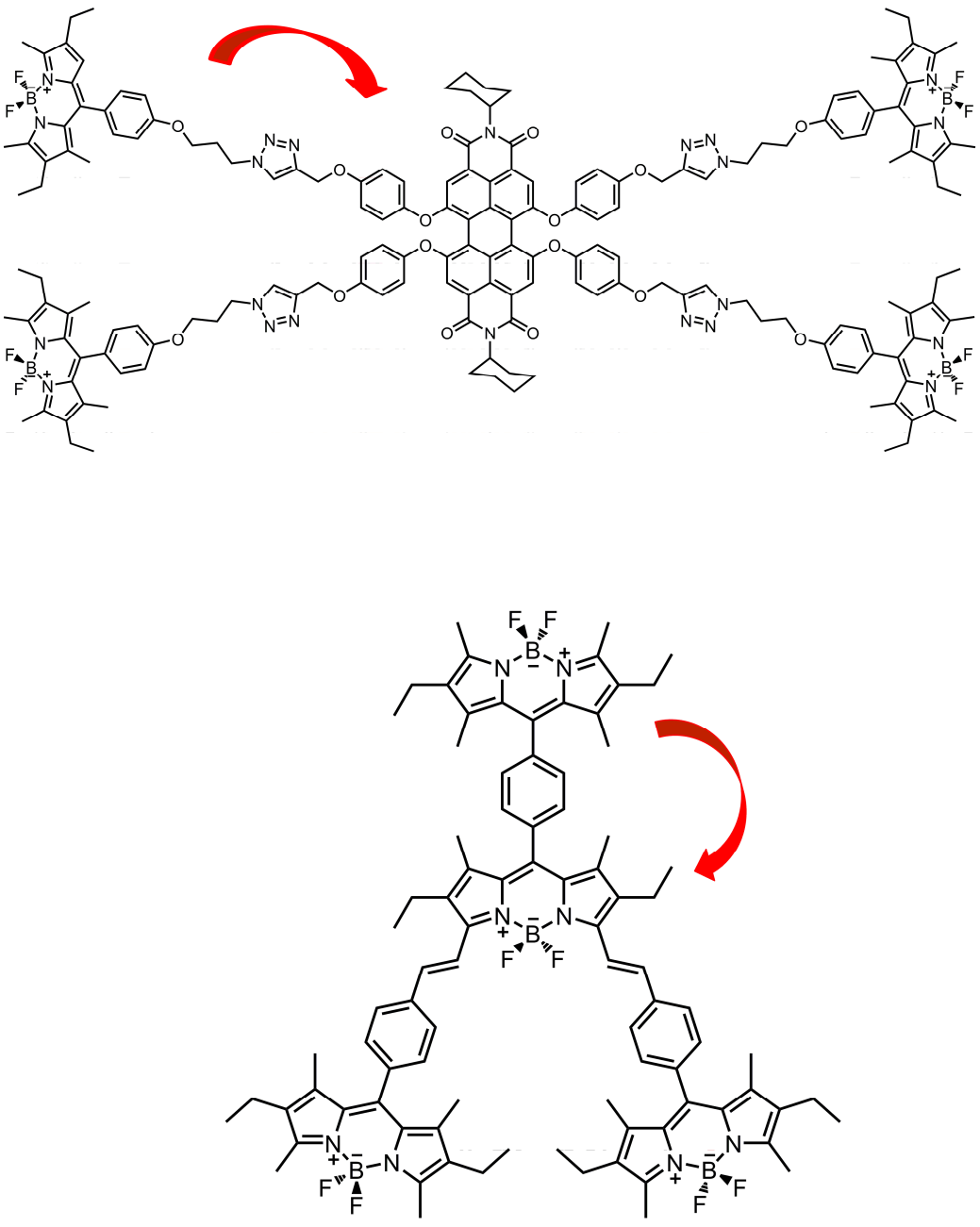

Figure 15. Some BODIPY-based Förster type energy transfer systems[130-131]

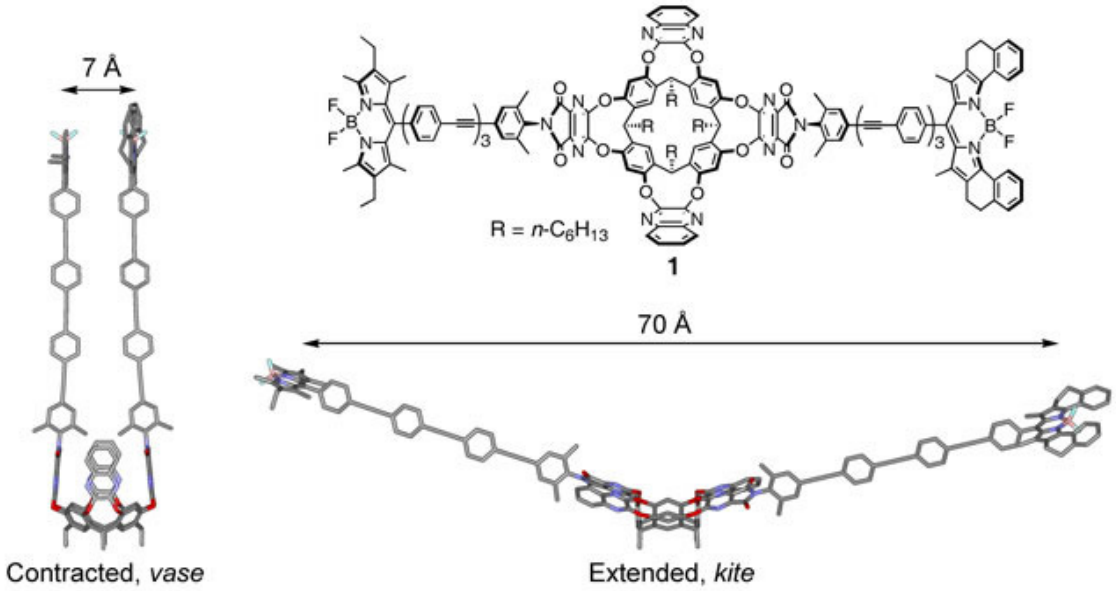

Figure 16. pH-controlled FRET.[132]

One interesting example of FRET was shown in Figure 16 where donor and acceptor distance depends on the pH of the media. In acidic conditions, FRET is abolished and donor emission was observed at 542 nm.[132] In this case, the whole molecule is extended such that the distance between donor and acceptor is 7 nm. On the other hand in the contracted form, the distance decreases almost ten folds, thus, energy transfer is observed. Change in FRET efficiency upon conformational transformation is extensively used in protein labeling and enzyme dynamics.

Apart from conformational change analysis, FRET systems are used to construct chemical or biological sensors, to determine ligand-receptor interaction, membrane organization assays, to monitor hybridization of nucleic acids and a number of other applications.[126]

1.3.2 Light Harvesting

Scientists usually admire the biological mechanisms which are shaped through millions of years of optimization processes to yield a system, perfectly tuned to work efficiently under the rules of earth. Photosynthesis is one such marvelous system in organisms that is evolved to convert sun light into chemical energy in the form of adenosine triphosphate (ATP).[133] Architectural design and synergistic functionality of elements of this energy conversion complex is inspired, hence, researches try to mimic certain parts of this system for a variety of purposes such as frequency conversion, signal amplification, artificial photosynthetic systems, dye-sensitized solar energy and molecular optoelectronic applications.[134-137]

Light harvesting (antenna) complex simply means array of different chromophores with different but mutual spectral properties interacting photophysically to funnel energy in certain part of the complex.[138] X-ray crystallographic structure and functionality of antenna complex in purple bacteria were well-studied and a number of artificial systems were designed and synthesized.[139]

1.3.2.1 Light Harvesting in Purple Bacteria

In purple bacteria, extensive study on light harvesting complex and subsequent redox reactions were done. Femtosecond energy transfer between units allows channeling of light energy to the core structure called reaction center. This reaction center initiates the redox processes leading to generation of proton gradient and release of oxygen at the end.[140]

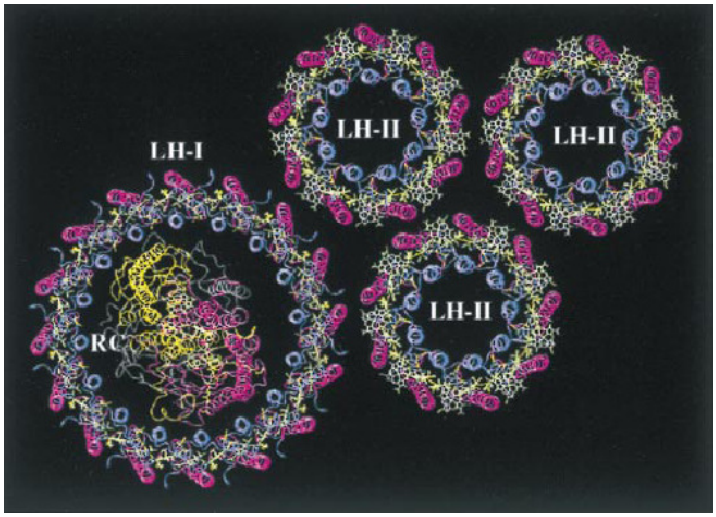

Figure 17. Antenna system in purple bacteria.[141]

Antenna system in purple bacteria composed of approximately 250 chlorophyll (BChl *a*) pigments and carotenoids having slightly different spectroscopic properties.[141] As shown in Figures 17 and 18, energy is transferred from outer LH-III comlex to the inner reaction center. Hopping energy is either within the complex (dashed lines) or between different complexes (solid line) as shown in Figure 18. Although most purple bacteria have LH-I, LH-II complexes and reaction center, not all have LH-III complex.[141]

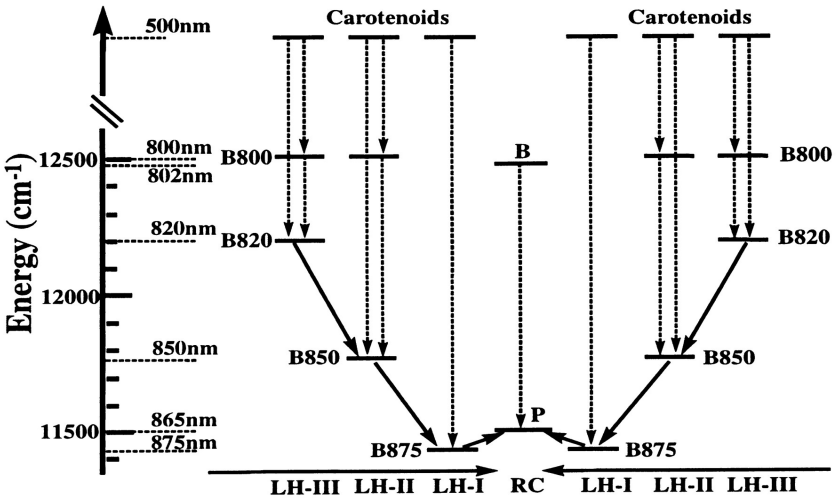

Figure 18. Energy levels of photosynthetic elements in purple bacteria.[141]

Within the LH-II complex, there are two different chlorophylls absorbing at 800 and 850 nm (B800 and B850 respectively). Rapid energy transfer from B850 (green) to B800 (blue) within 700 fs occurs.[140-141] In all complexes, carotenoids contribute to harvesting by transferring its energy to exciton states of the B850 with 100% efficiency. These exciton states are formed as a result of interaction of intimately arranged chlorophylls. Both Dexter and Förster type mechanisms are involved in whole light harvesting processes.[141]

1.3.2.2 Artificial Antenna Systems

Artificial antenna complexes that resemble biological counterparts in organization and light harvesting were published. These systems mimic the circular arrangement of pigments in LH-II complex of purple bacteria. One such example is shown in Figure 19, twelve porphyrins are assembled noncovalently to form circular array where maximum separation, namely radius of antenna is 4.1 nm.[142]

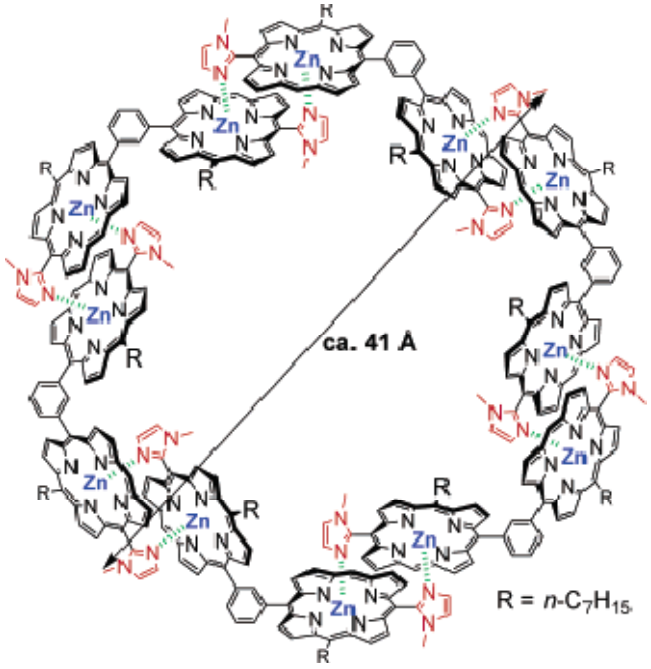

Figure 19. Artificial antenna in the form of slipped-cofacial array of chromophores.[142]

In this synthetic system, no protein matrix assistance is required as in the case of biological antenna since chromophores readily self-arrange through coordination of imidazolyl to Zn at the core of porphyrin to form perfect circular geometry. Thus, in this example "slipped-cofacial" placement which is crucial in the accomplishment of antenna is mimicked.[142]

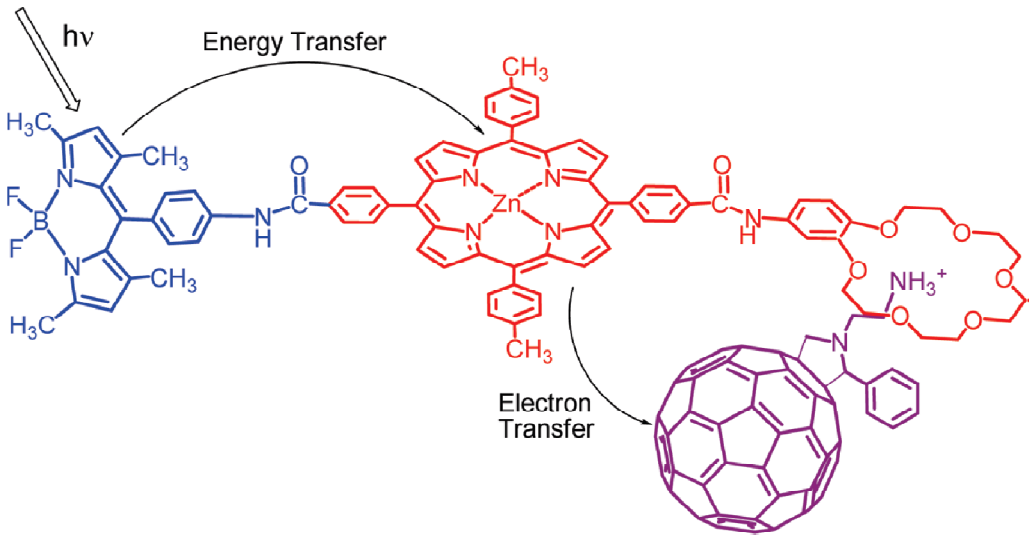

Figure 20. Artificial antenna and reaction center.[143]

One very exciting work was published by Tkachenko and D'Souza *et al.* and shown in Figure 20.[143] Primitive but entire mimicry of photosynthetic system was constructed with an energy donor BODIPY, acceptor Zn-porphyrin two of which resembles antenna part of biological counterpart and finally an electron acceptor fullerene self-assembled to other part. Fullerene corresponds to reaction center, accepts electron from Zn-porphyrin and charge separation persists quite long time.[143]

1.3.2.3 Light Harvesting Dendrimers

From their first synthesis on, dendrimers with branched construction are a focus for a variety of research due to their rational and versatile structure. Since proximity of donor-acceptor affects efficiency of energy transfer exponentially in Dexter type and sixth power of distance in Förster type, appropriate placement of chromophores in light harvesting systems is essential.[126] Hence, dendritic architecture provides a suitable scaffold for this type of systems by enabling arrangement in an array of spectral overlap. Further, it was postulated that energy dissipation due to collisions are diminished in dendritic scaffolds.[138]

First dendritic type energy transfer system was published by Balzani *et al*. in 1992 which was composed of complexes of Ruthenium and Osmium.[144-145] Following this, first unidirectional energy transfer from the phenyl acetylene outer units to perylene core was reported by Xu and Moore *et al*.[146] Dendritic benzyl ether ligands coordinated to core lanthanide was also observed to enhance core luminescence as reported by others.[147] In addition, a number of pophyrin-based dendritic antennas were synthesized and their photophysical properties were studied.[148-149]

Frechet *et al.* synthesized an antenna that consists of multiple chromophores with regular arrangement (Figure 21).[150] At the heart of the antenna, there lies perylene dye (λ_{abs} = 555 nm) as final acceptor. This core was decorated with four fluorol 7GA (λ_{abs} = 415 nm, λ_{em} = 520 nm). At the outer shell of the dendrimer eight Coumarin 2 donors are present (λ_{abs} = 350 nm, λ_{em} = 440 nm). Suitable spectral overlap and distance between donor-acceptor conjugates allows successful energy transfer in a cascade system from the terminal to the center. Förster resonance energy transfer efficiencies are very high even between coumarin 2 and perylene units which have smallest spectral overlap.[150]

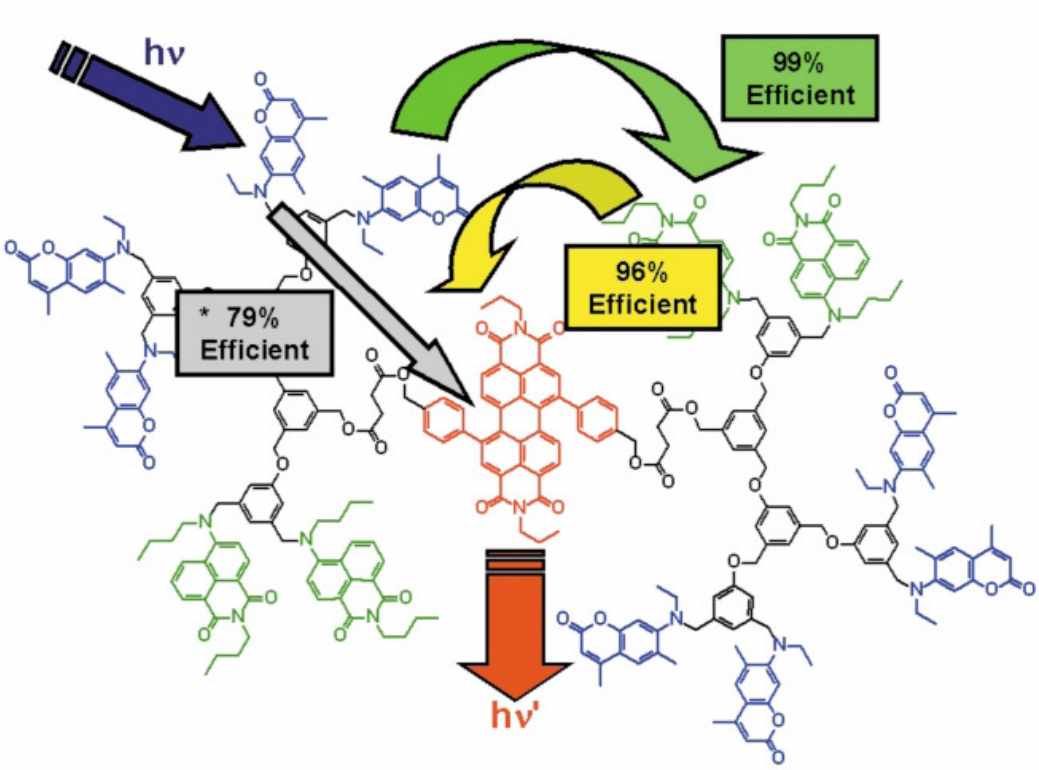

Figure 21. Cascade energy transfer in multichromatic antenna[150]

In conclusion, dendritic light harvesting systems allow proper arrangement of spectrally mutual chromophores in close proximity and enables unidirectional energy transfer to the core chromophore. Large complex of biological counterpart can be effectively constructed with this kind of chemical approach.

CHAPTER 2

EXPERIMENTAL PROCEDURES

2.1 General

All chemicals and solvents purchased from Sigma-Aldrich were used without further purification. 1-2 nm X 500 nm SWNT was purchased from Aldrich (catalog no: 652512). PEG-N_3 was synthesized according to literature.[151] Spectra of ^1H NMR and ^{13}C NMR were recorded using a Bruker DPX-400 in $CDCl_3$ with TMS as internal reference. Splittings in the spectra are shown as s (singlet), d (doublet), t (triplet), q (quartet), m (multiplet), p (pentet), dt (doublet of triplet), and br (broad).

Absorption spectrometry was performed using a Varian spectrophotometer. Steady state fluorescence measurements were conducted using a Varian Eclipse spectrofluorometer. Column chromatography of all products was performed using Merck Silica Gel 60 (particle size: 0.040–0.063 mm, 230–400 mesh ASTM). Reactions were monitored by thin layer chromatography using fluorescent coated aluminum sheets. Solvents used for spectroscopy experiments were spectrophotometric grade. Mass spectrometry measurements were done at the Ohio State University Mass Spectrometry and Proteomics Facility, Ohio, U.S.A.

AFM images were acquired in UNAM, Ankara, using PSIA XE-100E AFM and Multi75AI AFM tip. TEM images were aquired in UNAM, Ankara, using FEI Technai G2 F30 high resolution transmission electron microscope and carbon grid.

Quantum yield measurements and calculations were done using Rhodamine G6 (excitation 488 nm, water), Sulforhodamine 101(excitation 550 nm, ethanol) and Cresyl Violet (excitation 610 nm, methanol) as standard chromophores having quantum yields 0.95, 0.90 and 0.66 respectively. All absorbance values were below 0.1 to avoid self quenching. Following formula was used for calculations: [127]

$$\mathbf{Q = Q_R\,(I/I_R)*(A_R/A)*(n^2/n_R^2)} \qquad (6)$$

where Q_R stands for quantum yield of reference, I and I_R for integrated area of emission spectrum for specific wavelength for sample and for standard respectively, A and A_R represents absorbance of corresponding wavelength for sample and standard, n and n_R refer to refractive indices of solvents in which sample and standard compounds were dissolved respectively. Refractive index values were taken to be 1.333 for water, 1.3624 for ethanol and 1.329 for methanol. All samples except standards were dissolved in chloroform which has an n value of 1.49.

Lifetime measurements were done at Photon Technology International (Canada) Inc. Fast Kinetic Application Laboratories, Ontario Canada. The measurements were carried out with the TM-3 LaserStrobe time-resolved fluorometer from PTI utilizing a pulsed nitrogen/dye laser excitation and the stroboscopic detection system. The dye laser excitation was at 526, 590 and 653 nm. The instrument response function was measured with an aqueous Ludox solution. The decays were analyzed with a multiexponential fitting function by iterative reconvolution and chi-square minimization. Fluorescence decay results were given in Appendix C.

2.2 Experimental Part-I

2.2.1 Design of Photosensitizer

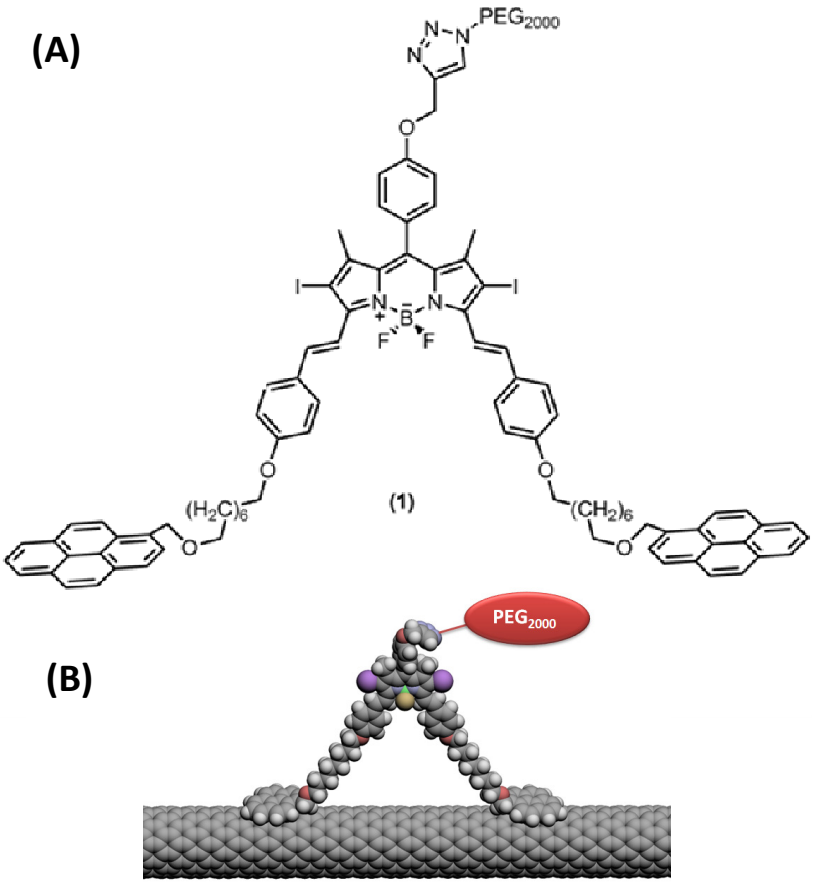

Figure 22. (a) Structure of target PS, compound **1**, (b) 3D structure of compound **1** on SWNT

As shown in Figure 22, BODIPY-based compound **1** is designed as photosensitizer in this research. Iodines are attached to enhance intersystem crossing, thus provide spin forbidden singlet-triplet transition. PEG is attached through triazole ring to make the photosensitizer water solubility. Presence of pyrenes enables SWNT attachment.

2.2.2 Synthesis of Photosensitizer

2.2.2.1 Synthesis of 4-(8-chlorooctyloxy)benzaldehyde (3)

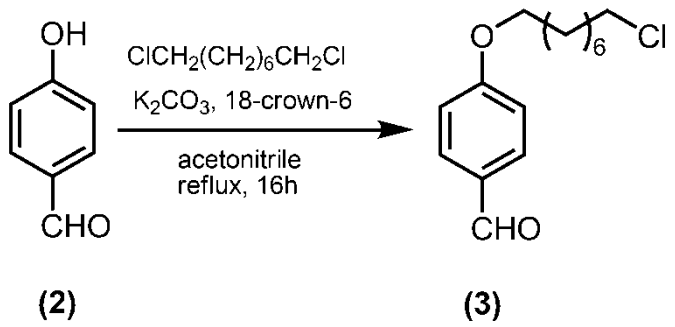

Figure 23. Synthesis of compound **3**

1,4-hydroxybenzaldehyde (1.25 g, 10 mmol) and 1,8 dichlorooctane (2.75 g, 15 mmol) were dissolved in acetonitrile (100 ml). K_2CO_3 (2.76 g, 20 mmol) and a few crystals of 18-crown-6 were added. The reaction mixture was refluxed for 16h. Then, acetonitrile was evaporated in vacuo and extracted with water and chloroform. Organic layer as dried with Na_2SO_4 and evaporated in vacuo**.** The product was purified by silica gel column chromatography using $CHCl_3$/Hexane (80:20, v/v). Fraction containing compound **3** was collected then the solvent was removed under reduced pressure (3 mmol, 806 mg, 30%).

^{1}H NMR ($CDCl_3$, 400 MHz, δ ppm) 1.30-1.52 (m, 8H), 1.72-1.89 (m, 4H), 3.54 (t, *J*= 6.7 Hz, 2H), 4.05 (t, *J*= 6.5 Hz, 2H), 6. 98 (d, *J*= 8.76 Hz, 2H), 7.83 (d, *J*= 8.8 Hz, 2H), 9.89 (s, 1H)

^{13}C NMR ($CDCl_3$, 100 MHz, δ ppm) 22.85, 26.76, 28.76, 29.00, 29.13, 32.56, 45.08, 68.33, 114.74, 131.97, 164.22, 190.78.

HRMS-ESI: calculated for [M+H] 269.1308, found 269.1303, Δ= 1.9 ppm

2.2.2.2 Synthesis of 4-(8-(pyren-1-ylmethoxy)octyloxy) benzaldehyde (4)

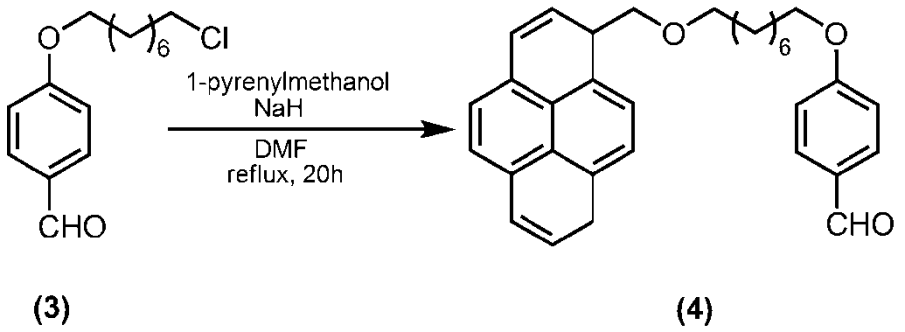

(3) (4)

Figure 24. Synthesis of Compound **4**

Pyrenyl methanol (696.84 mg, 3 mmol) was dissolved in DMF (5 ml). 120 mg 60% NaH was added slowly and the reaction mixture was stirred at room temperature for 20 min. 1,8-dichlorooctane **3** dissolved in DMF (5 ml) and added into the previous solution. After 20h of reflux, it was extracted with saturated $NaHCO_3$ aqueous solution and $CHCl_3$, organic layer was dried with Na_2SO_4 and evaporated under reduced pressure. The product was purified by silica gel column chromatography using $CHCl_3$/Hexane (75:25, v/v). Fraction containing compound **4** was collected then the solvent was removed under reduced pressure (279 mg, 0.6 mmol, 20%).

^{1}H NMR ($CDCl_3$, 400 MHz, δ ppm) 1.22-1.42 (m, 8H), 1.62-1.79 (m, 4H), 3.62 (t, *J*= 6.5 Hz, 2H), 3.96 (t, *J*= 6.6 Hz, 2H), 5.23 (s, 2H), 6.96 (d, *J*=8.7 Hz, 2H), 7.82 (d, *J*=8.8 Hz, 2H), 8.01-8.13 (m, 4H), 8.14-8.21 (m, 4H), 8.40 (d, *J*=9.2 Hz, 1H), 9.88 (s, 1H).

^{13}C NMR ($CDCl_3$, 100 MHz, δ ppm) 25.8, 26.1, 29.0, 29.2, 29.8, 68.3, 70.4, 71.5, 114.7, 123.6, 124.5, 125.0, 125.2, 125.9, 126.9, 127.3, 127.4, 127.6, 129.4, 129.7, 130.8, 131.2, 131.3, 131.8, 132.0, 164.2, 190.8.

HRMS-ESI: calculated for M+Na 487.2249, found 487.2217, Δ= 6.6 ppm

2.2.2.3 Synthesis of 4-(prop-2-ynyloxy)benzaldehyde (5)

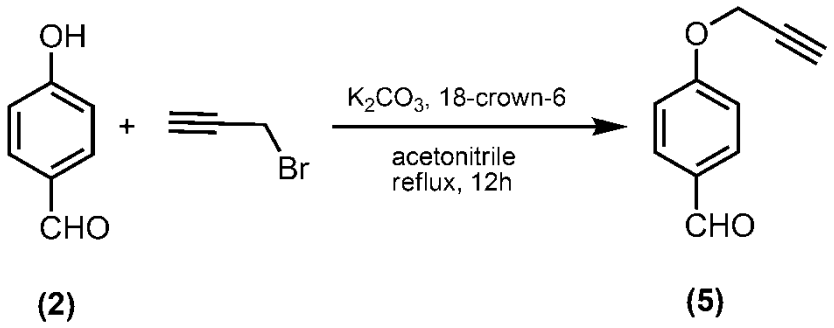

Figure 25. Synthesis of compound **5**

4-hydroxybenzaldehyde (2.45 g, 20 mmol) and propargyl bromide (2.5 g, 30 mmol) were dissolved in 100 ml acetonitrile. K_2CO_3 (5.5 g, mmol) and a few crystals of 18-crown-6 were added. The reaction was refluxed until all 4-hydroxybenzaldehyde consumed. The solvent was evaporated in vacuo, extracted with water and $CHCl_3$. Organic layer was dried with Na_2SO_4 and evaporated under reduced pressure. The product was purified by silica gel column chromatography using $CHCl_3$/Hexane (50:50, v/v). Fraction containing compound **5** was collected then the solvent was removed under reduced pressure (2.85 g, 17.8 mmol, 89%).

^{1}H NMR ($CDCl_3$, 400 MHz, δ ppm) 2.58 (t, *J*=2.5 Hz, 1H) 4.79 (dd, J=1.48, 0.9 Hz), 7.11 (d, *J*=7.1 Hz, 2H), 7.87 (d, *J*=7.0 Hz, 2H), 9.92 (s, 1H).

^{13}C NMR ($CDCl_3$, 100 MHz, δ ppm) 55.9, 76.4, 77.5, 115.2, 131.9, 162.4, 190.8, 207.7.

HRMS-ESI: calculated for M+Na 183.0422, found 183.0422, Δ= 0 ppm.

2.2.2.4 Synthesis of 1,3,5,7-Tetramethyl-8-(4-Propargyloxiphenyl)-4,4-difloroboradiaza-*s*-indacene (**6**)

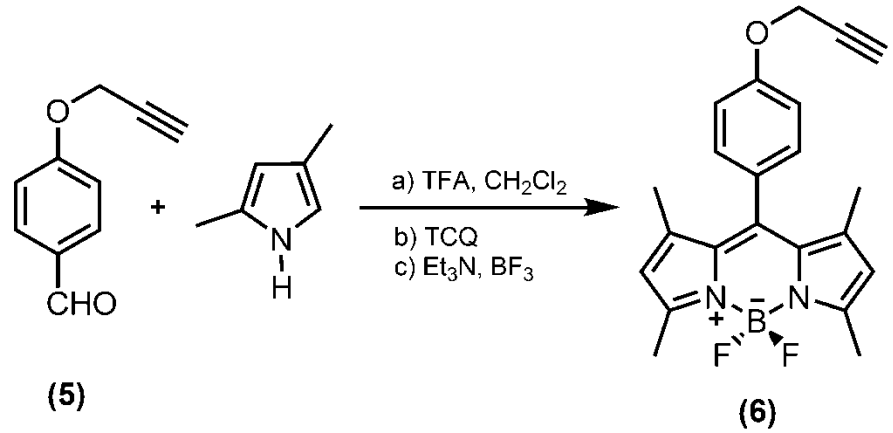

Figure 26. Synthesis of compound **6**

CH_2Cl_2 (300 ml) was purged with Ar for 30 min. 4-(prop-2-ynyloxy)benzaldehyde **5** (1 g, 6.2 mmol) and 2,4-dimethyl pyrrole (1.2 g, 12.6 mmol) were added. The color of the solution turned into red after the addition of 3 drops of trifluoroacetic acid. The reaction mixture was stirred at room temperature for 12h. Then, tetrachloro-1,4-benzoquinone (1.52 g, 6.2 mmol) was added and the reaction mixture was stirred at room temperature for 45 min. Then triethyl amine (6 ml) and boron trifluoride diethyl etherate (6 ml) were added sequencially. After stirring at room temperature for 30 min, it was extracted with water. Organic layer was dried with Na_2SO_4 and evaporated

under reduced pressure. The product was purified by silica gel column chromatography using $CHCl_3$ as mobile phase. Fraction containing compound **6** was collected then the solvent was removed under reduced pressure (260 mg, 0.68 mmol, 11%).

^{1}H NMR ($CDCl_3$, 400 MHz, δ ppm) 1.43 (s, 6H), 2.56-2.58 (m, 6H+1H), 4.77 (d, *J*=2.4 Hz, 2H), 5.99 (s, 2H), 7.10 (d, *J*=8.7 Hz), 7.21 (d, *J*=8.7 Hz, 2H).

^{13}C NMR ($CDCl_3$, 100 MHz, δ ppm) 14.5, 14.6, 56.0, 75.9, 78.0, 115.6, 121.2, 128.0, 129.2, 131.8, 141.5, 143.1, 155.4, 158.1.

HRMS-ESI: calculated for M+Na 401.1617, found 401.1644, Δ= 6.7 ppm.

2.2.2.5 Synthesis of 2,6-Diiodo-1,3,5,7-tetramethyl-8-(4-Propargyloxiphenyl) -4,4-difloroboradiaza-*s*-indacene (7)

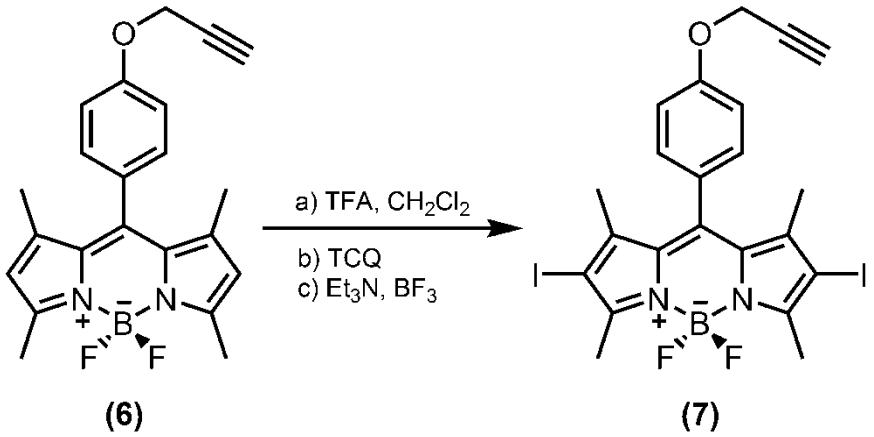

Figure 27. Synthesis of compound **7**

1,3,5,7-Tetramethyl-8-(4-Propargyloxiphenyl)-4,4-difloroboradiaza-*s*-indacene **6** (50 mg, 0.13 mmol) and I_2 (83 mg, 0.33 mmol) were dissolved in ethanol (100 ml). Iodic acid, HIO_3 (45.74 mg, 0.26 mmol) was dissolved in a few drops of water and added into previous solution. The reaction mixture was stirred at 60^{o}C for a few hours untill all reeactant was consumed. Then, saturated sodium thiosulfate solution was added (50 ml) and it was stirred at rrom

temparature for additional 30 min. Then, it was extracted with $CHCl_3$ and water. Organic layer was dried with Na_2SO_4 and evaporated under reduced pressure. The product was purified by silica gel column chromatography using $CHCl_3$/Hexane (50/50, v/v). Fraction containing compound **7** was collected then the solvent was removed under reduced pressure (59 mg, 0.09 mmol, 72%).

^{1}H NMR ($CDCl_3$, 400 MHz, δ ppm) 1.36 (s, 6H), 2.49 (s, 1H), 2.56 (s, 6H), 4.70 (s, 2H), 7.04 (d, *J*=8.8 Hz, 2H), 7.09 (d, *J*=8.8 Hz, 2H).

^{13}C NMR ($CDCl_3$, 100 MHz, δ ppm) 16.0, 17.1, 56.1, 76.1, 85.8, 100.1, 116.0, 127.8, 129.1, 131.6, 141.4, 146.0, 156.7, 158.6.

HRMS-ESI: calculated for M+Na 652.9550, found 652.9515, Δ= 5.4 ppm.

2.2.2.6 Double Knoevenagel Condensation Reaction (8)

2,6-Diiodo-1,3,5,7-tetramethyl-8-(4-Propargyloxiphenyl)-4,4-difloroboradiaza-*s*-indacene **7** (38 mg, 0.06 mmol) and 1-(8-(4-formyl)-phenyloxiheksyloxi methyl)-pyrene **4** (70 mg, 0.15 mmol) dissolved in benzene (45 ml). Piperidine (0.2 ml) and glacial acetic acid (0.2 ml) were added. The solution was refluxed using Dean-Stark apparatus. When the solution was concentrated, reaction was followed by TLC until green-colored product became the major product. Then, benzene was evaporated in vacuo. It was extracted with $CHCl_3$ and water. Organic layer was dried with Na_2SO_4 and evaporated under reduced pressure. The product was purified by silica gel column chromatography using $CHCl_3$ as mobile phase. Fraction containing compound **8** was collected then the solvent was removed under reduced pressure (40 mg, 0.026 mmol, 44%).

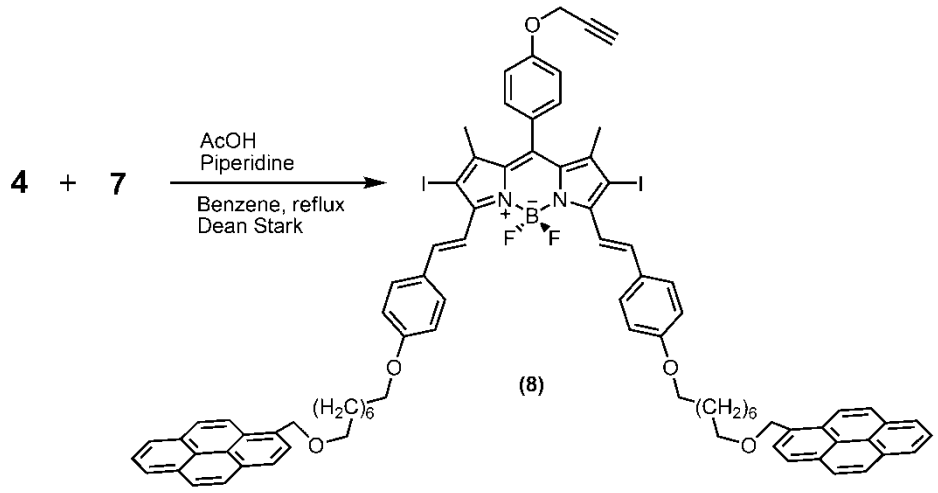

Figure 28. Synthesis of compound **8**

^{1}H NMR ($CDCl_3$, 400 MHz, δ ppm) 1.15-1.78 (m, 30H), 2.61 (s, 1H), 3.61 (t, *J*= 6.6 Hz, 4H), 3.89 (t, *J*= 6.4 Hz, 4H), 4.81 (d, *J*=2.2 Hz, 2H), 5.21 (s, 4H), 6.85 (d, *J*=8.7 Hz, 4H), 7.11 (d, *J*=8.8 Hz, 2H), 7.19 (d, *J*=8.8 Hz, 2H), 7.55-7.64 (m, 4H+2H), 7.99-8.09 (m, 8H), 8.13-8.21 (m, 8H+2H), 8.39 (d, *J*=9.2 Hz, 2H).

^{13}C NMR ($CDCl_3$, 100 MHz, δ ppm) 15.1, 18.2, 22.3, 25.9, 26.1, 29.1, 29.2, 29.3, 29.7, 29.8, 58.4, 68.0, 70.4, 71.5, 114.8, 123.6, 124.5, 125.1, 125.9, 126.9, 127.3, 127.4, 127.6, 129.2, 129.4, 131.2, 131.3, 131.8, 132.0, 160.3.

MALDI: calculated for **8,** 1522.414, found 1522.319, Δ= 6.2 ppm.

2.2.2.7 Synthesis of Compound 1 (Click Reaction)

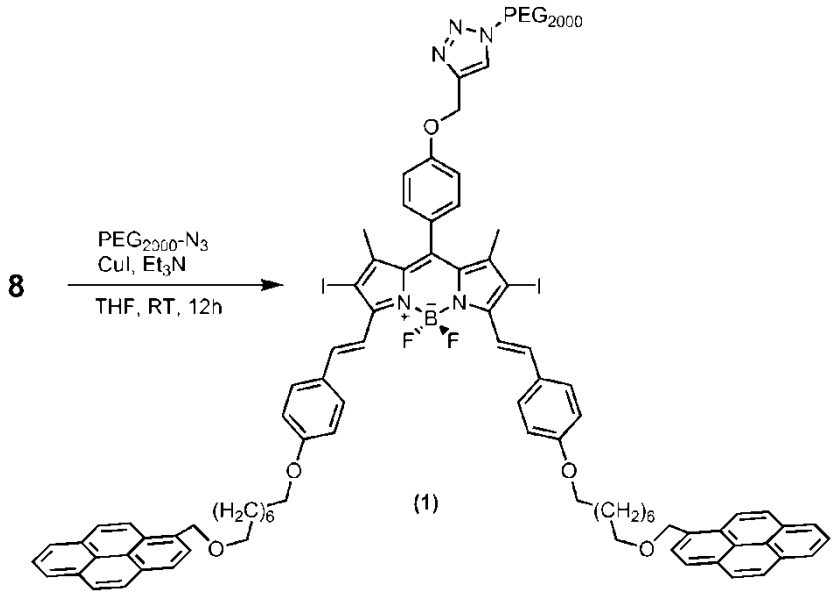

Figure 29. Synthesis of compound **1**.

Click reaction was performed according to literature.[152] Double Knoevenagel condension product, compound **8** (40 mg, 0.027 mmol) was dissolved in THF (2 ml). 2 molar equavalent CuI (10.3 mg, 0.054mmol), 50 molar equavalent triethyl amine (135.6 mg, 1.34 mmol) and 2 molar equavalent 1-azido polyethylene glycol (MW: 2000) (108 mg, 0.054 mmol) were added. The reaction mixture was stirred at room temperature for 12h, THF and triethyl amine were evaporated in vacuo. Organic layer was dried with Na_2SO_4 and evaporated under reduced pressure. The product was purified by silica gel column chromatography using $CHCl_3$/methanol (95/5, v/v). Fraction containing compound **1** was collected then the solvent was removed under reduced pressure (91 mg, 0.026 mmol, 95%).

^{1}H NMR ($CDCl_3$, 400 MHz, δ ppm) 1.19-1.42 (m, 16H), 1.47 (s, 6H), 1.60-1.71 (m, 8H), 3.37 (s, 3H), 3.51-3.71 (m, "PEG" approximately 210H), 3.78-3.90 (m, 8H), 5.17 (s, 4H), 5.25 (s, 2H), 6.84 (d, *J*=8.8 Hz, 4H), 7.11-7.17 (m, 4H), 7.53-

7.62 (m, 4H+2H), 7.91 (s, 1H), 7.95-8.05 (m, 8H), 8.07-8.20 (m, 8H+2H), 8.45 (d, *J*=9.2 Hz, 2H).

^{13}C NMR ($CDCl_3$, 100 MHz, δ ppm) 17.6, 25.8, 26.0, 29.0, 29.2, 29.6, 29.7, 46.9, 50.6, 59.0, 62.0, 68.0, 70.0, 70.6, 70.7, 71.9, 94.2, 106.0, 114.8, 123.5, 124.4, 125.1, 126.9, 127.3, 127.4, 127.5, 129.2, 129.3, 130.8, 131.1, 131.8, 139.1, 143.2, 150.4, 159.3, 160.3.

MALDI: Distribution around 3298.384 with separation of 44.287 corresponding to etylene glycole unit.

2.2.3 Non-covalent Functionalization of SWNT with Compound 1

Compound **1** was adsorbed on to the SWNT by means of sonication and unadsorbed molecules were eliminated through filtration as described elsewhere.[153] PBS buffer was prepared by dissolving 8 g NaCl, 0.2 g KCl, 1.44 g Na_2HPO_4 and 0.24 g KH_2PO_4 in 1L water. 1 mM solution of photosensitizer was prepared by dissolving 70 mg compound **1** in 20 ml ethanol-PBS mixture (50/50, v/v). 3 mg SWNT was put into a veil containing 5 ml 1:1 ethanol-PBS mixture and sonicated for 15 min. Then, 5 ml of previous solution was added into the viel. The resultant mixture was sonicated for 1h while tempeature of the sonicator was maintained at around room temperature.

The sample was centrifuged at 11000g for 2 hours to get rid of unsoluble SWNT via precipitation. Following this, the sample was centrifuged using Millipore 30kDa filter at 13000 g for 15 min to get rid of unadsorbed compound **1**. The filtrate was discarded and one more centrifugation was done. All green colored samples remained on the filter which was then collected into a tube by centrifugation of the filter upside down at 1000 g for 3 min.

Non-covalent attachment of compound **1** on SWNT was characterized through quenching of pyrene emission, AFM and TEM images.

2.2.4 Singlet Oxygen Generation Experiment

Singlet oxygen generating capability of compound 1 and SWNT-adsorbed compound 1 was done using singlet oxygen trap molecule 1,3-diphenylisobenzofuran (DPBF). Singlet oxygen can be monitored using photobleaching and subsequent decrease in absorbance of DPBF as shown in Figure 21.

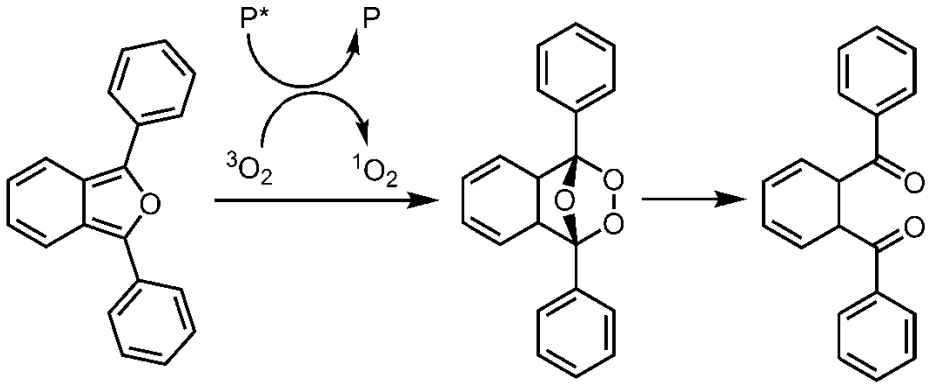

Figure 30. Photobleaching of DPBF

660 nm emitting 3000 mCd lead source was used as light source. A solution containing DPBF (50 μM) and SWNT-adsorbed compound 1 (62 nM) was prepared in isopropanol. Concentration of the SWNT-adsorbed compound 1 was determined by comparing its UV-absorbance to the absorbance of compound 1 solution with known concentration. Another solution was prepared with same concentration of DPBF but with 62 nM compound 1 only. Both solutions were aerated for 5 minutes. Then, absorbance spectrum of each solution was taken in 5 minutes intervals while the solutions were kept in dark. Then 660 nm light was exposed from 3-4 cm cell distance for 40 minutes and absorbance was taken in 5 minutes intervals for each solution. Same experiment was performed with a control solution of DPBF (50 μM) alone.

2.3 Experimental Part-II

2.3.1 Design of the Light Harvesting Dendrimers

Light harvesting dendrimer was designed in such a way that there is an efficient, unidirectional energy transfer from the terminal chromophore to the core of the dendrimer. This was achieved by convergent synthesis of dendrimer as seen in Figures 31-33. This design provides Förster type energy transfer (through space), thus, architectural structure of the dendrimer was determined taking spectral overlap of three different chromophores into account. Final acceptor chromophore was placed at the center of the dendrimer and other chromophores, mono styryl-BODIPY and BODIPY were placed accordingly.

Chromophores were covalently attached to one another using facile click reactions. In order to compare energy transfer from BODIPY (orange) directly to monostyryl-BODIPY compound **21** was designed (Figure 31). To assess FRET from mono-styryl BODIPY (red) to di-styryl BODIPY (green), two different dendrimers were designed with a core di-styryl-BODIPY carying two or four mono-styryl-BODIPY, compounds **23** and **24** respectively (Figures 32-33). Finally, cascade type light harvesting dendrimer composed of three different types of chromophores were designed as shown in Figure 33.

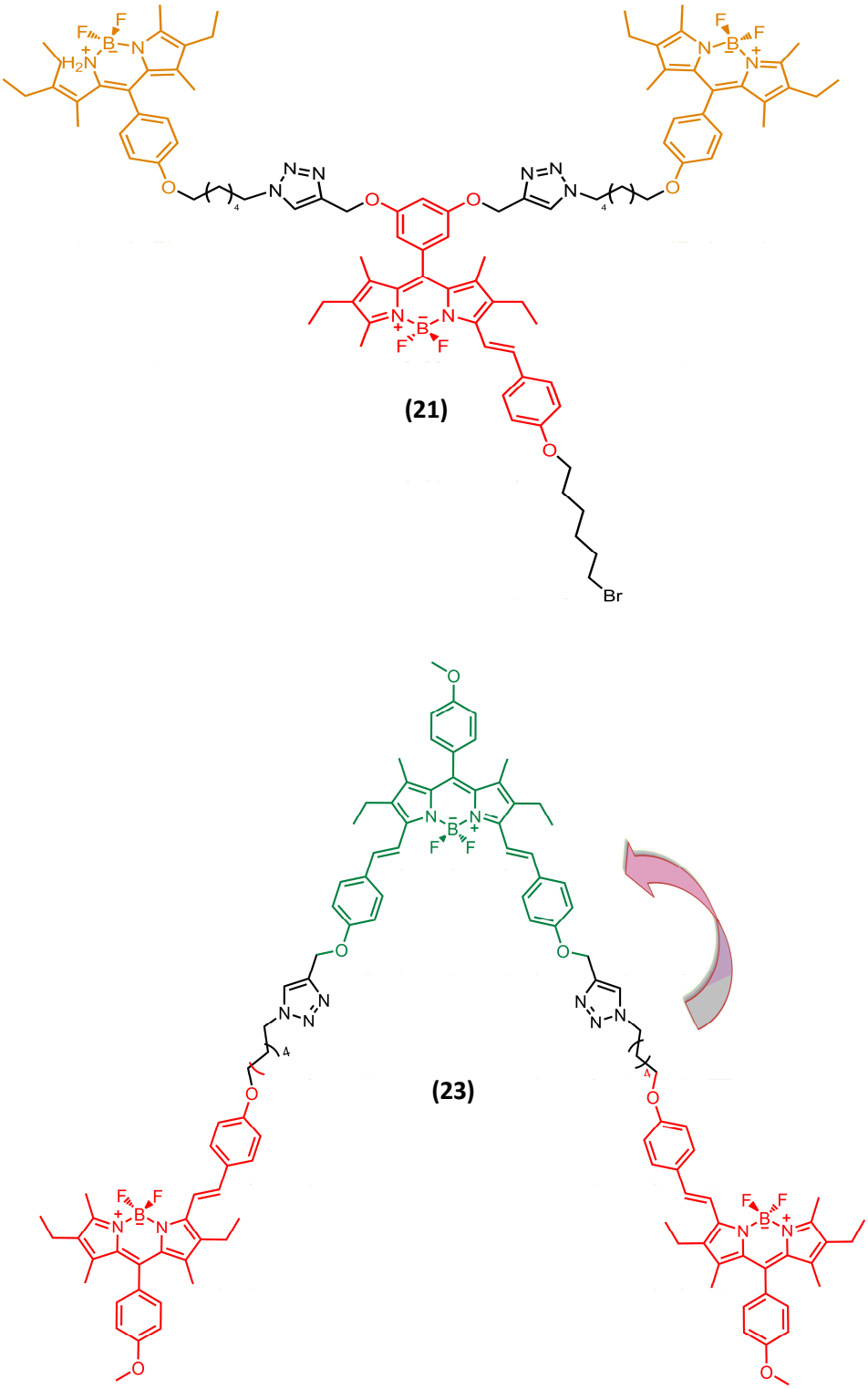

Figure 31. Structure of the light harvesting dendrimers (compound **21** and **23**)

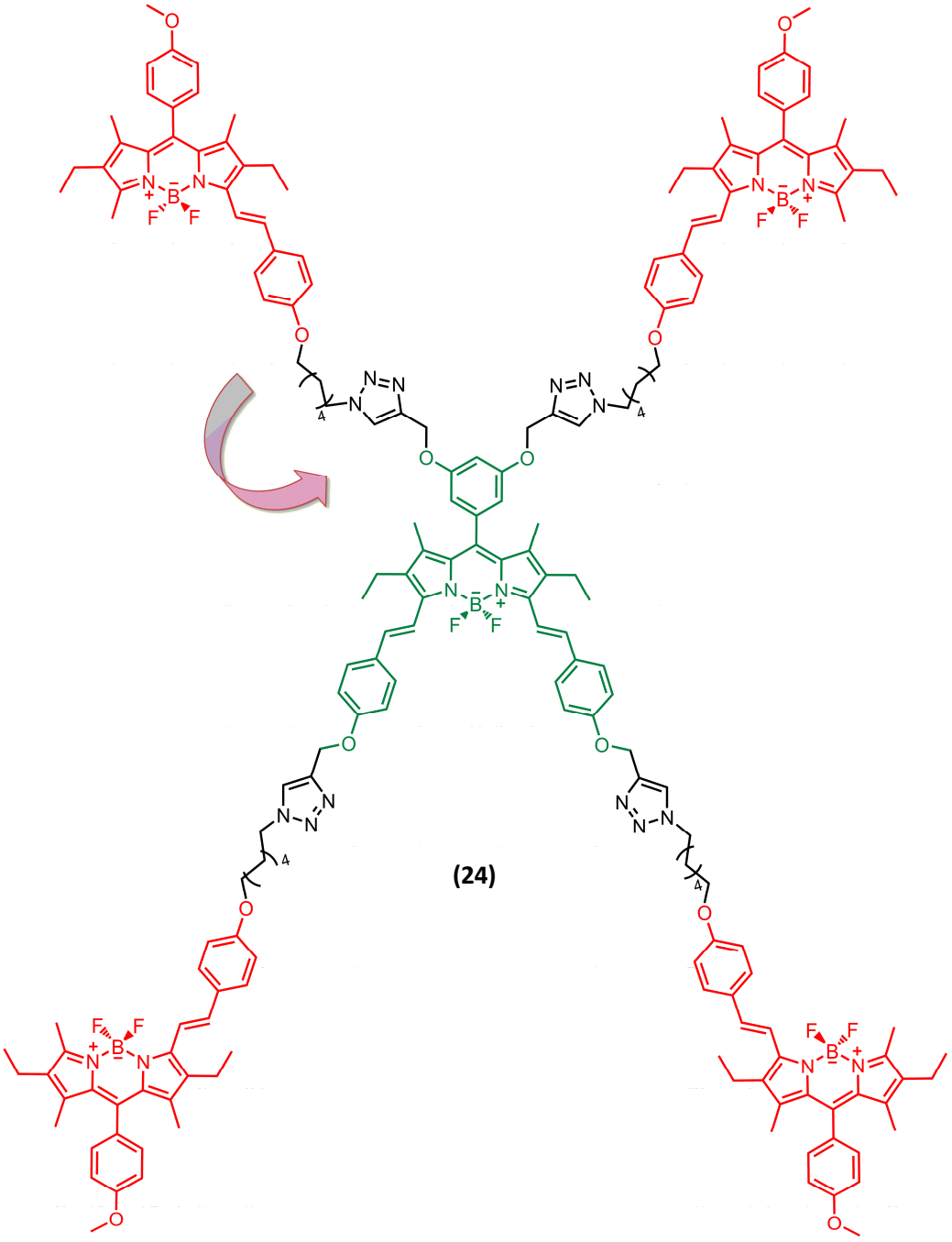

Figure 32. Structure of light harvesting dendrimer (compound **24**)

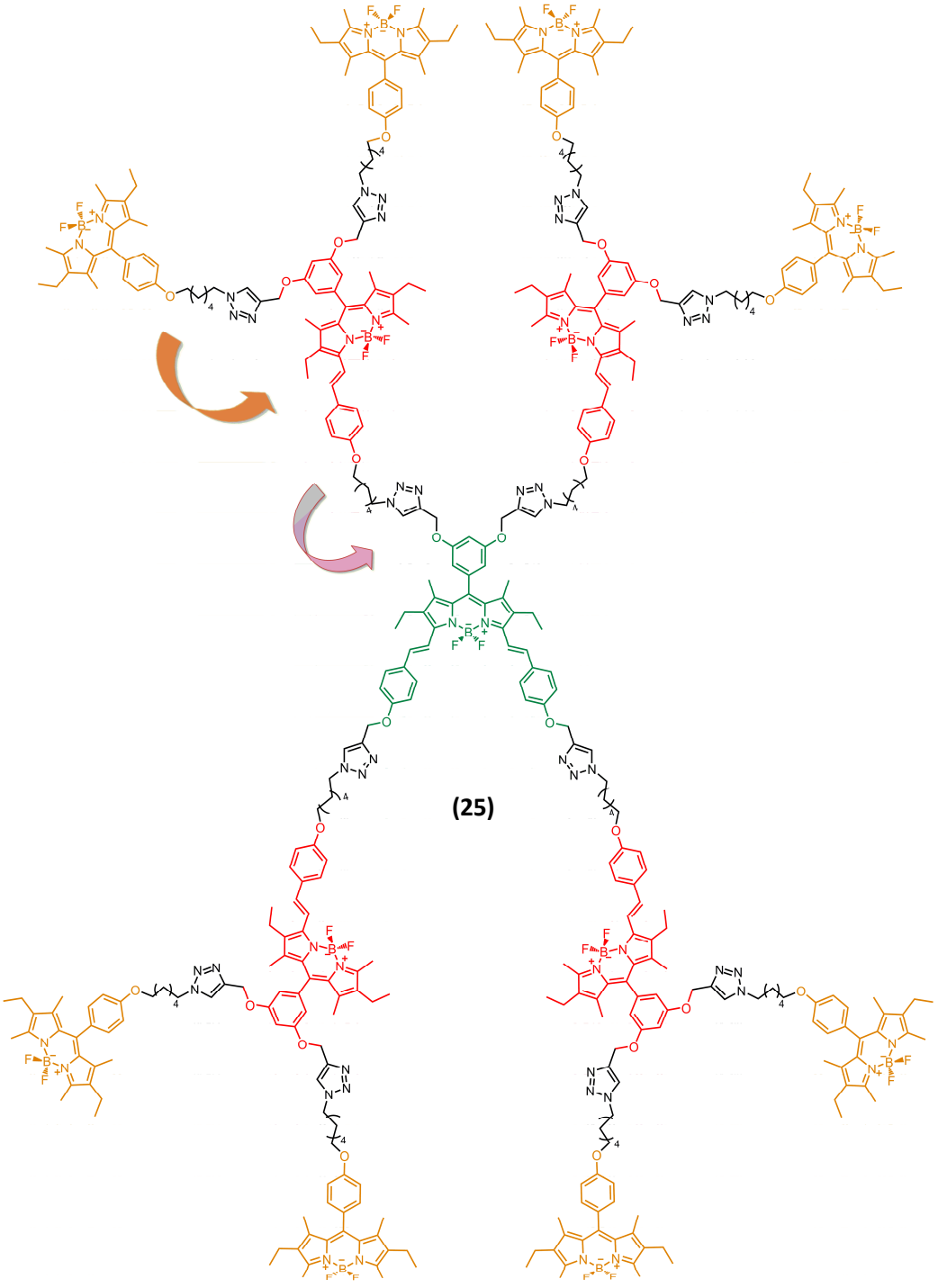

Figure 33. Structure of light harvesting dendrimer (compound **25**).

2.3.2 Synthesis of Light Harvesting Dendrimers

2.3.2.1 Synthesis of 4-(6-bromohexoxy)benzaldehyde (9)

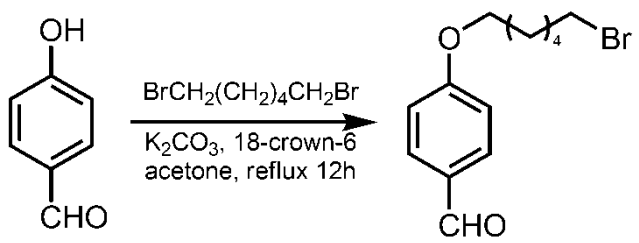

(2) (9)

Figure 34. Synthesis of compound **9**.

1,4-hydroxybenzaldehyde (5 g, 41 mmol) and 1,8 dibromohexane (2 g, 82 mmol) were dissolved in acetone (150 ml). K_2CO_3 (17.2 g, 123 mmol) and a few crystals of 18-crown-6 were added. The reaction mixture was refluxed for 12h. Then, acetone was evaporated in vacuo and extracted with water and chloroform. Organic layer as dried with Na_2SO_4 and evaporated in vacuo**.** The product was purified by silica gel column chromatography using $CHCl_3$/Hexane (75:25, v/v). Fraction containing compound **9** was collected then the solvent was removed under reduced pressure (6.7 mmol, 1.906 g, 16%).

^{1}H NMR ($CDCl_3$, 400 MHz, δ ppm) 1.35 (m, 4H), 1.65 (m, 4H), 3.4 (t, *J*= 6.68 Hz, 2H), 3.88 (t, *J*= 6.4 Hz, 2H), 6. 82 (d, *J*= 8.76 Hz, 2H), 7.68 (d, *J*= 8.64 Hz, 2H), 9.7 (s, 1H).

^{13}C NMR ($CDCl_3$, 100 MHz, δ ppm) 25.24, 26.51, 28.83, 32.39, 44.91, 68.09, 114.68, 129.73, 131.86, 164.08, 190.58.

2.3.2.2 Synthesis of 10-(4-(6-bromohexoxy)phenyl)-2,8-diethyl-5,5-difluoro-1,3,7,9-tetramethyl-5H-dipyrrolo[1,2-c:1',2'-f][1,3,2]diazaborinin-4-ium-5-uide (10)

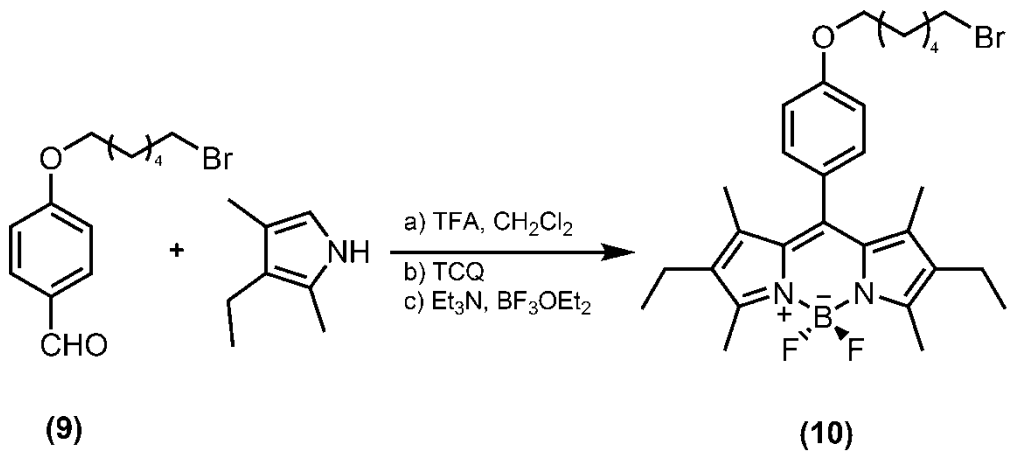

Figure 35. Synthesis of compound **10**.

CH_2Cl_2 (300 ml) was purged with Ar for 30 min. 4-(6-bromohexoxy)benzaldehyde **9** (1.089 g, 3.82 mmol) and 2,4-dimethyl pyrrole (0.94 g, 7.7 mmol) were added. The color of the solution turned into red after the addition of 3 drops of trifluoroacetic acid. The reaction mixture was stirred at room temperature for 12h. Then, tetrachloro-1,4-benzoquinone (0.93 g, 3.82 mmol) was added and the reaction mixture was stirred at room temperature for 45 min. Then triethyl amine (8 ml) and boron trifluoride diethyl etherate (8 ml) were added sequencially. After stirring at room temperature for 30 min, it was extracted with water. Organic layer was dried with Na_2SO_4 and evaporated under reduced pressure. The product was purified by silica gel column chromatography using $CHCl_3$ as mobile phase. Fraction containing compound **10** was collected then the solvent was removed under reduced pressure (670 mg, 1.2 mmol, 31%).

^{1}H NMR ($CDCl_3$, 400 MHz, δ ppm) 1.0 (t, J= 7.52, 6H), 1.35 (s, 6H), 1.58 (m, 4H), 1.85 (m, 4H), 2.3 (q, J= 7.56, 4H), 2.55 (s, 6H), 3.59 (t, *J*= 6.64 Hz, 2H), 4.05 (t, *J*= 6.45 Hz, 2H), 7.0 (d, *J*= 8.56 Hz, 2H), 7.15 (d, *J*= 8.56 Hz, 2H).

^{13}C NMR ($CDCl_3$, 100 MHz, δ ppm) 11.84, 12.46, 14.61, 17.06, 25.43, 26.67, 29.11, 32.48, 44.96, 67.87, 114.95, 127.78, 129.44, 130.10, 132.60, 138.43, 140.0, 153.46, 159.47.

MALDI: calculated for M= 558.2229, found 558.

2.3.2.3 Synthesis of 10-(4-(6-azidohexoxy)phenyl)-2,8-diethyl-5,5-difluoro-1,3,7,9-tetramethyl-5H-dipyrrolo[1,2-c:1',2'-f][1,3,2]diazaborinin-4-ium-5-uide (11)

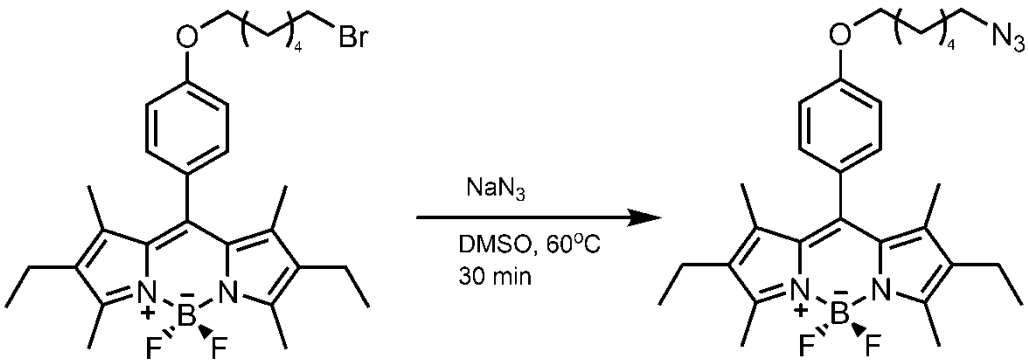

(10) **(11)**

Figure 36. Synthesis of compound **11**.

10-(4-(6-bromohexoxy)phenyl)-2,8-diethyl-5,5-difluoro-1,3,7,9-tetra methyl-5H-dipyrrolo[1,2-c:1',2'-f][1,3,2]diazaborinin-4-ium-5-uide **10** (190 mg, 0.34 mmol) was dissolved in 20 ml DMSO. Excess amount of sodium azide

(600 mg, 9.23 mmol) was added. The reaction mixture was stirred for 30 minutes at 60°C. After 30 minutes, sample was extracted with water and $CHCl_3$ a few times to get rid of DMSO and excess NaN_3. Organic layer containing compound **11** was dried with Na_2SO_4 and evaporated under reduced pressure No further purification was required.

^{1}H NMR ($CDCl_3$, 400 MHz, δ ppm) 1.0 (t, J= 7.52 Hz, 6H), 1.35 (s, 6H), 1.54 (m, 4H), 1.68 (m, 2H), 1.85 (m, 2H), 2.3 (q, J= 7.56 Hz, 4H), 2.55 (s, 6H), 3.32 (t, *J*= 6.64 Hz, 2H), 4.05 (t, *J*= 6.45 Hz, 2H), 7.0 (d, *J*= 8.56 Hz, 2H), 7.15 (d, *J*= 8.56 Hz, 2H).

^{13}C NMR ($CDCl_3$, 100 MHz, δ ppm) 11.84, 12.46, 14.62, 17.07, 25.71, 26.56, 28.80, 29.13, 51.38, 67.86, 114.95, 127.77, 129.44, 131.19, 132.61, 138.43, 140.33, 153.46, 159.46.

HRMS-ESI: calculated for M+H 522.3216, found 522.3240, Δ= 0.8 ppm.

2.3.2.4 Synthesis of (3,5-bis(prop-2-ynyloxy)phenyl)methanol (12)

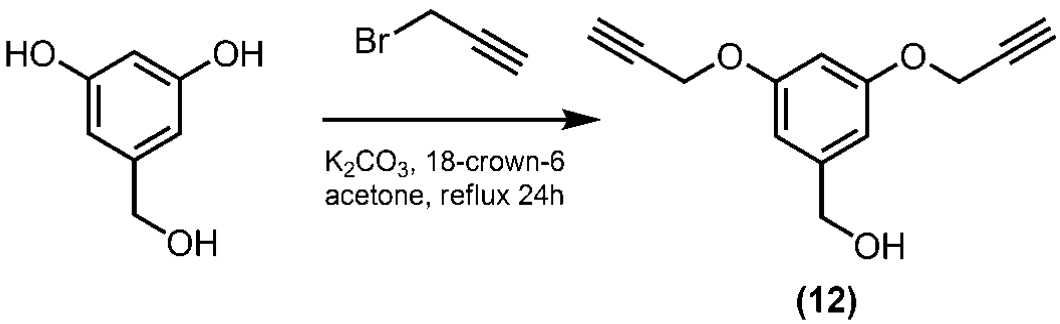

Figure 37. Synthesis of compound **12**.

5-(hydroxymethyl)benzene-1,3-diol (5 g, 35.7 mmol) was dissolved in 200 ml acetone in round bottom flask. K_2CO_3 (5 g, 35.7 mmol) and a few crystals of 18-crown-6 were added. Propargyl bromide (10.5 g, 71.4 mmol) was added to the flask and the reaction mixture was refluxed for 24h. Then, acetone

was evaporated in vacuo and extracted with water and chloroform. Organic layer as dried with Na_2SO_4 and evaporated in vacuo**.** The product was purified by silica gel column chromatography using $CHCl_3$/Methanol (97:3, v/v). Fraction containing compound **12** was collected then the solvent was removed under reduced pressure (30.5 mmol, 6.6 g, 86%).

^{1}H NMR ($CDCl_3$, 400 MHz, δ ppm) 2.45 (s, 2H), 4.60 (s, 6H), 6.49 (s, 1H), 6.51 (s, 2H) as reported elsewhere.[154]

2.3.2.5 Synthesis of 3,5-bis(prop-2-ynyloxy)benzaldehyde (13)

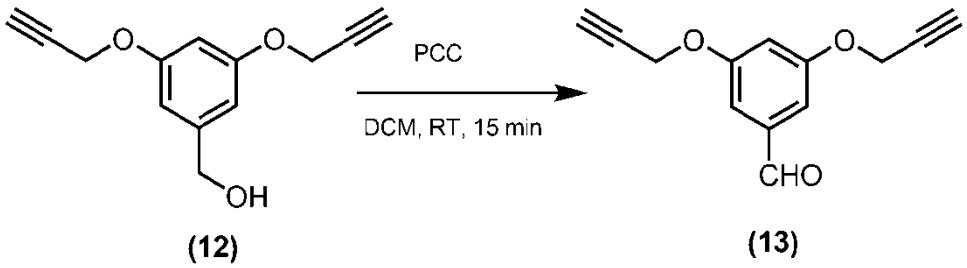

(12) (13)

Figure 38. Synthesis of compound **13.**

(3,5-bis(prop-2-ynyloxy)phenyl)methanol **12** (1 g, 4.625 mmol) was dissolved in 50 ml dichloromethane. Pyridinium chlorochromat (2 g, 9.25 mmol) was added and the reaction mixture was stirred at room temperature. After 15 minutes all of the compound **12** was converted to compound **13** as followed by TLC. Dichloromethane was evaporated in vacuo and the product was purified by silica gel column chromatography using $CHCl_3$ as mobile phase. Fraction containing compound **13** was collected then the solvent was removed under reduced pressure.

^{1}H NMR ($CDCl_3$, 400 MHz, δ ppm) 2.58 (t, J=2.36 Hz, 2H), 4.73 (d, J=2.40 Hz, 4H), 6.85 (t, J= 2.32 Hz, 1H), 7.1 (d, J=2.36 Hz, 2H), 9.9 (s, 1H).

^{13}C NMR ($CDCl_3$, 100 MHz, δ ppm) 56.15, 76.27, 77.78, 108.8, 138.39, 159.09, 191.42.

2.3.2.6 Synthesis of 10-(3,5-bis(prop-2-ynyloxy)phenyl)-2,8-diethyl-5,5-difluoro-1,3,7,9-tetramethyl-5H-dipyrrolo[1,2-c:1',2'-f][1,3,2]diazaborinin-4-ium-5-uide (14)

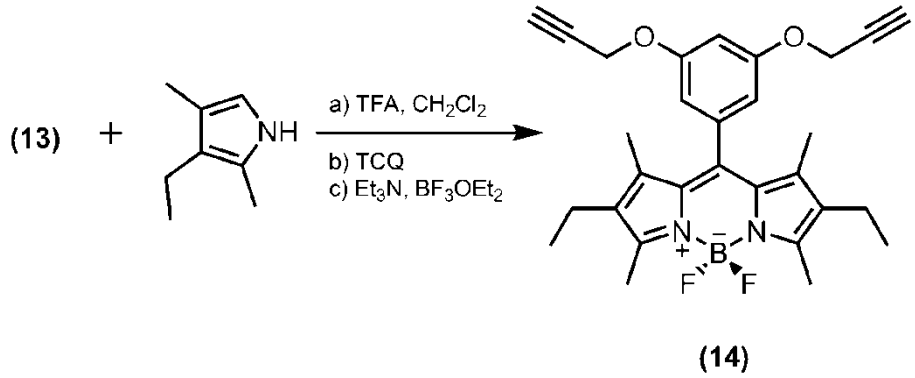

Figure 39. Synthesis of compound **14**.

CH_2Cl_2 (300 ml) was purged with Ar for 30 min. 3,5-bis(prop-2-ynyloxy)benzaldehyde **13** (1.0 g, 4.6 mmol) and 2,4-dimethyl pyrrole (1.141 g, 9.2 mmol) were added. The color of the solution turned into red after the addition of 3 drops of trifluoroacetic acid. The reaction mixture was stirred at room temperature for 12h. Then, tetrachloro-1,4-benzoquinone (1.12 g, 4.6 mmol) was added and the reaction mixture was stirred at room temperature for 45 min. Then triethyl amine (8 ml) and boron trifluoride diethyl etherate (8 ml) were added sequencially. After stirring at room temperature for 30 min, it was extracted with water. Organic layer was dried with Na_2SO_4 and evaporated under reduced pressure. The product was purified by silica gel column chromatography using $CHCl_3$:Hexane (66:33, v/v) as mobile phase. Fraction

containing compound **14** was collected then the solvent was removed under reduced pressure (470 mg, 0.96 mmol, 21%).

^{1}H NMR ($CDCl_3$, 400 MHz, δ ppm) 1.0 (t, J= 7.48 Hz, 6H), 1.44 (s, 6H), 2.3 (q, J=7.56 Hz, 4H), 2.5-2.55 (m, 6H+2H), 4.69 (d, J=2.08 Hz, 4H), 6.6 (d, J=2.28 Hz, 2H), 6.7 (t, J=2.28 Hz, 1H).

^{13}C NMR ($CDCl_3$, 100 MHz, δ ppm) 11.54, 12.50, 14.63, 17.07, 56.04, 75.94, 78.10, 103.50, 107.93, 130.39, 132.80, 137.56, 138.40, 139.18, 153.89, 159.35.

HRMS-ESI: calculated for M+Na 489.2525, found 489.2509, Δ= -3.2 ppm.

2.3.2.7 Synthesis of (E)-10-(3,5-bis(prop-2-ynyloxy)phenyl)-7-(4-(6-bromo hexyloxy)styryl)-2,8-diethyl-5,5-difluoro-1,3,9-trimethyl-5H-dipyrrolo[1,2-c:1',2'-f][1,3,2]diazaborinin-4-ium-5-uide (15)

Compound **9** (72 mg, 0.25 mmol) dissolved in benzene (45 ml). Piperidine (0.2 ml) and glacial acetic acid (0.2 ml) were added. The solution was refluxed using Dean-Stark apparatus. When the solution was concentrated, reaction was followed by TLC until purple-colored product became the major product. Then, benzene was evaporated in vacuo. It was extracted with $CHCl_3$ and water. Organic layer was dried with Na_2SO_4 and evaporated under reduced pressure. The product was purified by silica gel column chromatography using Ethyl Acetate:Hexane (25:75, v/v) as mobile phase. Fraction containing compound **15** was collected then the solvent was removed under reduced pressure (78 mg, 0.1 mmol, 29%).

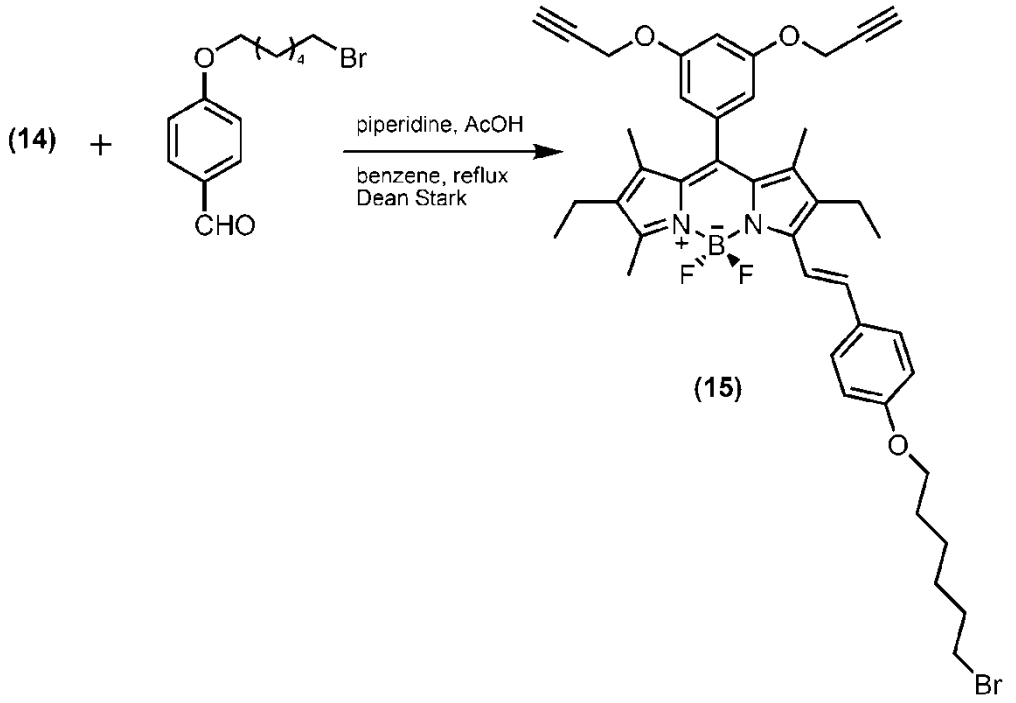

Figure 40. Synthesis of compound **15**.

^{1}H NMR ($CDCl_3$, 400 MHz, δ ppm) 1.0 (t, J= 6.48 Hz, 3H), 1.18 (t, J= 7.56 Hz), 1.45-1.55 (m, 3H + 3H + 4H), 1.82 (m, 4H), 2.33 (q, J=7.52 Hz, 2H), 2.5-2.65 (m, 3H + 2H + 2H), 3.6 (t, J= 6.68 Hz, 2H), 4.05 (t, J= 6.44 Hz, 2H), 4.69 (s, 4H), 6.6 (d, J=2.32 Hz, 2H), 6.7 (t, J=2.32 Hz, 1H), 6.9 (d, J= 8.6 Hz, 2H), 7.19 (d, J= 16.69 Hz, 1H), 7.5 (d, J= 8.72 Hz, 2H), 7.62 (d, J= 16.72 Hz, 1H).

^{13}C NMR ($CDCl_3$, 100 MHz, δ ppm) 11.27, 11,61, 12.75, 14.10, 14.56, 17.12, 18.33, 25.41, 26.66, 29.08, 30.32, 32.52, 44.99, 56.07, 67.84, 75.91, 78.09, 103.57, 108.14, 114.74, 117.89, 128.61, 130.19, 135.00, 137.73, 159.35, 159.58.

HRMS-ESI: calculated for M+Na 755.2831, found 755.2811, Δ= 2.6 ppm.

2.3.2.8 Synthesis of 4-(6-azidohexoxy)benzaldehyde (16)

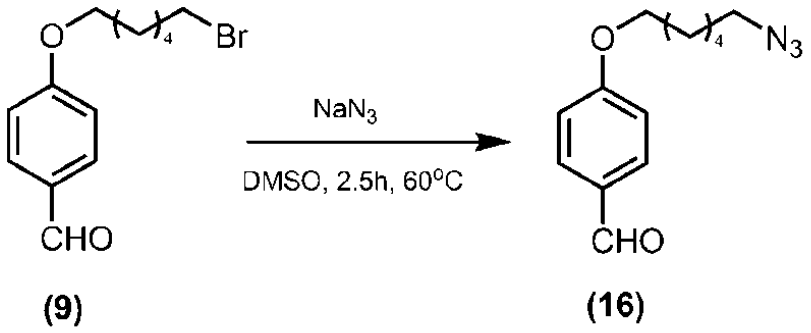

Figure 41. Synthesis of compound **16.**

4-(6-bromohexoxy)benzaldehyde **9** (1.5 g, 5.3 mmol) was dissolved in 25 ml DMSO. Sodium azide (1.37 g, 21.2 mmol) was added and the reaction mixture was stirred at 60°C for 2.5 hours. Then, it was extracted with water and $CHCl_3$ a few times and organic layer was collected, dried with Na_2SO_4 and evaporated under reduced pressure. No further purification was required.

^{1}H NMR ($CDCl_3$, 400 MHz, δ ppm) 1.4-1.55 (m, 4H), 1.55-1.65 (m, 2H), 1.75-1.85 (m, 2H), 3.28 (t, J=6.80 Hz, 2H), 4.05 (t, J=6.40 Hz, 2H), 7.00 (d, J=8.76 Hz, 2H), 7.82 (d, J= 7.86 Hz, 2H), 9.86 (s, 1H).

^{13}C NMR ($CDCl_3$, 100 MHz, δ ppm) 25.57, 26.43, 28.74, 28.89, 51.31, 68.12, 114.73, 129.80, 131.96, 164.14, 190.75.

2.3.2.9 Synthesis of 2,8-diethyl-5,5-difluoro-10-(4-methoxyphenyl)-1,3,7,9-tetramethyl-5H-dipyrrolo[1,2-c:1',2'-f][1,3,2]diazaborinin-4-ium-5-uide (17)

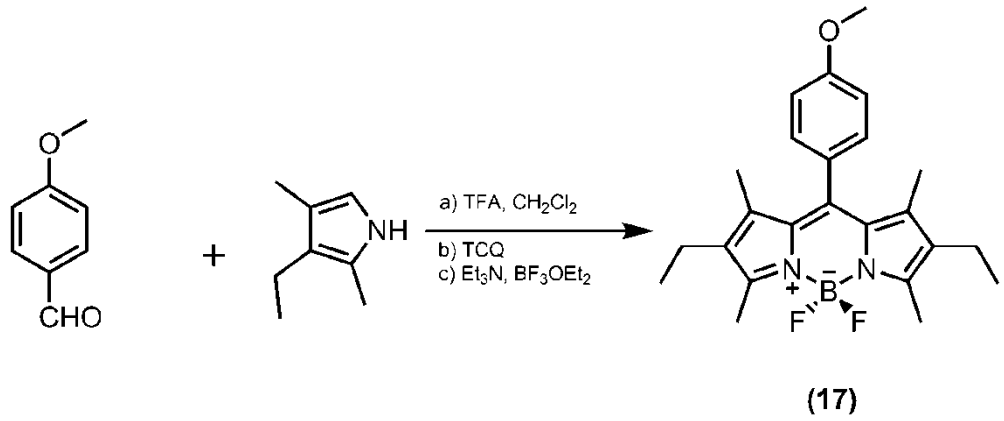

Figure 42. Synthesis of compound **17.**

CH_2Cl_2 (300 ml) was purged with Ar for 30 min. 4-methoxy benzaldehyde (394 mg, 2.89 mmol) and 2,4-dimethyl pyrrole (0.75 g, 5.78 mmol) were added. The color of the solution turned into red after the addition of 3 drops of trifluoroacetic acid. The reaction mixture was stirred at room temperature for 12h. Then, tetrachloro-1,4-benzoquinone (0.72 g, 2.89 mmol) was added and the reaction mixture was stirred at room temperature for 45 min. Then triethyl amine (6 ml) and boron trifluoride diethyl etherate (6 ml) were added sequencially. After stirring at room temperature for 30 min, it was extracted with water. Organic layer was dried with Na_2SO_4 and evaporated under reduced pressure. The product was purified by silica gel column chromatography using $CHCl_3$ as mobile phase. Fraction containing compound **17** was collected then the solvent was removed under reduced pressure (412 mg, 1 mmol, 35%).

^{1}H NMR ($CDCl_3$, 400 MHz, δ ppm) 1.0 (t, J= 7.52 Hz, 6H), 1.35 (s, 6H), 2.3 (q, J=7.56 Hz, 4H), 2.52 (s, 6H), 3.90 (s, 3H), 7.00 (d, J=8.76 Hz, 2H), 7.16 (d, J= 8.76 Hz, 2H),

^{13}C NMR ($CDCl_3$, 100 MHz, δ ppm) 11.81, 12.46, 14.61, 17.06, 55.30, 114.42, 127.87, 129.46, 131.19, 132.62, 138.43, 140.27, 153.48, 159.99.

HRMS-ESI: calculated for M+H 411.2419, found 411.2424, Δ= 0.2 ppm.

2.3.2.10 Synthesis of 2,8-diethyl-5,5-difluoro-10-(4-methoxyphenyl)-1,9-dimethyl-3,7-bis(4-(prop-2-ynyloxy)styryl)-5H-dipyrrolo[1,2-c:1',2'-f][1,3,2] diazaborinin-4-ium-5-uide (18)

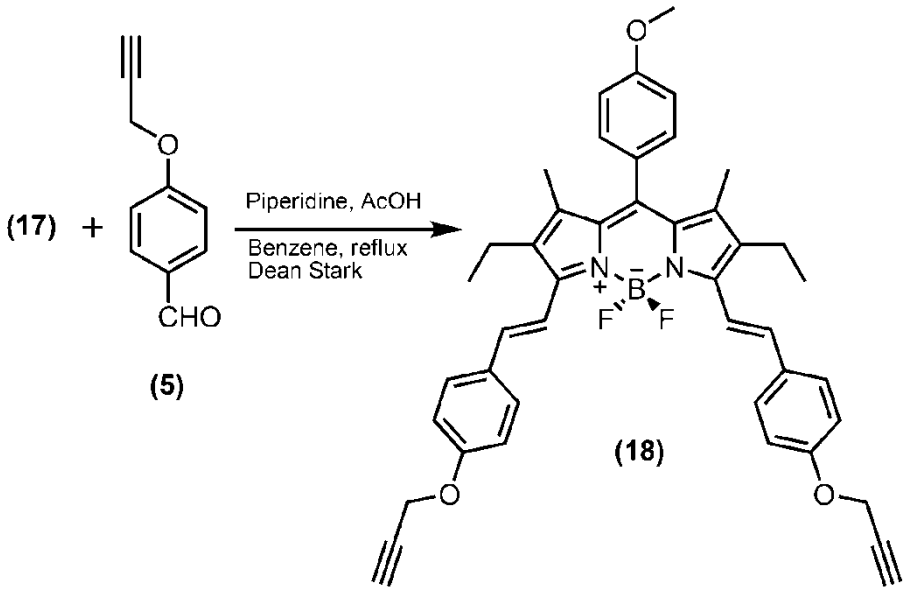

Figure 43. Synthesis of compound **18**.

Compound **17** (100 mg, 0.24 mmol) and 4-(prop-2-ynyloxy) benzaldehyde **5** (98 mg, 0.6 mmol) dissolved in benzene (45 ml). Piperidine (0.4 ml) and glacial acetic acid (0.4 ml) were added. The solution was refluxed using Dean-Stark apparatus. When the solution was concentrated, reaction was followed by TLC until green-colored product became the major product. Then, benzene was evaporated in vacuo. It was extracted with $CHCl_3$ and water. Organic layer was dried with Na_2SO_4 and evaporated under reduced pressure. The product was purified by silica gel column chromatography using Ethyl

Acetate:Hexane (25:75, v/v) as mobile phase. Fraction containing compound **18** was collected then the solvent was removed under reduced pressure (150 mg, 0.22 mmol, 90%).

^{1}H NMR ($CDCl_3$, 400 MHz, δ ppm) 1.15 (t, J= 7.48 Hz, 6H), 1.38 (s, 6H), 2.55-2.65 (m, 4H+2H), 3.90 (s, 3H), 4.75 (d, J=2.36 Hz, 4H), 7.00-7.06 (m, 4H + 2H), 7.17-7.24 (m, 2H+2H), 7.06 (d, J=8.76 Hz, 4H), 7.70 (d, J=16.56 Hz, 2H)

^{13}C NMR ($CDCl_3$, 100 MHz, δ ppm) 11.67, 14.04, 18.00, 55.58, 56.04, 75.50, 78.10, 115.20, 116.00, 118.50, 127.50, 128.69, 129.50, 130.00, 133.50, 158.00, 159.50.

HRMS-ESI: calculated for M+Na 717.3076, found 717.3060, Δ= -2.2 ppm.

2.3.2.11 Synthesis of 10-(3,5-bis(prop-2-ynyloxy)phenyl)-2,8-diethyl-5,5-difluoro-1,9-dimethyl-3,7-bis(4-(prop-2-ynyloxy)styryl)-5H-dipyrrolo[1,2-c:1',2'-f][1,3,2]diazaborinin-4-ium-5-uide (19)

Compound **14** (200 mg, 2.05 mmol) and 4-(prop-2-ynyloxy) benzaldehyde **5** (800.9 mg, 5 mmol) dissolved in benzene (45 ml). Piperidine (0.5 ml) and glacial acetic acid (0.5 ml) were added. The solution was refluxed using Dean-Stark apparatus. When the solution was concentrated, reaction was followed by TLC until green-colored product became the major product. Then, benzene was evaporated in vacuo. It was extracted with $CHCl_3$ and water. Organic layer was dried with Na_2SO_4 and evaporated under reduced pressure. The product was purified by silica gel column chromatography using Ethyl Acetate:Hexane (20:80, v/v) as mobile phase. Fraction containing compound **19** was collected then the solvent was removed under reduced pressure.

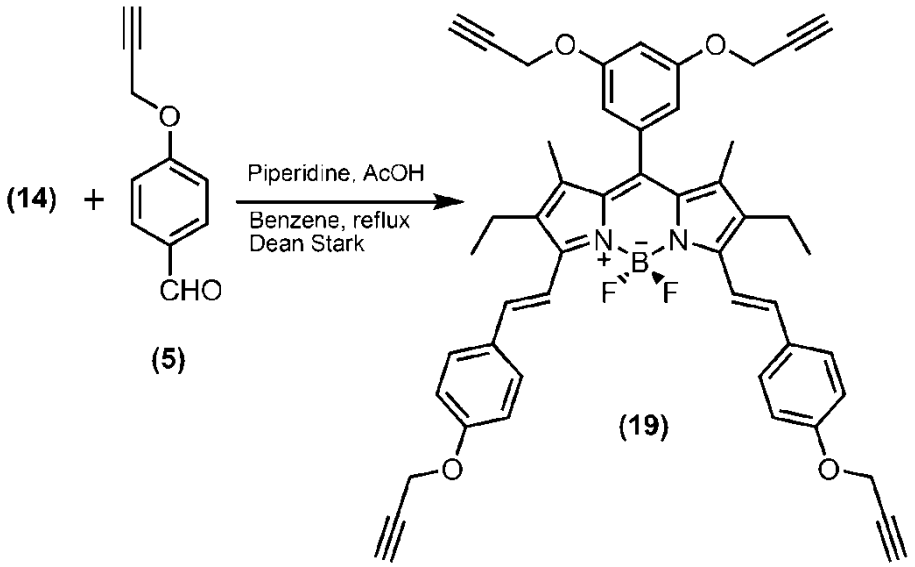

Figure 44. Synthesis of compound **19.**

^{1}H NMR ($CDCl_3$, 400 MHz, δ ppm) 1.15 (t, J= 7.44 Hz, 6H), 1.5 (s, 6H), 2.52 (t, J=2.36 Hz, 2H), 2.55 (t, J=2.36 Hz, 2H), 2.63 (q, J=7.56 Hz, 4H), 4.70 (d, J=2.4 Hz, 4H), 4.75 (d, J= 2.36 Hz, 4H), 6.63 (d, J=2.32 Hz, 2H), 6.72 (t, J=2.28 Hz, 1H), 7.05 (d, J=8.80 Hz, 4H), 7.21 (d, J=16.77 Hz, 2H), 7.60 (d, J=8.80 Hz, 4H), 7.68 (d, J= 16.73 Hz, 2H).

^{13}C NMR ($CDCl_3$, 100 MHz, δ ppm) 11.37, 14.04, 18.39, 55.89, 56.08, 75.73, 75.94, 78.10, 103.61, 108.32, 115.22, 118.58, 128.73, 130.00, 131.17, 135.26, 137.86, 158.04, 159.37.

HRMS-ESI: calculated for M+Na 795.3182, found 795.3199, Δ= 2.2 ppm.

2.3.2.12 Synthesis of (E)-7-(4-(6-azidohexyloxy)styryl)-2,8-diethyl-5,5-difluoro-10-(4-methoxyphenyl)-1,3,9-trimethyl-5H-dipyrrolo[1,2-c:1',2'-f][1,3,2]diazaborinin-4-ium-5-uide (20)

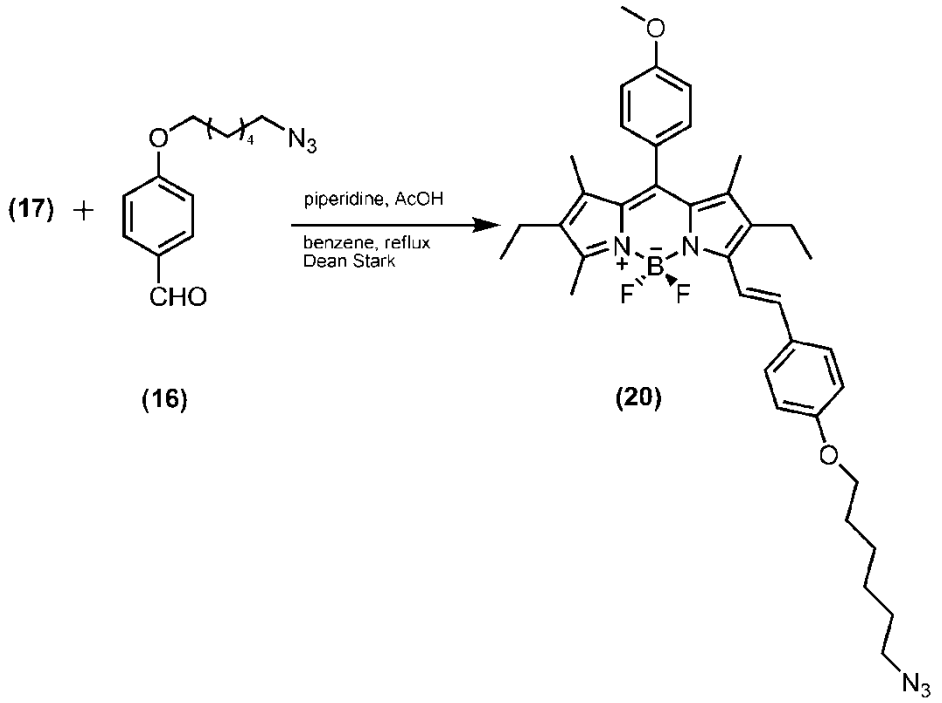

Figure 45. Synthesis of compound **20.**

Compound **17** (410 mg, 1 mmol) and 4-(6-azidohexoxy) benzaldehyde **16** (120 mg, 0.49 mmol) dissolved in benzene (45 ml). Piperidine (0.5 ml) and glacial acetic acid (0.5 ml) were added. The solution was refluxed using Dean-Stark apparatus. When the solution was concentrated, reaction was followed by TLC until purple-colored product became the major product. Then, benzene was evaporated in vacuo. It was extracted with $CHCl_3$ and water. Organic layer was taken, dried with Na_2SO_4 and evaporated under reduced pressure. The product was purified by silica gel column chromatography using Ethyl Acetate:Hexane (20:80, v/v) as mobile phase. Fraction containing **20** was collected then the solvent was removed under reduced pressure (100 mg, 0.16 mmol, 16 %)

^{1}H NMR ($CDCl_3$, 400 MHz, δ ppm) 1.0 (t, J= 7.48 Hz, 3H), 1.15 (t, J= 7.56 Hz, 3H), 1.36 (s, 3H), 1.38 (s, 3H), 1.50 (m, 4H), 1.68 (m, 2H), 1.84 (m, 2H), 2.34 (q, J= 7.48 Hz, 2H), 2.58 (m, 2H+3H), 3.32 (t, J= 6.84 Hz, 2H), 3.90 (s, 3H), 4.02 (t, J=6.32 Hz, 2H), 6.91 (d, J=8.72 Hz, 2H), 7.03 (d, J=8.68 Hz, 2H), 7.15-7.22 (m, 2H+1H), 7.54 (d, J=8.76 Hz, 2H), 7.62 (d, J=16.69 Hz, 1H)

^{13}C NMR ($CDCl_3$, 100 MHz, δ ppm) 11.58, 11.91, 12.71, 14.11, 14.56, 17.11, 18.32, 25.68, 26.52, 28.81, 29.11, 51.40, 55.33, 67.81, 114.44, 114.72, 118.00, 128.03, 128.57, 129.65, 130.27, 134.73, 138.63, 149.90, 155.00, 159.49, 160.02.

HRMS-ESI: calculated for M+Na 640.3634, found 640.3604, Δ= -4.8 ppm.

2.3.2.13 Synthesis of Compound 21 (Click Reaction)

Synthesis was done according to literature.[155] Compound **11** (107 mg, 0.21 mmol) and compound **15** (78 mg, 0.1 mmol) were dissolved in 8 ml THF. A few drops of Et_3N was added and the reaction mixture was stirred for 5 minutes at room temperature. In a viel, $CuSO_4.5H_2O$ (30% mole equavalent of compound **15**, 7.5 mg, 0.03 mmol) was dissolved in 4 ml water separately. Sodium ascorbate (60% mole equavalent of compound **15**, 11.88 mg, 0.06 mmol) was dissolved in 4 ml water in another viel. Solutions of sodium ascorbate and $CuSO_4$ were added to the first reaction mixture sequantially and the resultant mixture was stirred at room temperature untill all compound **15** was consumed, as followed by TLC. Then, it was extracted with $CHCl_3$ and water. Organic layer was dried with Na_2SO_4 and evaporated under reduced pressure. The product was purified by silica gel column chromatography using $CHCl_3$ as mobile phase. Fraction containing compound **21** was collected then the solvent was removed under reduced pressure (65 mg, 0.035mmol, 35 %).

^{1}H NMR ($CDCl_3$, 400 MHz, δ ppm) 1.0 (m, 15H), 1.16 (t, J= 7.40 Hz, 3H), 1.34 (s, 12H), 1.42-1.62 (m, 3H + 3H + 12H), 1.84 (m, 8H), 2.00 (m, J= 8H), 2.3 (m, 8H + 2H), 2.54 (s, 12H), 2.58-2.64 (m, 2H+3H), 3.58 (t, J=6.68 Hz, 2H), 4.01

(m, 6H), 4.42 (t, J=7.12 Hz, 4H), 5.20 (s, 4H), 6.61 (d, J=2.20, 2H), 6.78 (t, J=2.20 Hz, 1H), 6.90 (d, J= 8.76 Hz, 2H), 6.98 (d, J=8.60 Hz, 4H), 7.15 (d, J=8.52, 4H), 7.19 (d, J=16.286 Hz, 1H), 7.54 (d, J=8.72 Hz, 2H), 7.61 (d, J=16.85 Hz, 1H), 7.66 (s, 2H).

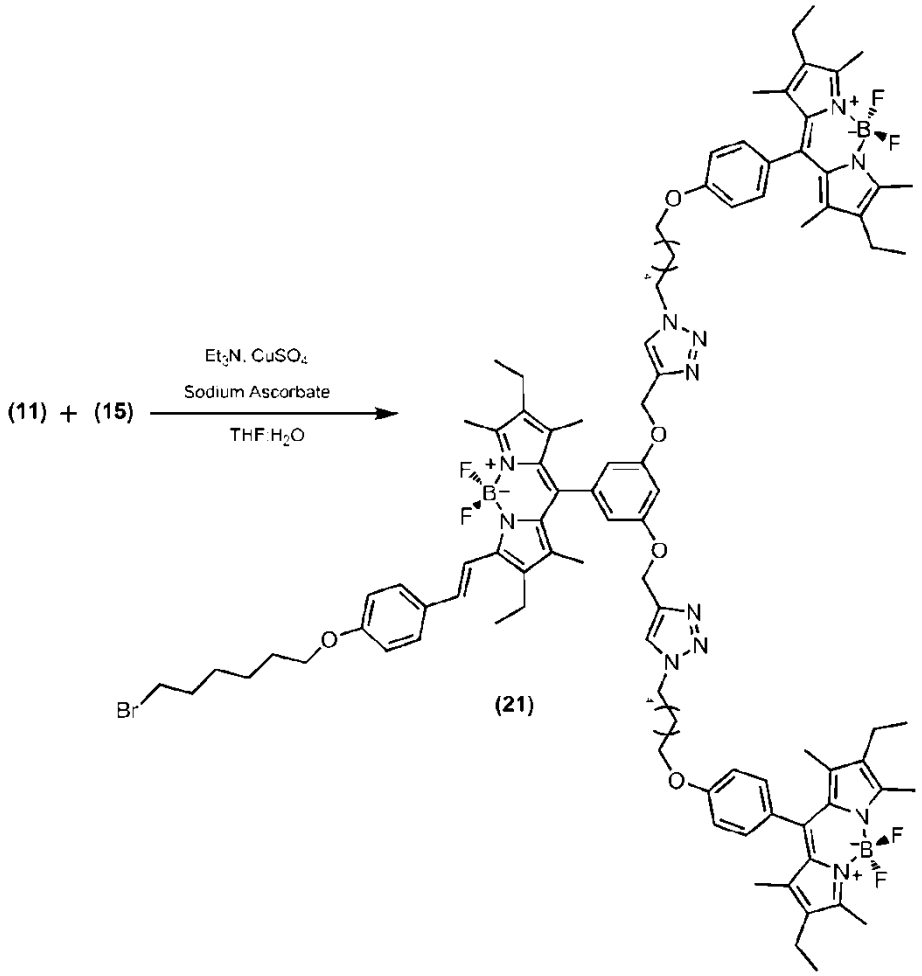

Figure 46. Synthesis of compound **21**

^{13}C NMR ($CDCl_3$, 100 MHz, δ ppm) 11.32, 11.66, 11.85, 12.46, 14.10, 14.57, 14.62, 17.06, 25.40, 25.61, 26.37, 26.66, 29.08, 30.25, 32.51, 44.99, 50.36, 62.27, 67.75, 67.84, 100.00, 102.00, 108.00, 114.75, 114.91, 122.64, 127.83, 128.61, 129.46, 130.13, 132.62, 135.05, 137.86, 138.40, 140.27, 143.44, 153.49, 159.41, 160.22.

MALDI: calculated for compound **21** 1782.8871, found 1755.

2.3.2.14 Synthesis of Compound 22

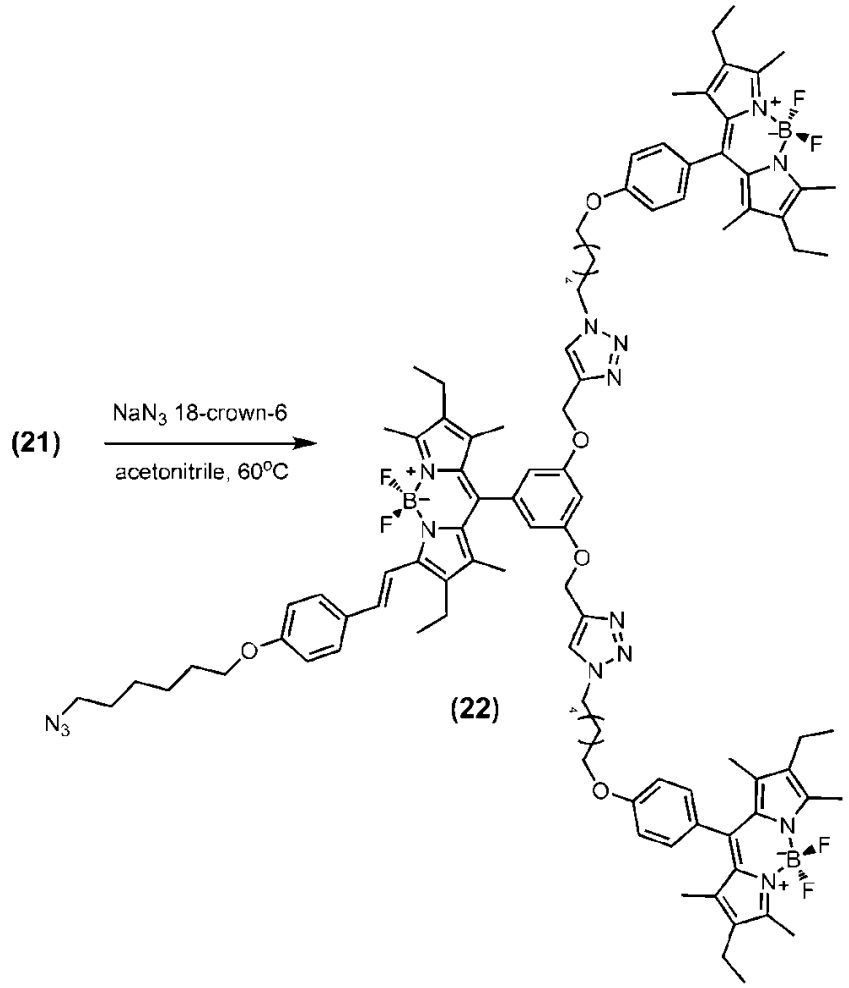

Figure 47. Synthesis of compound **22**.

Compound **21** (40 mg, 0.022 mmol) and sodium azide (7.23 mg, 0.11 mmol) was dissolved in 15 ml acetonitrile. A few crystals of 18-crown-6 was added and the reaction mixture was stirred 2 days at 60°C. Then, it was extracted with ethyl acetate and water. Organic layer was collected, dried with Na_2SO_4 and evaporated under reduced pressure. No further purification was required.

^{1}H NMR ($CDCl_3$, 400 MHz, δ ppm) 1.0 (m, 15H), 1.16 (t, J= 7.16 Hz, 3H), 1.34 (s, 12H), 1.42-1.62 (m, 3H + 3H + 12H), 1.84 (m, 8H), 2.00 (m, 8H), 2.3 (m, 8H + 2H), 2.50-2.65 (m, 12H+2H+3H), 3.30 (t, J=6.84 Hz, 2H), 4.05 (m, 6H), 4.42 (t, J=7.12 Hz, 4H), 5.20 (s, 4H), 6.61 (d, J=1.68, 2H), 6.78 (t, J=2.20 Hz, 1H), 6.90 (d, J= 8.56 Hz, 2H), 6.98 (d, J=8.28 Hz, 4H), 7.15-7.20 (m,4H+1H), 7.54 (d, J=8.60 Hz, 2H), 7.61 (d, J=16.53 Hz, 1H), 7.66 (s, 2H).

2.3.2.15 Synthesis of Compound 23 (Click Reaction)

Synthesis was done according to literature.[155] Compound **18** (22 mg, 0.03 mmol) and compound **20** (60 mg, 0.094 mmol) were dissolved in 3 ml THF. A few drops of Et_3N was added and the reaction mixture was stirred for 5 minutes at room temperature. In a viel, $CuSO_4.5H_2O$ (30% mole equavalent of compound **18**, 2.3 mg, 0.009 mmol) was dissolved in 1.5 ml water separately. Sodium ascorbate (60% mole equavalent of compound **18**, 3.6 mg, 0.018 mmol) was dissolved in 1.5 ml water in another viel. Solutions of sodium ascorbate and $CuSO_4$ were added to the first reaction mixture sequantially and the resultant mixture was stirred at room temperature untill all compound **18** was consumed, as followed by TLC. Then, it was extracted with $CHCl_3$ and water. Organic layer was dried with Na_2SO_4 and evaporated under reduced pressure. The product was purified by silica gel column chromatography using $CHCl_3$:Methanol (95:5, v/v) as mobile phase. Fraction containing compound **23** was collected then the solvent was removed under reduced pressure.

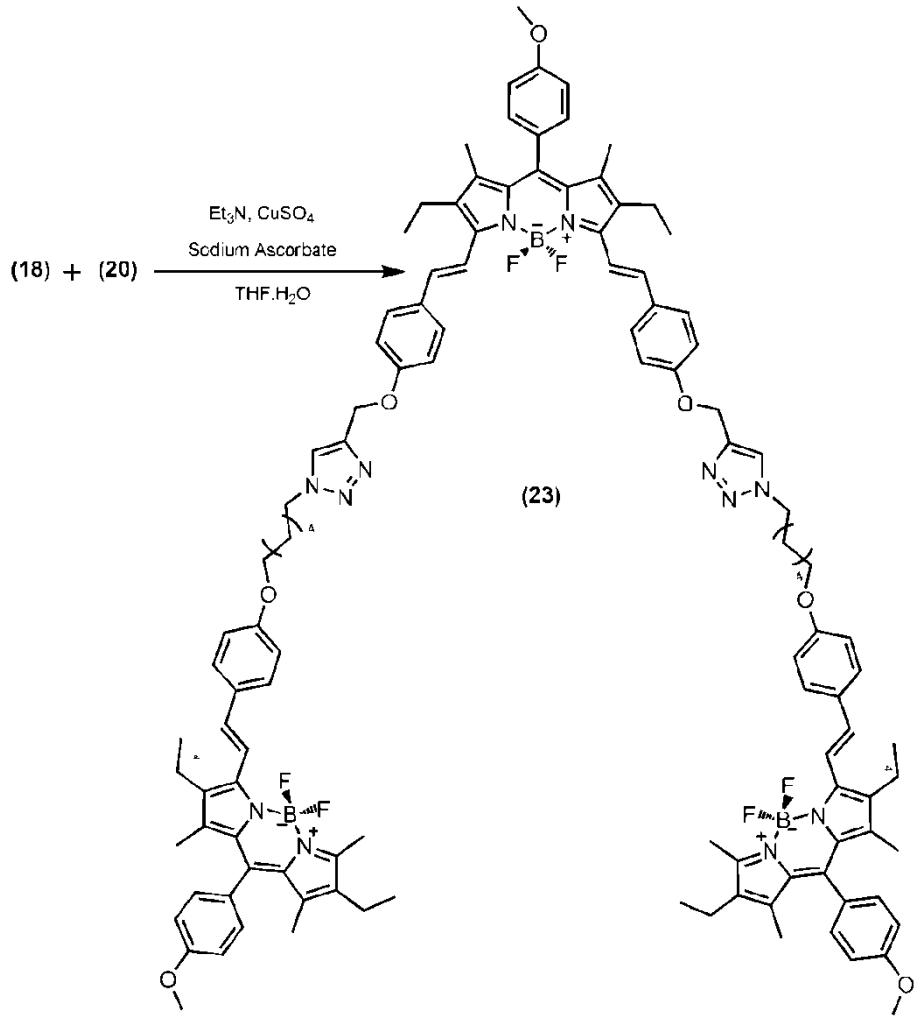

Figure 48. Synthesis of compound **23**.

^{1}H NMR ($CDCl_3$, 400 MHz, δ ppm) 1.0 (t, J= 7.52 Hz, 6H), 1.15 (M, 12H), 1.35 (m, 12H+6H+2H), 1.54 (m, 4H), 1.78 (m, 4H), 1.98 (m, 4H), 2.32 (m, 4H), 2.55-2.65 (m, 6H+8H), 3.9 (s, 9H), 3.98 (t, J= 6.20 Hz, 4H), 4.4 (m, 4H), 5.3 (s, 4H), 6.88 (d, J= 8.80 Hz, 4H), 7.03 (m, 4H+2H+4H), 7.12-7.24 (m, 4H+2H+4H), 7.52 (d, J= 8.72 Hz, 4H), 7.55-7.65 (m, 2H+4H+2H), 7.68 (d, J= 16.61 Hz, 2H)

^{13}C NMR ($CDCl_3$, 100 MHz, δ ppm) 11.91, 12.72, 14.06, 14.11, 14.57, 17.11, 18.32, 18.38, 25.50, 26.23, 28.97, 30.19, 50.33, 55.33, 62.19, 67.68, 114.44, 114.47, 114.72, 115.15, 122.58, 128.02, 128.55, 128.77, 129.65, 129.85, 130.24, 130.86, 134.73, 158.72, 159.47, 160.02, 160.06.

MALDI: calculated for compound **23** 1973.0291, found 1973.

2.3.2.16 Synthesis of Compound 24 (Click Reaction)

Synthesis was done according to literature.[155] Compound **19** (13.3 mg, 0.017 mmol) and compound **20** (55 mg, 0.086 mmol) were dissolved in 3 ml THF. A few drops of Et_3N was added and the reaction mixture was stirred for 5 minutes at room temperature. In a viel, $CuSO_4.5H_2O$ (21.5 mg, 0.086 mmol) was dissolved in 1.5 ml water separately. Sodium ascorbate (25.6 mg, 0.129 mmol) was dissolved in 1.5 ml water in another viel. Solutions of sodium ascorbate and $CuSO_4$ were added to the first reaction mixture sequantially and the resultant mixture was stirred at room temperature untill all compound **19** was consumed, as followed by TLC. Then, it was extracted with $CHCl_3$ and water. Organic layer was dried with Na_2SO_4 and evaporated under reduced pressure. The product was purified by silica gel column chromatography using $CHCl_3$ as mobile phase and then $CHCl_3$:Methanol (98:2, v/v) as mobile phase. Fraction containing compound **24** was collected then the solvent was removed under reduced pressure.

^{1}H NMR ($CDCl_3$, 400 MHz, δ ppm) 0.8-1.65 (m, 24H+24H+8+8+8+6+6), 1.75 (m, 8H), 1.95 (m, 8H), 2.32 (m, 8H), 2.6 (m, 20H+4H), 3.9 (s, 12H), 4.00 (m, 8H), 4.40 (m, 8H), 5.2 (m, 8H), 6.6 (d, J= 3.84 Hz, 2H), 6.9 (m, 8H+4H+1H), 7.00 (m, 8H+4H), 7.1-7.25 (m, 8H+ 4H + 2H), 7.45-7.70 (m, 4H+8H+2H+4H+4H).

MALDI: calculated for compound **24**, 3329.7508, found 3329.

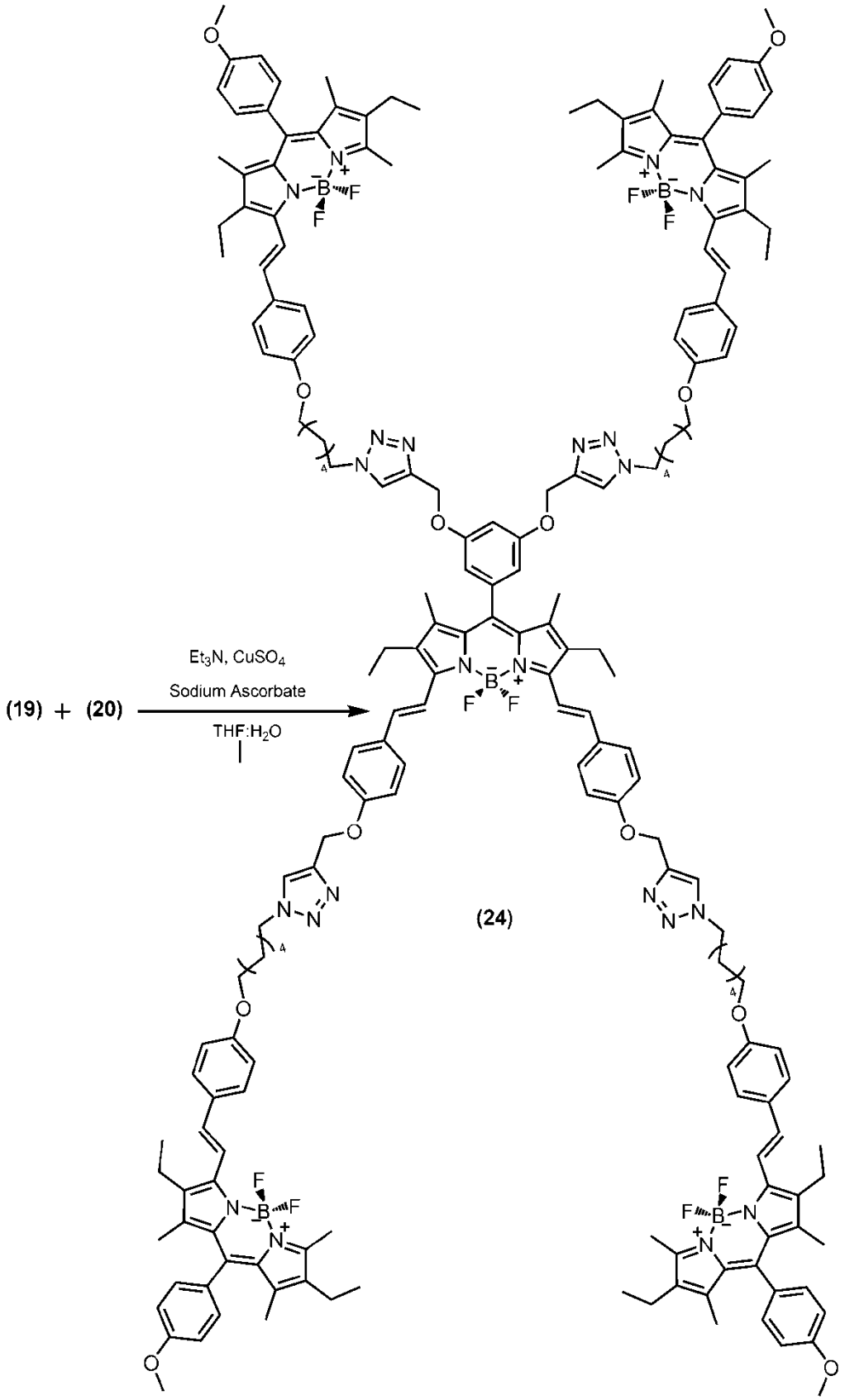

Figure 49. Synthesis of compound **24**

2.3.2.17 Synthesis of Compound 25 (Click Reaction)

Synthesis was done according to literature.[155] Compound **19** (4.39 mg, 0.0057 mmol) and compound **43** (50 mg, 0.028 mmol) were dissolved in 3 ml THF. A few drops of Et_3N was added and the reaction mixture was stirred for 5 minutes at room temperature. In a viel, $CuSO_4.5H_2O$ (19 mg, 0.076 mmol) was dissolved in 0.75 ml water separately. Sodium ascorbate (35.1 mg, 0.177 mmol) was dissolved in 0.75 ml water in another viel. Solutions of sodium ascorbate and $CuSO_4$ were added to the first reaction mixture sequantially and the resultant mixture was stirred at room temperature untill all compound **19** was consumed, as followed by TLC. Then, it was extracted with $CHCl_3$ and water. Organic layer was dried with Na_2SO_4 and evaporated under reduced pressure. The product was purified by silica gel column chromatography using $CHCl_3$:Methanol (95:5, v/v) as mobile phase. Fraction containing compound **25** was collected then the solvent was removed under reduced pressure.

^1H NMR ($CDCl_3$, 400 MHz, δ ppm) 1.0 (m, 60H), 1.18 (m, 12H+6H), 1.22-1.70 (m, 120H + 6H + 8H), 1.82 (m, 32H), 2.00 (m, 24H), 2.34 (m, 40H), 2.5-2.64 (m, 12H+8H+48H+4H), 4.00 (m, 16H+8H), 4.40 (m, 16H+8H), 5.2 (m, 16H+8H), 6.6 (8H+2H), 6.79 (4H+1H), 6.86 (8H), 7.00(16H+4H), 7.18 (16H+4H+2H), 7.48-7.62 (8H+4H+4H+2H), 7.65 (8H+4H).

MALDI: calculated for compound **25**, 7812.3031, found 7794.

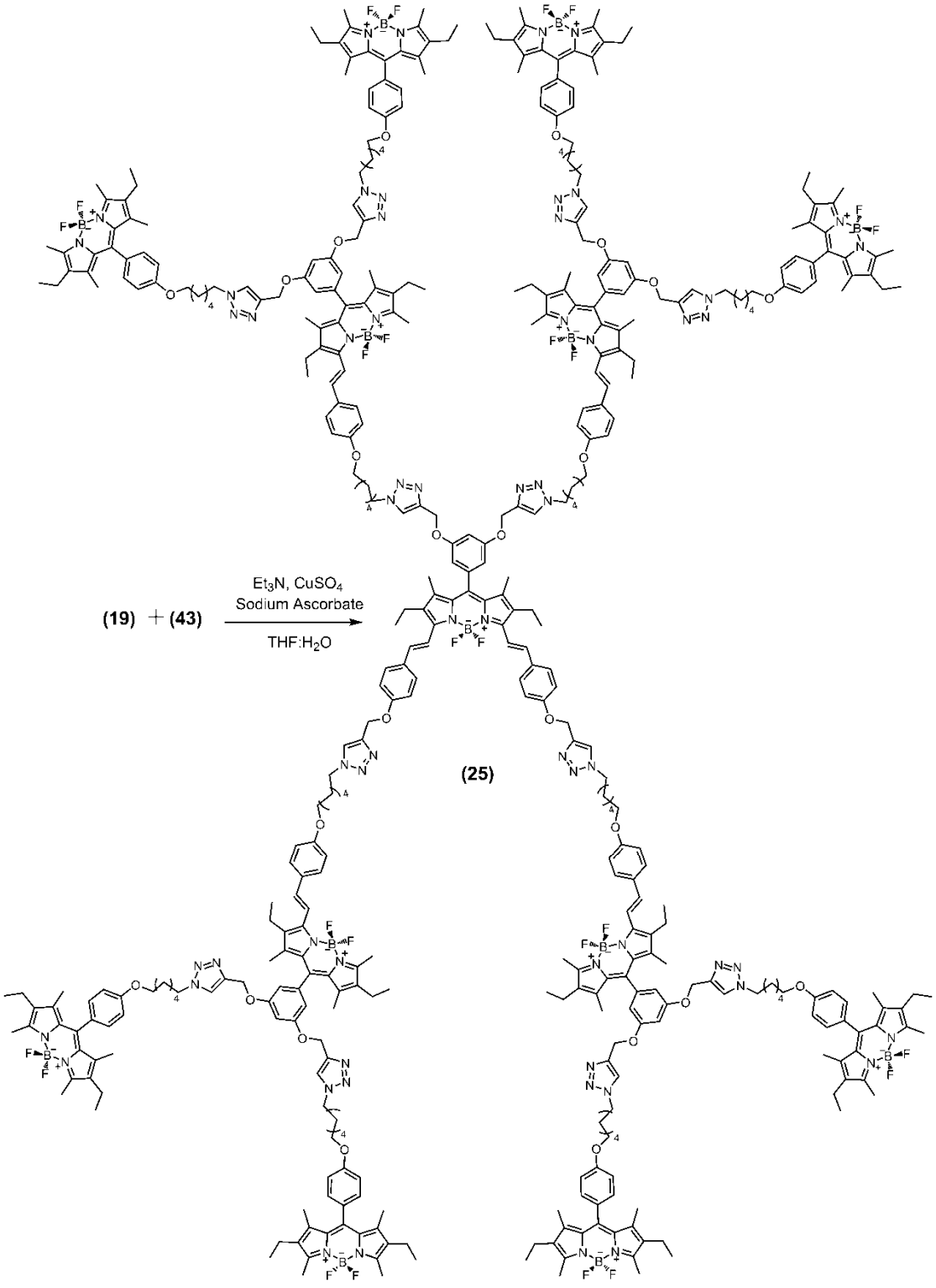

Figure 50. Synthesis of compound **25**.

CHAPTER 3

RESULTS AND DISCUSSIONS

3.1 SWNT as a Delivery System for Photosensitizer

Carbon nanotubes are suitable delivery system for drugs and related agents when their biocompatibility and easy non-covalent modifications are considered. In this research, SWNT is used for delivery agent for photodynamic therapy reagent. Photodynamic therapy is a growing field of research due to promising results obtained in clinical applications. This approach allows local treatment of tumors and gives minimum damage to surrounding normal tissue compared to other conventional therapies such as radio or chemotherapies. Even in the absence of specific targeting group, photosensitizers tend to localize in tumor tissue due to enhanced permeation and retention in this region, in addition light is exposed to only region of interest maintaining further selectivity.

Here, we present a novel photodynamic therapy reagent based on BODIPY where SWNT is used as delivery system. BODIPY core was synthesized through standard BODIPY reactions. BODIPY is preferred due to its photostability and high extinction coefficient.[45] Besides, core BODIPY can be modified in a number of regions easily.[45] In this research for instance, 2, 6 positions were decorated with iodines. Spin forbidden transition from singlet excited state of photosensitizer to triplet state is enhanced in the presence of heavy atom as a result of increased spin-orbit coupling.[32] Thus, iodination maintains this in our design.

Methyl groups in 3, 5 positions are acidic to participate in Knoevenagel condensation reactions. Hence, we obtained distyryl-BODIPY with pyrene containing moiety for the attachment on SWNT. Previously, SWNT-pyrene π-π

interaction was well studied and high stability against desorption was reported.[90-91] Recently, Akkaya et al. discovered that modification in 1, 7 positions of BODIPY is also possible through same kind of reaction (unpublished data).

Via facile click reaction polyetylene glycol moiety was attached to the photensitizer to maintain water solubility and nonspecific binding of proteins on the walls of SWNT.[156] PEG also increases blood circulation time of photosensitizer as reported by Liu and Dai et al.[157] All the compounds obtained after each reaction were characterized using ^{1}H, ^{13}C NMR spectra and Mass spectrometry analysis. NMR spectra were measured using $CDCl_3$ as solvent. All these data are given in appendices A and B.

Maximum absorbance wavelength of photosensitizer is determined to be 725 nm in aqueous solution (Figure 51) which is very suitable for PDT applications since penetration depth of light of this wavelength, namely, light in near IR region, is considerably high.

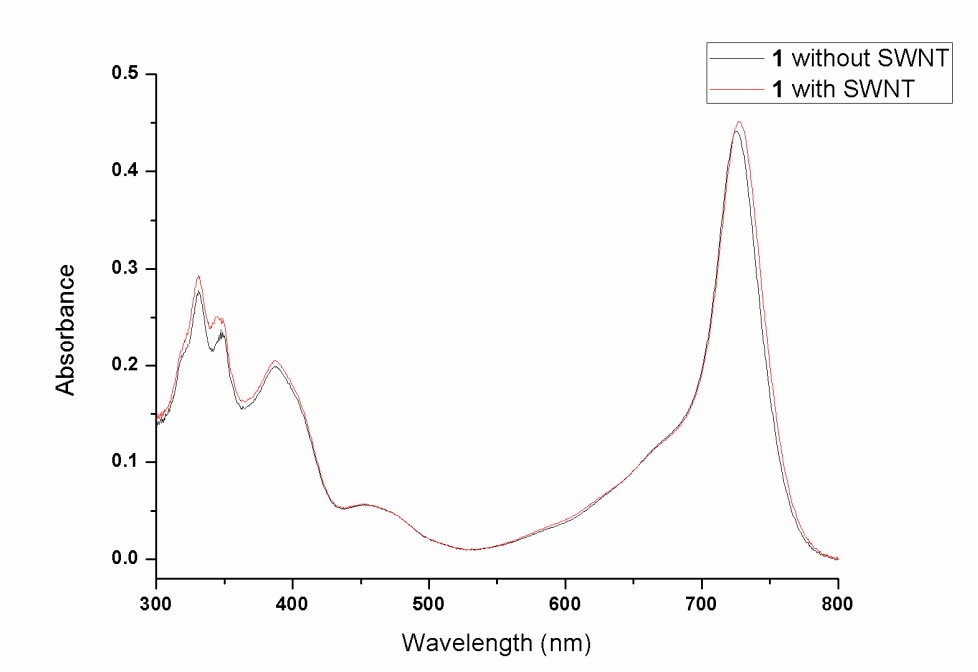

Figure 51. Absorbance of compound **1** in ethanol-PBS mixture (50/50, v/v). Black line: compound **1** before adsorption on to SWNT; red line: compound **1** after adsorption on to SWNT.

Non-covalent attachment of pyrene containing photosensitizer on SWNT was performed through sonication method as reported elsewhere.[153] Through sonication, nanotube bundles are expected to be disrupted and dispersed. Attachment of PEG containing PS solubilizes nanotubes afterwards. Through filtration method, unattached, free compound **1** was eliminated. Millipore filter used for this purpose allows the passage of small molecules, molecules with molecular mass lower than 30kDa, thus only free compound **1** can pass through pores of filter. Strikingly, the filtrate was transparent indicating, owing to strong pyrene-SWNT interaction, only spectroscopically insignificant, minute amount of compound **1** remains unattached.

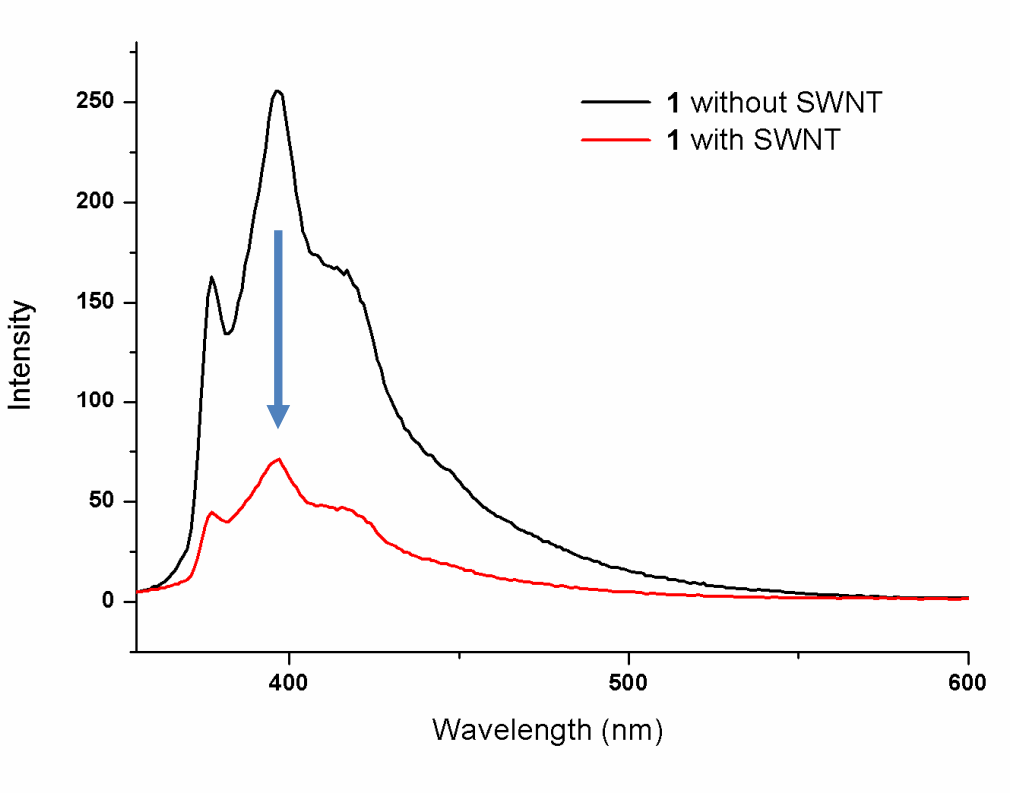

Figure 52. Fluorescence spectrum of compound **1** in ethanol-PBS mixture (50/50, v/v) excited at 343 nm. Red line: compound **1** before adsorption on SWNT; blue line: compound **1** after adsorption on SWNT.

Pyrene emission was reported to be quenched after such attachment due to electron transfer from pyrene to SWNT.[158-159] In this research, this phenomenon is confirmed, thus pyrene-SWNT attachment was demonstrated. Upon excitation at 343 nm, almost three folds quenching of pyrene emission due to stacking of compound **1** on to the SWNT was observed (Figure 52) compared with the non-stacked compound **1** with equal absorbance (Figure 51).

Apart from quenching in pyrene emission, pyrene-SWNT non-covalent functionalization was characterized using atomic force microscopy (AFM) and high resolution transmission electron microscopy (TEM) measurements (Figure 53). Nanotubes are seen as separate entities rather than bundles in TEM image indicating that solubilization process was successful.[153] Besides, using non-contact mode, roughness of a few nanometer heights on SWNT was measured which clearly points out the presence of bulky molecule on otherwise smooth SWNT (Figure 54).[160-161]

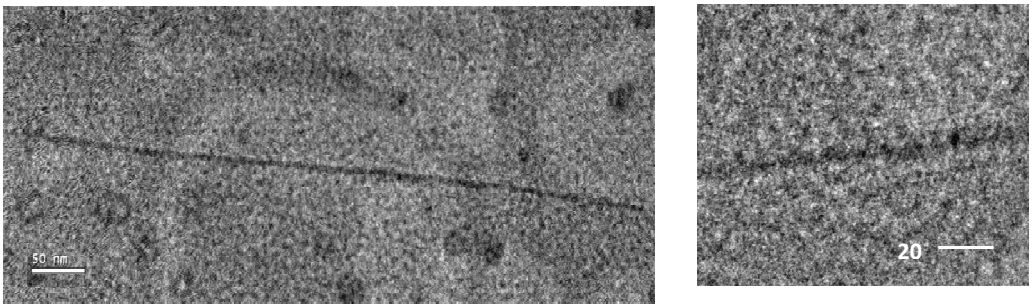

Figure 53. TEM image of SWNT functionalized with compound **1.**

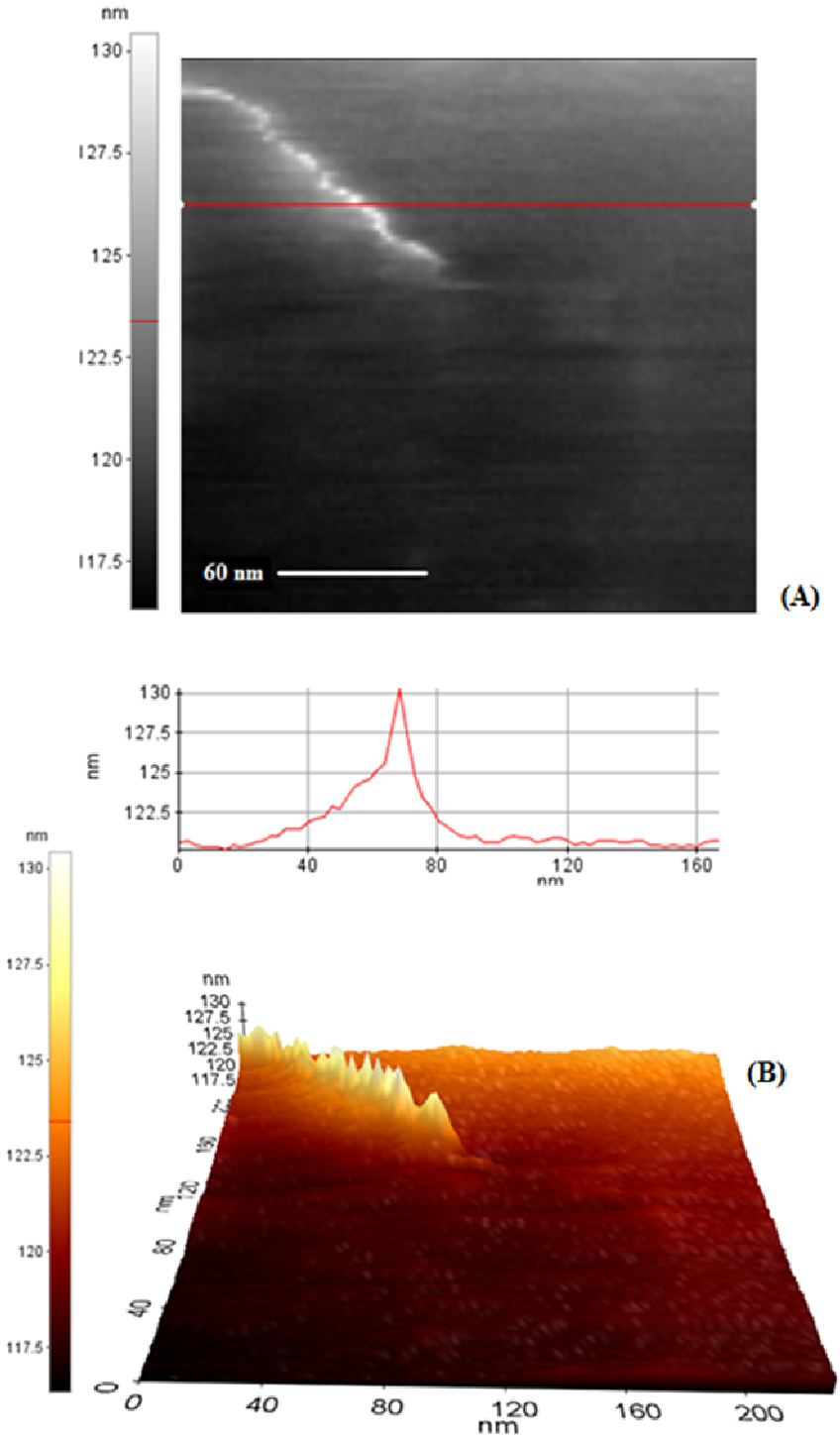

Figure 54. (a) AFM image of compound **1**-SWNT. (b) AFM 3D topographic view. PSIA XE-100E AFM and Multi75AI tip was used in noncontact mode with resonance frequency 75 KHz and force constant 3.0 N/m.

Singlet oxygen generation capability of compound 1 with and without SWNT was measured using photobleaching of singlet oxygen trap molecule 1,3-diphenylisobenzofuran (DPBF). As shown in Figure 21, DPBF reacts with $^1O_2$ and absorbance at 411 nm decreases consequently. $^1O_2$ is generated by excited photosensitizer. Since DPBF is soluble in isopropanol, experiment was performed in this solution. Maximum absorbance wavelength of compound 1 with SWNT in isopropanol is at about 666 nm, thus array of LEDs emitting 660 nm light is appropriate for excitation of PS (Figure 55).

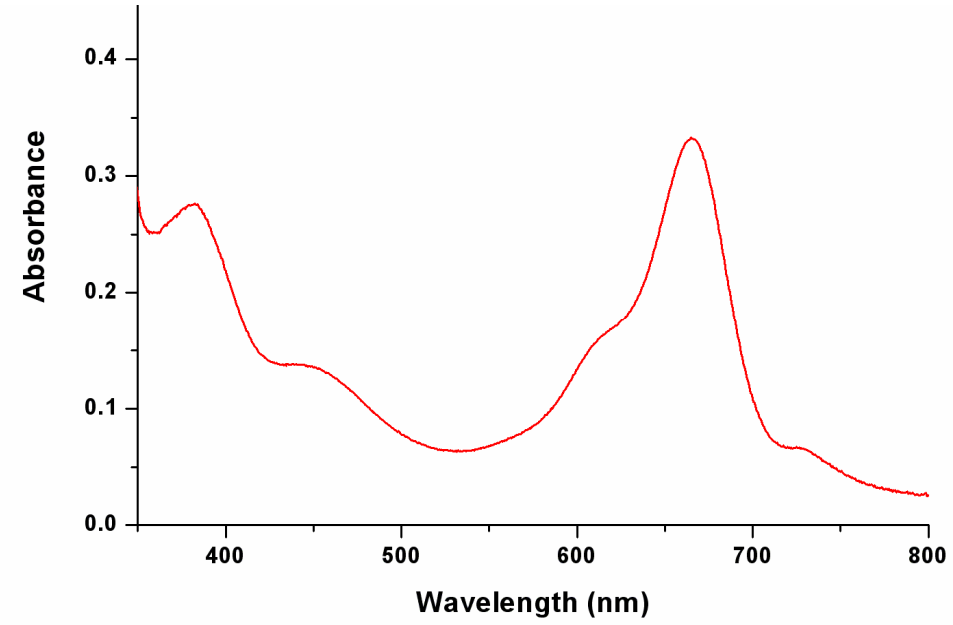

Figure 55. Absorbance spectrum of SWNT-adsorbed compound **1** in isopropanol.

We performed same experiment with three different samples. In control experiment, only 50 µM DPBF containing solution was monitored for 5 minutes intervals for 15 min in dark and 40 min under 660 nm light illumination. No significant decrease in absorbance was detected even under irradiation as shown in Figure 56 and Figure 57 as expected. Same experiment was performed with same concentration of DPBF together with 62 nM compound **1** only and compound **1** stacked on SWNT. Results indicate that photobleaching rate is

slightly higher in sample containing free compound **1**. However, this difference in rate of photobleaching is not too important to obstruct phodynamic action of photosensitizer, namely singlet oxygen generation capability. SWNTs are known to react with $^1O_2$ and act as scavenger $^1O_2$ to some extent.[162-163] This would be the reason of minor decrease in photobleaching rate. However, the alkyl-spacer between SWNT binding moiety and BODIPY core seems to be effective in preserving PDT ability of PS by separating donor-acceptor moieties hence reduces quenching.

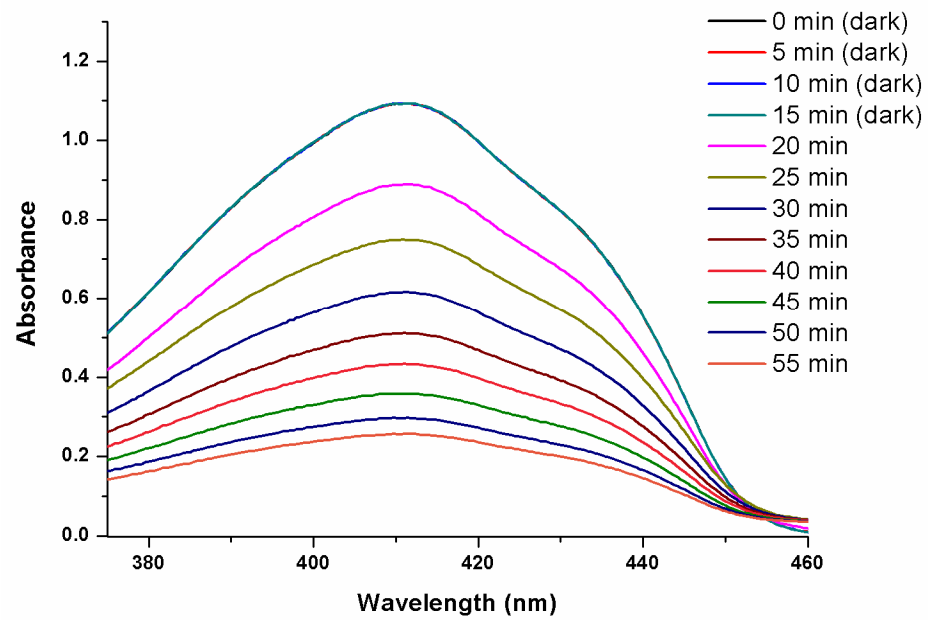

Figure 56. Bleaching of 50 μM DPBF in isopropanol in the presence of 62 nM SWNT-adsorbed compound 1. For the first 15 minutes sample was kept at dark, then irradiated with 660 nm light for 40 minutes. Absorbance was measured in 5 minutes intervals.

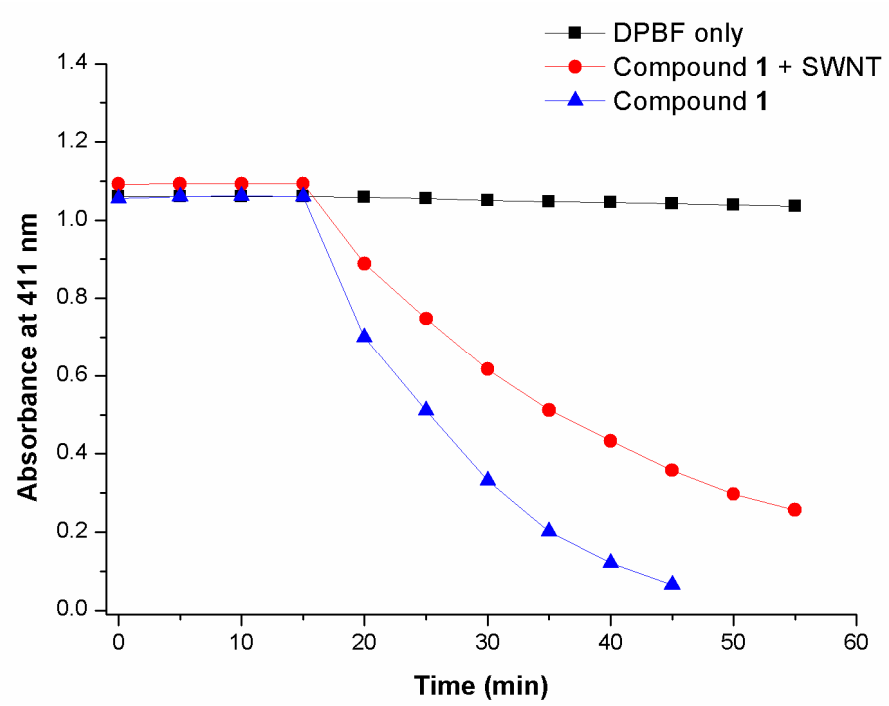

Figure 57. Absorbance of DPBF in isopropanol at 411 nm without compound **1** (square), in the presence of compound **1** only (triangle) and in the presence of compound **1** non-covalently attached to SWNT (circle).

3.2 Light Harvesting Dendrimer

In the knowledge of science, understanding the working principles of biological systems provides direct use of experience of millions of years of evolutionary processes. Living organisms naturally select certain traits that are tuned to work efficiently under earths' conditions. One such marvelous trait is their ability to use sun energy. Living in a world where energy demand is severely increasing, understanding and mimicking such traits are becoming meaningful. Thus, array of chromophores that harvest light efficiently is a primitive but promising approach.

In this research, four different light harvesting dendrimers were designed and synthesized. Efficient and unidirectional energy transfer from the terminal units to the interior of the dendrimer was achieved by convergent synthesis. The light harvesting system was designed to allow Förster type resonance energy transfer in a cascade from the surface of the dendrimer to the core. Placement of each chromophore on the structure of the dendrimer was determined taking spectral overlap between adjacent chromophores into account. Final acceptor unit, distyryl BODIPY was placed at the center of the dendrimer and other chromophores, mono styryl-BODIPY and BODIPY were located in the outer shell of the dendrimer in succession. Through out this chapter, BODIPY, monostyryl-BODIPY and distyryl-BODIPY were shown in orange, red and green respectively. To assess energy transfer from mono-styryl BODIPY to di-styryl BODIPY, two dendrimers were synthesized with a core di-styryl-BODIPY carying two or four mono-styryl-BODIPYs (**23** and **24** in that order). Direct energy transfer from BODIPY to monostyryl-BODIPY was examined using **21** that carries two BODIPY attached to one monostyryl-BODIPY.

BODIPYs were synthesized using standard BODIPY reactions and in order to construct spectrally appropriate chromophores, conjugation was extended through Knoevenagel condensation reactions. Chromophores were covalently attached to one another using facile copper (I) catalyzed click reactions between azido and ethynyl groups of compounds. Azido compounds were characterized monitoring ^{1}H NMR shift from δ3.5 to δ3.3 as the bromo reagent is consumed to generate azido product. Click reaction products have distinct singlet peak at around δ7.6 in ^{1}H NMR corresponding to triazole hydrogen.

Photophysical characterization shown in Table 2 confirms that as the number of specific BODIPY units increases, extinction coefficient at that BODIPY's maximum absorbance wavelength increases in accordance. Extinction coefficient of BODIPY (**11**) was determined to be 76154 at 526 nm. This number increases to 539807 in compound **25** which carries 8 BODIPY units. This increase is more than 7-folds which is consistent with the number of

BODIPYs on the structure. In compounds **23** and **24**, increase in monostyryl-BODIPY extinction coefficient is 2.2 and 4.5 folds respectively, consistent with number of this units, 2 and 4 in each compound in that order.

Table 2. Photophysical properties of dendrimers and dendrimer elements.

Compound	**ε (λ_{max}) ($M^{-1}cm^{-1}$)(nm)**	**λ_{em} (nm)**	**Φ_F λ_{exc}(488nm)**	**Φ_F λ_{exc}(550nm)**	**Φ_F λ_{exc}(610nm)**
11	76154 (526)	539	0.80	-	-
15	59434 (590)	605	-	0.85	-
18	71214 (651)	670	-	-	0.67
19	71587 (653)	672	-	-	0.68
20	-	624	-	0.89	-
21	-	605	0.14		-
23	63850 (654) 131539 (590)	605 672	-	0.08 (605) 0.42 (672)	-
24	88084 (656) 269745 (590)	605 672	-	0.06 (605)	-
25	81875 (655) 298750 (590) 539807(527)	539 605 672	- - 0.02	- 0.09 -	- - -

Quantum yields were calculated using three different standard chromophores, Rhodamine 6G (488 nm, water), Sulforhodamine 101 (550 nm, ethanol) and Cresyl Violet (610 nm, methanol) and given in table 2. Formula 6 given at page 37 was used for calculations. Since for accuracy, absorbance and emission spectra of standard and sample should be overlapping, no ideal standard exists to calculate the quantum yields of dendrimers, absorbing at 520 nm, emitting at 672 nm. Thus, calculations were done for those having satisfactory overlap in each spectrum. Otherwise, lack of overlap would lead to underestimation of quantum yields, hence misleading.

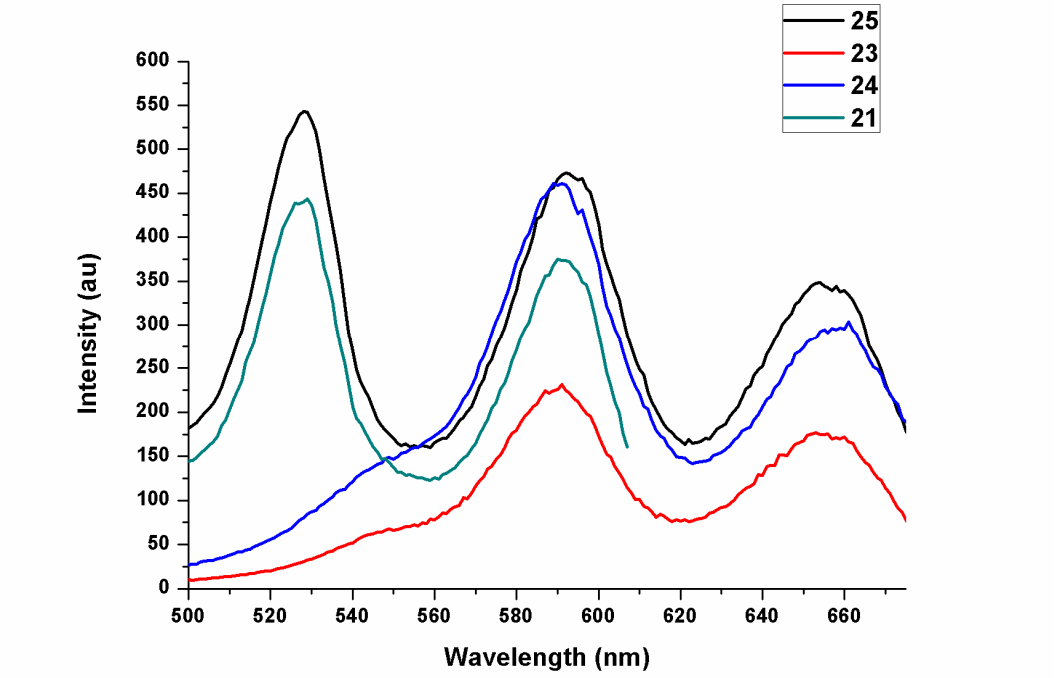

Figure 58. Excitation spectra of compounds **21**, **23**, **24** and **25**.

Excitation spectra are given in Figure 58. As it can be seen in Figures 59, 62, 65, 68, absorbance spectra of compounds **21, 23**, **24** and **25** show distinct peaks (526 nm, 590 nm, 653nm) corresponding to individual chromophores in the structure of the dendrimer, which indicates absence of ground state interactions between different units of dendrimer.

In order to understand energy transfer between BODIPYand mono-styryl BODIPY in the absence of di-styryl BODIPY, FRET efficiency in compound **21** was analyzed. Even though, **11** and **21** absorb equally at 526 nm, corresponding emission at 539 nm was quenched significantly in **21** due to FRET (Figure 59, 60). In addition, highly enhanced emission at 605 nm (more than 8-fold increase) compared to **15**, was observed even when the compound **21** was excited from BODIPY. Energy trsnsfer from outer BODIPY is also obvious considering the decrease in quantum yield from 0.80 to 0.14 upon excitation at BODIPY's absorbance wavelength for compound **21** (Table 2). Consistently, lifetime of BODIPY decreased from 4.3 ns to 0.14 ns (Table 3).

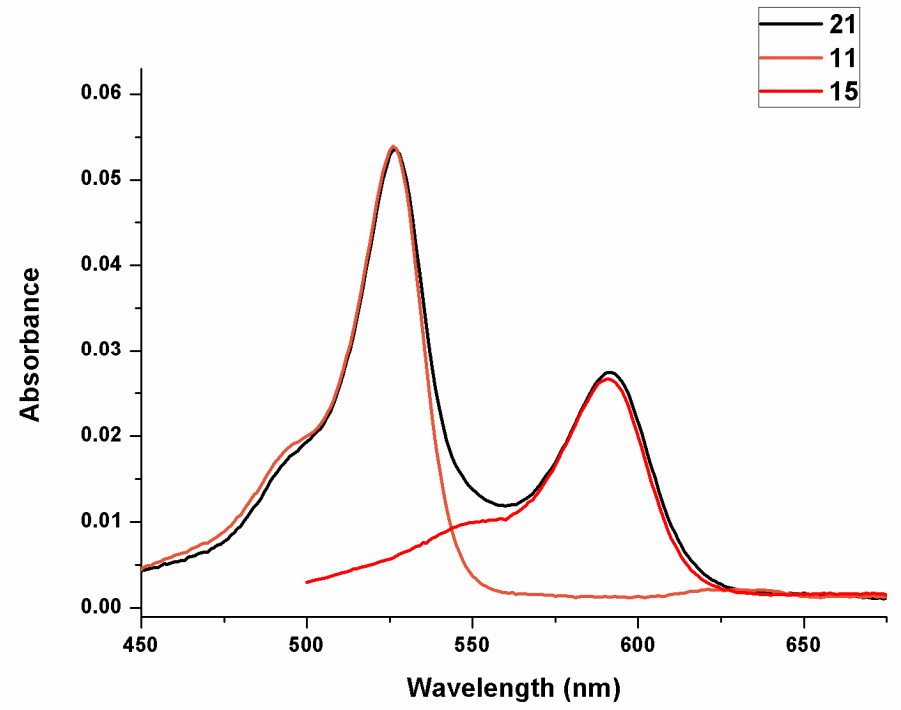

Figure 59. Absorbance spectra of compounds **11, 15** and **21**.

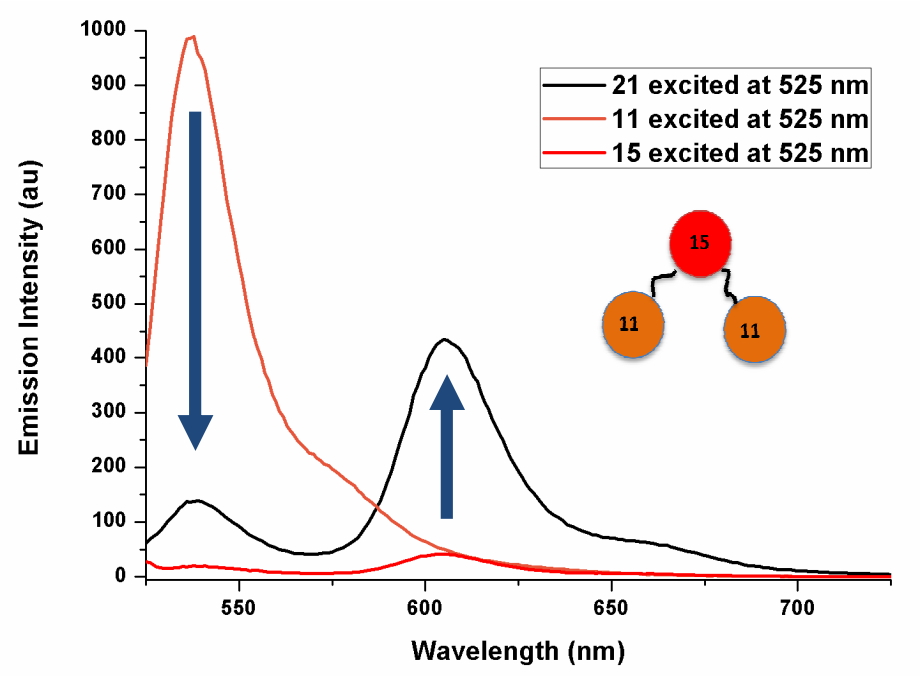

Figure 60. Emission spectra of compounds **11, 15** and **21** with equal absorbance.

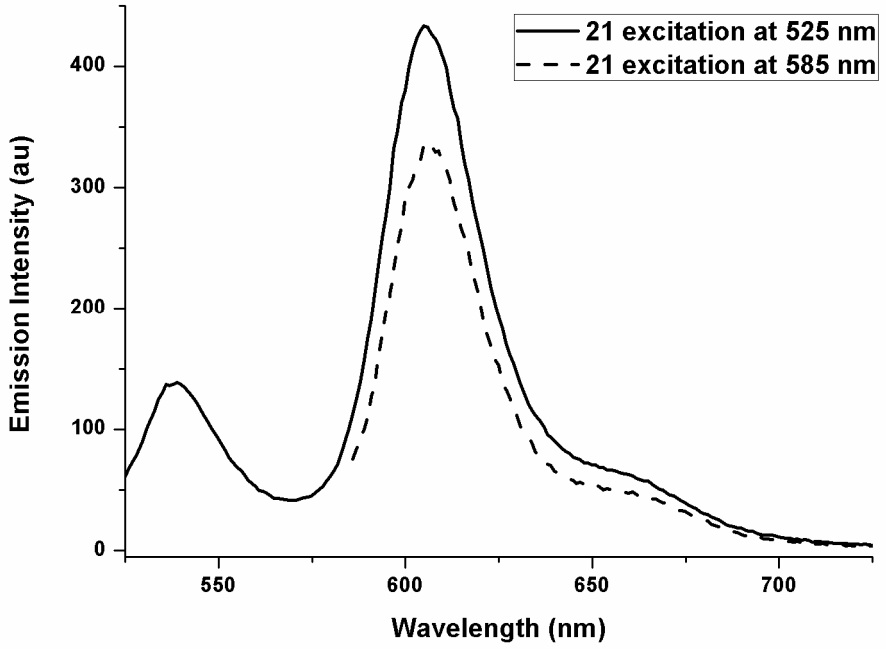

Figure 61. Comparison of emissions of compound **21** excited at 525(solid line) and 585 nm (dashed line).

For compound **21**, excitation at 525 nm results in enhancement in emission of acceptor monostyryl BODIPY. Much more interestingly, emission upon excitation at 525 nm is more than emission upon excitation at core's own absorption maxima, namely at 585 nm (Figure 61). This indicates nothing but efficient channeling of energy to the core from the surrounding BODIPY moieties.

FRET efficiencies can be calculated either using steady state or time-resolved method. The latter is accepted to be more accurate since it lacks problems associated with inner filter effect and integration errors. Comparing the results obtained using quantum yields (steady state approach) or excited state lifetimes of donor alone and donor in the presence of acceptor (time-resolved approach), shows that in steady for compound 21, first method slightly underestimate the energy transfer efficiency. 83% and 97% efficiency were found using each method respectively. Being more accurate, FRET efficiency

calculations were done using time-resolved method (Formula 7 and 8) at page 29, which estimates 97% efficiency of FRET from outer BODIPY units to distyryl BODIPYs. For some other compounds however, quantum yields were used since lifetime data is not available yet. For all calculations, lifetime of BODIPY was taken to be 4.3 ns as tabulated elsewhere.[164] For compound **21**, rate of energy transfer was determined to be $6.91*10^9$ s^{-1}. Lifetime of donor BODIPY, (compound **11**) decreases significantly from 4.3 ns to 0.14 ns, which can be attributed to energy transfer. All available lifetimes, FRET rate constants and calculated FRET efficiencies were given in Table 3. Rate constants were calculated using Equation 7 on page 29 or for those of compounds lacking τ_{DA}, following formula was used.[126]

$$k_{FRET} = 1/\tau_D \left[(1/\varepsilon_{FRET})-1\right]^{-1} \quad (10)$$

Table 3. Lifetimes, FRET rate constants and efficiencies of compounds.

Compound	**τ (ns)**			**$k_{FRET}(s^{-1})$**	**ε_{FRET}**
	λ_{em}(529)	λ_{em}(605)	λ_{em}(675)		
15	-	5.57	-	-	-
19	-	-	4.97	-	-
20	-	4.57	-	-	-
21	0.14	5.03	-	$6.91*10^9$	97%
23	-	-	4.80	$2.21*10^9$	91%
24	-	-	4.44	$2.9*10^9$	93%
25; exc 526 nm	0.31	-	4.6	$3.09*10^9$	93%
25; exc 585 nm	-	-	-	$1.97*10^9$	90%

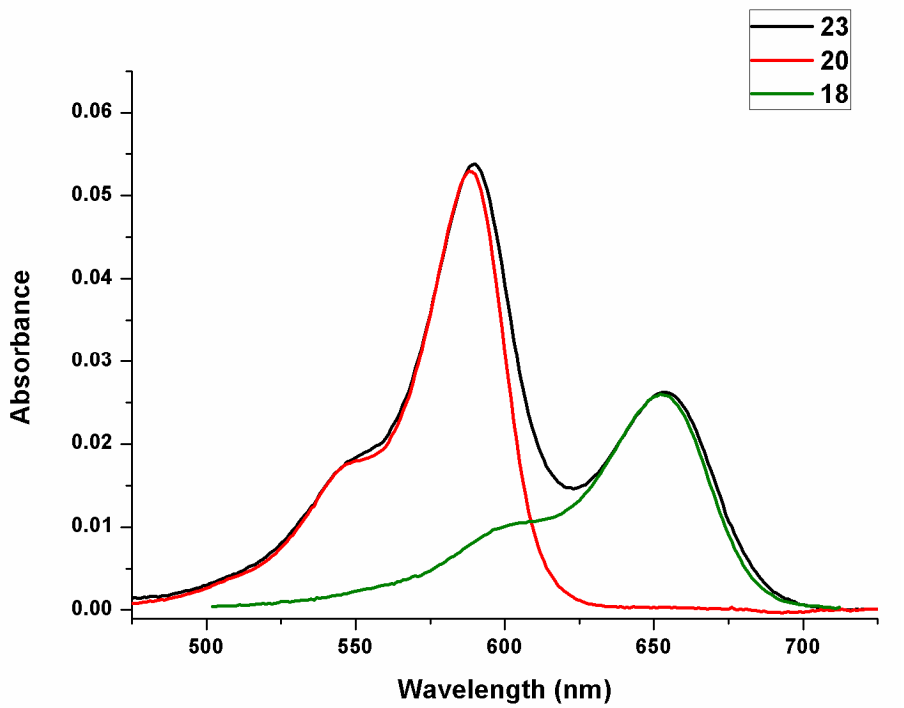

Figure 62. Absorbance spectra of compounds **18**, **20**, **23**.

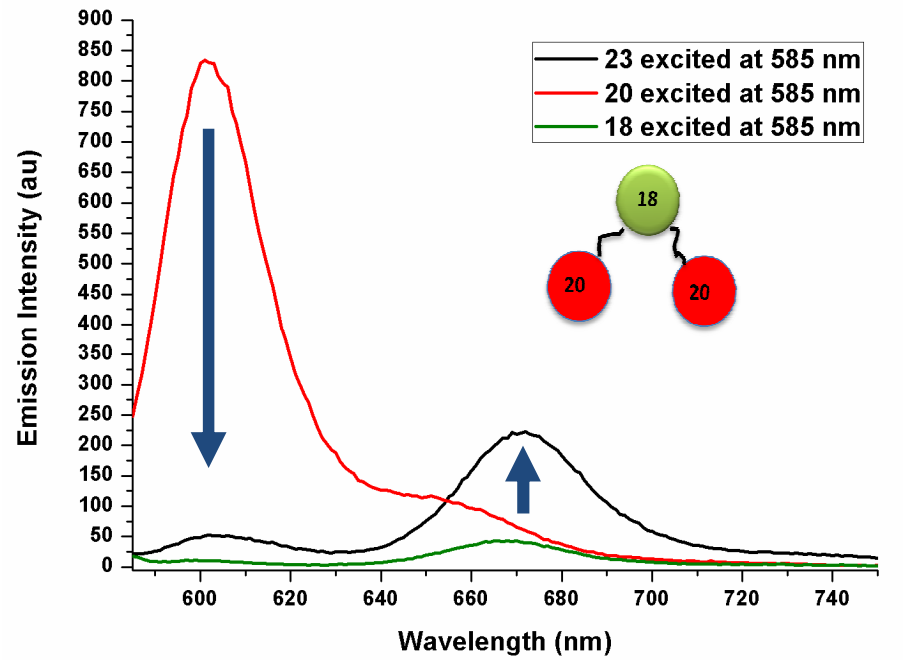

Figure 63. Emission spectra of compounds **18**, **20** and **23** with equal absorbance excited at 585 nm

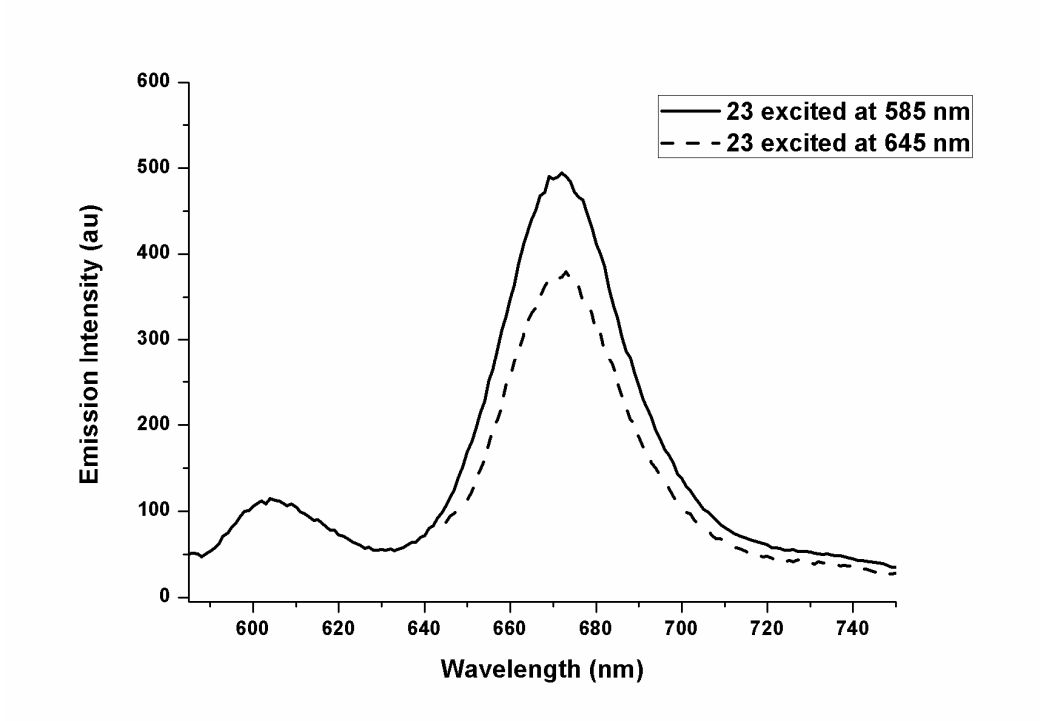

Figure 64. Comparison of emission of 23 excited at 585 nm (solid line) and 645 nm (dashed line)

To determine FRET efficiency from monostyryl-BODIPY to core distyryl-BODIPY two different dendrimers; compounds **23** and **24** were synthesized. With equal absorbance (Figure 62 and 65) emission spectra of these compounds were analyzed (Figure 63 and 66). Emission of distyryl BODIPY at 624 nm decreased more than 5-folds in each compound. Energy transfer efficiencies from monostyryl to distyryl BODIPYs were determined to be 91% and 93% for **23** and **24** respectively. Quantum yield calculations indicate a decrease from 0.89 (compound **20**) to 0.08 (compound **23**) and 0.06 (compound **24**) for emission at 624 nm corresponding to distryl-BODIPY emission which is expected.Furthermore, as it can be seen in Figure 64 and 67, both compounds **23** and **24** display higher emission intensity upon excitation at donor's absorption wavelength compared to excitation at acceptor's own absorption wavelength. All these data undoubtly confirms efficient FRET from monostyryl to distyryl-BODIPY in each dendrimer.

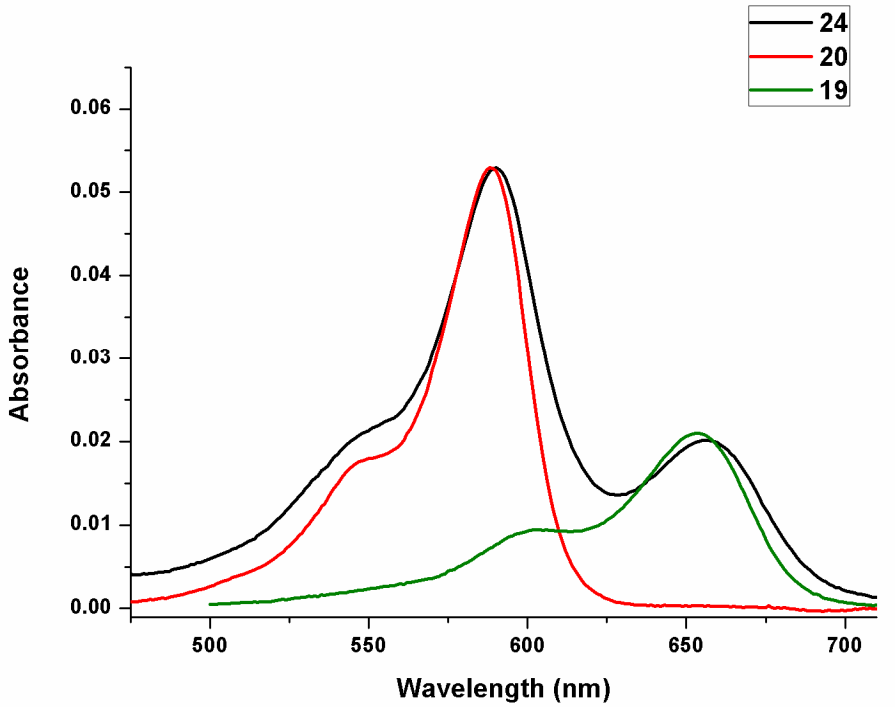

Figure 65. Absorbance spectra of compounds **19**, **20** and **24**.

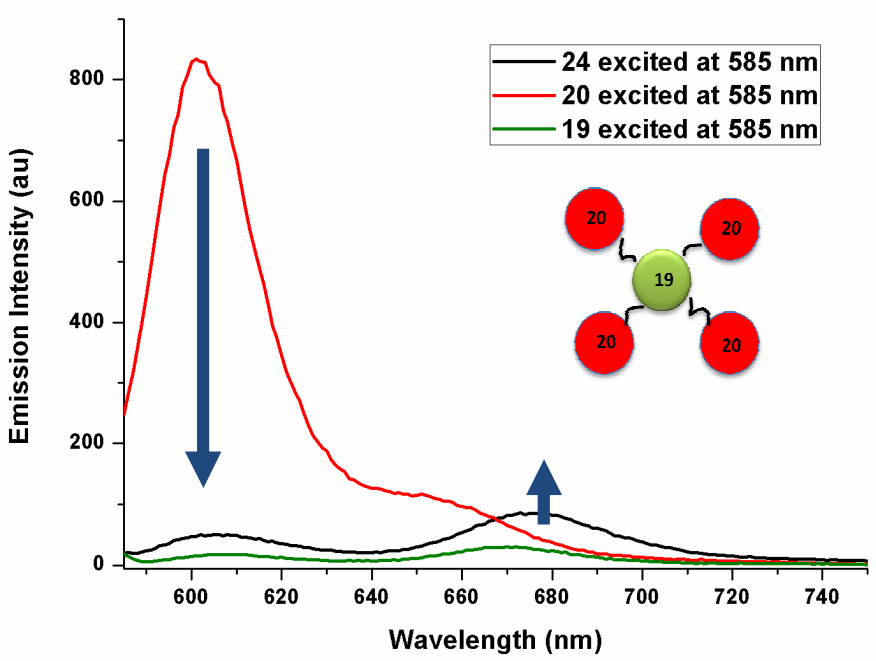

Figure 66. Emission spectra of compounds **19, 20** and **24** with equal absorbance excited at 585 nm.

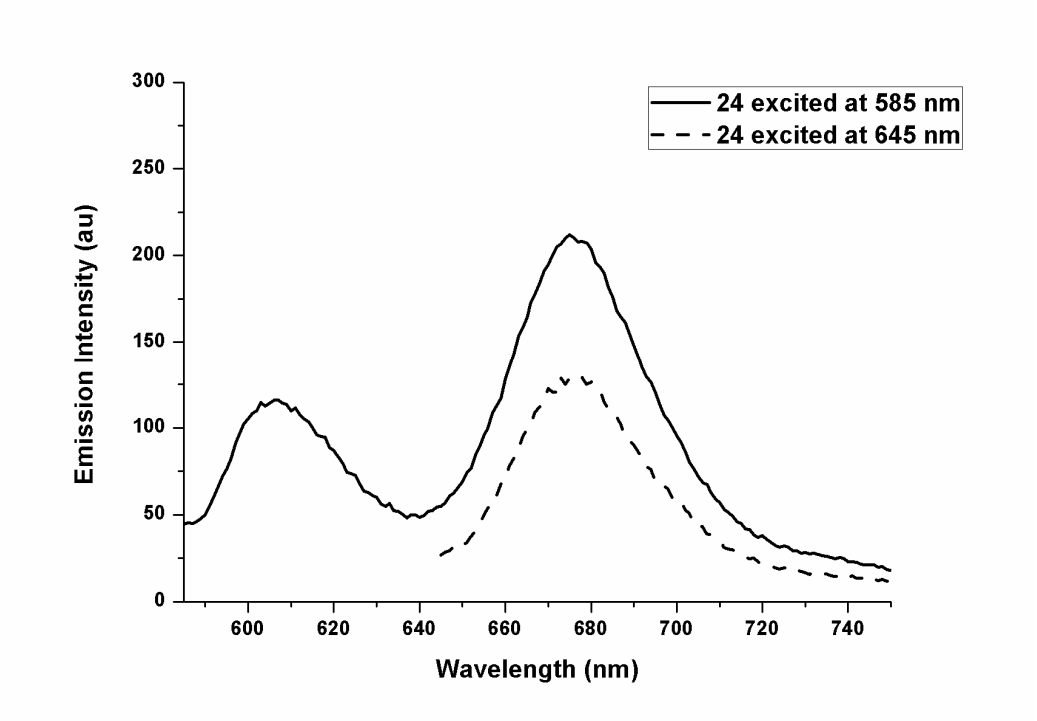

Figure 67. Comparison of emission of **24** excited at 585 nm (solid line), 645 nm (dashed line).

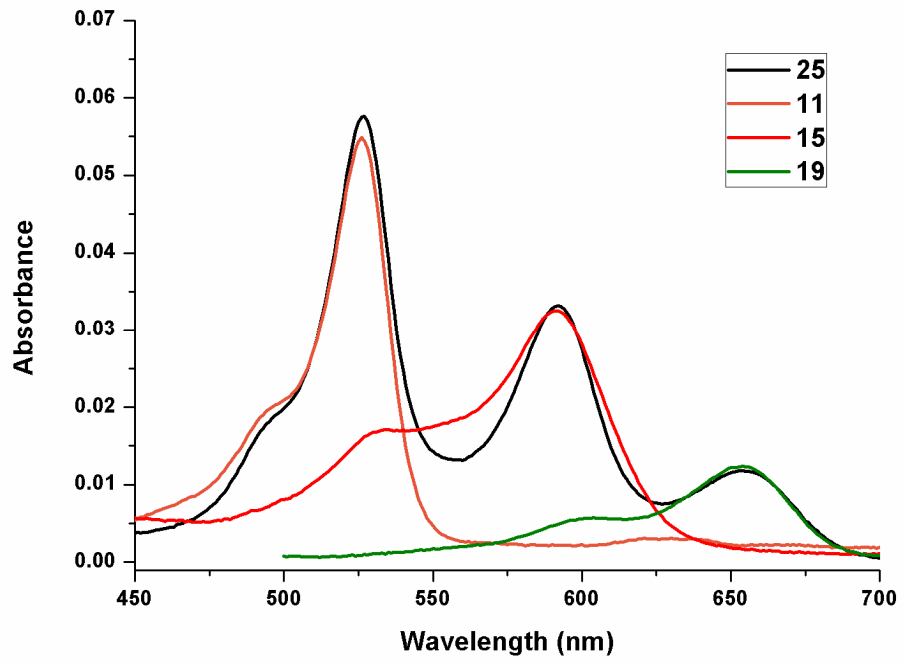

Figure 68. Absorbance spectra of compounds **11, 15, 19, 25.**

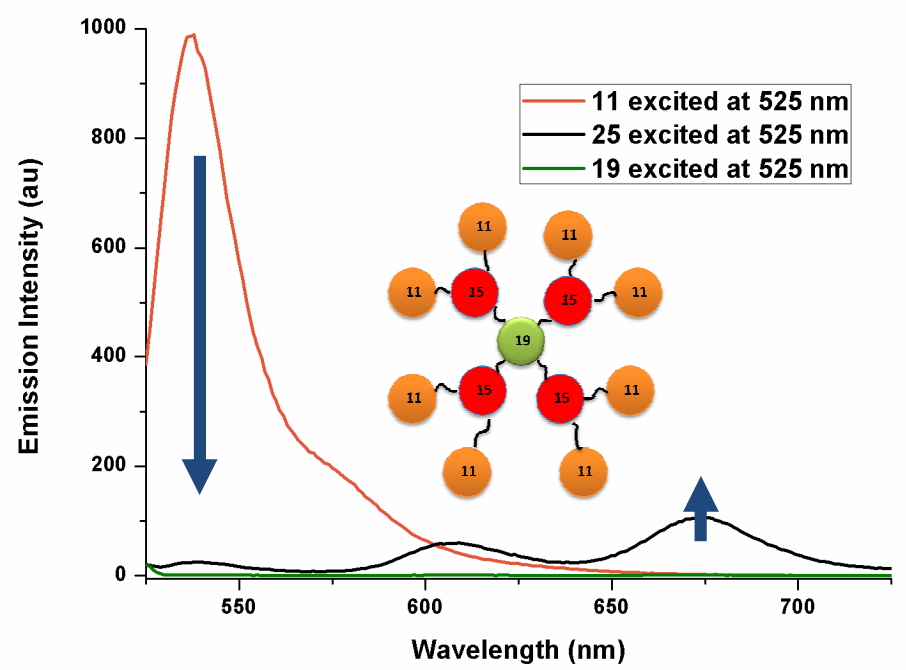

Figure 69. Emission spectra of compounds **11, 19** and **25** with equal absorbance excited at 525 nm.

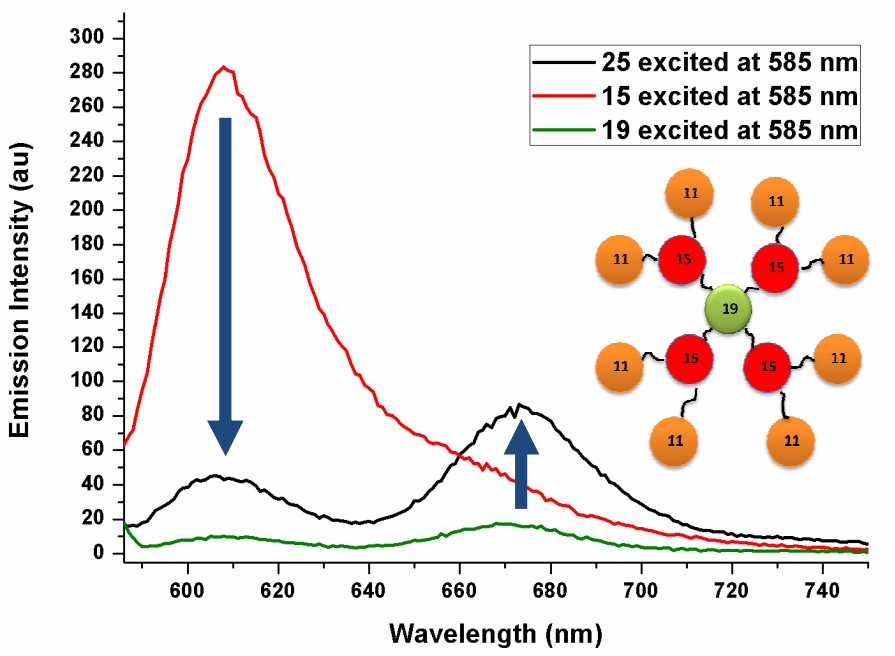

Figure 70. Emission spectra of compounds **11, 19** and **25** with equal absorbance excited at 585 nm.

For compound **25** carries two different types of donors, namely BODIPY and monostyryl-BODIPY. Emission spectra with equally absorbing compounds (Figure 63) show that both emissions at 539 nm and 606 nm decrease substantially upon excitation at 525 nm and 585 nm respectively, due to energy transfer (Figure 69 and 70). Energy transfer efficiencies were determined to be 90% from the BODIPY terminal units to either mono or distyryl-BODIPYs and 93% from monostyryl-BODIPY to the core. Interestingly, with this dendrimer, emission at 672 nm is achieved even when the compound is excited at 150 nm below, at 525 nm. This enables spanning of a large region of the visible spectrum with a single molecule and to funnel energy in certain part, which is gorgeous. More strikingly, emission intensity at 672 nm is larger when the compound is excited at 525 nm compared to excitations at 585 nm and 645 nm as shown in Figure 71.

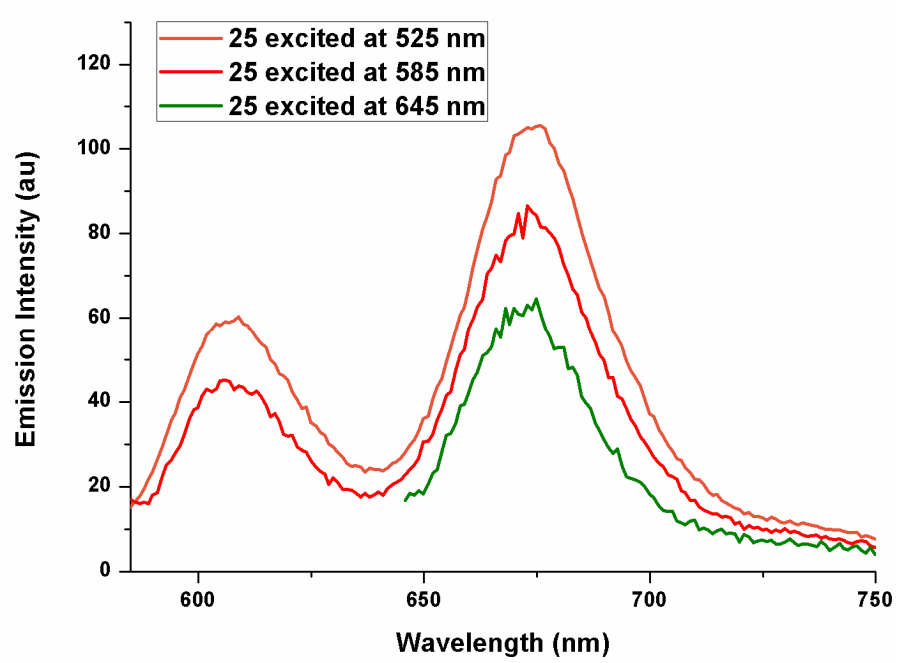

Figure 71. Comparison of emission of 25 excited at 525 nm (orange), 585 nm (red) and 645 nm (green).

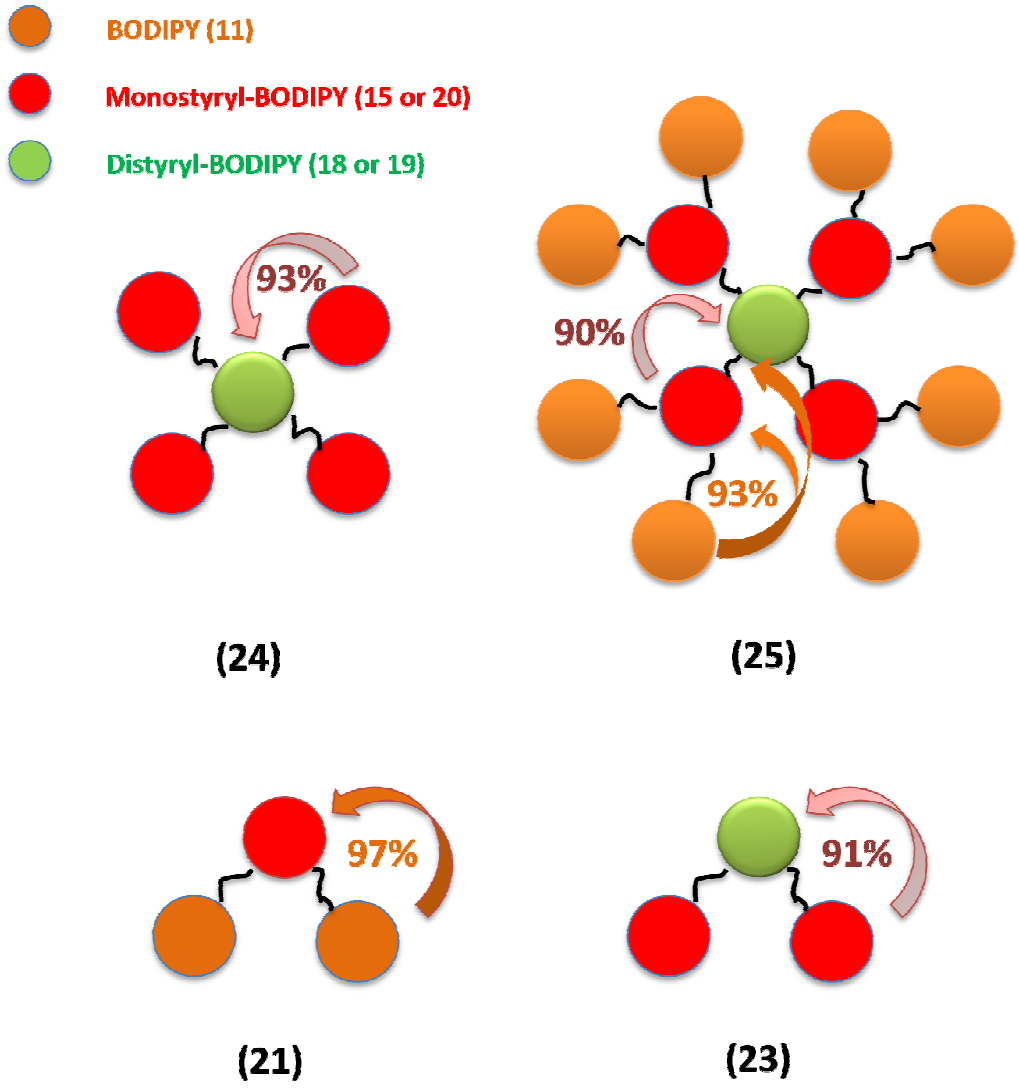

Figure 72. Schematic representations and FRET efficiencies of compounds **21**, **23**, **24** and **25**.

To sum up, direction of energy transfer and FRET efficiencies for compounds **21**, **23**, **24** and **25** are illustrated in Figure 72. Core distyryl-BODIPY is shown in color green, monostyryl-BODIPY that surrounds core is shown in red and finally outer BODIPY units are in orange. To generalize, FRET efficiency varies from 90% (compound **25**) to 97% (compound **21**). Maximum energy transfer is achieved from BODIPY to monostyryl-BODIPY with FRET efficiency of 97%. Considering the distance dependence of FRET rate constant and efficiency, using shorter linkers between chromophores may increase the efficiencies even more. Here, 6-carbon flexible linkers were used.

In this research, highly efficient energy harvesting with BODIPY-based dendrimeric antenna is presented. This antenna shows cascade property by channeling energy to the core and enhancing core fluorescence emission. This enhancement is larger when the dendrimer was excited at primary donor, namely terminal BODIPY units.This system can be used in a number of applications such as to label proteins, to produce panchromatic dyes for dye-sensitized solar cells, for signal amplification and frequency conversion purposes or in construction of a variety of optoelectronic devices.

CHAPTER 4

CONCLUSION

In this research novel, water soluble BODIPY-based photodynamic therapy reagent was synthesized and characterized. SWNTs were non-covalently functionalized with these photosensitizers and suscessfull photodynamic ability was observed. In addition, four different BODIPY-based dendrimers were synthesized and energy transfer efficiencies were examined.

Compound **1** is designed to be used in PDT. Through rational synthesis, PDT requirements such as water solubility, enhanced intersystem crossing is provided using PEG and iodines respectively. SWNTs are used as potential delivery system for PS and non-covalent functionalization was achieved through pyrene-SWNT π–π interactions. Attachment was characterized well using quenching of pyrene emission and AFM, TEM electron micrographs. Singlet oxygen generation experiments show that compound **1** is an efficient singlet oxygen generator in nanomolar concentrations, even when it is stacked on SWNT. In the second part, four different dendrimers each carrying different number of donors and acceptors were synthesized and spectral and fluorescence decay analyses were done. More than 90% energy transfer from donors to core acceptor was observed through either using decrease in lifetime of donors or from quantum yields. Cascade-like energy transfer system result in enhanced emission at the core even the system was excited at 150 nm below elucidating the efficiency of light harvesting.

In conclusion, we have demonstrated that SWNTs can be used in the delivery of PS for the use in PDT while preserving their singlet oxygen generation capability and highly efficient FRET in multichromatic cascade-type BODIPY dendrimers were revieled.

REFERENCES

1. Triesscheijn, M.; Baas, P.; Schellens, J.H. M.; Stewart, F.A. *The Oncologist,* **2006**, 11, 1034.
2. Tralau, C.J.; Barr, H.; Sandeman, D.R.; Barton, T.; Lewin, M.R.; Brown, S.G. *J. Photochem. Photobiol*., **1987**, 46, 777.
3. Castano, A.P., Demidova, T.N., Hamblin, M.R. *Photodiagnosis Photodyn. Ther.,* **2004**, 1, 279.
4. Miyamoto, S.; Ronsein, G.E.; Prado, F.M.; Uemi, M.; Correa, T.C.; Toma, I.N.; Bertolucci, A.; Oliveira, M.C. B.; Motta, F.D.; Medeiros, M.H.G. *IUBMB Life*., **2007**, 59, 322.
5. Davies, K.J.A. *J. Biol. Chem.,* **1987**, 162, 9895.
6. Dolmans, D.E.; Fukumura, D.; Jain, R. *Nat. Rev. Cancer*., **2003**, 3, 380.
7. Prat, F.; Hou, C.; Foote, C.S. *J. Am. Chem. Soc*., **1997**, 119, 5051.
8. Castano, A.P.; Mroz, P.; Hambli, M.R. *Nature Reviews Cancer,* **2006**, 6, 535.
9. Szaciowski, K.; Macyk, W.; Drzewiecka-Matuszek, A.; Brindell, M.; Stochel, G. *Chem. Rev*., **2005**, 105, 2647.
10. Raab, O.*Z Biol.,* **1900**, 39, 524.
11. Ackroyd, R.; Kelty, C.; Brown, N.; Reed, M. *Photochem Photobiol.,* **2001**, 74, 656.
12. Mitton, D.; Ackroyd, M.D.; *FRCS*., **2008**, 5, 103.
13. Von Trappeiner, H.; Jodlbauer, A. *Med. Worchenschr.,* **1903**, 47, 2042.
14. Von Trappeiner, H.; Jodlbauer, A. Die Sensibilisierende Wirkung Fluorieszierender Substanzer. Gesammte Unter-suchungen uber die photodynamische erscheinung, Voger, F.C., Leipzig, **1907**.
15. Moan, J.; Wold, E. *Nature,* **1979**, 279, 450.
16. Meyer-Betz, F. *Dtsch. Arch. Klin*., **1913**, 112, 476.
17. Dougherty, T.J.; Kaufman, J.E.; Goldfarb, A.; Weishaupt, K.R.; Boyle, D.; Mittleman, A. *Cancer Res.,* **1978**, 38, 2628.

18. Lakowicz, J.R., *Principles of Fluorescence Spectroscopy*, 2nd ed., Kluwer/Plenum, New York, **1999**.

19. Henderson, B.; Dougherty T.J. *Photochem. Photobiol*., **1992**, 55, 145.

20. Prutz, W.A. *Arch. Biochem. Biophys*. **1996**, 332, 110.

21. Buytaert, E.; Dewaele, M.; Agostinis, P. *Biochimica et Biophysica Acta 1776*, **2007**, 86.

22. Wright, A.; Hawkins, C.L.; Davies, M.J.P. *Free Radic. Biol. Med.,* **2003**, 34, 637.

23. Cadet, J.; Di Mascio, P. Peroxides in biological system. In the chemistry of peroxides (Rappaport, Z., *et al*., eds). **2006**. Pp.915-999, John Wiley and Sons Ltd, Chichester.

24. Ochsner, M. *J. Photochem. Photobiol*., **1997**, 39, 1.

25. Boegheim, J.P.; Scholte, H.; Dubbehnan, T.M.A.R.; Beems, E.; Raap, A.K.; van Steveninck, J. *J. Photochem. Photobiol. B: Biol.,* **1987**, 1, 61.

26. Oleinick, N. L.; Morris, R.L.; Belichenko, I. *Photochem. Photobiol. Sci*., **2002**, 1, 1.

27. Korbelik, M.J. *Clin. Laser Med. Surg*. **1996**, 14, 329.

28. Elmore, S. *Toxicol. Pathol*., **2007**, 35, 495.

29. Zhang, A.; Wu, Y.; Lai, H.W.L.; Yew, D.T. *Neuro-embriology*, **2004-05**, 3, 47.

30. Korbelik, M.; Sun, J.; Cecic, I. *Cancer Res.,* **2005**, 65, 1018.

31. Korbelik, M.; Sun, J. *Cancer Immunol. Immunother.,* **2005**, 55, 900.

32. Turro, N. J. In Modern Molecular Photochemistry; University Science Books: Sausalito, CA, **1991**, pp 191-195.

33. Lower, S.K.; El-Sayed, M.A. *Chem. Rev.,* **1966**, 66, 199.

34. Gorman, A.; Killoran, J.; O'Shea, C.; Kenna, T.; Gallagher, M. W.; O'Shea, D. F. *J. Am. Chem. Soc*., **2004**, 126, 10619.

35. Spikes, J.D.; Bommer, J.C. *Photochem. Photobiol.,* **1993**, 58, 346.

36. Innovations in Fluorescence (2009). Retrieved from http://www.iss.com (18 july 2009)

37. Graczykowa, A. Photodynamic method of diagnosis and therapy of tumors (in Polish); Dom Wydawniczy Bellona: Warszawa, **1999**.

38. Zhu, T.C.; Finlay, J.C. *Med. Phys*., **2008**, 35, 3127.

39. Yukruk, F. PhD Thesis, METU, 2005.

40. Killoran, J.; Allen, L.; Gallapher, J.F.; Gallapher, W.M.; O'Shea, D.F. *Chem. Commun*., **2002**, 1862.

41. Wang, S.; Gao, R.; Zhou, F.; Selke, M. *J. Mater. Chem*., **2004**, 14, 487.

42. Yogo, T.; Urano, Y.; Ishitsuka, Y.; Maniwa, F.; Nagano, T. *J. Am. Chem. Soc.,* **2005**, 127, 12162.

43. Atilgan, S.; Ekmekci, Z.; Dogan, A. L.; Guc, D.; Akkaya, E. U. *Chem. Commun*., **2006**, 4398.

44. Ozlem S.; Akkaya E. U. *J. Am. Chem. Soc.*, **2009**, 131, 48.

45. Loudet, A.; Burgess, K. *Chem. Rev.,* **2007**, 107, 4891.

46. Montcourrier, P.; Mangeat, P.H.; Valembois, C.; Salazar, G.; Sahuquet, A.; Duperray, C.; Rochefort, H. *J. Cell Sci.,* **1994**, 107, 2381.

47. Cameron, I.L.; Smith, N.K.R.; Pool, T.B.; Sparks, R.L. *Cancer Res.,* **1980**, 40, 1493.

48. Yogo, T.; Urano, Y.; Mizushima, A.; Sunahara, H.; Inoue, T.; Hirose, K.; Iino, M.; Kikuchi, K.; Nagano, T. *Proc. Natl. Acad. Sci.,* **2008**, 105, 28.

49. Clo, E.; Snyder, J.W.; Voigt, N.V.; Ogilby, P.R.; Gothelf, K.V. *J. Am. Chem. Soc.*, **2006**, 128, 4200.

50. Förster, T. *Ann. Phys.,* **1948**, 2, 55.

51. Förster, T. *Z. Naturforsch.,* **1949**, 4, 321.

52. Marras, S.; Kramer, F.R.; Tyagi, S. *Nucleic Acids Res.,* **2002**, 30, e122.

53. Abravaya, K.; Huff, J.; Marshall, R.; Merchant, B.; Mullen, C.; Schneider, G.; Robinson, *J. Clin. Chem. Lab. Med*., **2003**, 41, 468.

54. Zheng, G.; Chen, J.; Stefflova, K.; Jarvi, M.; Li, H.; Wilson, B.C. *Proc. Natl. Acad. Sci.,* **2007**, 104, 8989.

55. Choi, Y.; Weissleder, R.; Tung, C.H. *Cancer Res*., **2006**, 66, 7225.

56. Shiomi, T.; Okada, Y. *Cancer Metast. Rev.,* **2003**, 22, 145.

57. Zhu, Z.; Tang, Z.; Phillips, J.A.; Yang, R.; Wang, H.; Tan, W. *J. Am. Chem. Soc.,* **2008**, 130, 10856.

58. Dougherty, T.J.; Lawrence, G.; Kaufman, J.H.; Boyle, D.; Weishaupt, K.R.; Goldfarb, A. *J. Natl. Cancer Inst*., **1979**, 62, 231.

59. Bessler, N.M. *Retina*, **2004**, 24, 512.

60. Singh, A.D.; Kaiser, P.K.; Sears, J.E.; Gupta, M.; Rundle, P.A.; Rennie, I.G. *Br. J. Ophthalmol.,* **2004**, 88, 1414.

61. Feyh, J. *J.Photochem. Photobiol. B: Biol.,* **1996**, 36, 175.

62. Stummer W.; Reulen H. J.; Novotny A.; Stepp H.; Tonn J. C. *Acta Neurochir. Suppl.,* **2003**, 88, 9.

63. Marks P. V.; Belchetz P.E.; Saxena A.; Igbaseimokumo U.; Thomson S.; Nelson M.; Stringer M. R.; Holroyd J.A.; Brown S.B. *Br. J. Neurosurg.,* **2000**, 14, 317.

64. Huang, Z.A. *Technol. Cancer Res. Treat*., **2005**, 4, 283.

65. Iijima, S. *Nature*, **1991**, 354, 56.

66. Zhao, Y.L.; Hu, L.; Stoddart, J.F.; Gruner, G. *Adv. Mater*., **2008**, 20, 1910.

67. Diehl, M.R.; Steuerman, D.W.; Tseng, H.R.; Vignon, S.A.; Star, A.; Celestre, P.C.; Stoddart, J.F.; Heath, J.R. *Chem. Phys. Chem*., **2003**, 4, 1335.

68. Bianco, A.; Kostarelos, K.; Partidos, C.D.; Prato, M. *Chem. Commun*., **2005**, 571.

69. Ajayan, P.M. *Chem. Rev*., **1999**, 99, 1787.

70. Ajayan, P.M.; Tour, J.M. *Nature*, **2007**, 447, 1066.

71. Liu, J.; Rinzler, A.G.; Dai, H.; Hafner, J.H.; Bradley, R.K.; Boul, P.J.; Lu, A.; Iverson, T.; Shekimov, K.; Huffman, C.B.; Rodriguez-Macias, F.; Shon, Y.S.; Lee, T.R.; Colbert, D.T.; Smalley, R.E. *Science*, **1998**, 280, 1253.

72. Mawhinney, D.B.; Naumenko, V.; Kuznetsova, A.; Yates, J.T.J.; Liu, J.; Smalley, R.E. *Chem. Phys. Lett.,* **2000**, 324, 213.

73. Hu, H.; Bhowmik, P.; Zhao, B.; Hamon, M.A.; Itkis, M.E.; Haddon, R.C. *Chem. Phys. Lett*., **2001**, 345, 25.

74. Monthioux, M.; Smith, B.W.; Burteaux, B.; Claye, A.; Fischer, J.E.; Luzzi, D.E. *Carbon*, **2001**, 39, 1251.

75. Niyogi, S.; Hamon, M.A.; Hu, H.; Zhao, B.; Bhowmik, P.; Sen, R.; Itkis, M.E., Haddon, R.C. *Acc. Chem. Res*., **2002**, 35, 1105.

76. Chen, J.; Hamon, M.A.; Hu, H.; Chen, Y.; Rao, A.M.; Eklund, P.C.; Haddon, R.C. *Science*, **1998**, 282, 95.

77. Bahr, J.L.; Yang, J.; Kosynkin, D.V.; Bronikovski, M.J.; Smalley, R.E.; Tour, J.M. *J. Am. Chem. Soc*., **2001**, 123, 6536.

78. Bahr, J.L.; Tour, J.L. *Chem. Mater*., **2001**, 13, 3823.

79. Mickelson, E.T.; Chiang, I.W.; Zimmerman, J.L.; Boul, P.J.; Lozano, J.; Liu, J.; Smalley, R.E.; Hauge, R.H.; Margrave, J.L. *J. Phys. Chem. B*, **1999**, 103, 4318.

80. Holzinger, M.; Vostrowski, O.; Hirsch, A.; Hennrich, F.; Kappes, M.; Weiss, R.; Jellen, F. *Angew. Chem., Int. Ed.,* **2001**, 40, 4002.

81. Georgakilas, V.; Kordatos, K.; Prato, M.; Guldi, D.M., Holzinger, M.; Hirsch, A. *J. Am. Chem. Soc.*, **2002**, 124, 760.

82. Pekker, S.; Salvetat, J.P.; Jakab, E.; Bonard, J.M.; Forro, L.J. *Phys. Chem. B*, **2001**, 105, 7938.

83. Mickelson, E.T.; Huffman, C.B.; Rinzler, A.G.; Smalley, R.E.; Hauge, R.H.; Margrave, J.L. *Chem. Phys. Lett.,* **1998**, 296, 188.

84. Boul, P.J.; Liu, J.; Mickelson, E.T.; Huffman, C. B.; Ericson, L.M.; Chiang, I.W.; Smith, K.A.; Colbert, D.T.; Hauge, R.H.; Margrave, J.L.; Smalley, R.E. *Chem. Phys. Lett.,* **1999**, 310, 367.

85. Bandow, S.; Rao, A.M.; Williams, K.A.; Thess, A.; Smalley, R.E.; Eklund, P.C. *J. Phys. Chem. B*, **1997**, 101, 8839.

86. Curran, S.A.; Ajayan, P.M.; Blau, W.J.; Carroll, D.L.; Coleman, J.N.; Dalton, A.B.; Davey, A.P.; Drury, A.; McCarthy, B.; Maier, S.; Stevens, A. *Adv. Mater*., **1998**, 10, 1091.

87. Star, A.; Stoddart, J.F.; Steuerman, D.; Diehl, M.; Boukai, A.; Wong, E.W.; Yang, X.; Chung, S.W.; Choi, H.; Heath, J.R. *Angew. Chem.,* **2001**, 113, 1771; *Angew. Chem. Int. Ed*., **2001**, 40, 1721.

88. Tsang, S.S.; Guo, Z.; Chen, Y.K.; Green, M.L. H.; Hill, H.A. O.; Hambley, T.W.; Sadler, P.J. *Angew. Chem.,* **1997**, 109, 2291.

89. Guo, Z.; Sadler, P.J.; Tsang, S.C. *Adv. Mater*., **1998**, 10, 701.

90. Chen, R.J.; Zhang, Y.; Wang, D.; Dai, H. *J. Am. Chem. Soc*., **2001**, 123, 3838.

91. Nakashima, N. *Sci. Technol. Adv. Mater*., **2006**, 7, 609.

92. Ogoshi, T.; Takashima, Y.; Hiroyasu, Y.; Harada, A. *J. Am. Chem. Soc*., **2007**, 129, 4878.

93. D'Souza, F.; Chitta, R.; Sandanayaka, A.S.D.; Subbaiyan, N.K.; D'Souza, L.; Araki, Y.; Ito, O. *J. Am. Chem. Soc*., **2007**, 129, 15865.

94. Feng, W.; Fujii, A.; Ozaki, M.; Yoshino, K. *Carbon*, **2005**, 43, 2501.

95. Murakami, H.; Nomura, T.; Nakashima, N. *Chem. Phys. Lett.,* **2003**, 378, 481.

96. Hu, C.; Chen, Z.; Shen, A.; Shen, X.; Li, J.; Hu, S. *Carbon*, **2006**, 44, 428.

97. Pantarotto, D.; Briand, J.P.; Prato, M.; Bianco, A. *Chem. Commun*., **2004**, 16.

98. Sayes, C.M.; Liang, F.; Hudson, J.L.; Mendez, J.; Guo, W.; Beach, J.M.; Moore, V.C.; Doyle, C.D.; West, J.L.; Billups, W.E.; Ausman, K.D.; Colvin, V.L. *Toxicol. Lett*., **2006**, 161, 135.

99. Dumortier, H.; Lacotte, S.; Pastorin, G.; Marega, R.; Wu, W.; Bonifazi, D.; Briand, J.P.; Prato, M.; Muller, S.; Bianco, A. *Nano Lett.,* **2006**, 6, 1522.

100. Sigh, R.; Pantarotto, D.; Lacerda, L.; Pastorin, G.; Klumpp, C.; Prato, M.; Bianco, A.; Kostarelos, K. *Proc. Natl. Acad. Sci*., **2006**, 103, 3357.

101. Guo, J.; Zhang, X.; Li, Q.; Li, W. *Nucl. Med. Biol.,* **2007**, 34, 579.

102. Poland, C.A.; Duffin, R.; Kinloch, I.; Maynard, A.; Wallace, W.A.H.; Seaton, A.; Stone, V.; Brown, S.; Macnee, W.; Donaldson, K. *Nature Nanotech*., **2008**, 3, 423.

103. Liu, A.; Sun, K.; Yang, J.; Zhao, D. *J. Nanopart. Res.,* **2008**, 10, 1303.

104. Schipper, M.L.; Nakayama-Ratchford, N.; Davis, C.R.; Kam, N.W.S.; Chu, P.; Liu, Z.; Sun, X.; Dai, H.; Gambhir, S.S. *Nature Nanotech.,* **2008**, 3, 216.

105. Hu, H.; Ni, Y.; Montana, V.; Haddon, R.C.; Parpura, V. *Nano Lett.*, **2004**, 4, 507.

106. Feazell, R.P.; Ratchford, N.N.; Dai, H.; Lippard, S.J. *J. Am. Chem. Soc.*, **2007**, 129, 8438.

107. Chen, J.; Chen, S.; Zhao, X.; Kuznetsova, L.V.; Wong, S.S.; Ojima, I. J. Am. Chem. Soc., **2008**, 130, 16778.

108. Kam, N.W.S.; Jessop, T.C.; Wender, P.A.; Dai, H. *J. Am. Chem. Soc.*, **2004**, 126, 6850.

109. Kostarelos, K.; Lacerda, L.; Pastorin, G.; Wu, W.; Wieckowski, S.; Luangsivilay, J.; Godefroy, S.; Pantarotto, D.; Briand, J.P.; Muller, S.; Prato, M.; Bianco, A., *Nature Nanotech.*, **2007**, 2, 108.

110. Liu, Z.; Cai, W.; He, L.; Nakayama, N.; Chen, K.; Sun, X.; Chen, X.; Dai, H. *Nature Nanotech.,* **2007**, 2, 47.

111. Xu, Z.; Hu, P.; Wang, S.; Wang, X. *Appl. Surf. Sci.*, **2008**, 254, 1915.

112. Chen, R.J.; Bangsaruntip, S.; Drouvalakis, K.A.; Kam, N.W.S.; Shim, M.; Li, Y.; Kim, W.; Utz, P.J.; Dai, H. *Proc. Natl. Acad. Sci.*, **2003**, 100, 4984.

113. Konig, K. *J. Microsc.*, **2000**, 200, 83.

114. Kam, N.W.S.; O'Connell, M.; Wisdom, J.A.; Dai, H. *Proc. Natl. Acad. Sci.*, **2005**, 102, 11600.

115. Gannon, C.J.; Cherukuri, P.; Yakobson, B.I.; Cognet, L.; Kanzius, J.S.; Kittrell, C.; Weisman, R.B.; Pasquali, M.; Schmidt, H.K.; Smalley, R.E.; Curley, S.A. *Cancer*, **2007**, 110, 2654.

116. Kam, N.W.S.; Liu, Z.; Dai, H. *J. Am. Chem. Soc.*, **2005**, 127, 12492.

117. Liu, Z.; Winters, M.; Holodniy, M.; Dai, H. *Angew. Chem. Int. Ed.,* **2007**, 46, 2023.

118. Bhirde, A.A.; Patel, V.; Gavard, J.; Zhang, G.; Souza, A.A.; Masedunskas, A.; Leapman, R.D.; Weigert, R.; Gutkind, J.S.; Rusling, J.F. *ACS Nano*, **2009**, 3, 307.

119. Balzani, V.; Credi, A.; Venturi, M. *Molecular Devices and Machines – A Journey into the Nano World,* Wiley-VCH, **2002**.

120. Turro, N.J. *Modern Molecular Photochemistry*, University Science Books, Sausalito, **1991.**

121. Dexter, D.L. *J. Chem. Phys.*, **1953**, 21, 836.

122. Prathapan, S.; Johnson, T.E.; Lindsey, J.S. *J. Am. Chem. Soc.,* **1993**, 115, 7519.

123. Kim, T.G.; Castro, J.C.; Loudet, A.; Jiao, J.G.S.; Hochstrasser, R.M.; Burgess, K., Topp, M.R. J. Phys. Chem., 2006, 110, 20.

124. Barigelletti, F.; Flamigni, L. *Chem. Soc. Rev.*, **2000**, 29, 1.

125. Förster, T. *Disc. Faraday Soc.*, **1959**, 27, 7.

126. Valeur, B. *Molecular Fluorescence, Principles and Applications*, Wiley-WC, **2002**.

127. Lakowicz, J.R. *Principles of Fluorescence Spectroscopy*, Kluwer Acadamic, Plenum Publishers, **1999**.

128. Sharma, A.; Schulman, S.G. *Introduction to Fluorescence Spectroscopy*, Wiley Science, **1999**.

129. Adronov, A.; Gilat, S.L.; Frechet, J.M.J.; Ohta, K.; Neuwahl, F.V.R.; Fleming, G.R. *J. Am. Chem. Soc.*, **2000**, 122, 1175.

130. Yilmaz, M.D.; Bozdemir, O.A.; Akkaya, E.U. *Org. Lett.*, **2006**, 8, 2871.

131. Barın, G.; Yilmaz, M.D.; Akkaya, E.U. *Tet. Lett.*, **2009**, 50, 1738.

132. Azov, V.A.; Schlegel, A.; Diederich, F. *Angew. Chem., Int. Ed.,* **2005**, 44, 4635.

133. Nelson, N.; Ben-Shem, A. *Nat. Rev.*, **2004**, 5, 971.

134. Serin, J.M.; Brousmiche, D.W.; Frechet, J.M.J. *J. Am. Chem. Soc.*, **2002**, 124, 11848.

135. Brousmiche, D.W.; Serin, J.M.; Frechet, J.M.J.; He, G.S.; Lin, T.-C.; Chung, S. J.; Prasad, P.N. *J. Am. Chem. Soc.*, **2003**, 125, 1448.

136. Balzani, V.; Ceroni, P.; Gestermann, S.; Kauffmann, C.; Gorka, M.; Vögtle, F. *Chem. Commun.*, **2000**, 853.

137. Bignozzi, C.A.; Argazzi, R.; Kleverlaan, C.J. *Chem. Soc. Rev.*, **2000**, 29, 87.

138. Adronov, A.; Frechet, J.M.J. *Chem. Commun.*, **2000**, 1701.

139. Hu, X.; Damjanavic, A.; Ritz, T.; Schulten, K. *Proc. Natl. Acad. Sci. USA*. **1998**, 95, 5935.

140. Lehninger, A.L.; Nelson, D.L.; Cox, M.M. *Principles of Biochemistry,* Worth Publishers Inc., New York, **1993**.

141. Xu, X.; Damjanovic, A.; Ritz, T.; Schulten, K. *Proc.Natl. Acad. Sci. USA*., **1998**, 95, 5935.

142. Takahashi, R.; Kobuke, Y. *J. Am. Chem. Soc*., **2003**, 125, 2372.

143. Maligaspe, E.; Tkachenko, N.V.; Subbaiyan, N.K.; Chitta, R.; Zandler, M.E.; Lemmetyinen, H.; D'Souza, F. *J. Phys. Chem. A.,* **2009**, 113, 8478.

144. Campagna, S.; Denti, G.; Serroni, S.; Ciano, M.; Juris, A.; Balzani, V. *Inorg. Chem*., **1992**, 31, 2982.

145. Denti, G.; Champagna, S.; Serroni, S.; Ciano, M.; Balzani, V. *J. Am. Chem. Soc*., **1992**, 114, 2944.

146. Xu, Z.; Moore, J.S. *Acta Polym*., **1994**, 45, 83.

147. Kawa, M.; Frechet, J.M.J. *Chem. Mater*., **1998**, 10, 286.

148. Li, J.; Ambroise, A.; Yang, S.I.; Diers, J.R.; Seth, J.; Wack, C.R.; Bocian, D.F.; Holten, D.; Lindsey, J.S. *J. Am. Chem. Soc*., **1999**, 121, 8927.

149. Nakamura, Y.; Hwang, I.-W.; Aratani, N.; Ahn, T.K.; Ko, D.M.; Takagi, A.; Kawai, T.; Matsumoto, T.; Kim, D.; Osuka, A. *J. Am. Chem. Soc*., **2005**, 127, 236.

150. Serin, J.M.; Brousmiche, D.W.; Frechet, J.M.J. *Chem. Commun*., **2002**, 2605.

151. *Pat.,* 528 398. 2007. *US Pat*., 7 301 003, 2025.

152. Christian, W.T.; Christensen, C.; Meldal, M. *J. Org. Chem.,* **2002**, 67, 3057.

153. Z. Liu, W. Cai, L. He, N. Nakayama, K. Chen, X. Sun, *Nature Nanotechn.*, **2007**, 2,47.

154. *Pat*. 424 165. 2008. *USPTO*., 20080233047.

155. Wyszogrodzka, M.; Haag, R. *Chem. Eur. J*., **2008**, 14, 9202.

156. Shim, M.; Kam, N.W.S.; Chen, R.J.; Li, Y.; Dai, H. *Nano Lett*., *2002*, 2, 285.

157. Liu, Z.; Davis, C.; Cai, W.; He, L.; Chen, X., Dai, H. *Proc. Natl. Acad. Sci.,* **2008**, 105, 1410.

158. Guldi, D.M.; Rahman, G.M.A.; Jux, N.; Balbinot, D.; Hartnagel, U.; Tagmatarchis, N.; Prato, M. *J. Am. Chem. Soc*., **2005**, 127, 9830.

159. Alvaro, M.; Atienzar, P.; Bourdelande, J.L.; Garcia, H. *Chem. Phys. Lett*., **2004**, 384, 119.

160. Gomez, F.J.; Chen, R.J.; Wang, D.; Waymouth, R.M.; Dai, H. *Chem. Commun*., **2003**, 190.

161. Guo, Z.; Du, F.; Ren, D.; Chen, Y.; Zheng, J.; Liu, Z.; Tian, J. *J. Mater. Chem*., **2006**, 16, 3021.

162. Lebedkin, S.; Kareev, I.; Hennrich, F.; Kappes, M.M. *J. Phys. Chem. C*., **2008**, 112, 16236.

163. Hamon, M.A.; Stensaas, K.L.; Sugar, M.A.; Tumminello, K.C.; Allred, A.K. *Chem. Phys. Lett*., **2007**, 447, 1.

164. Liu, J.Y.; Yeung, H.S.; Xu, W.; Li, X.; Ng, D.K.P. *Org. Lett.* **2008**, 10 (23), 5421.

APPENDIX A

NMR SPECTRA

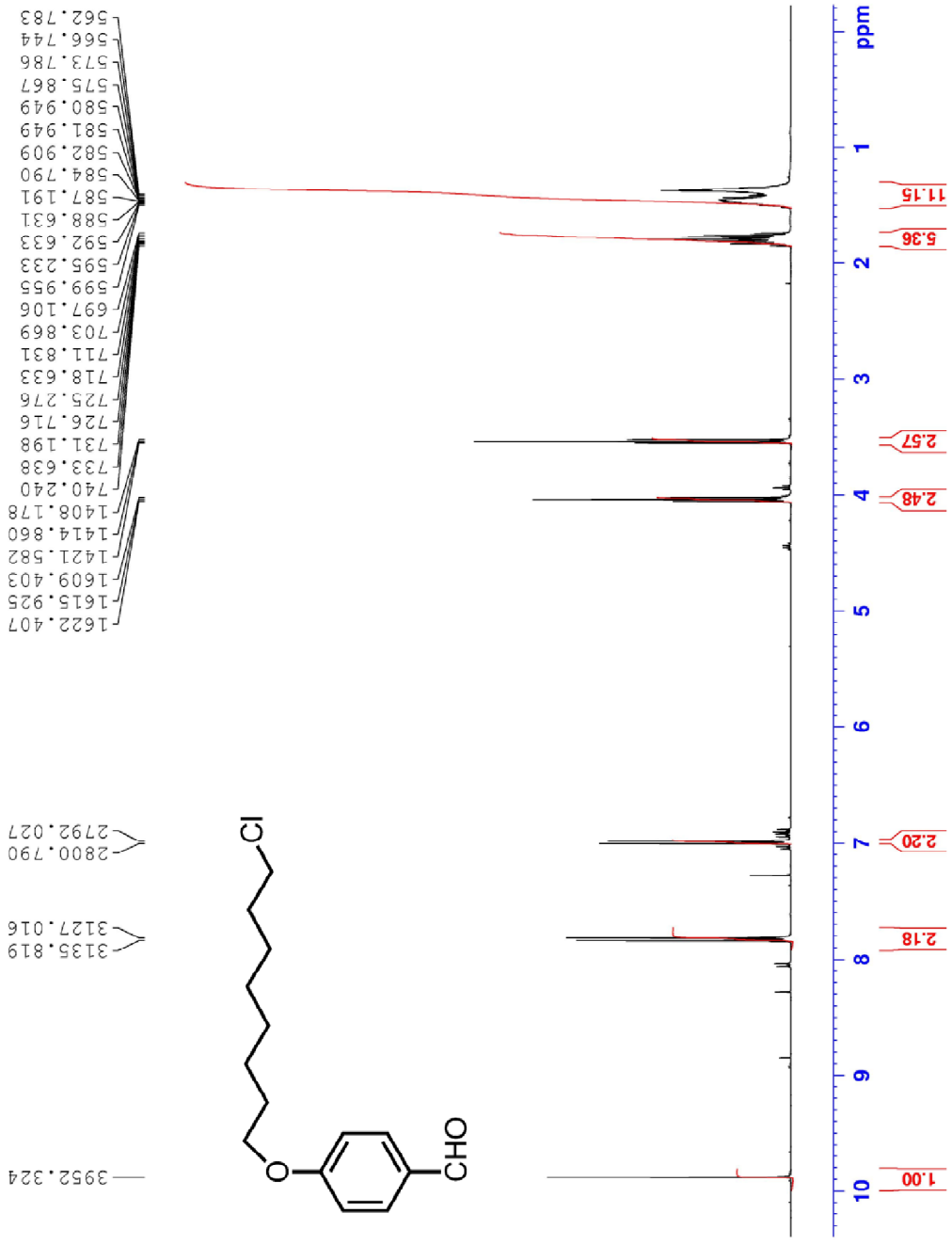

Figure 73. ^{1}H NMR spectrum of compound **3.**

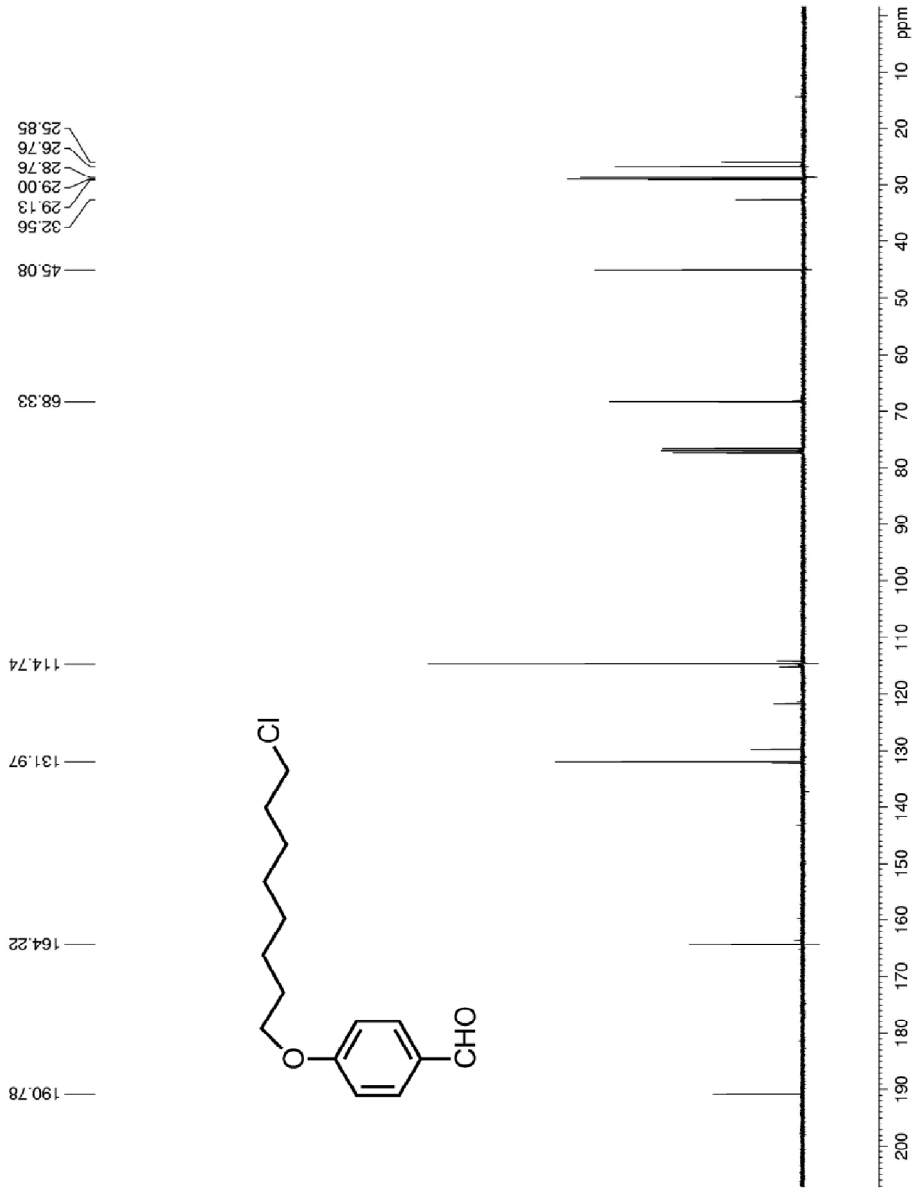

Figure 74. ^{13}C NMR spectrum of compound **3**

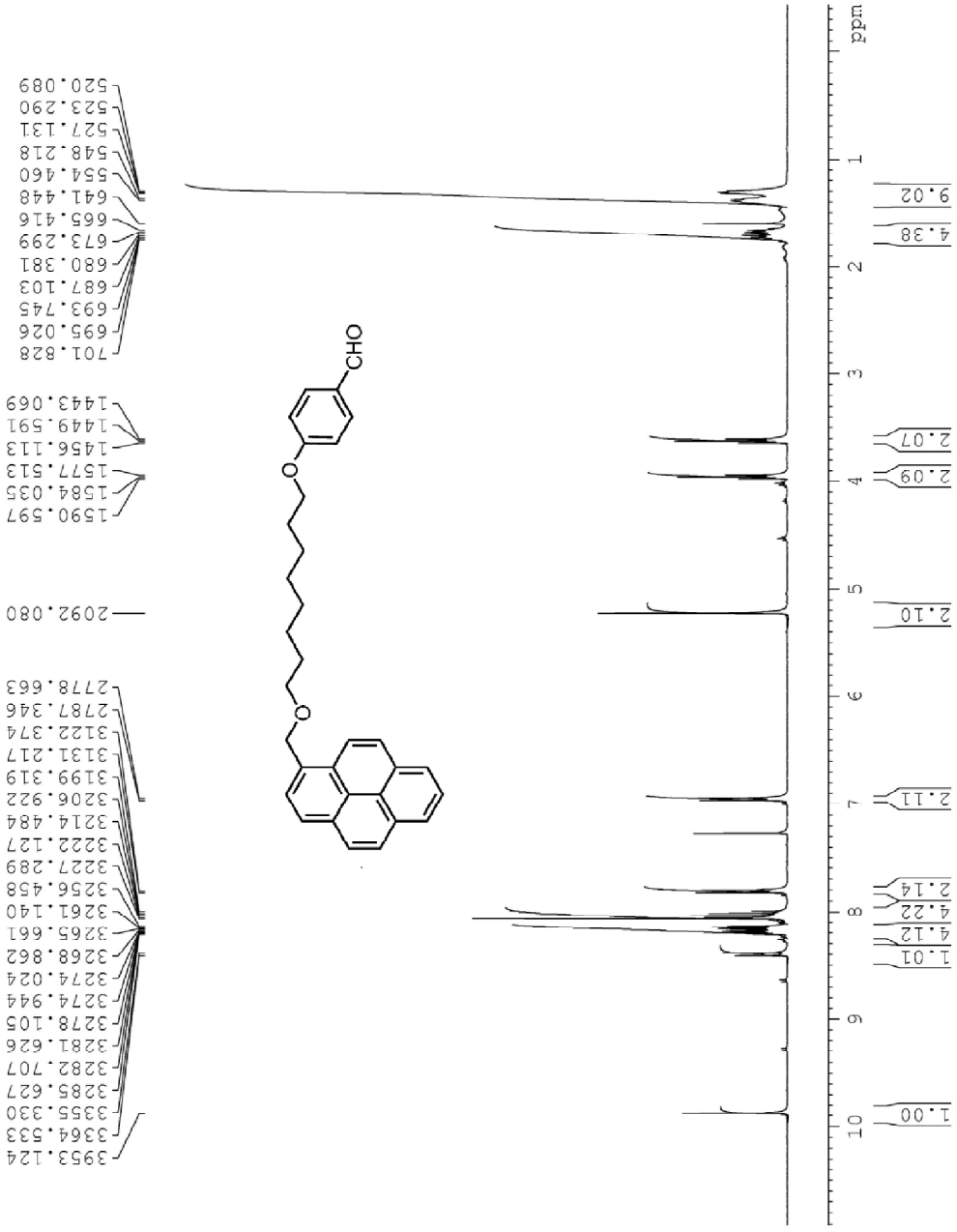

Figure 75. ^{1}H NMR spectrum of compound **4**

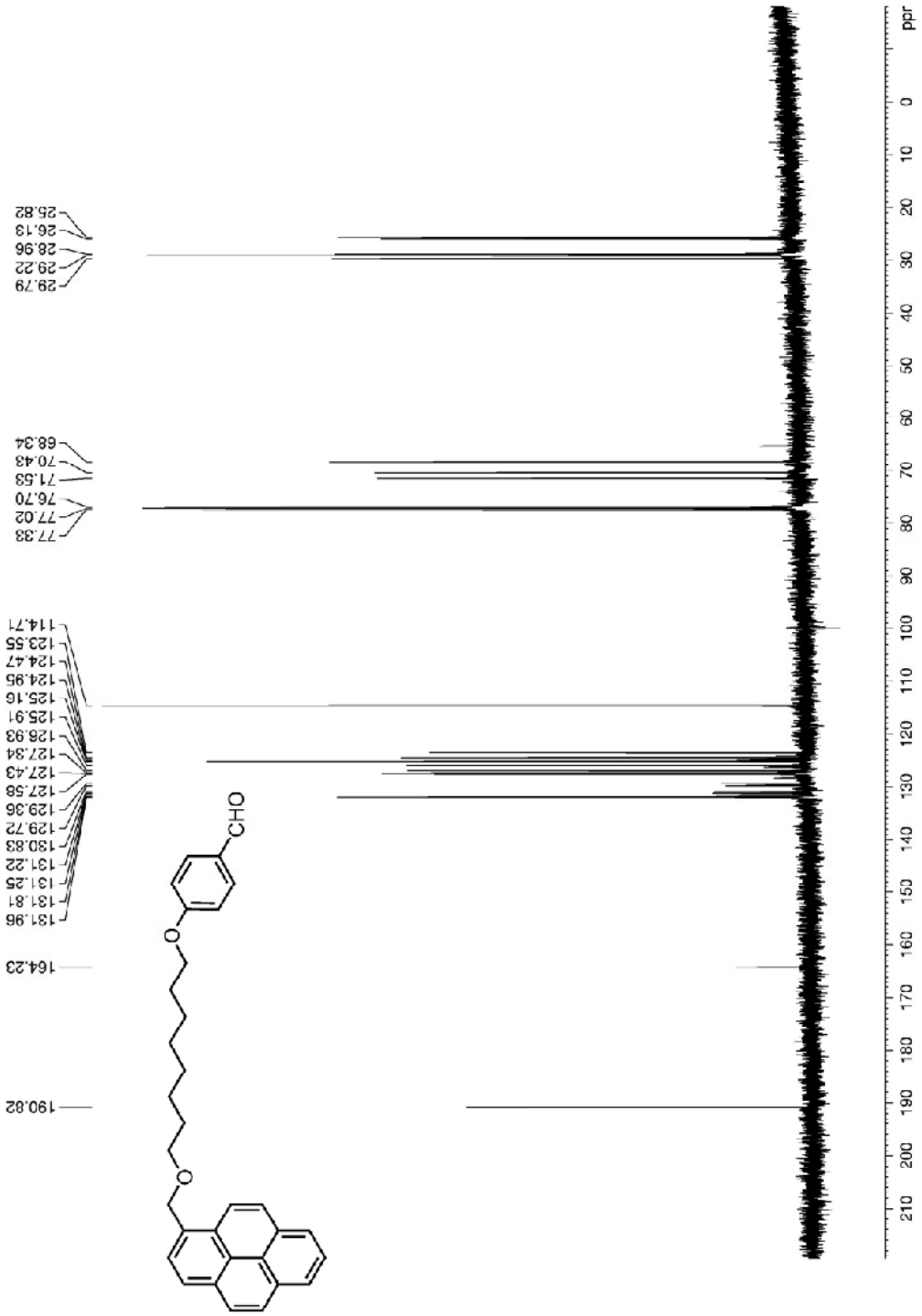

Figure 76. ^{13}C NMR spectrum of compound **4**

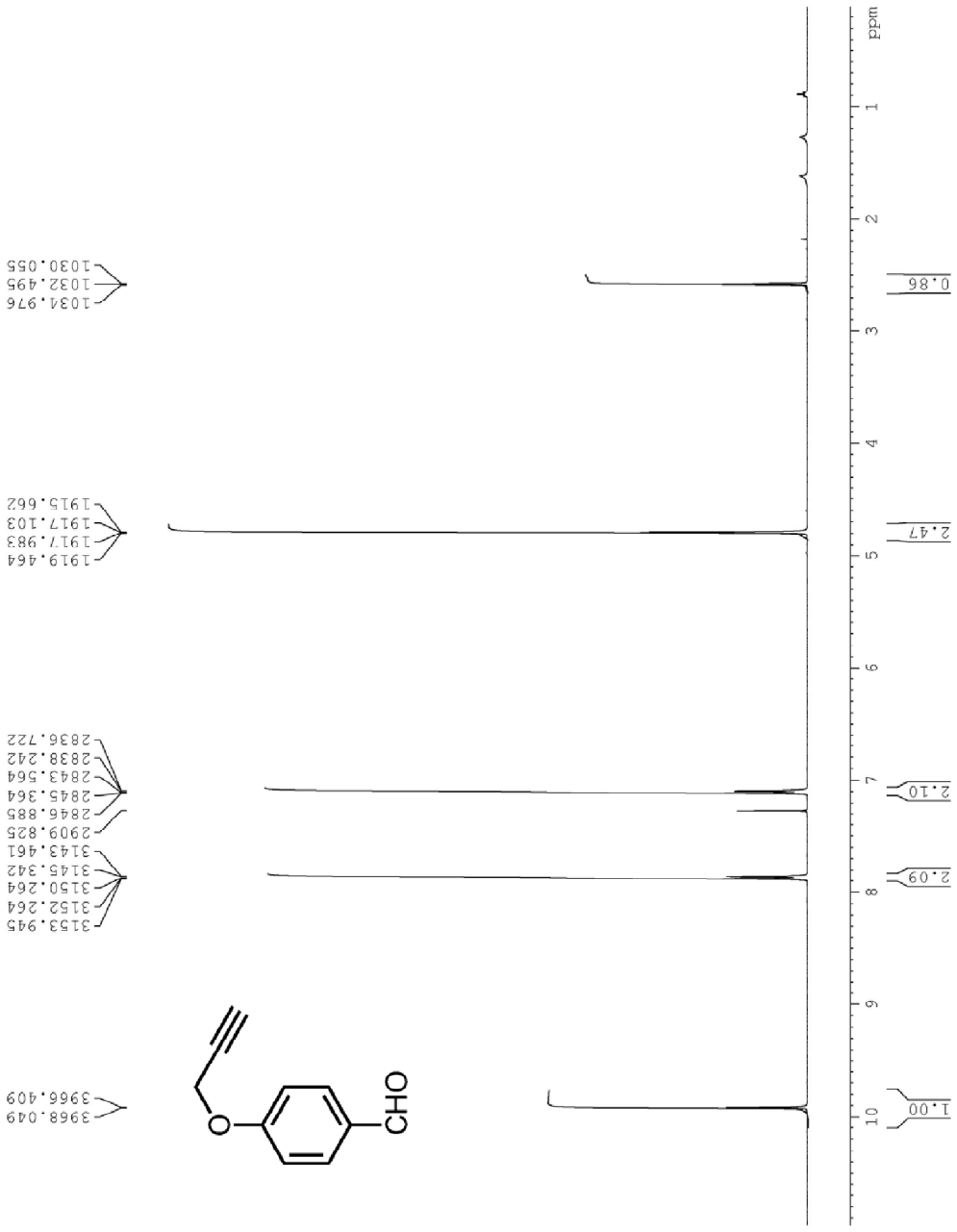

Figure 77. ^{1}H NMR spectrum of compound **5**

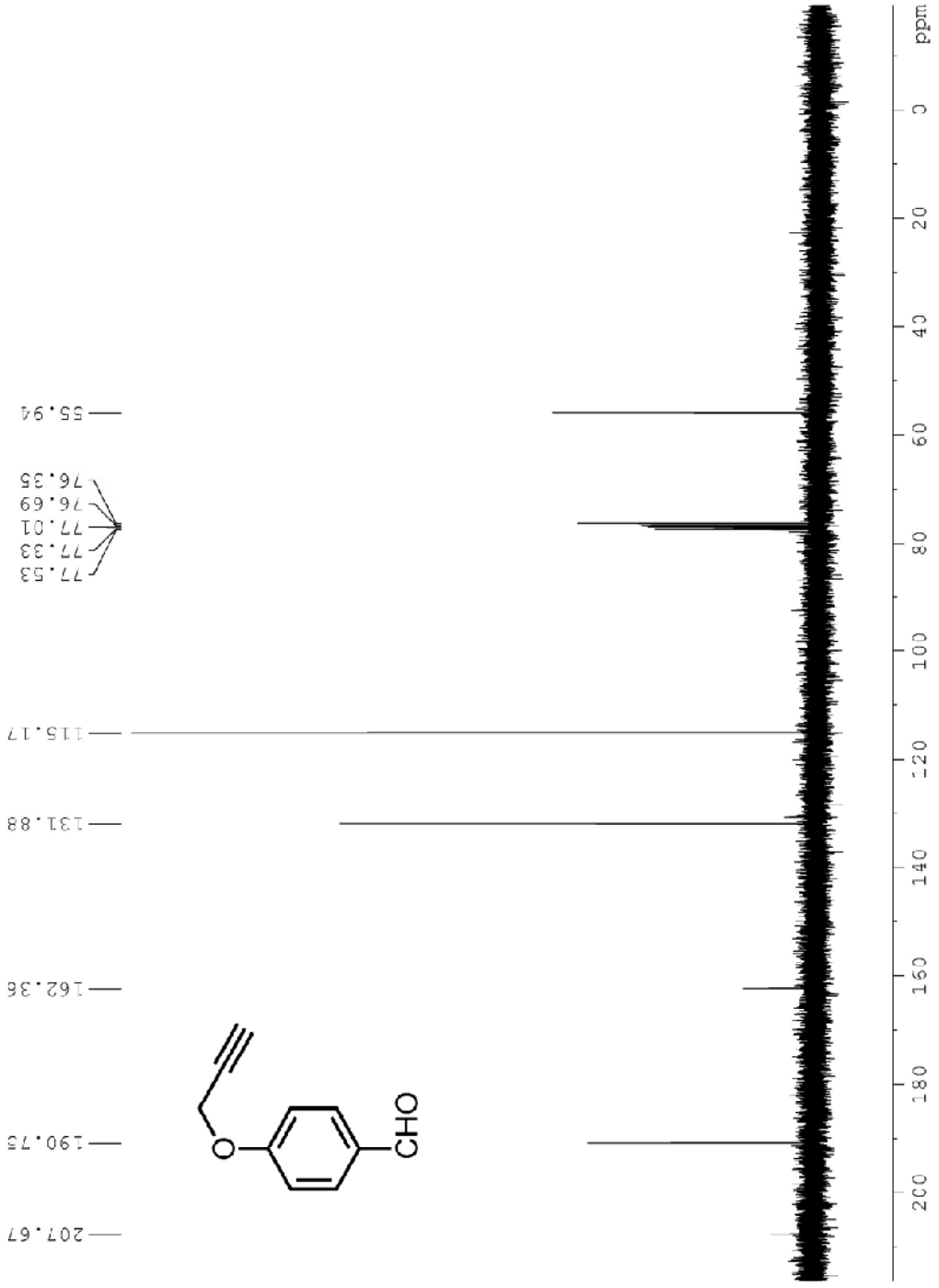

Figure 78. ^{13}C NMR spectrum of compound 5

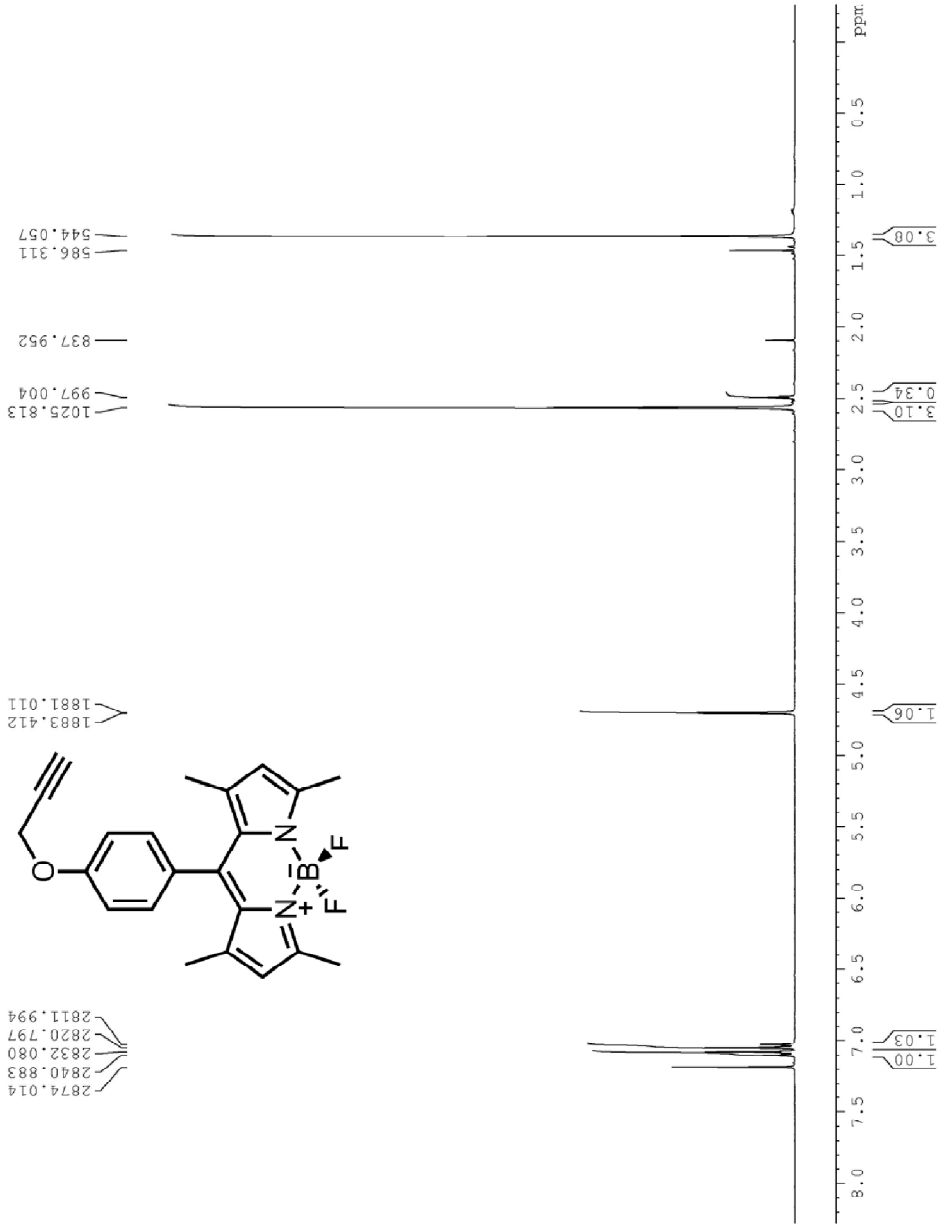

Figure 79. ^{1}H NMR spectrum of compound **6**

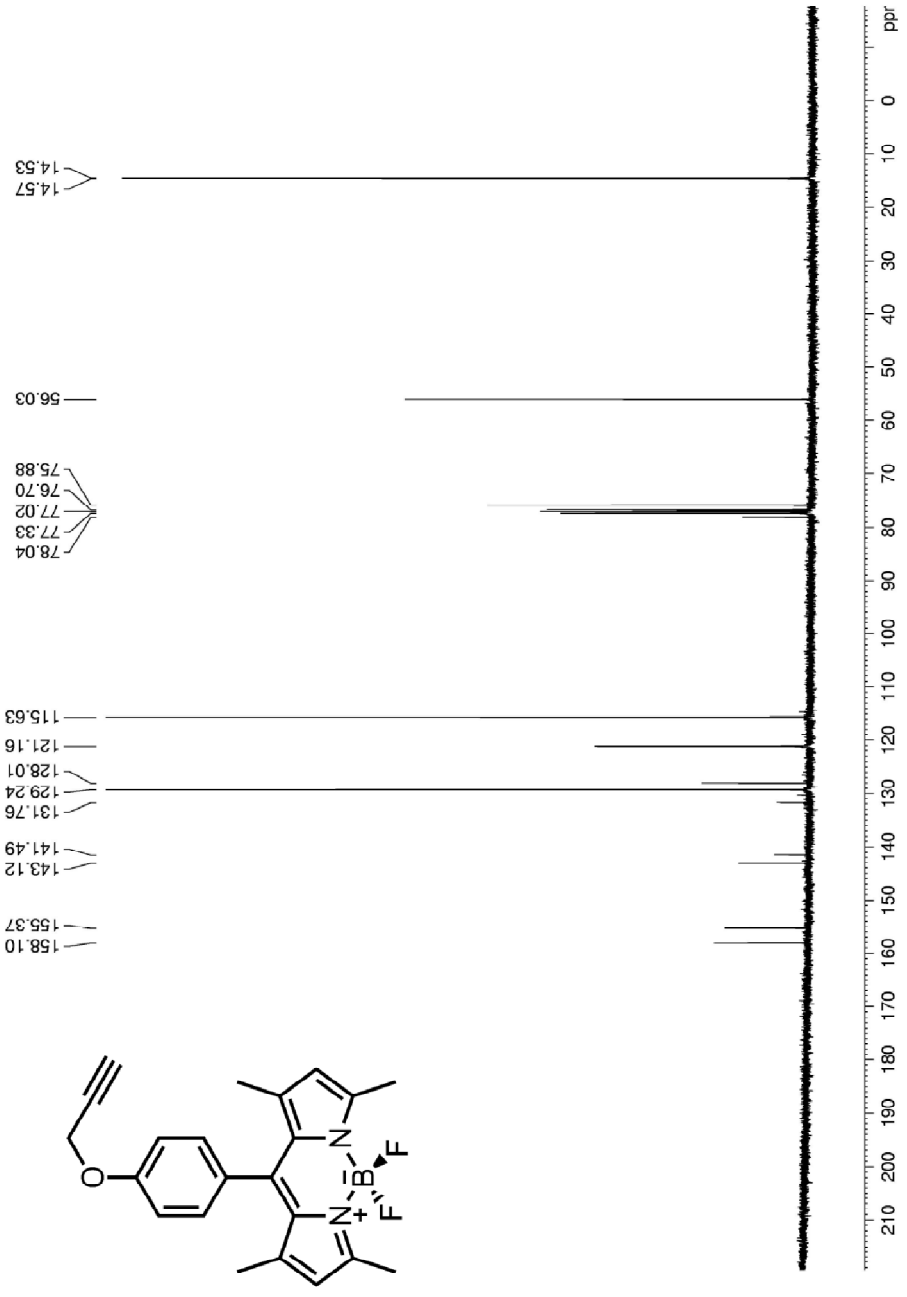

Figure 80. ^{13}C NMR spectrum of compound **6**

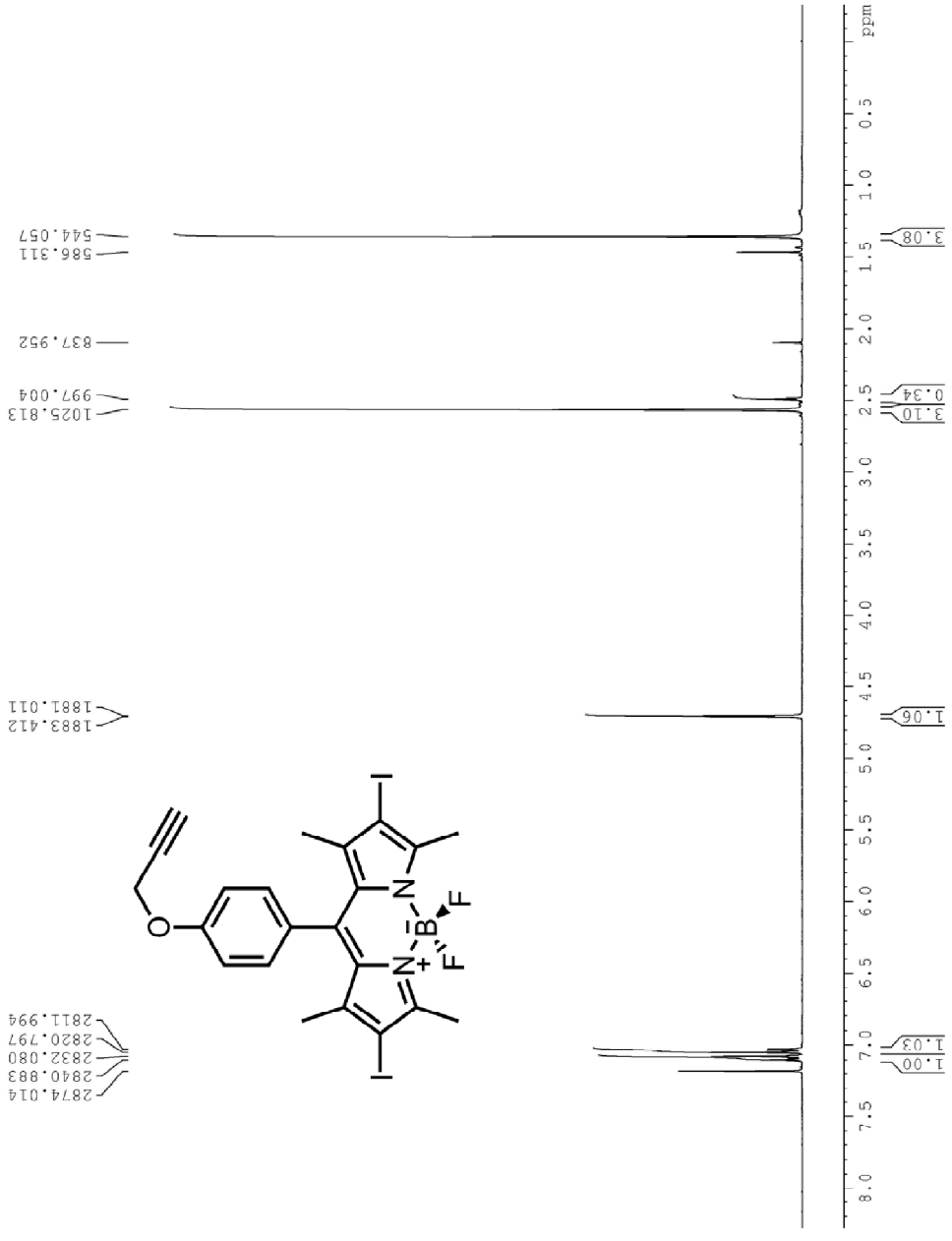

Figure 81. ^{1}H NMR spectrum of compound **7**

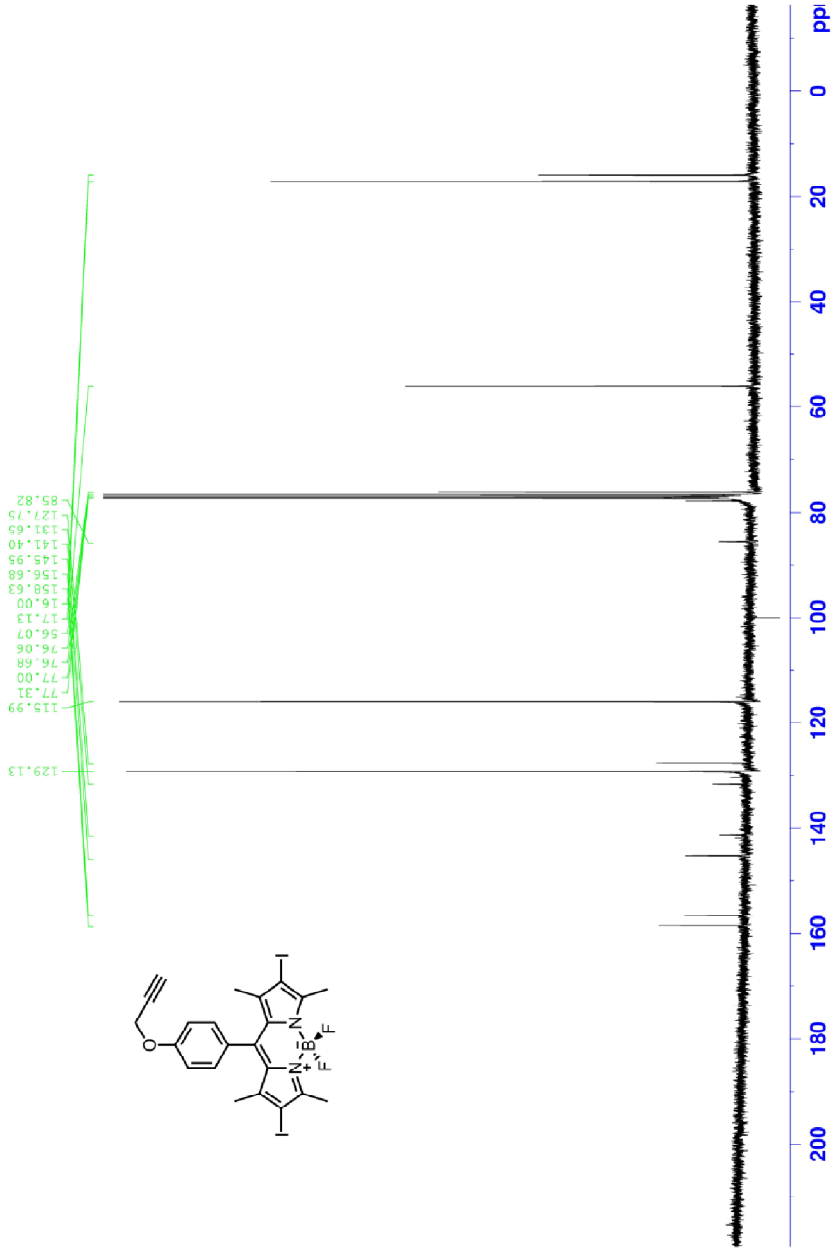

Figure 82. ^{13}C NMR spectrum of compound **7**

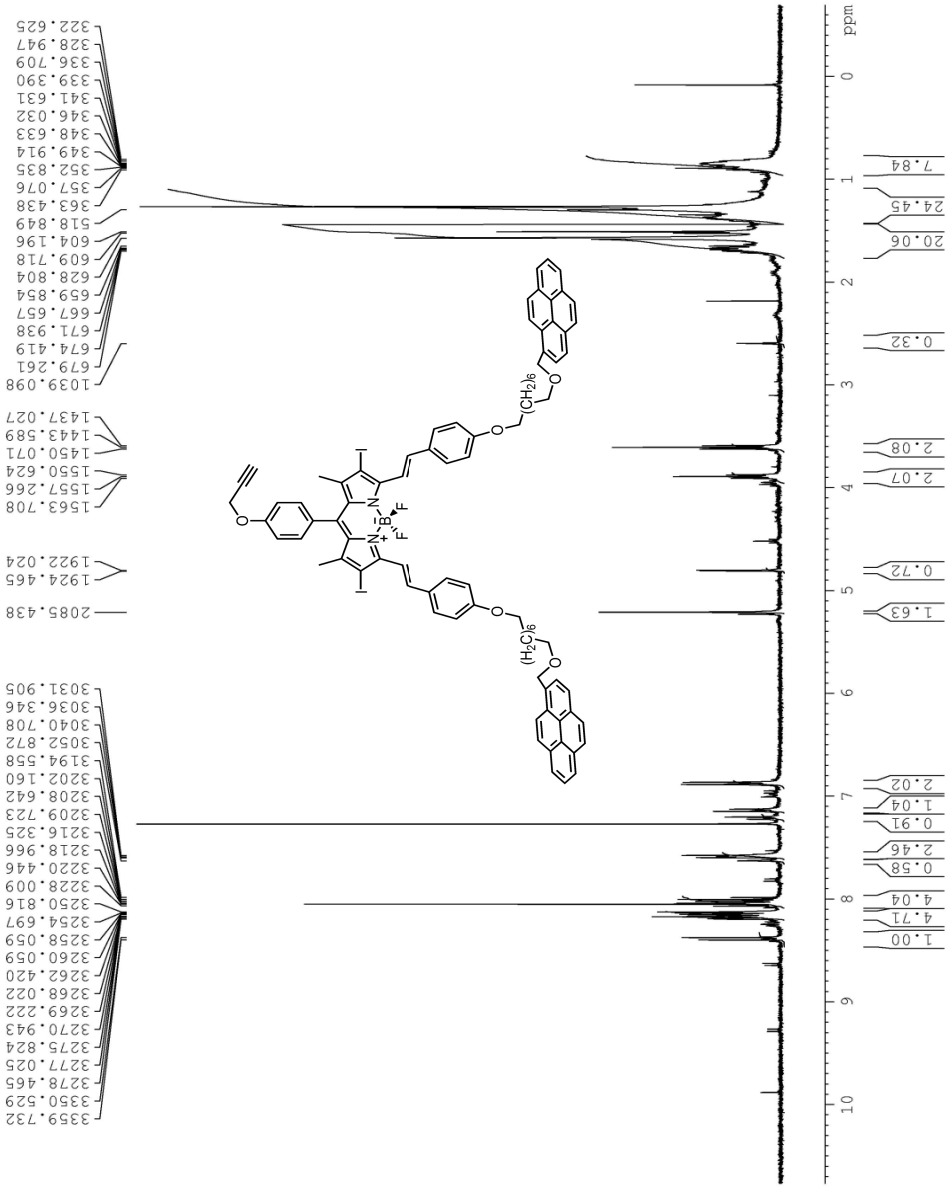

Figure 83. ^{1}H NMR spectrum of compound **8**

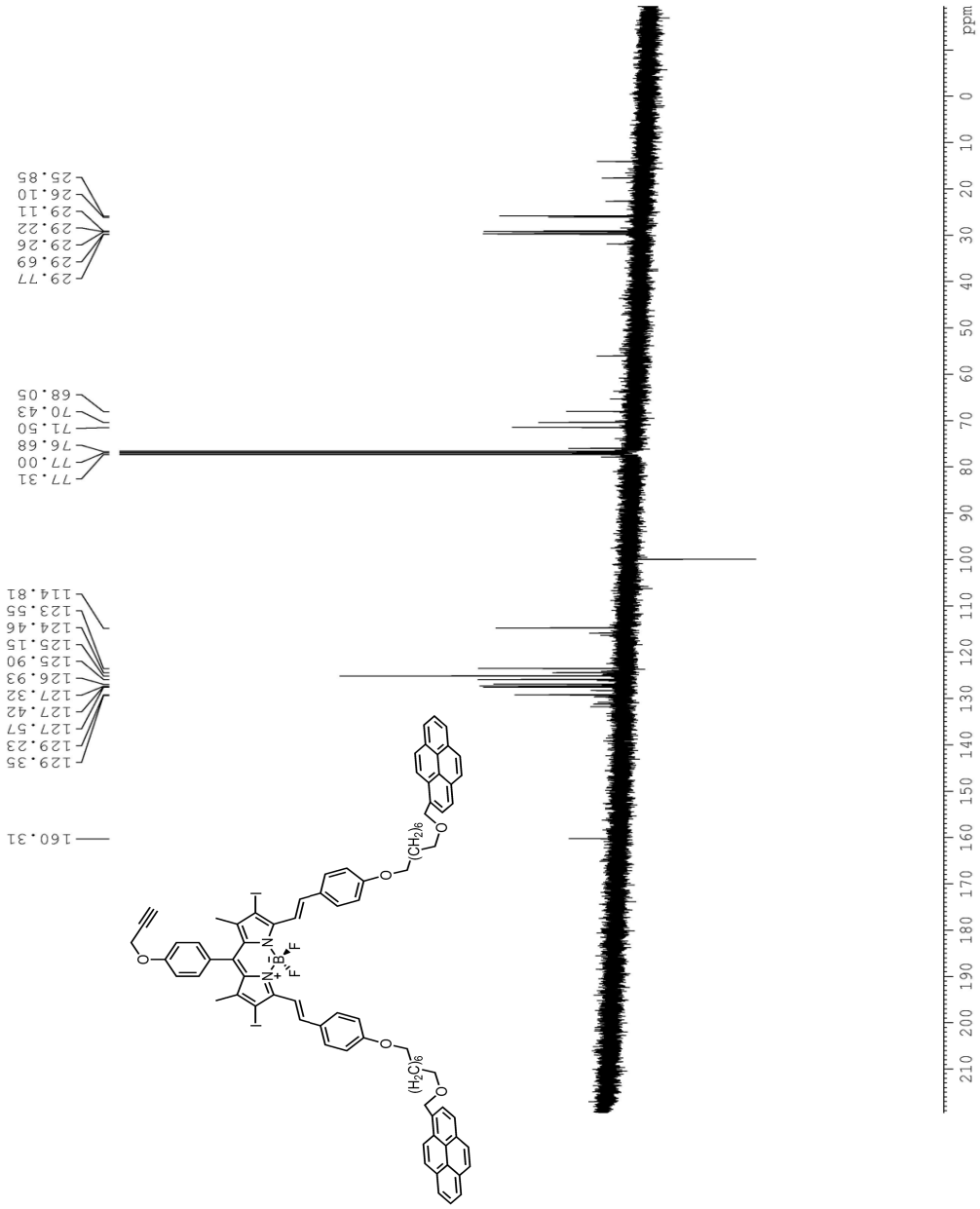

Figure 84. ^{13}C NMR spectrum of compound **8**

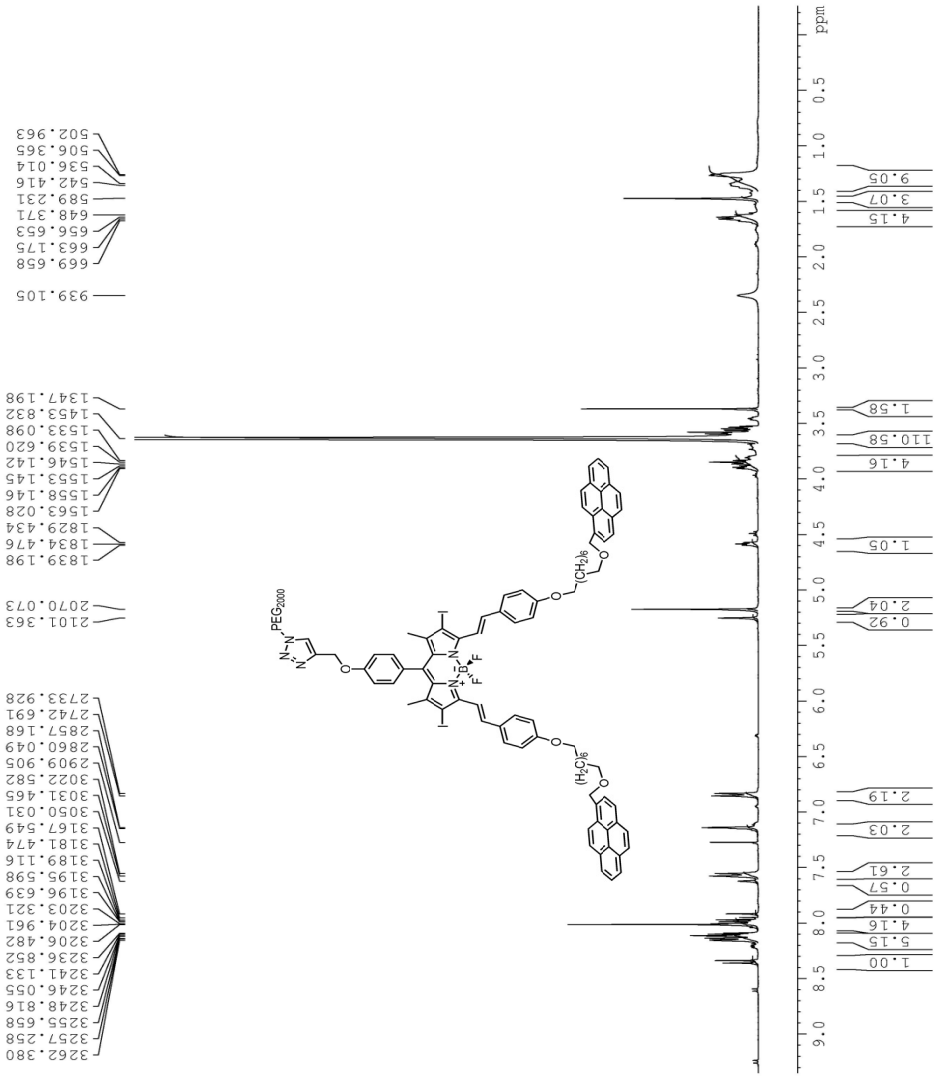

Figure 85. ^{1}H NMR spectrum of compound **1**

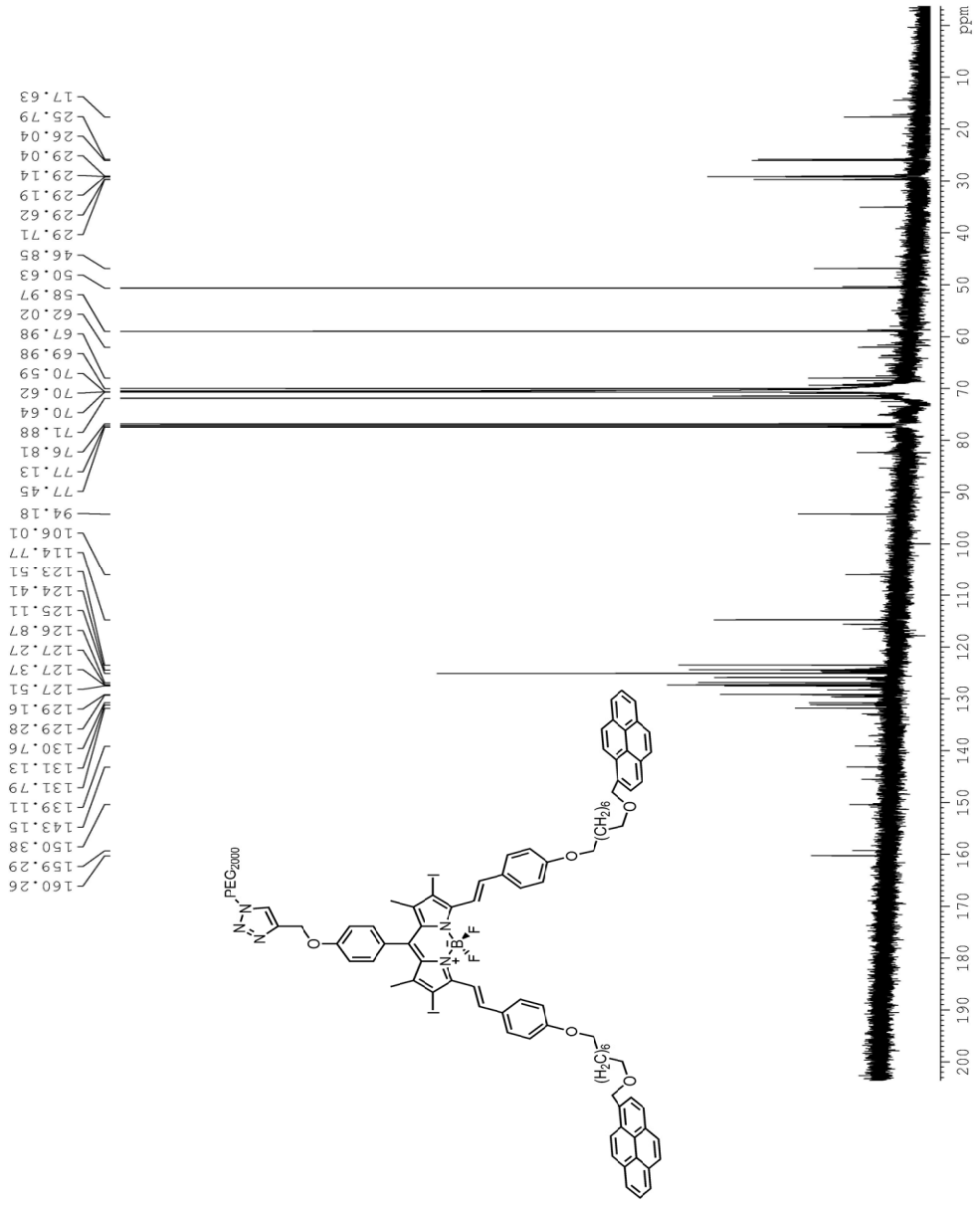

Figure 86. ^{13}C NMR spectrum of compound **1**

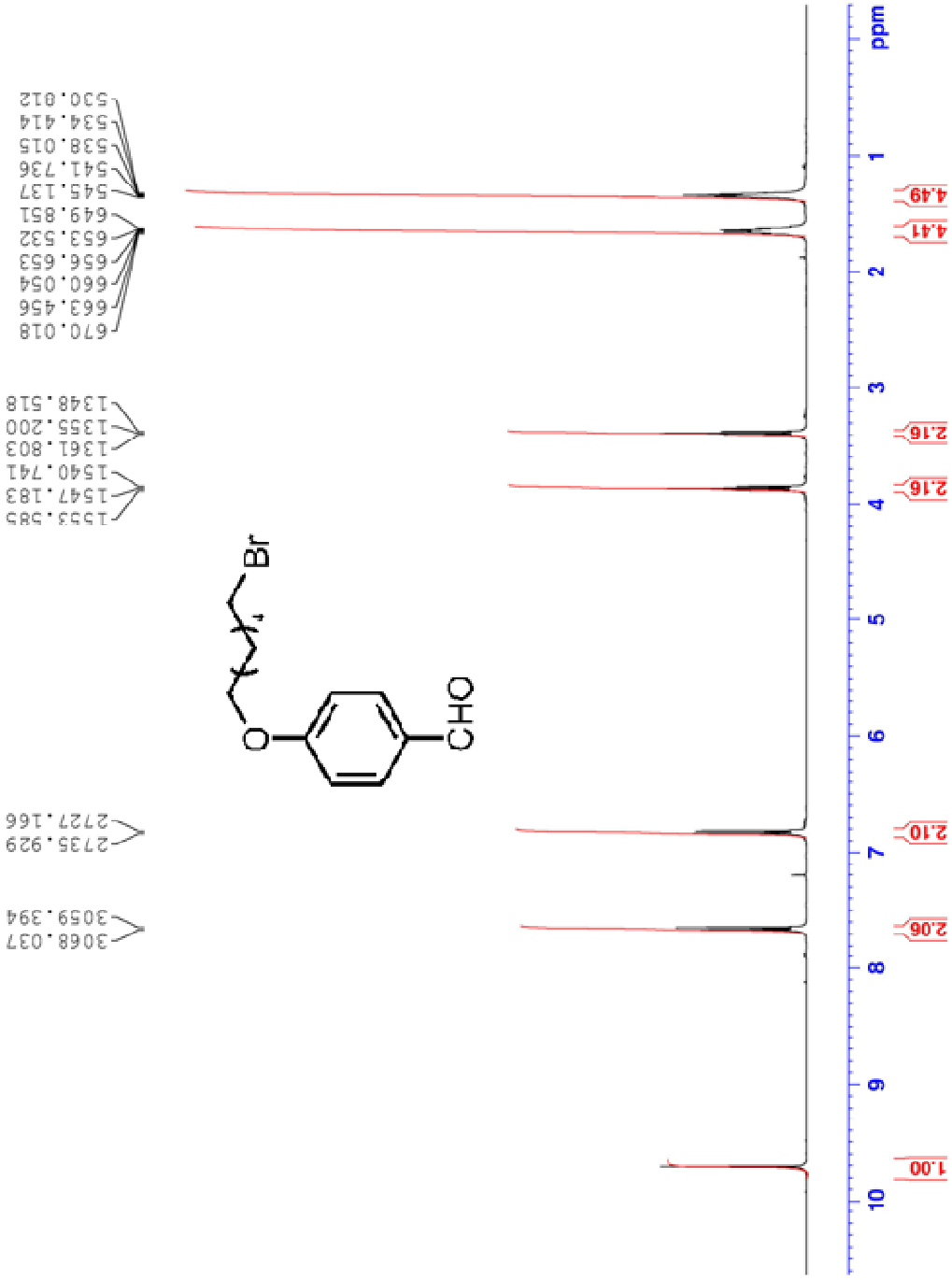

Figure 87. ^{1}H NMR spectrum of compound **9.**

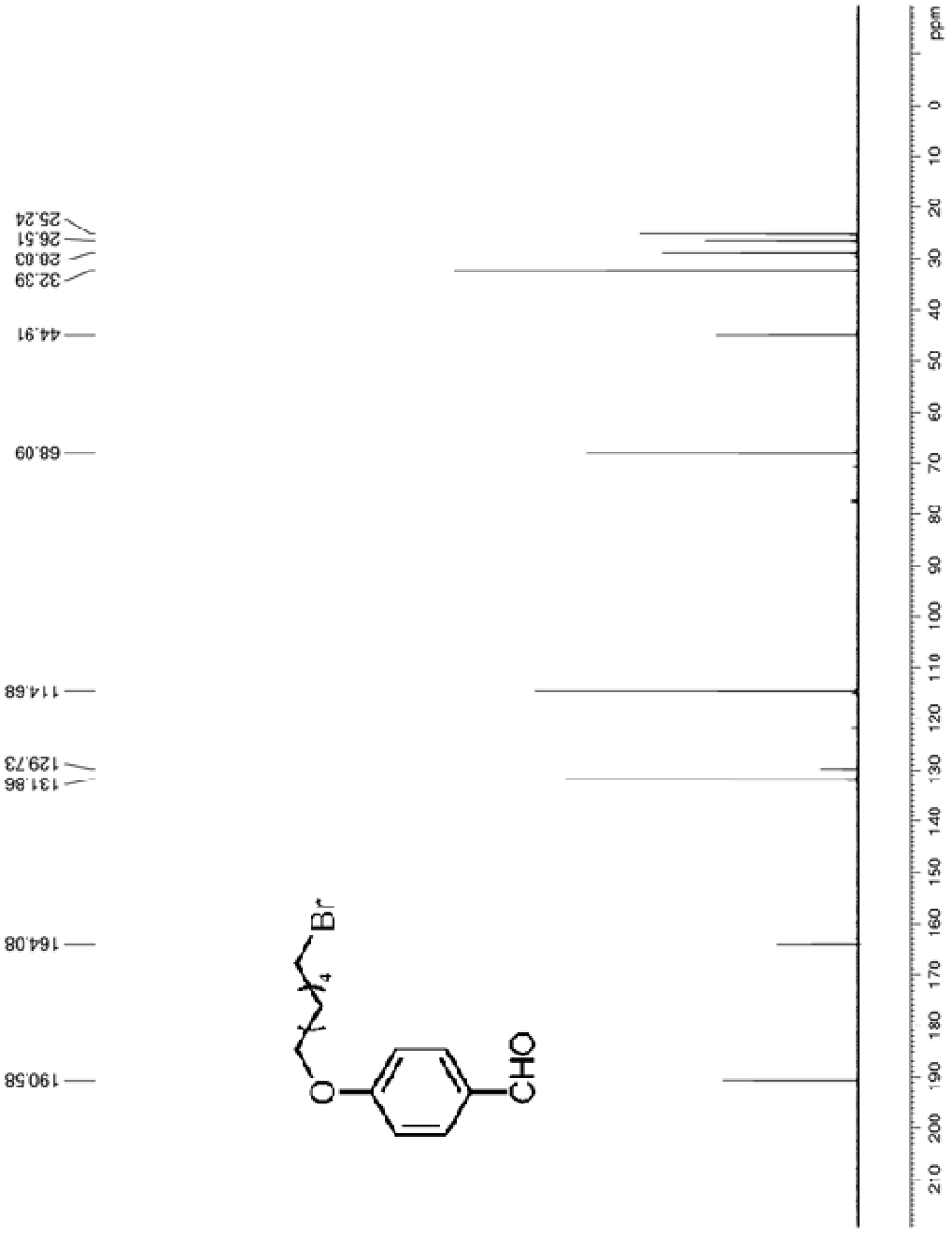

Figure 88. ^{13}C NMR spectrum of compound **9.**

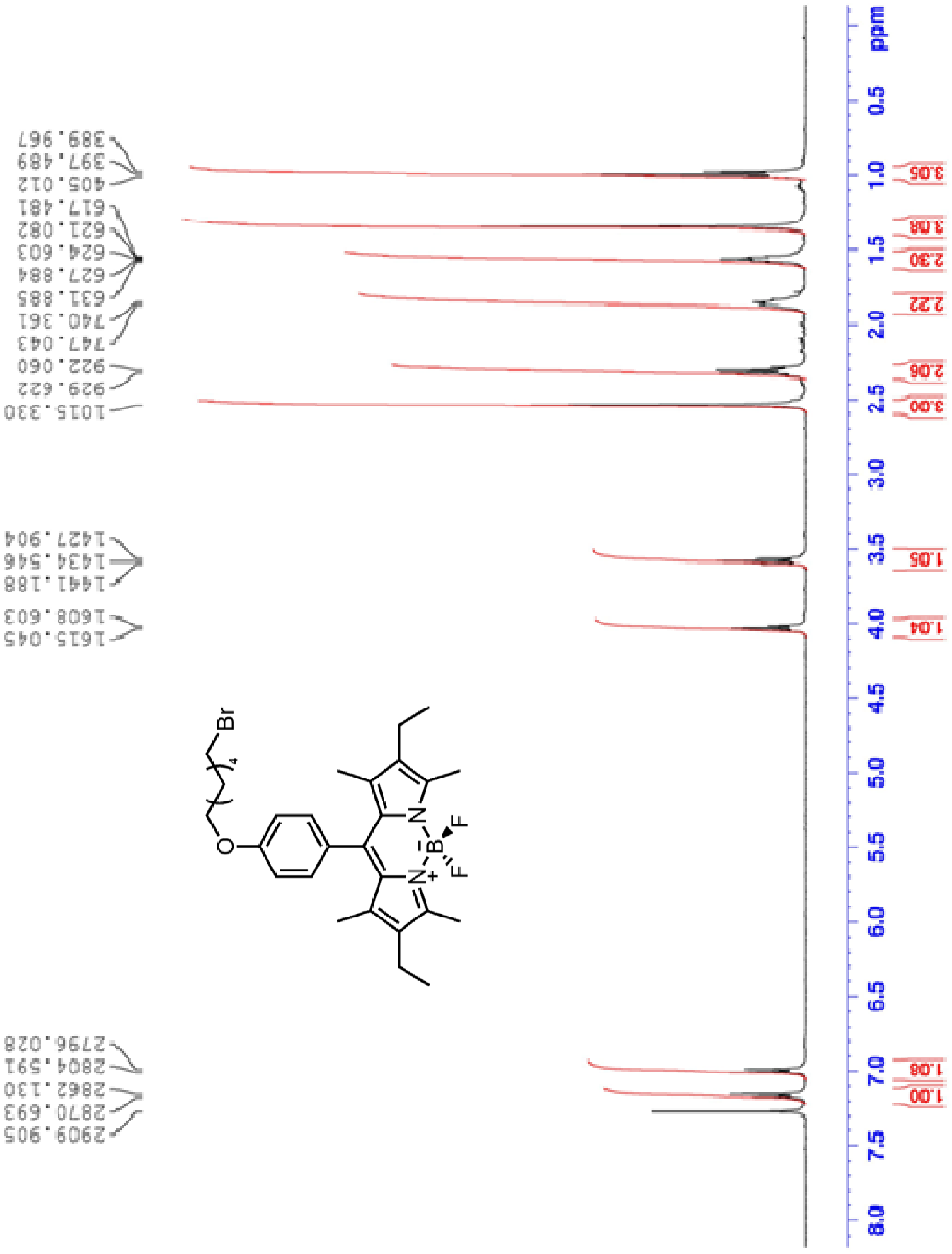

Figure 89. ^{1}H NMR spectrum of compound **10.**

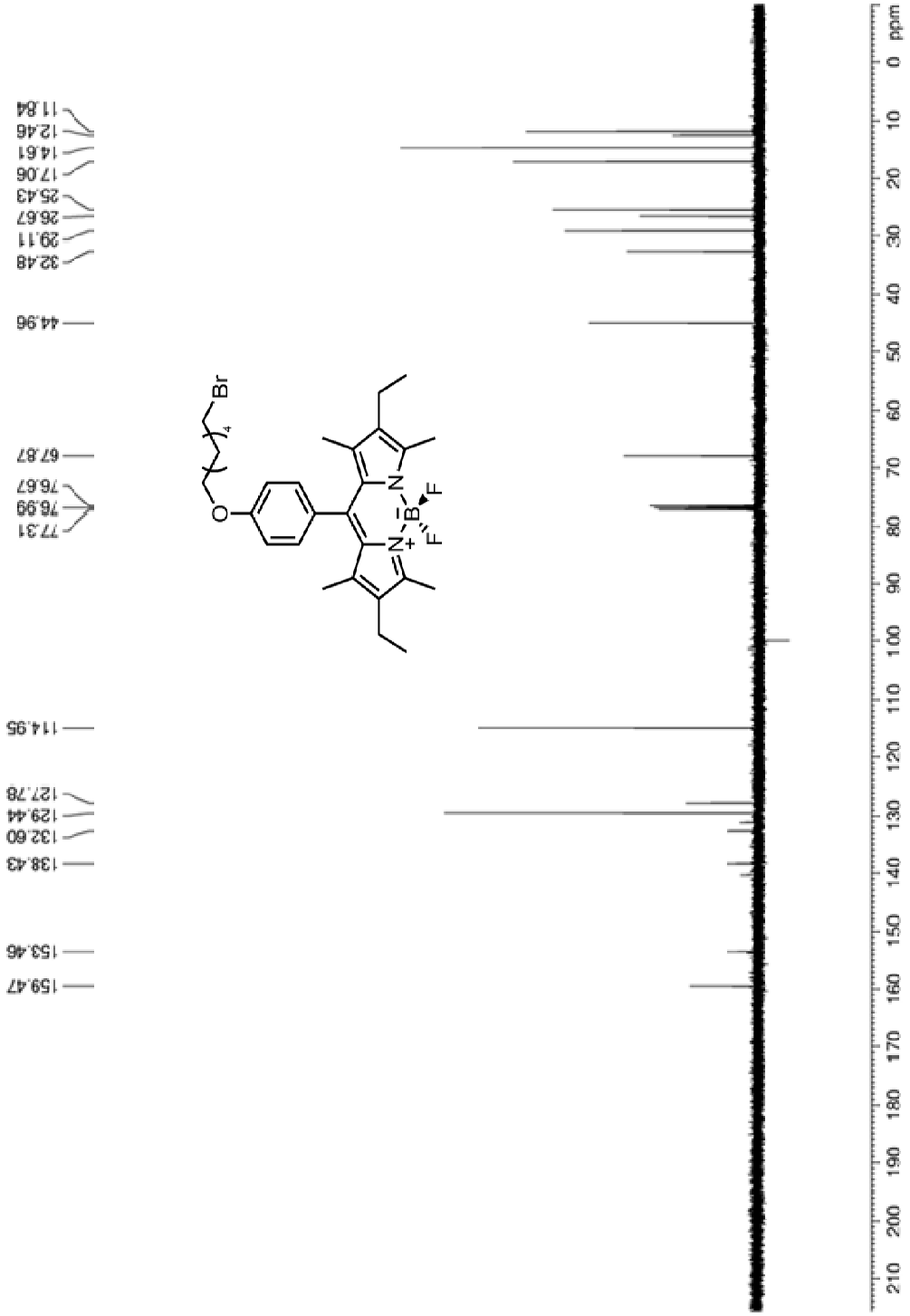

Figure 90. ^{13}C NMR spectrum of compound **10.**

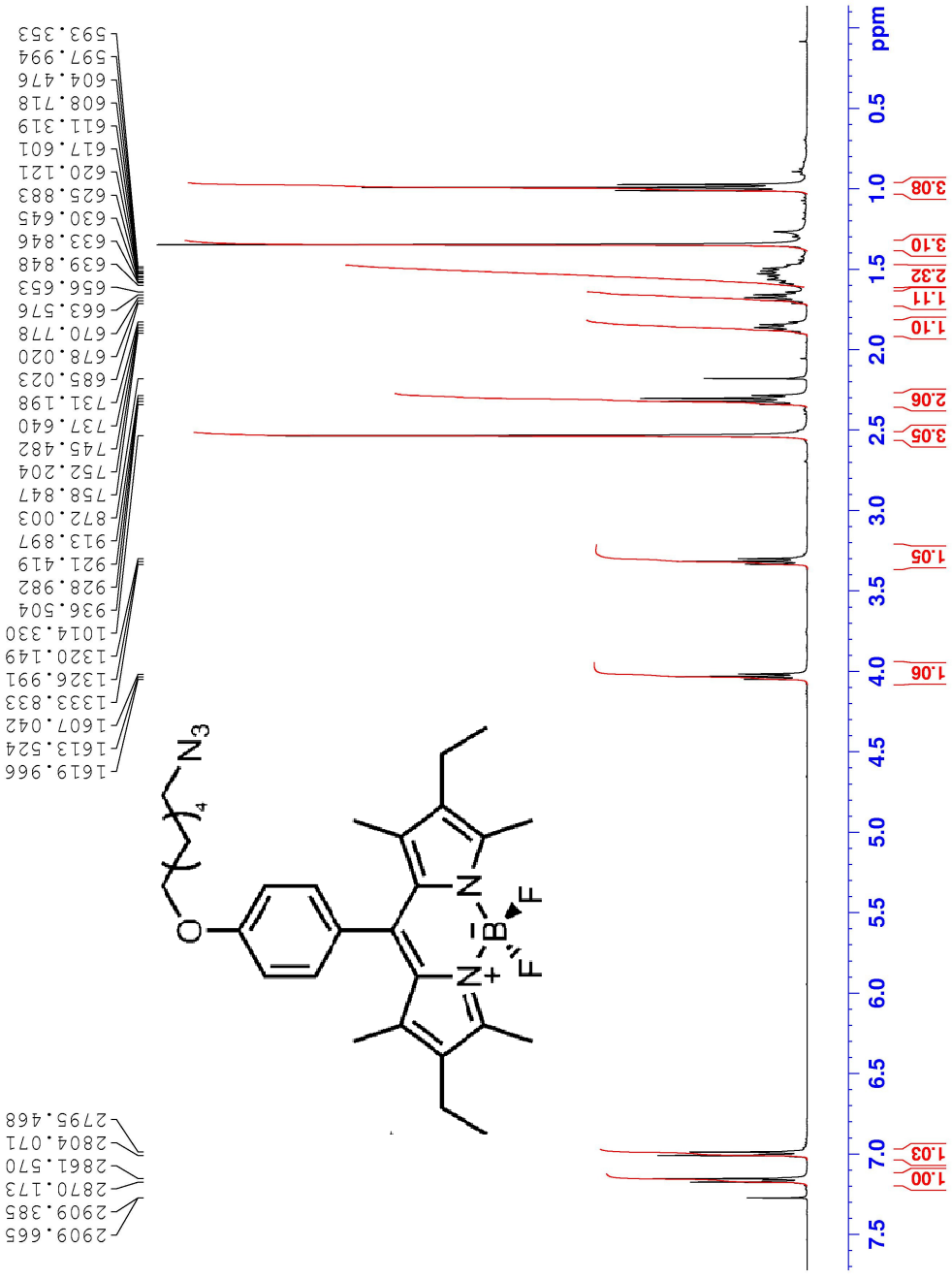

Figure 91. ^{1}H NMR spectrum of compound **11.**

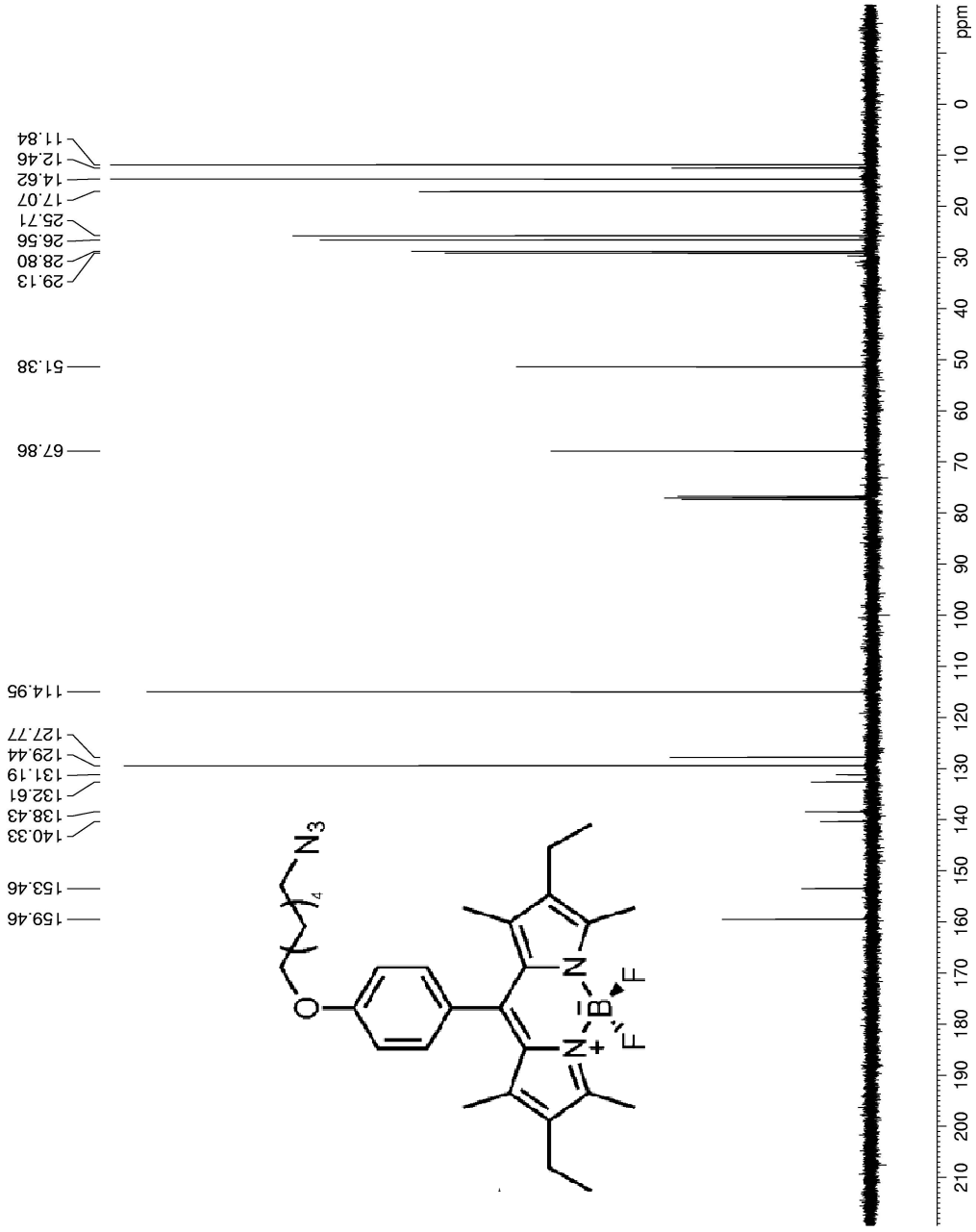

Figure 92. ^{13}C NMR spectrum of compound **11.**

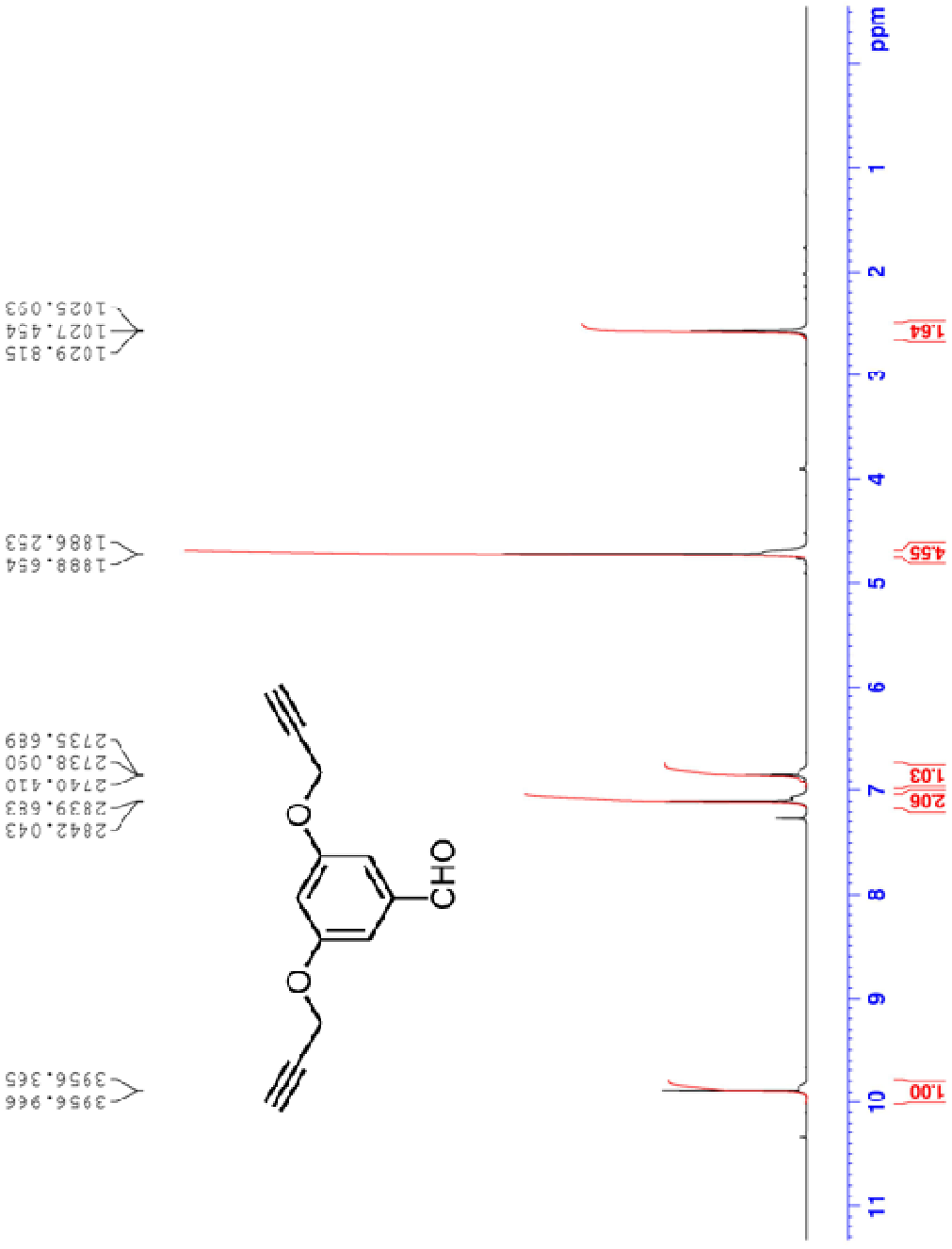

Figure 93. ^{1}H NMR spectrum of compound **13.**

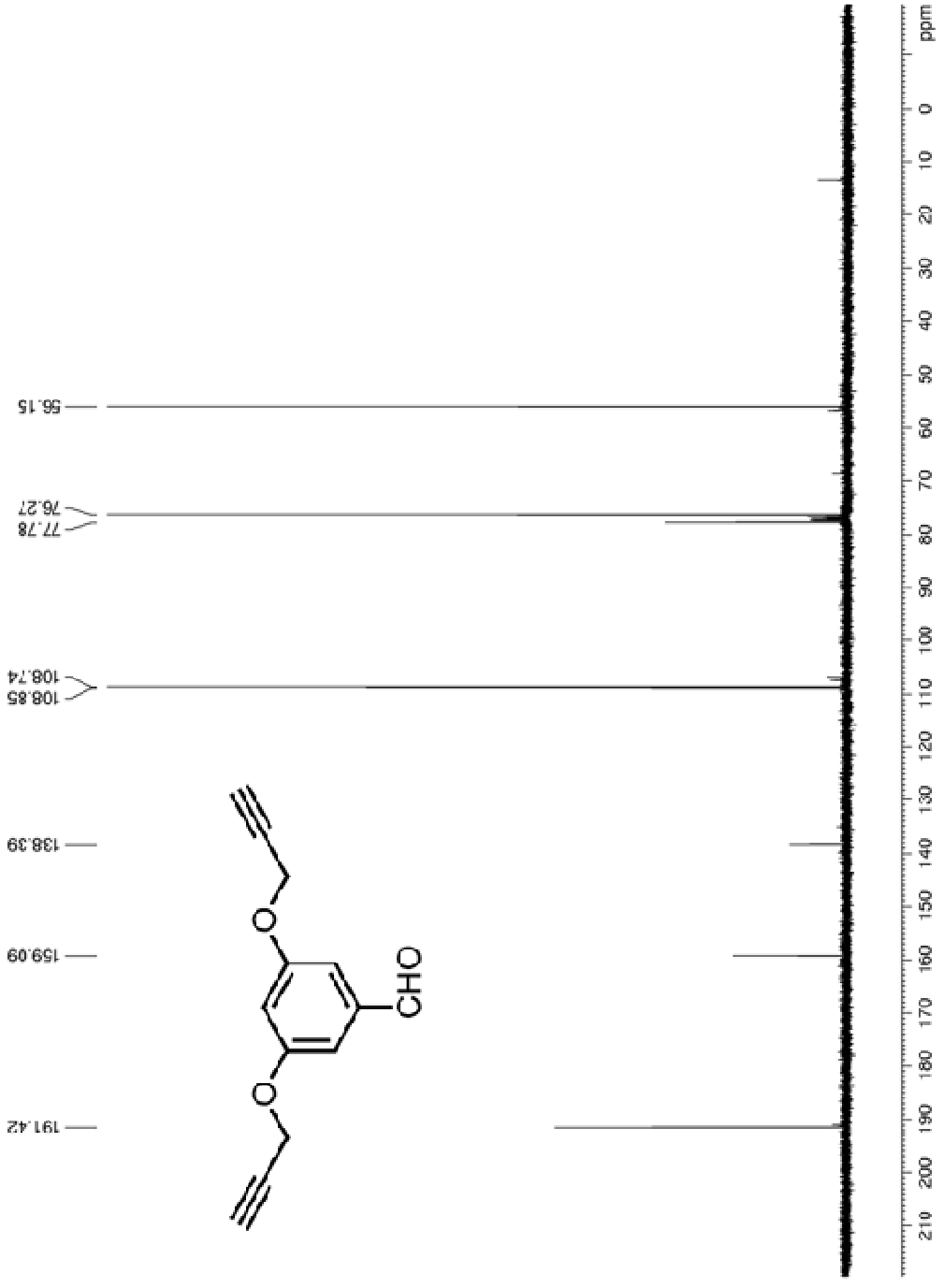

Figure 94. ^{13}C NMR spectrum of compound **13.**

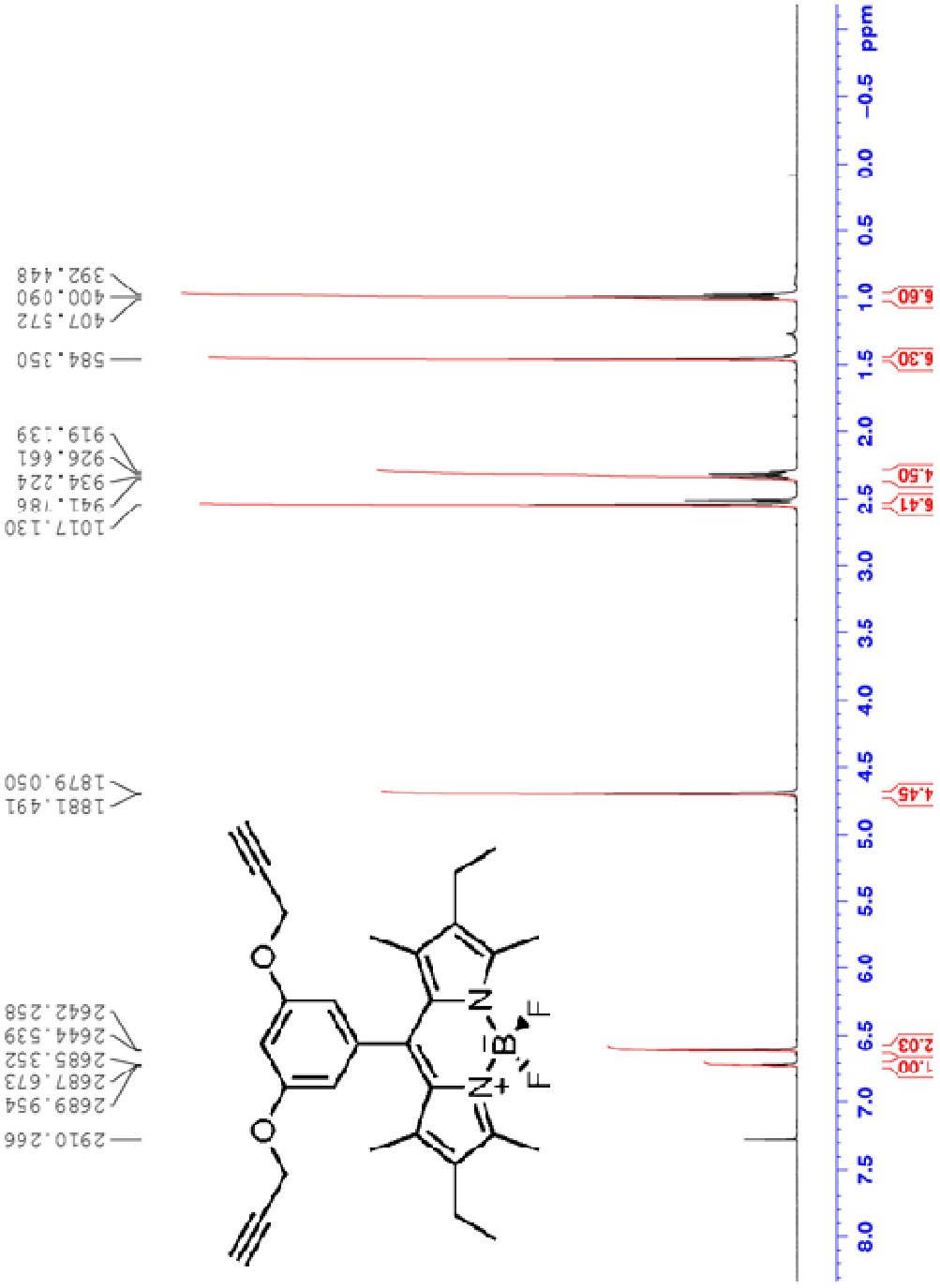

Figure 95. ^{1}H NMR spectrum of compound **14.**

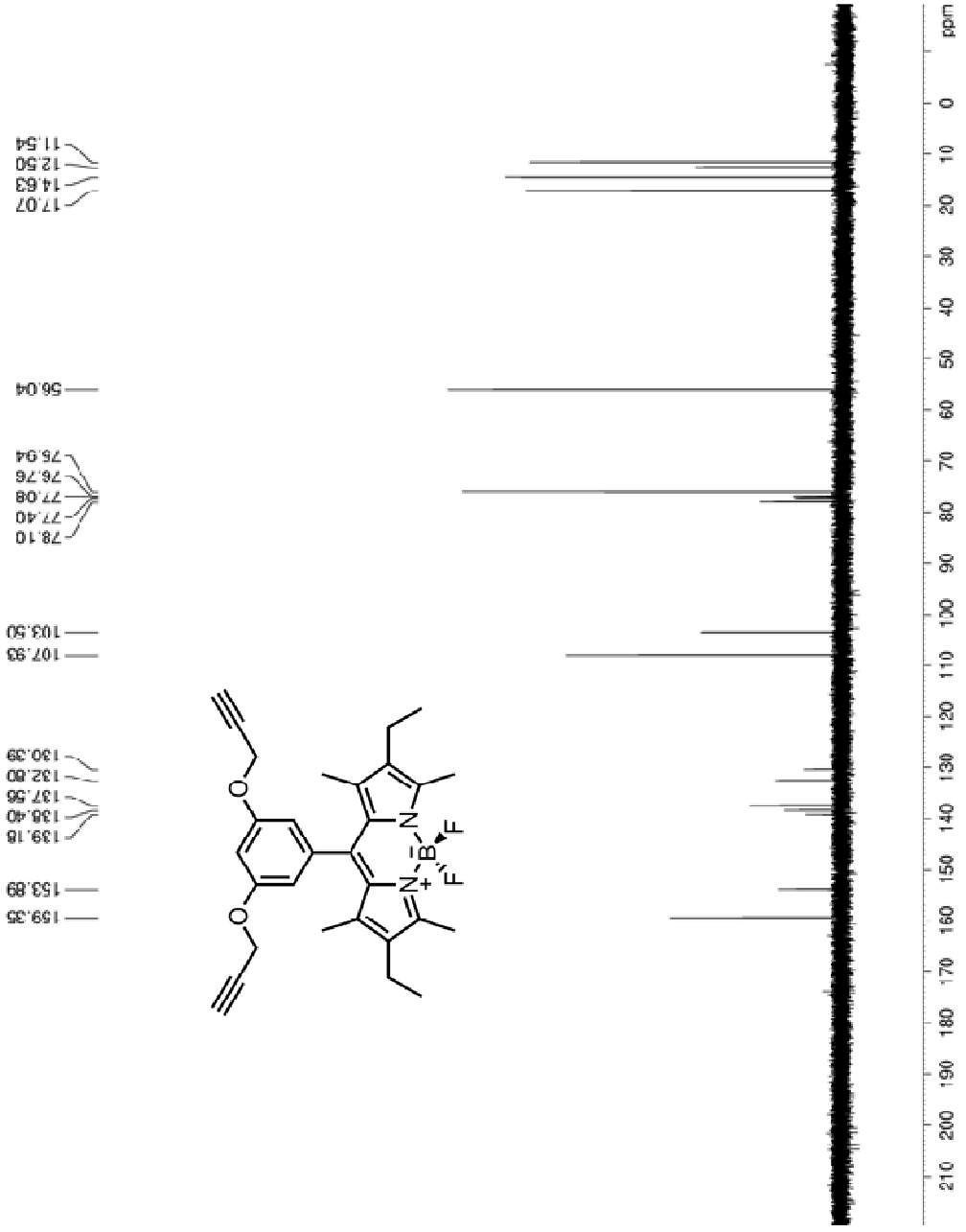

Figure 96. ^{13}C NMR spectrum of compound **14.**

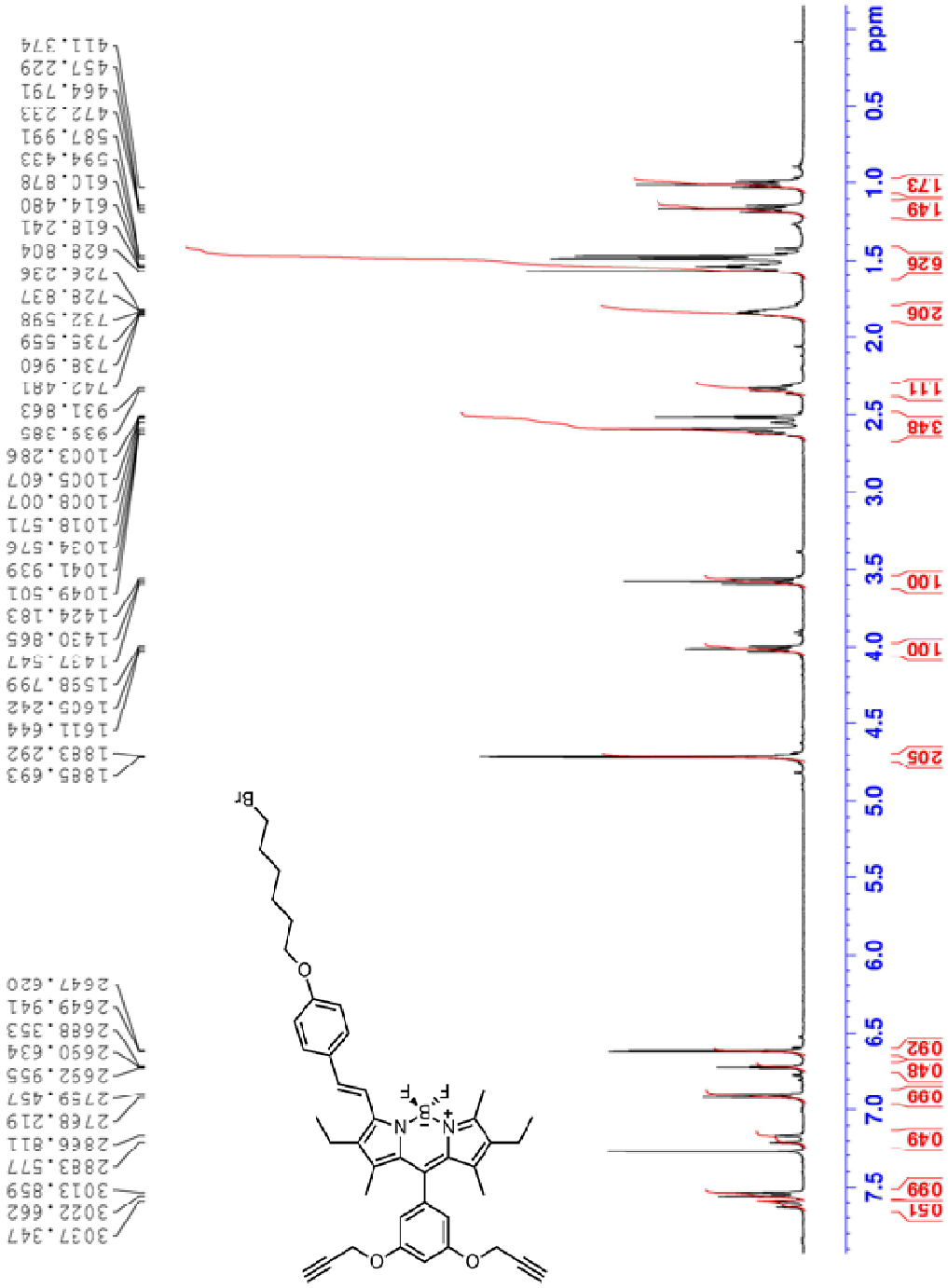

Figure 97. ^{1}H NMR spectrum of compound **15.**

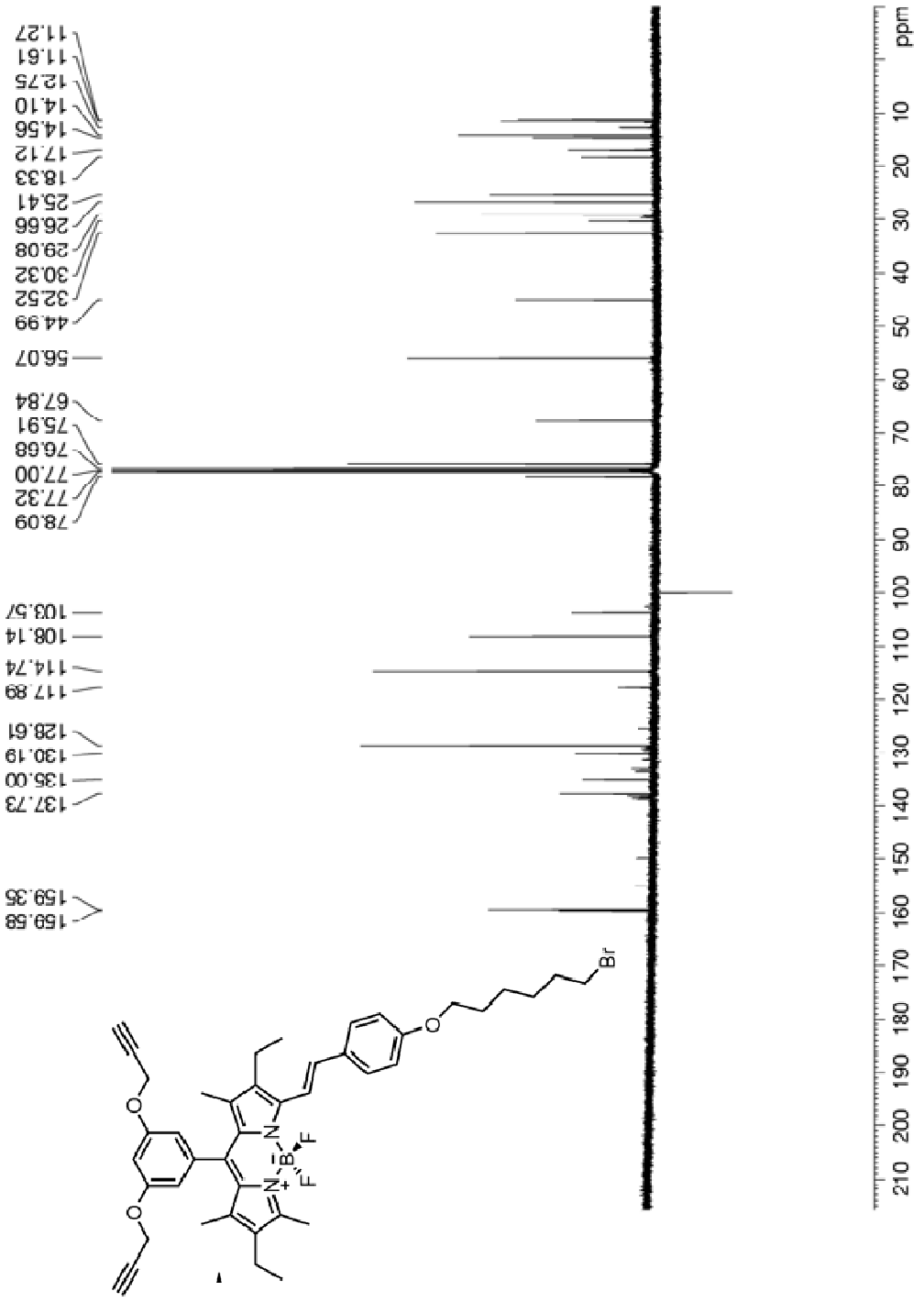

Figure 98. ^{13}C NMR spectrum of compound **15**.

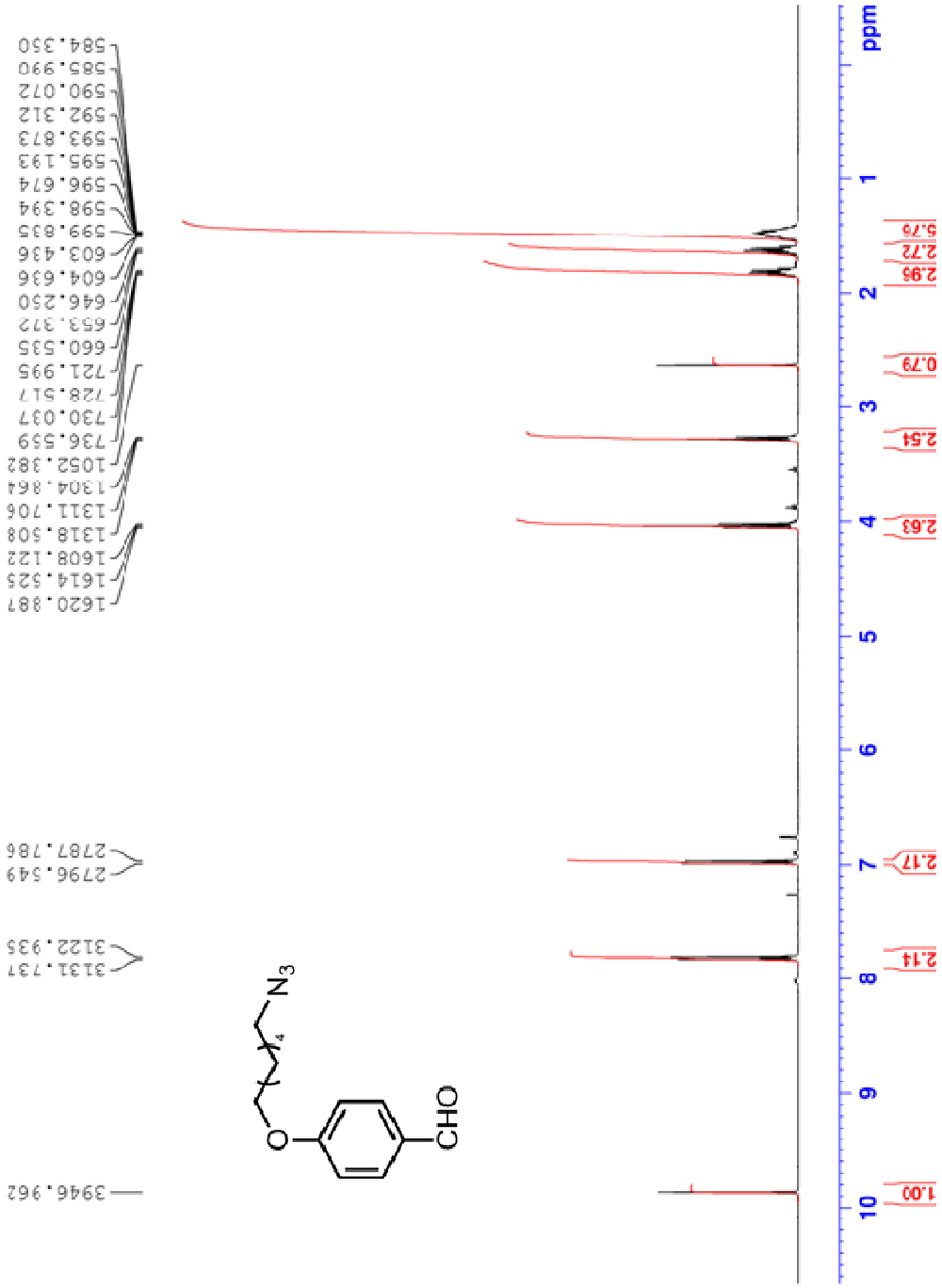

Figure 99. ^{1}H NMR spectrum of compound **16**.

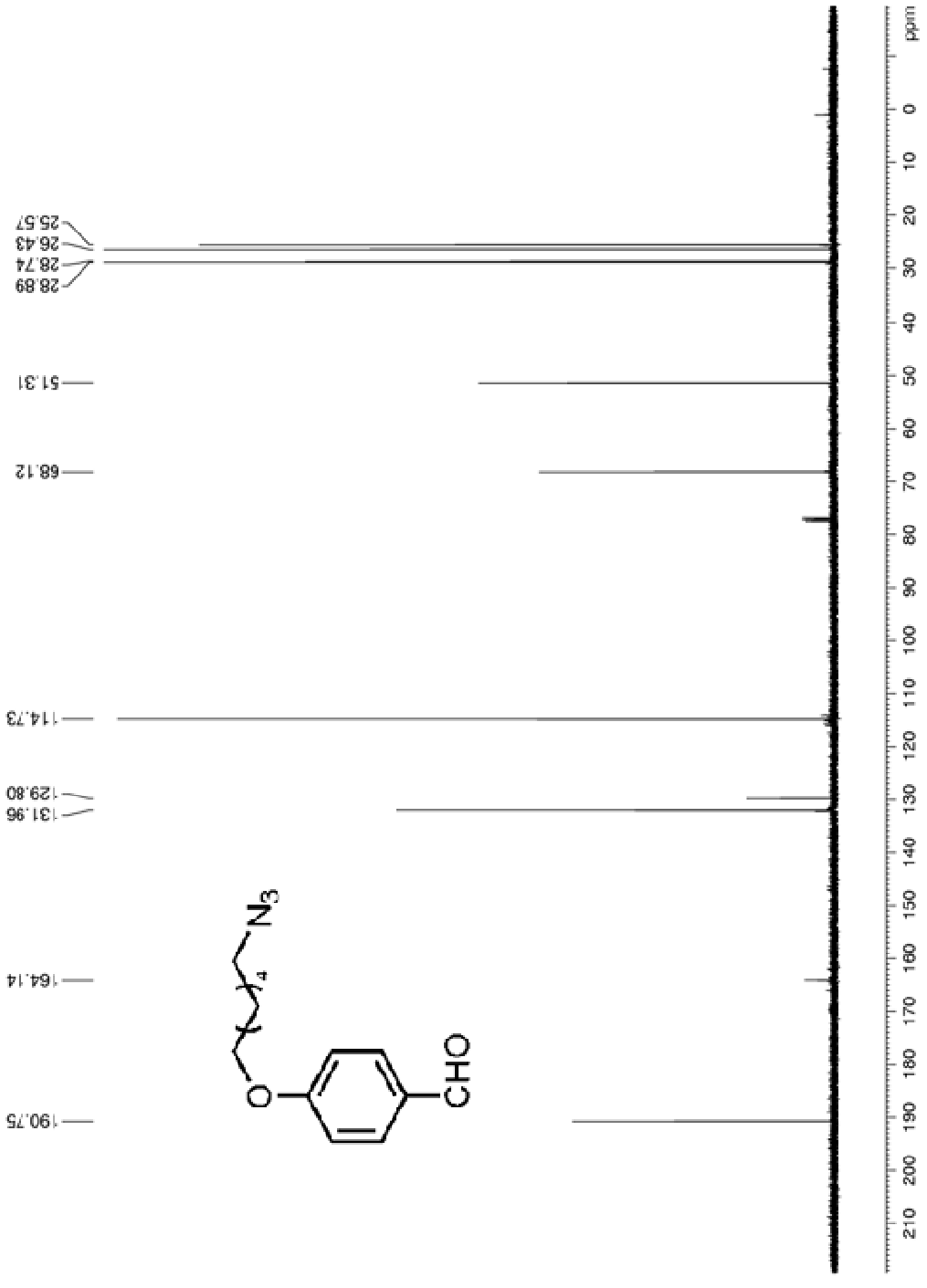

Figure 100. ^{13}C NMR spectrum of compound **16**.

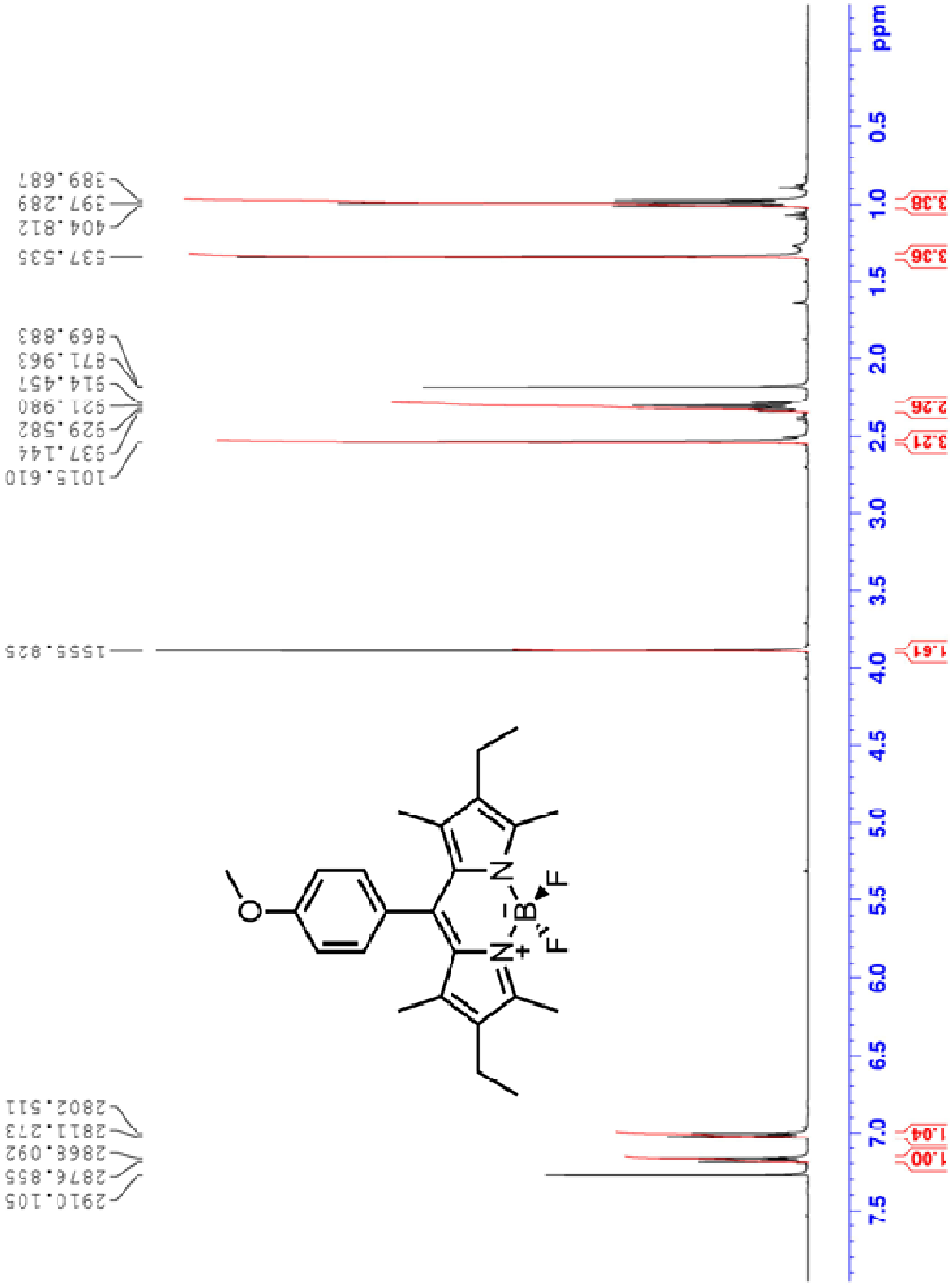

Figure 101.[1]H NMR spectrum of.compound **17**.

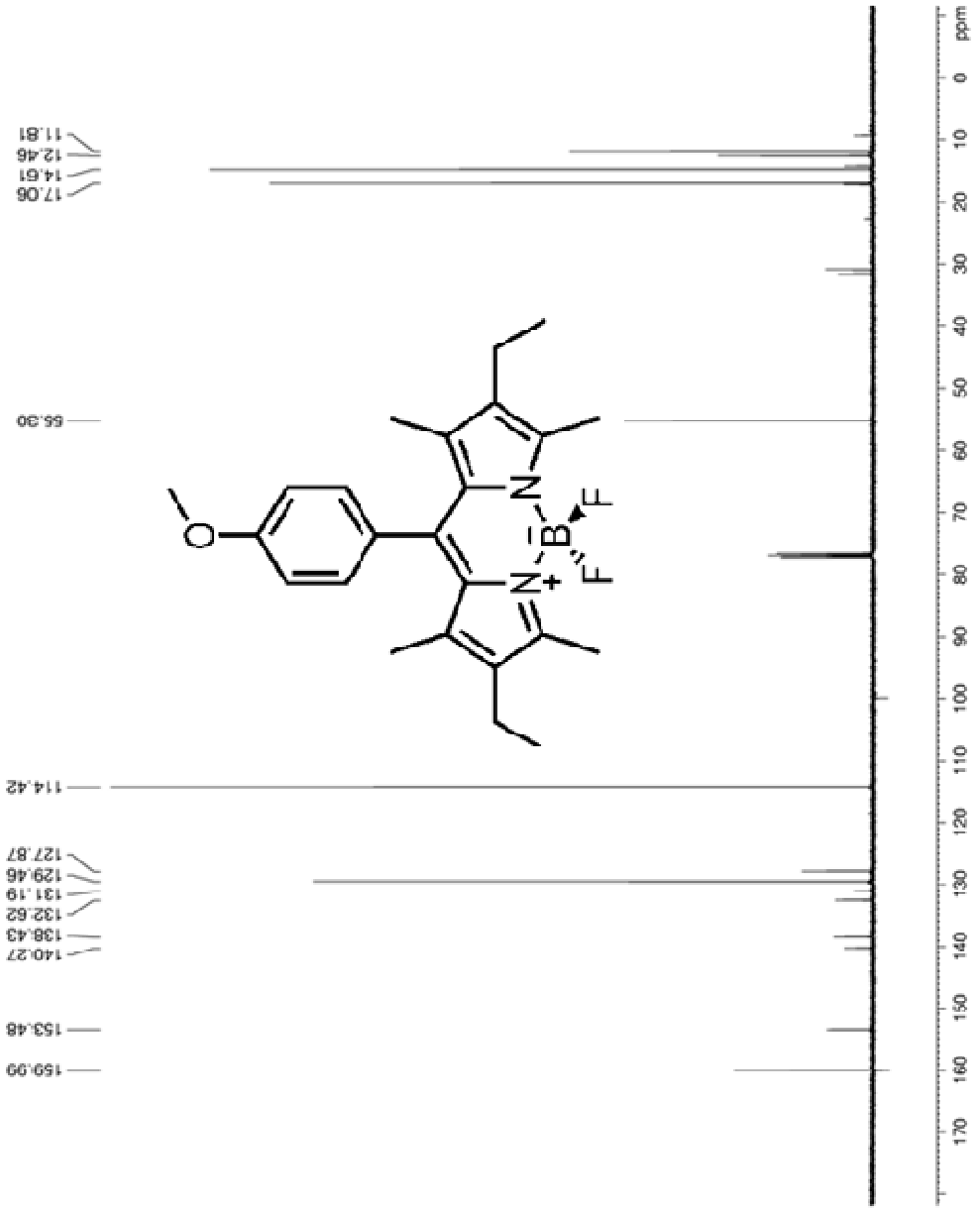

Figure 102. ^{13}C NMR spectrum of compound **17**.

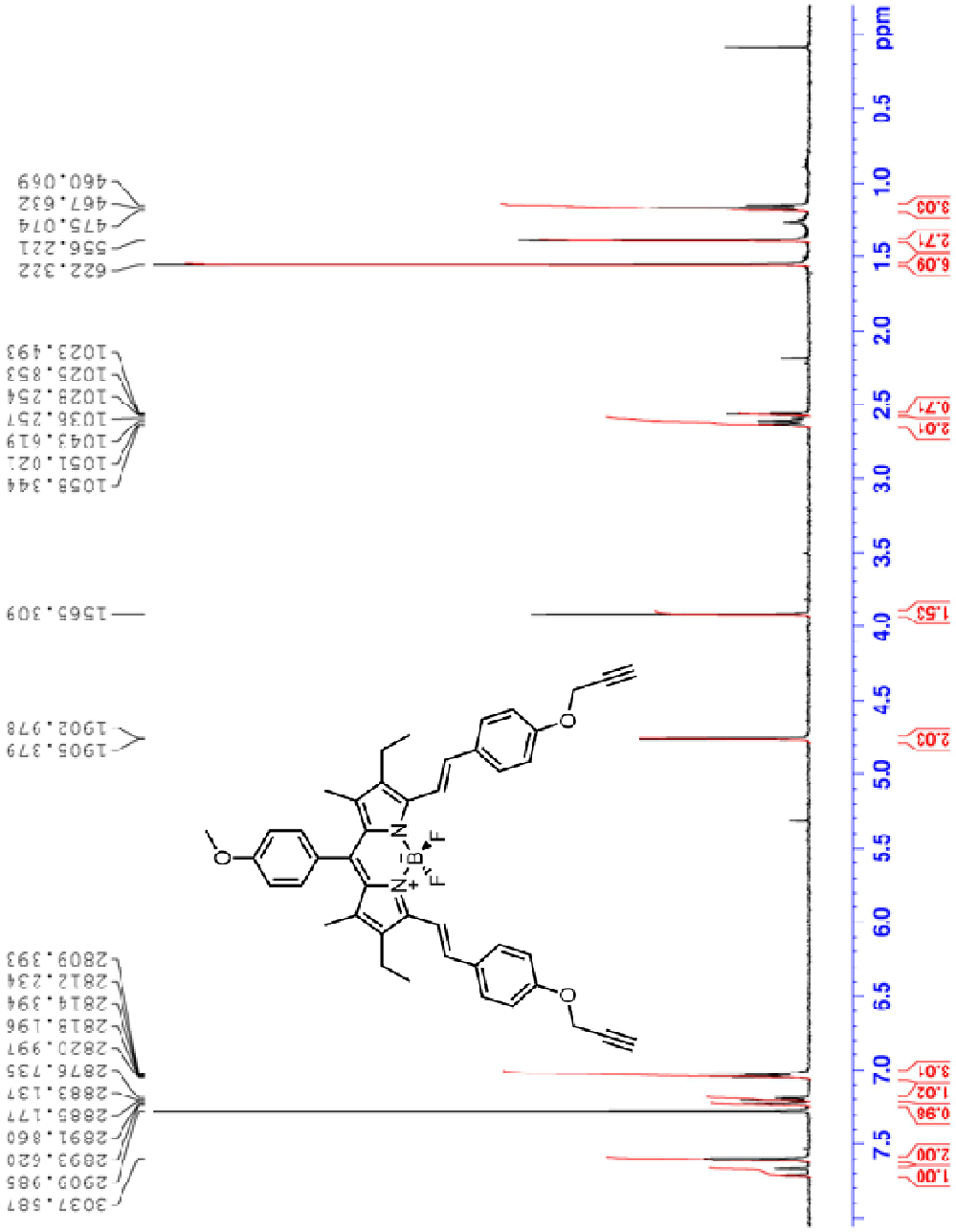

Figure 103. ^{1}H NMR spectrum of compound **18**.

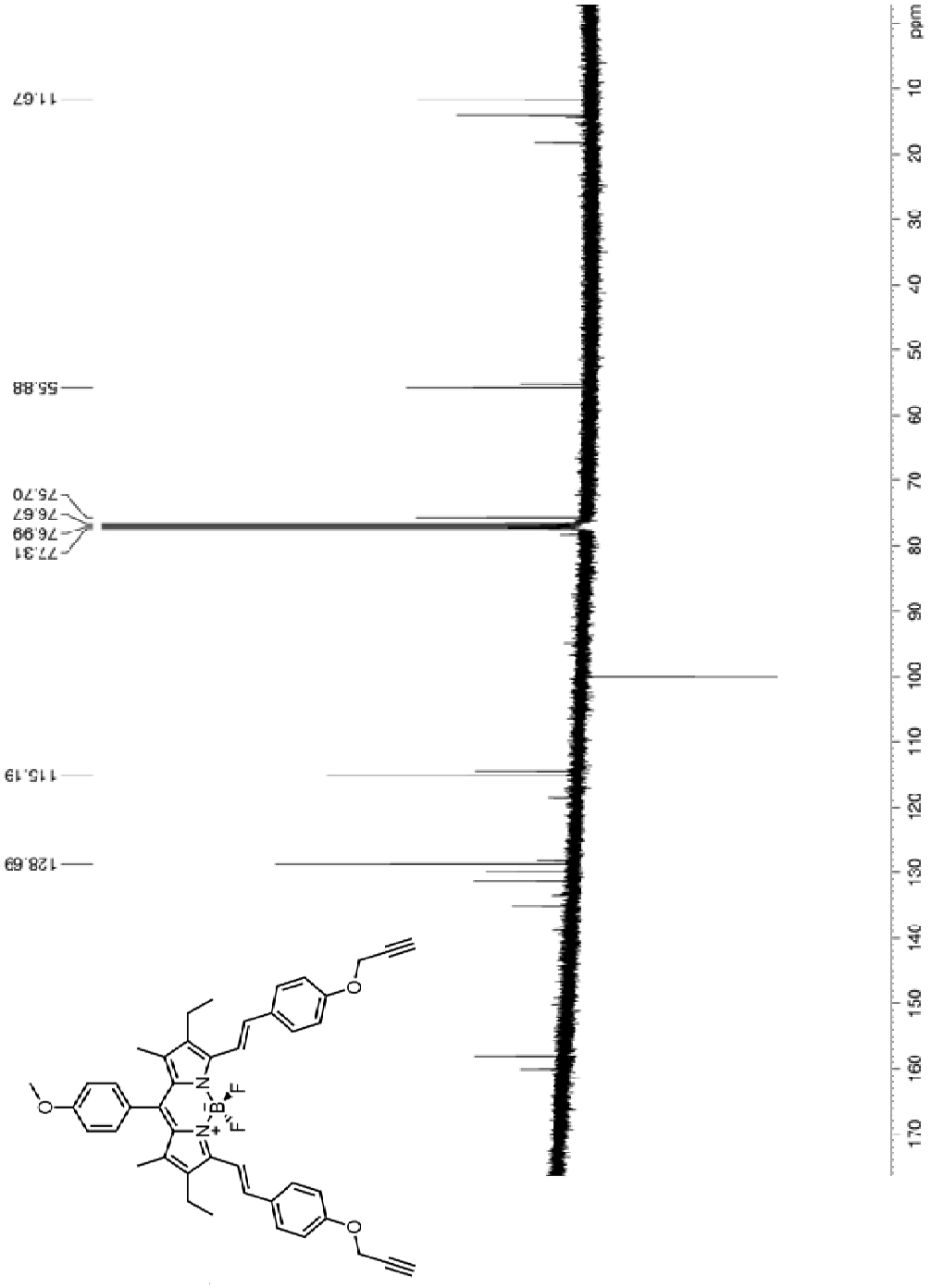

Figure 104. ^{13}C NMR spectrum of compound **18**.

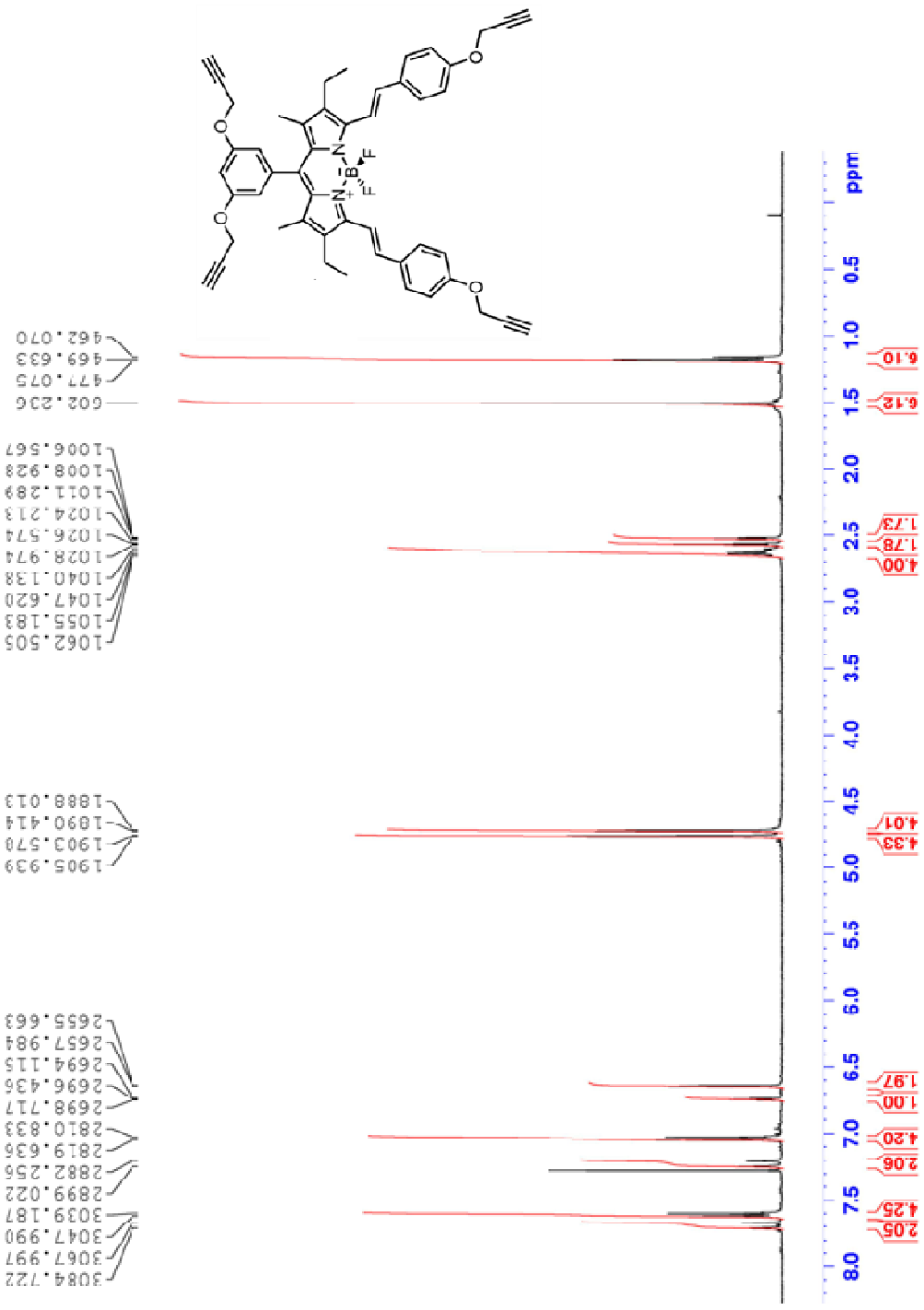

Figure 105. ^{1}H NMR spectrum of compound **19**.

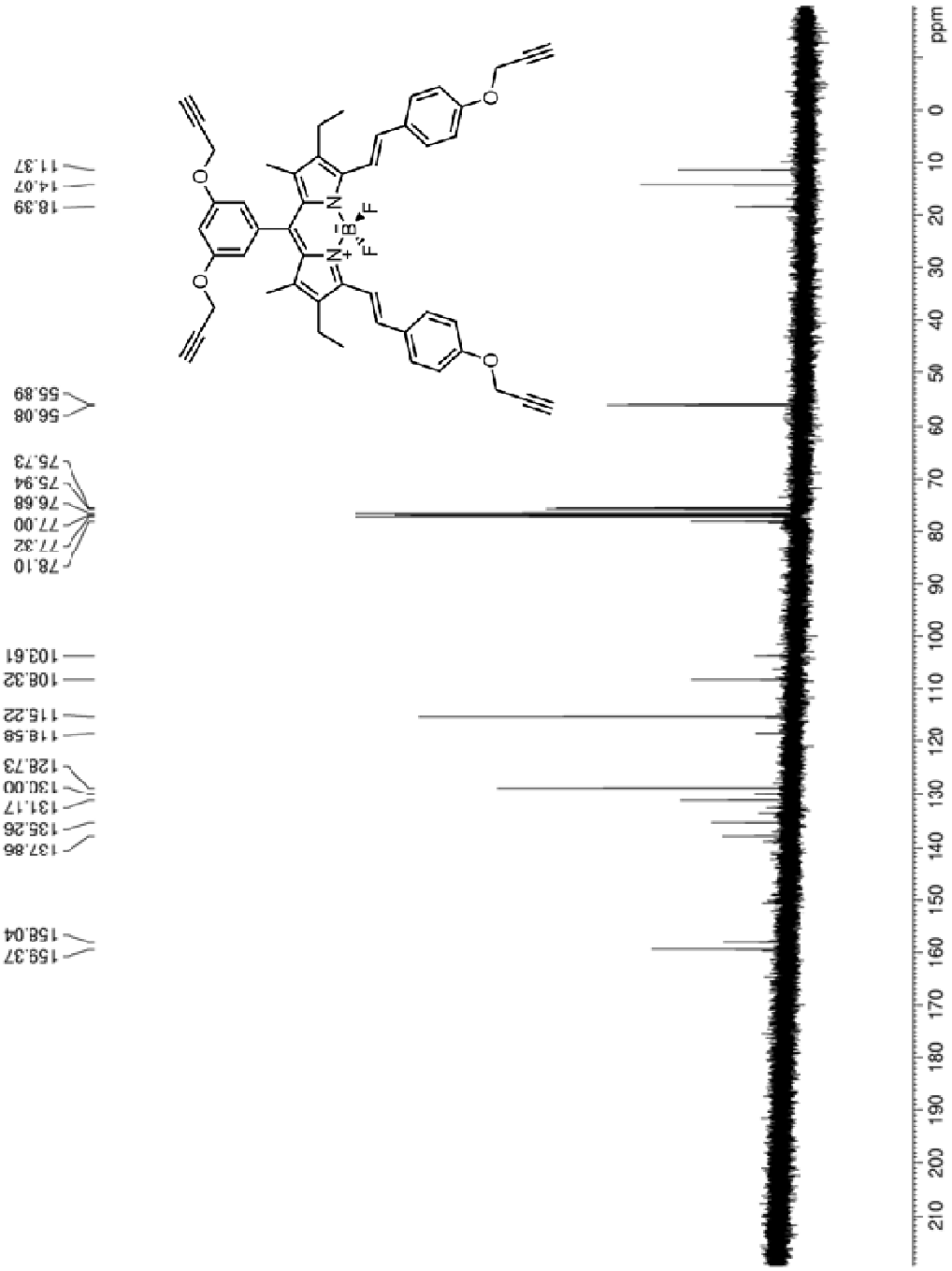

Figure 106. ^{13}C NMR spectrum of compound **19**.

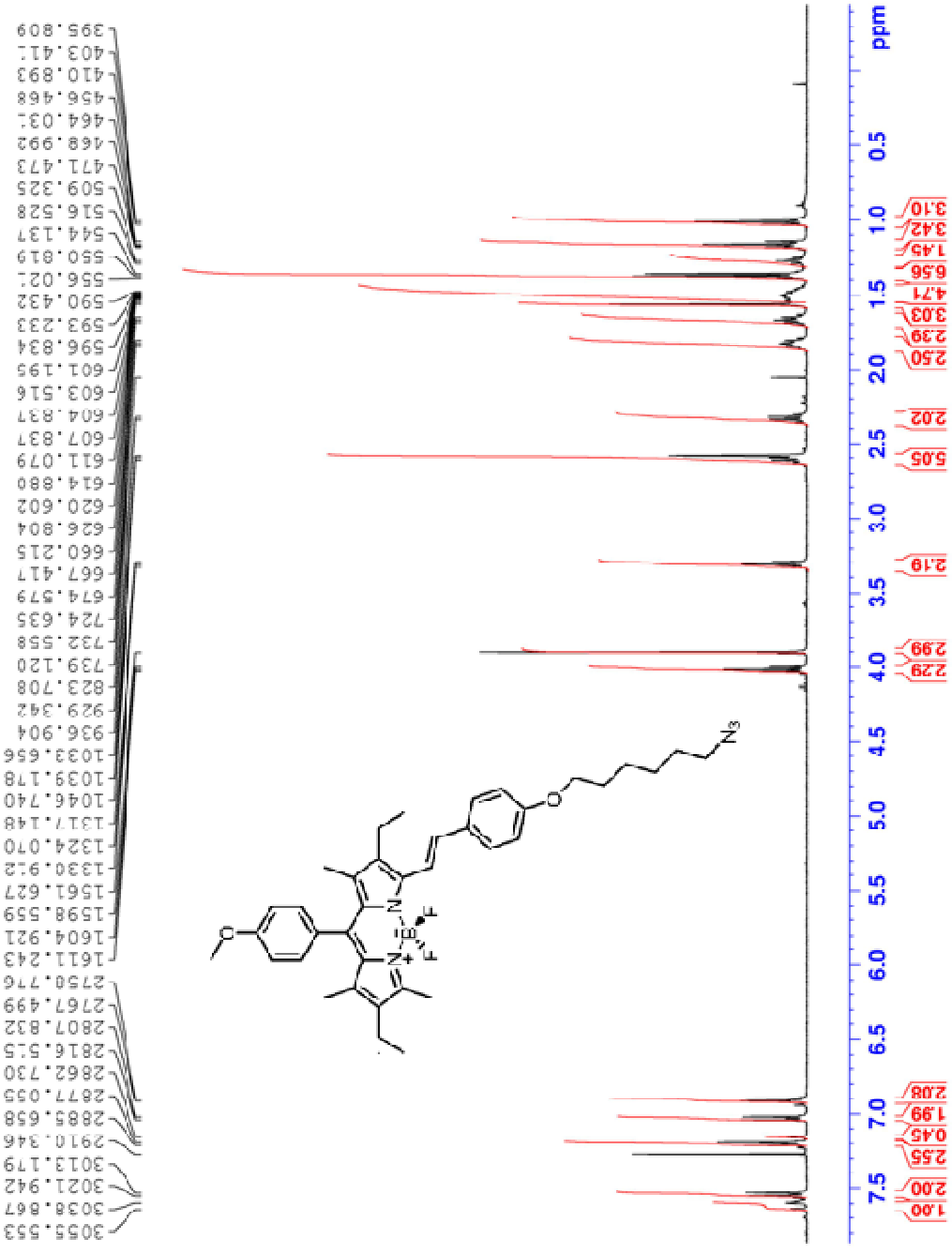

Figure 107. ^{1}H NMR spectrum of compound **20**.

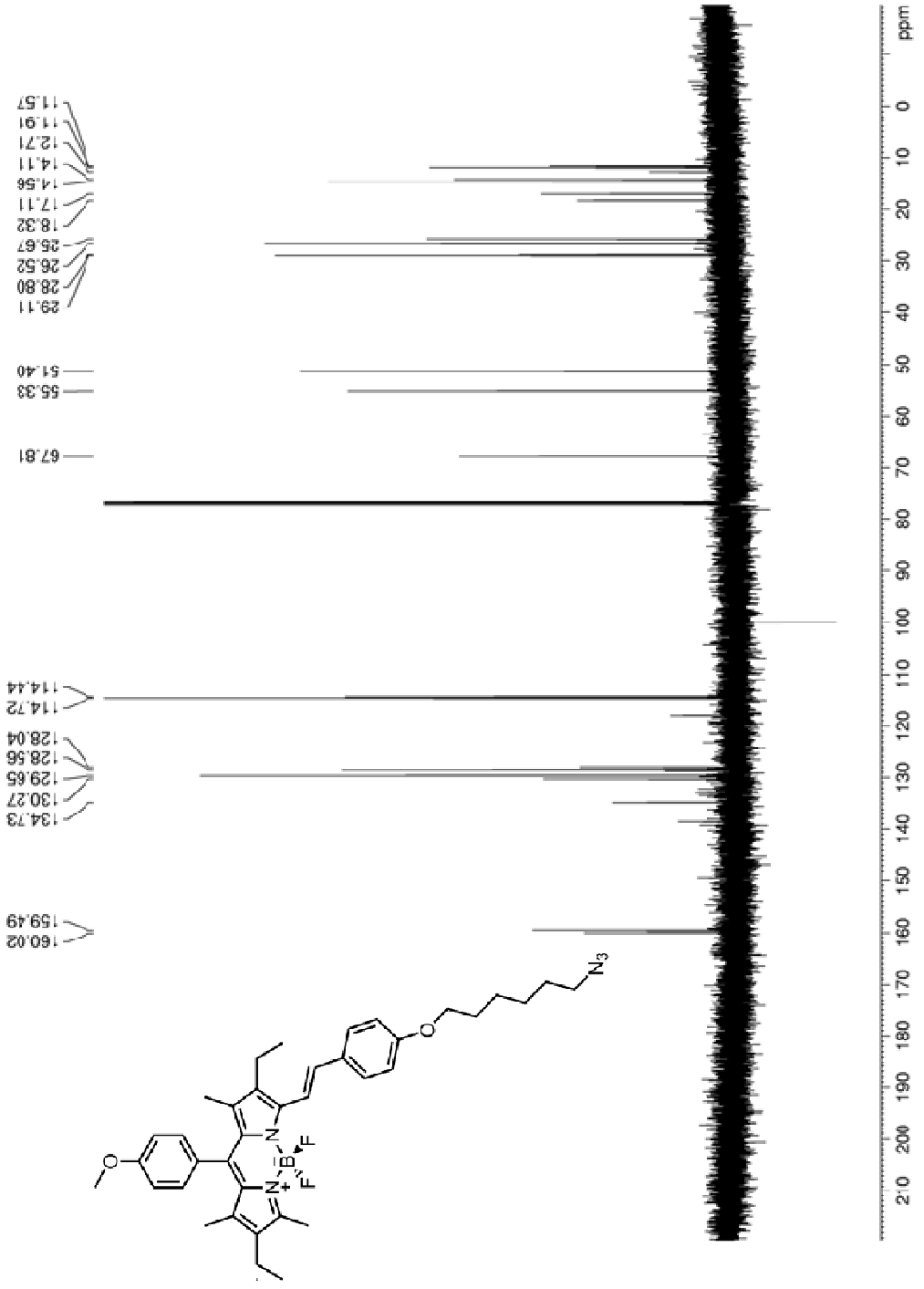

Figure 108. ^{13}C NMR spectrum of compound **20**.

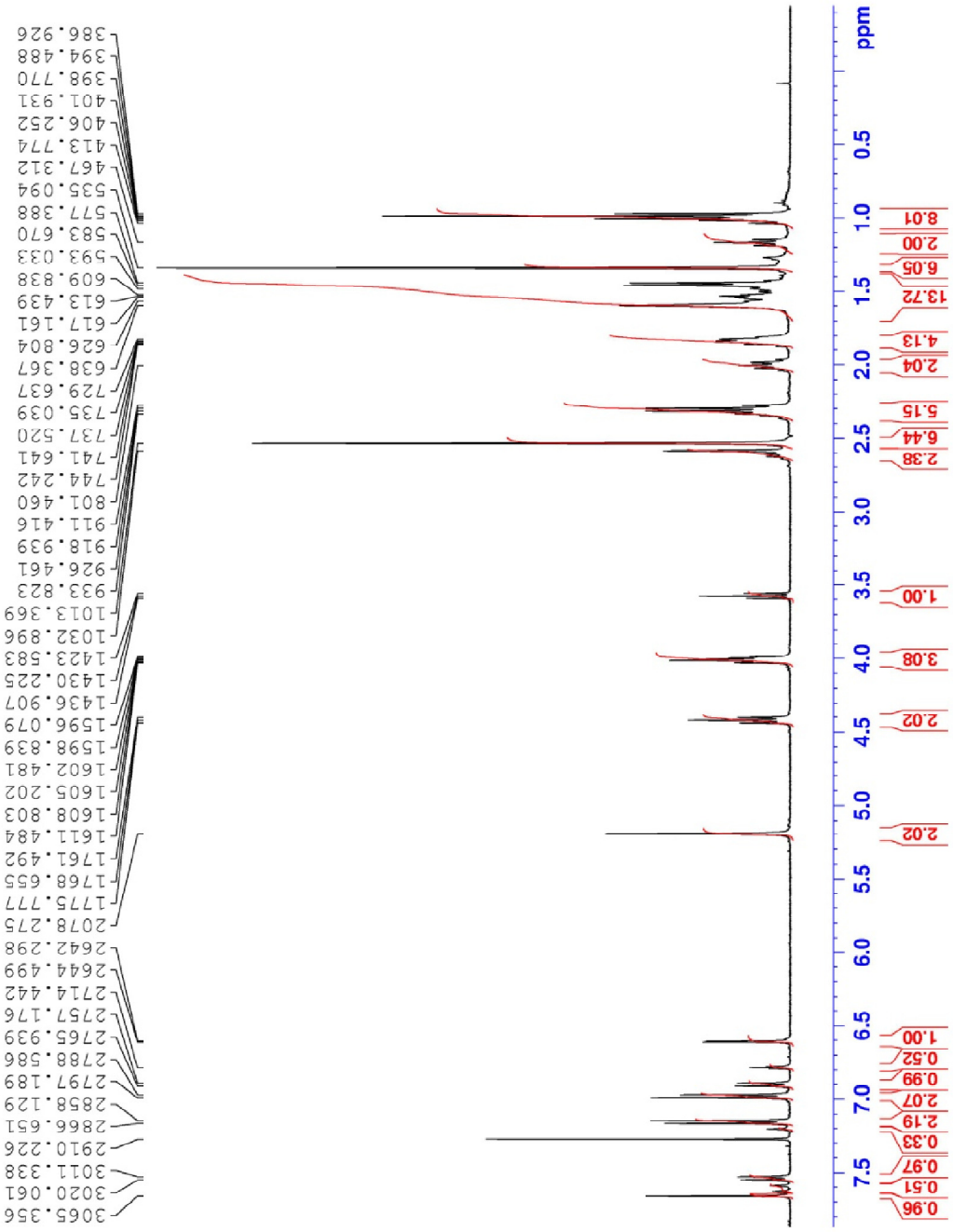

Figure 109. ^{1}H NMR spectrum of compound **21**.

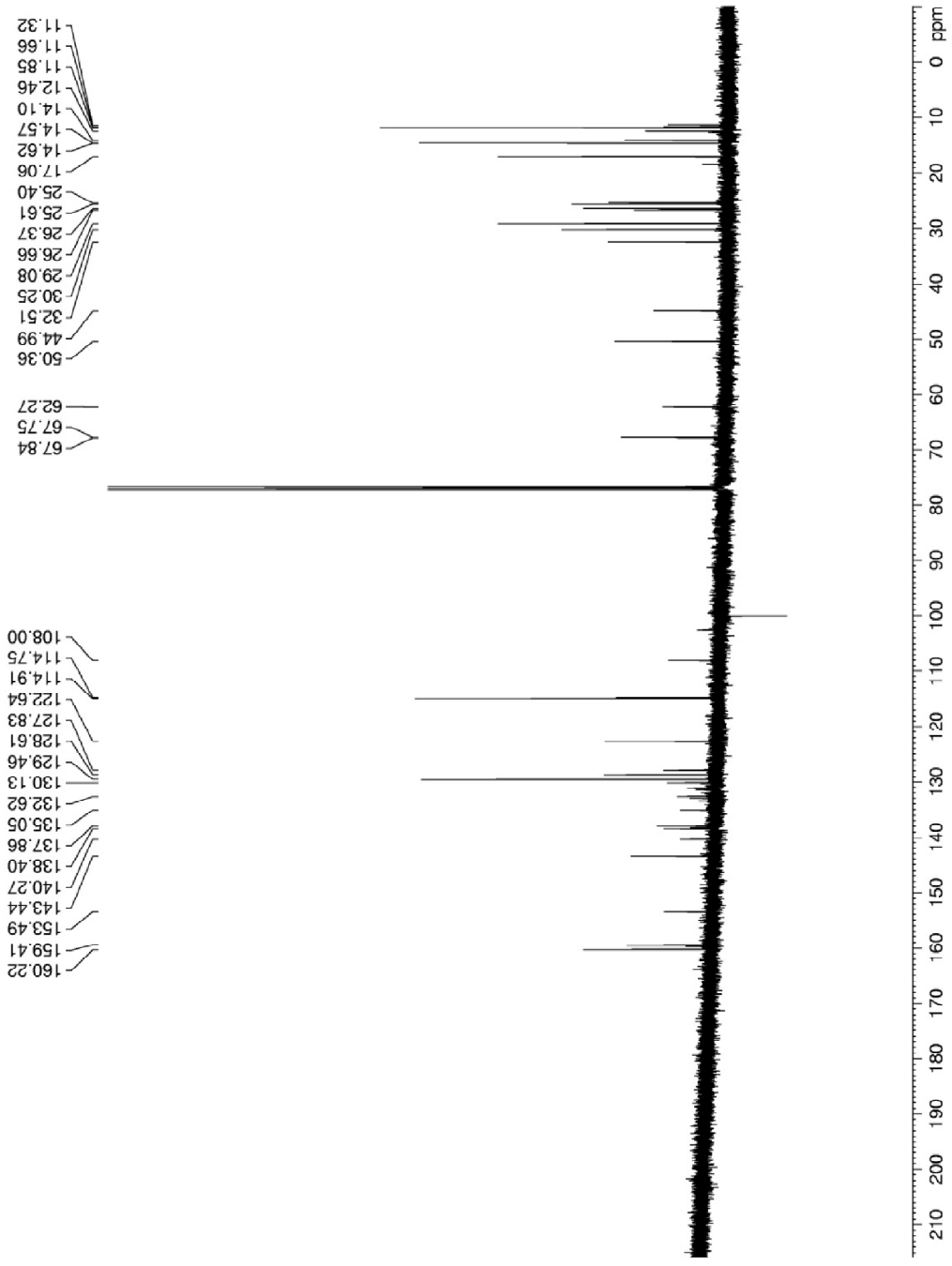

Figure 110. ^{13}C NMR spectrum of compound **21.**

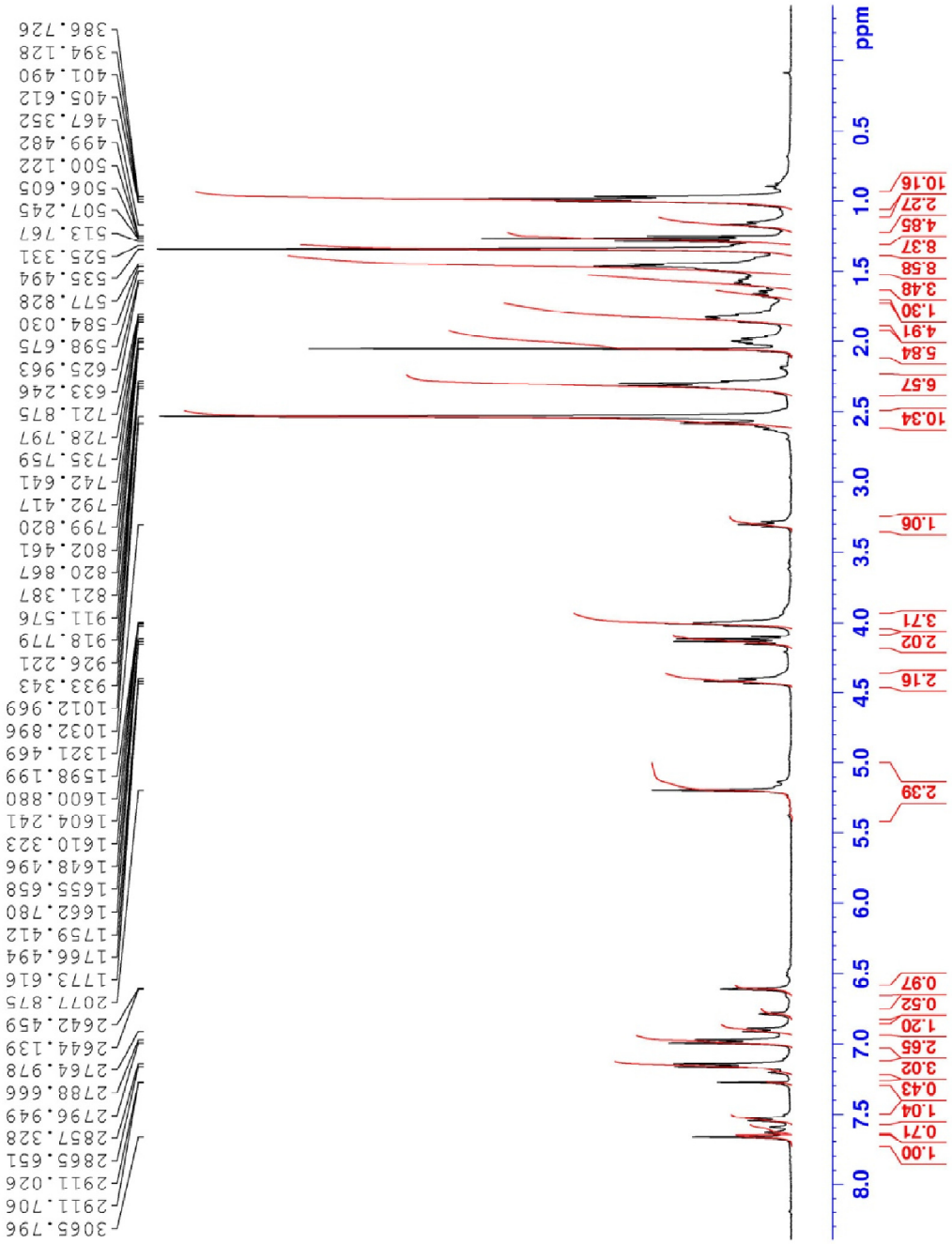

Figure 111.[1]H NMR spectrum of compound **22**.

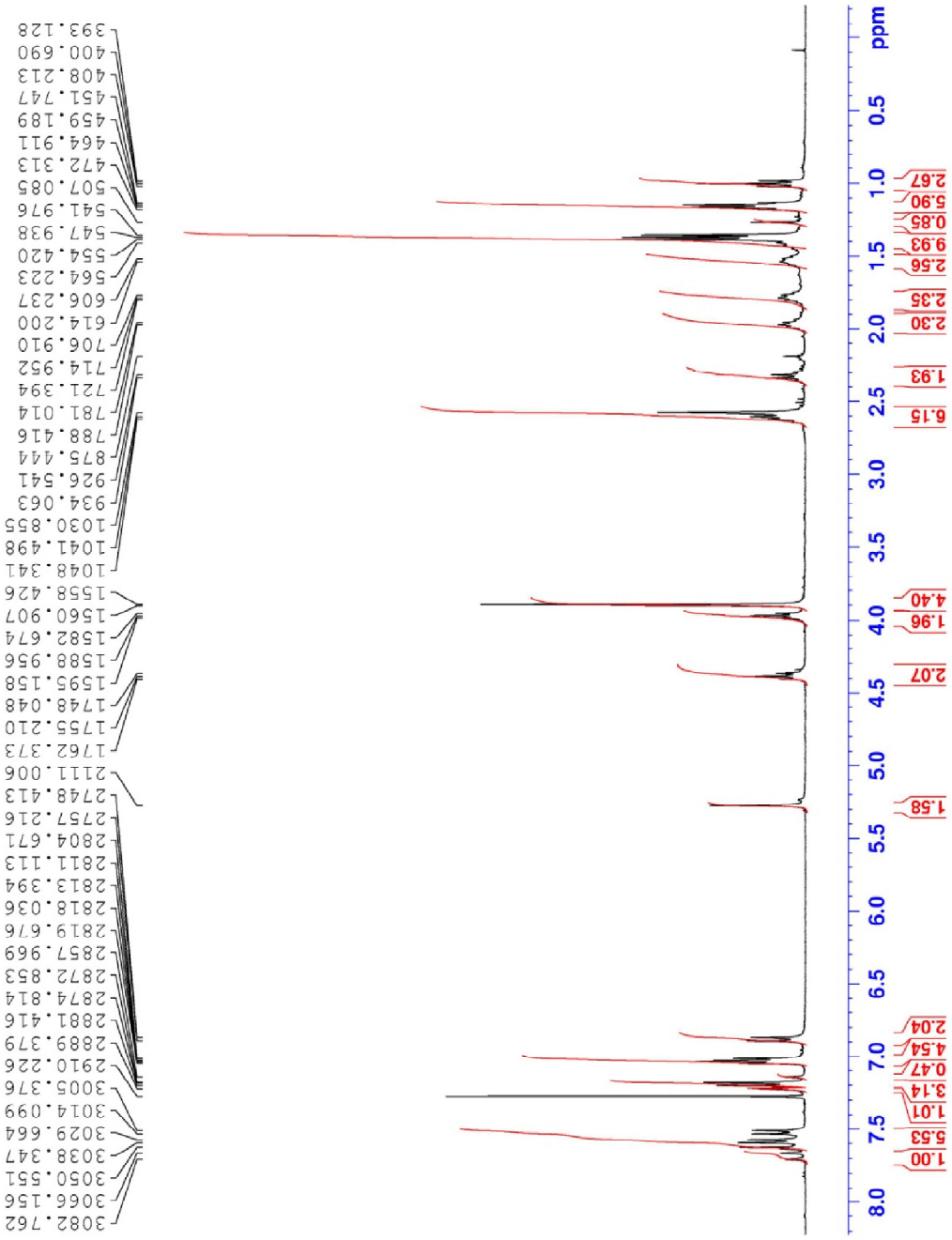

Figure 112. [1]H NMR spectrum of compound **23**.

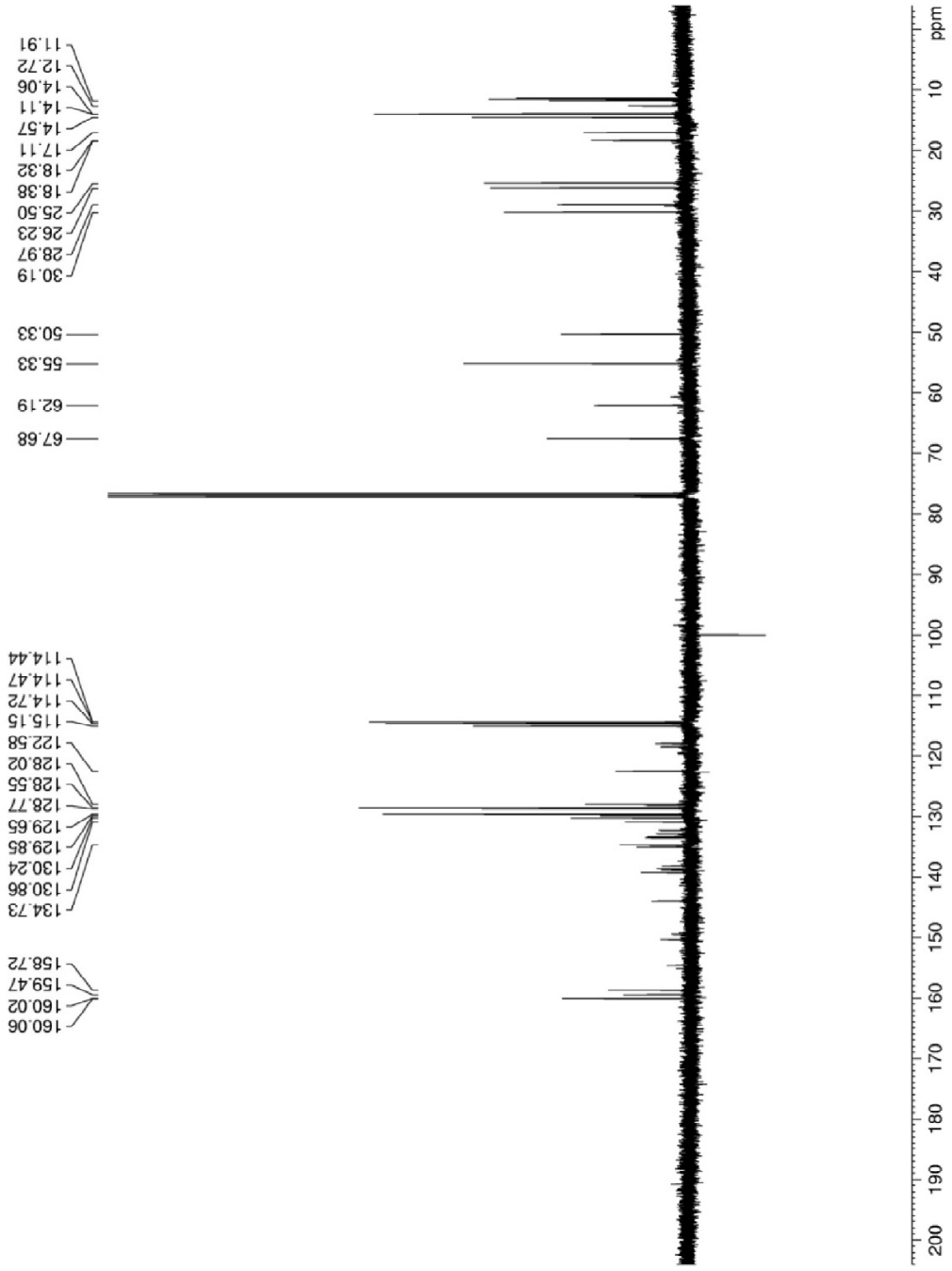

Figure 113. ^{13}C NMR spectrum of compound **23**.

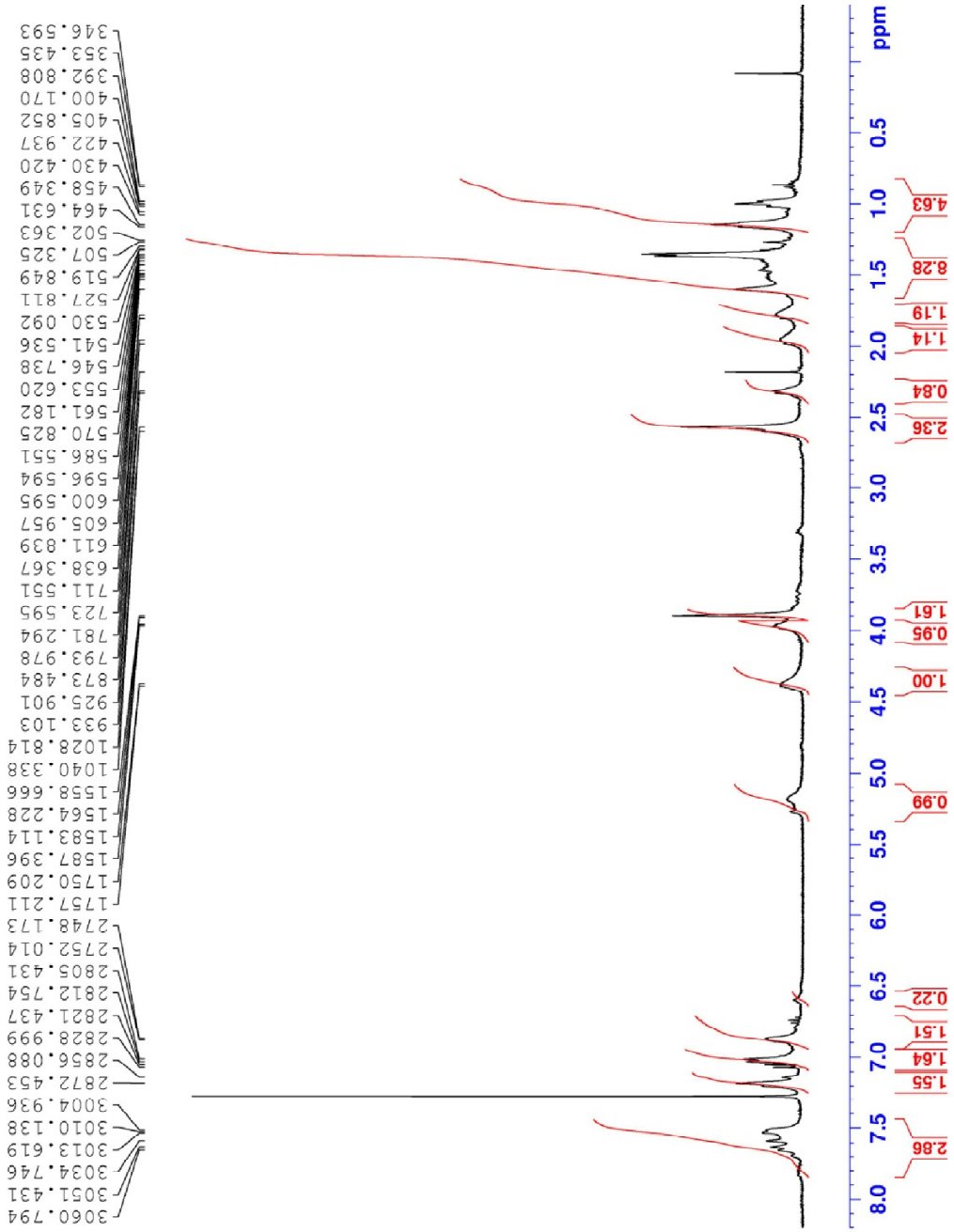

Figure 114. [1]H NMR spectrum of compound **24**.

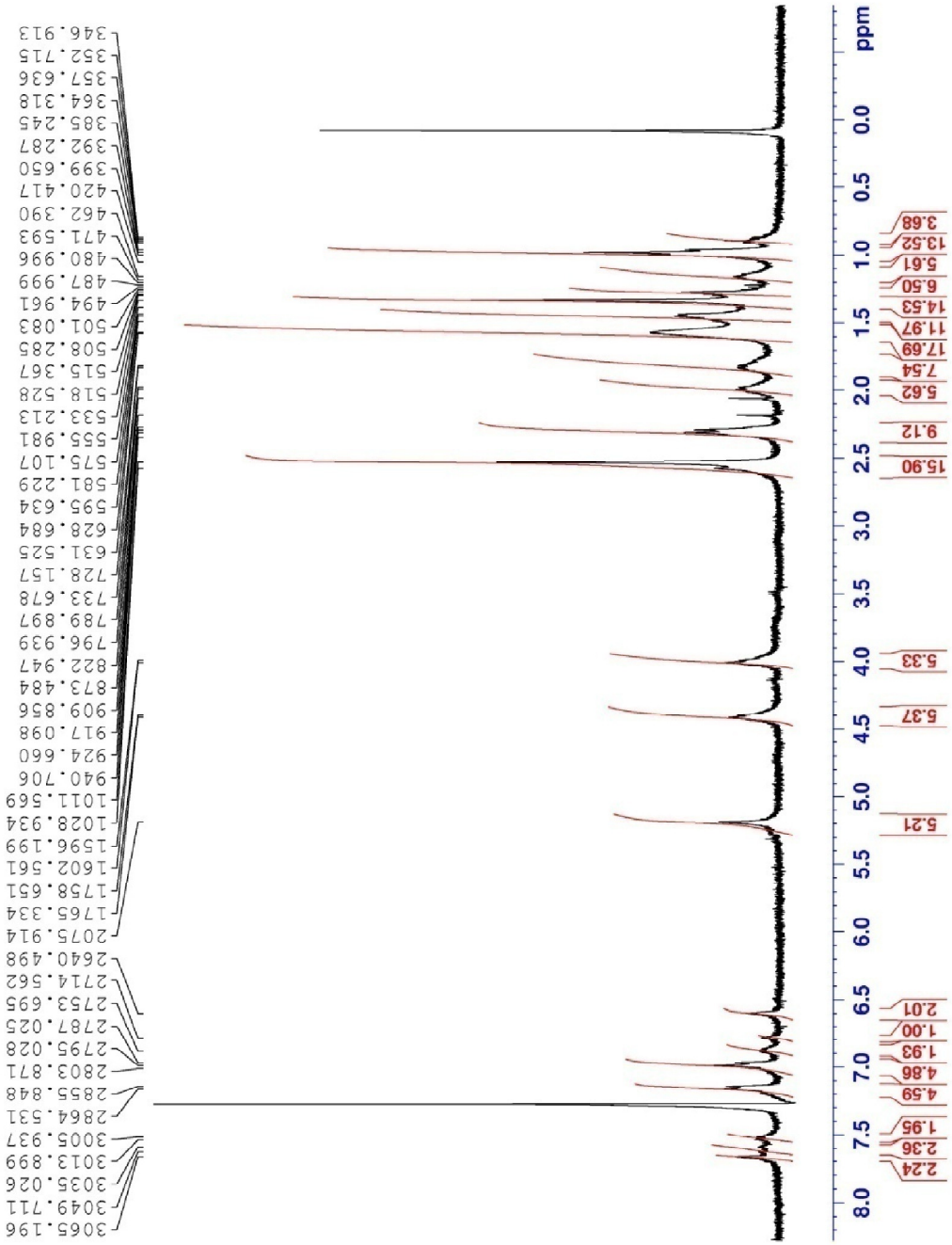

Figure 115. ^{1}H NMR spectrum of compound **25**.

APPENDIX B

MASS SPECTRA

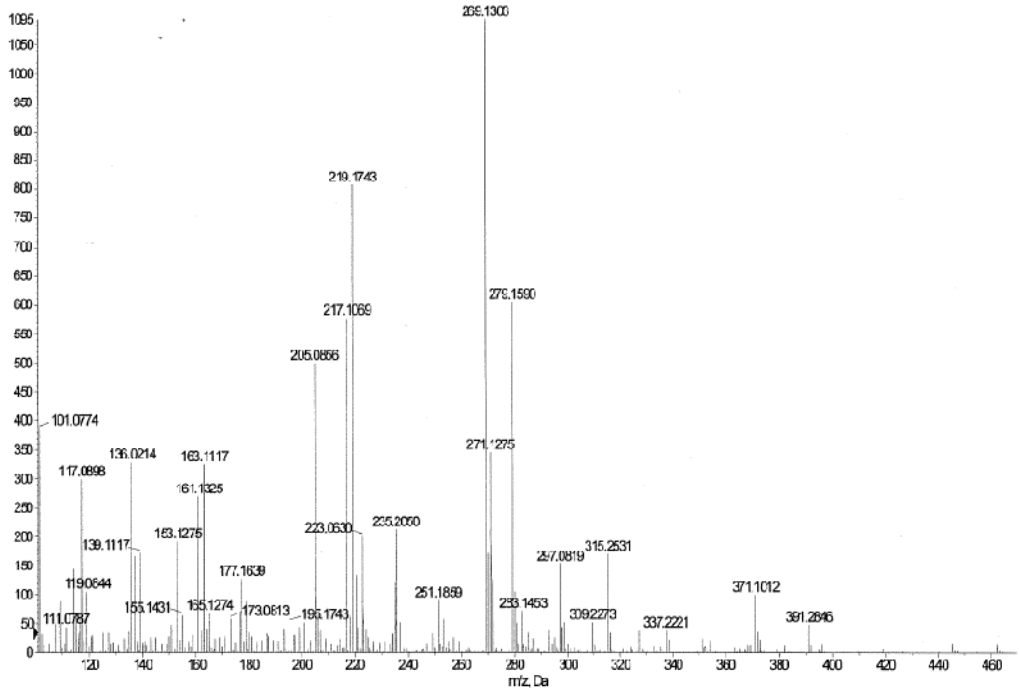

Figure 116. ESI-HRMS of compound **3**.

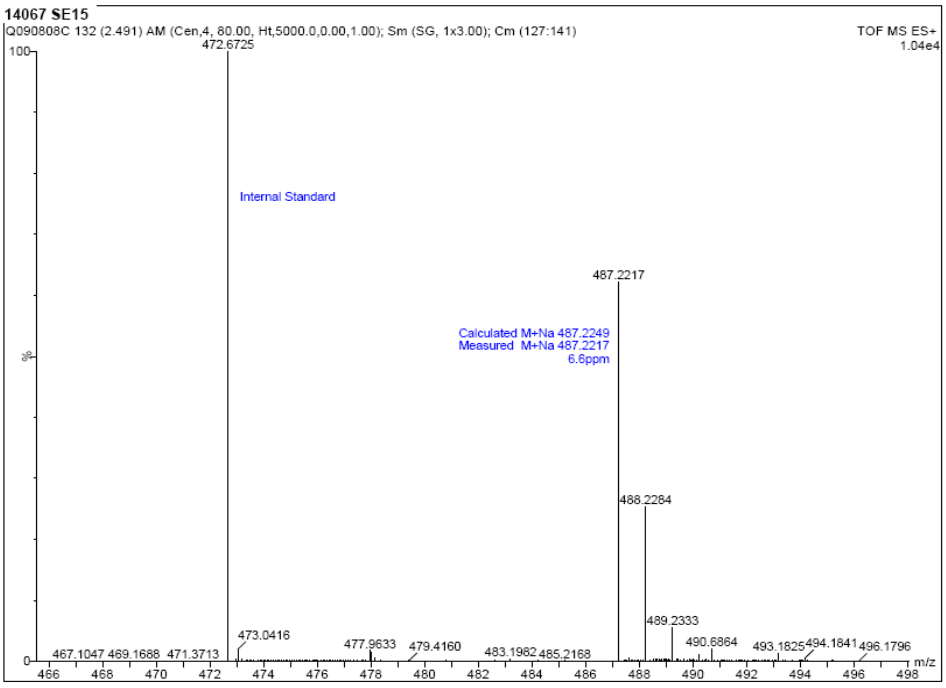

Figure 117. ESI-HRMS of compound **4**.

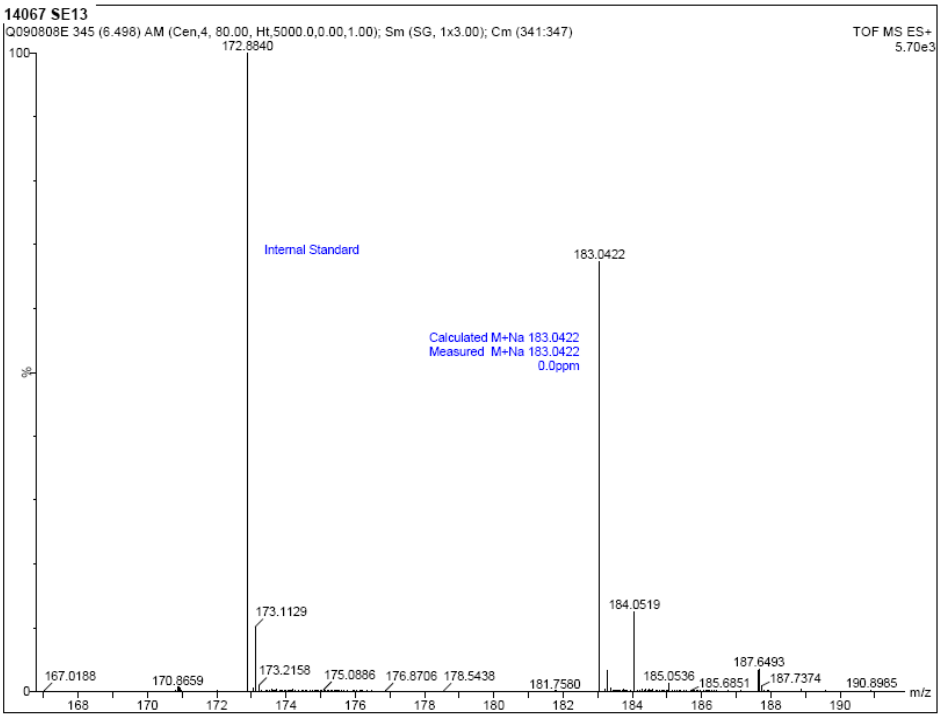

Figure 118 ESI-HRMS of compound **5**

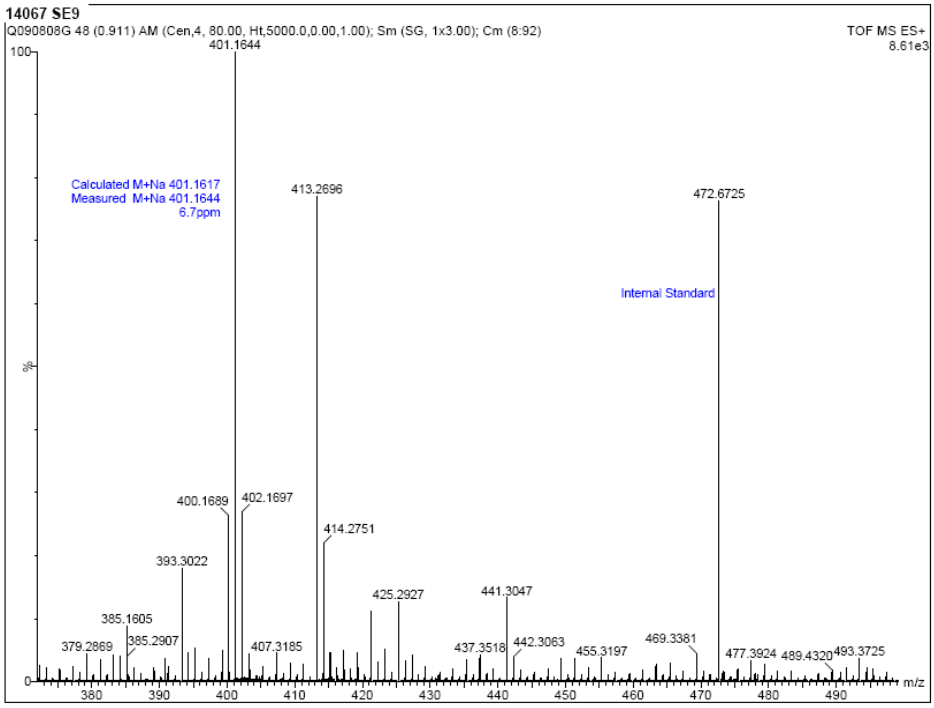

Figure 119. ESI-HRMS of compound **6**

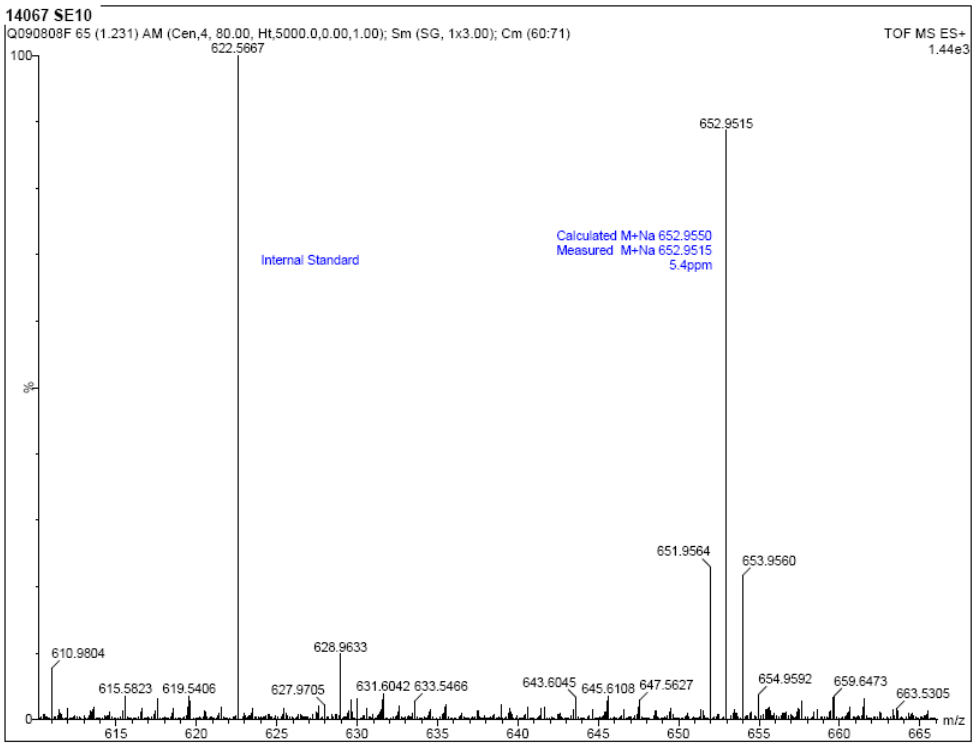

Figure 120. ESI-HRMS of compound **7**.

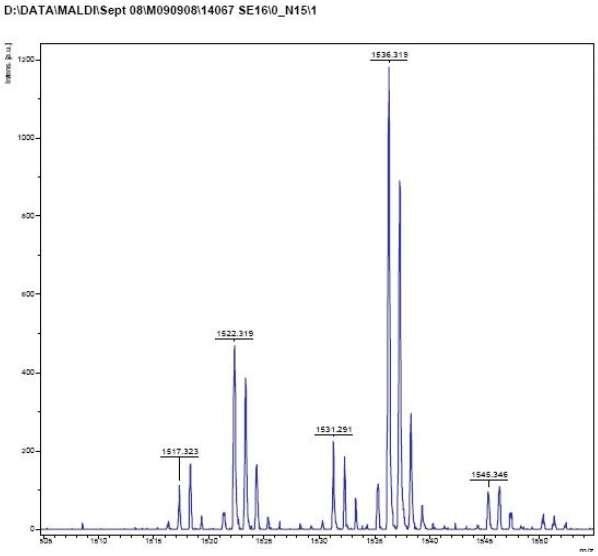

m/z	SN	Quality Fac.	Res.	Intens.	Area
1303.295	164.3	9934	8855	278.00	45
1308.291	47.9	2163	10490	81.00	12
1322.296	27.2	1688	14854	46.00	6
1390.462	42.0	1640	8124	71.00	12
1396.470	55.6	2599	7724	94.00	17
1407.409	123.9	8544	3830	208.00	81
1475.356	45.5	1581	20217	77.00	7
1489.314	109.9	3967	9943	186.00	30
1517.323	66.2	2637	11641	112.00	16
1522.319	277.2	17096	7404	469.00	103
1531.291	133.0	7596	11890	225.00	36
1536.319	697.5	48446	8712	1180.00	244
1545.346	56.2	2738	7949	95.00	20
1559.322	196.8	14178	9006	333.00	66
1573.308	11.8	265	34697	20.00	1

Figure 121. MALDI-MS of compound **8**

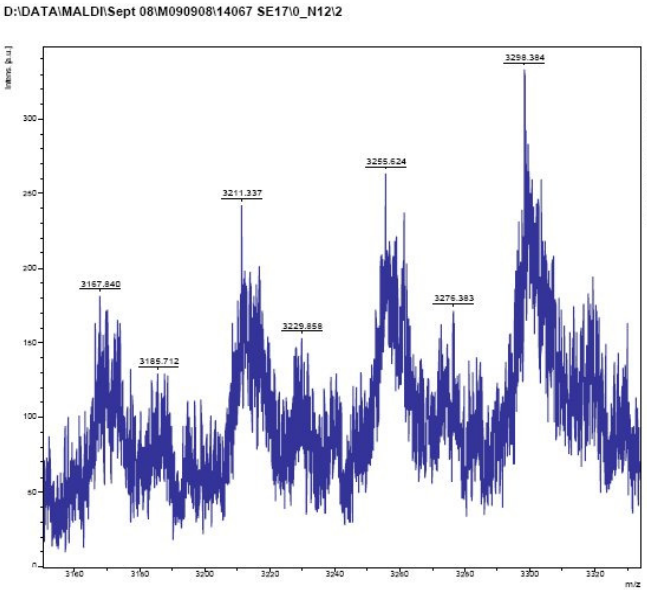

m/z	SN	Quality Fac.	Res.	Intens.	Area
1702.968	8.1	3239	8035	98.00	24
1734.952	2.0	772	23700	24.00	3
1746.995	12.7	7171	12876	154.00	30
1768.952	3.1	1269	8684	38.00	9
1790.985	18.8	9885	10949	227.00	52
1812.961	5.7	5020	17146	69.00	16
3167.840	15.0	726	4241	181.00	49
3185.712	9.6	425	3985	116.00	34
3211.337	20.0	505	3321	242.00	54
3229.858	12.7	731	1773	153.00	74
3255.624	21.8	597	678	263.00	151
3276.383	14.2	2035	3101	171.00	102
3298.384	27.6	2580	3341	333.00	150

Figure 122. MALDI-MS of compound **1**

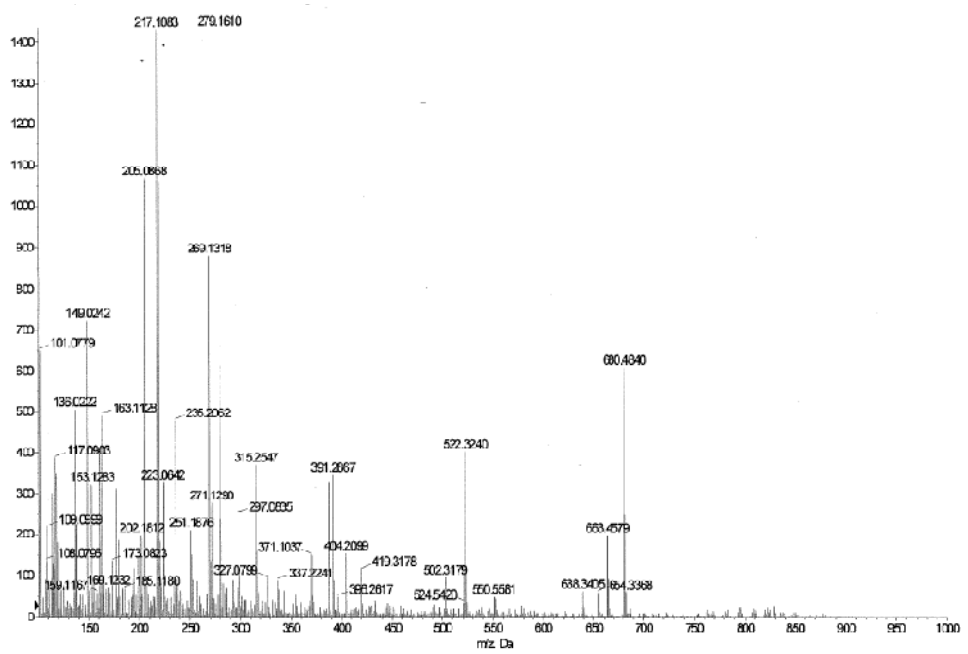

Figure 123. ESI-HRMS of compound **11**.

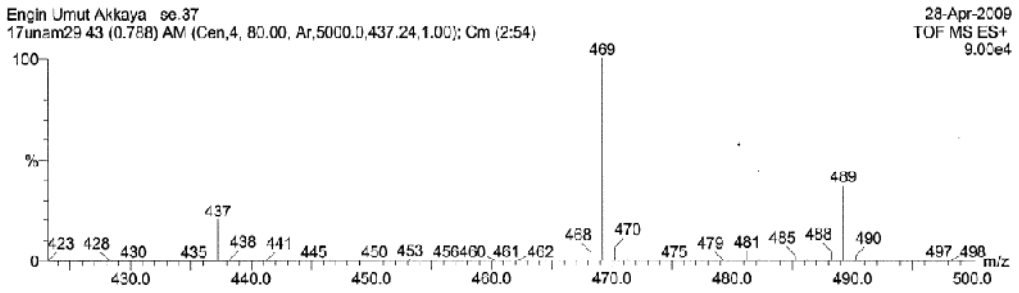

Minimum:				-1.5		
Maximum:		5.0	5.0	75.0		
Mass	Calc. Mass	mDa	PPM	DBE	Score	Formula
489.2509	489.2525	-1.5	-3.2	14.5	1	C29 H32 B N2 O2 P2

Figure 124. ESI-HRMS of compound **14**.

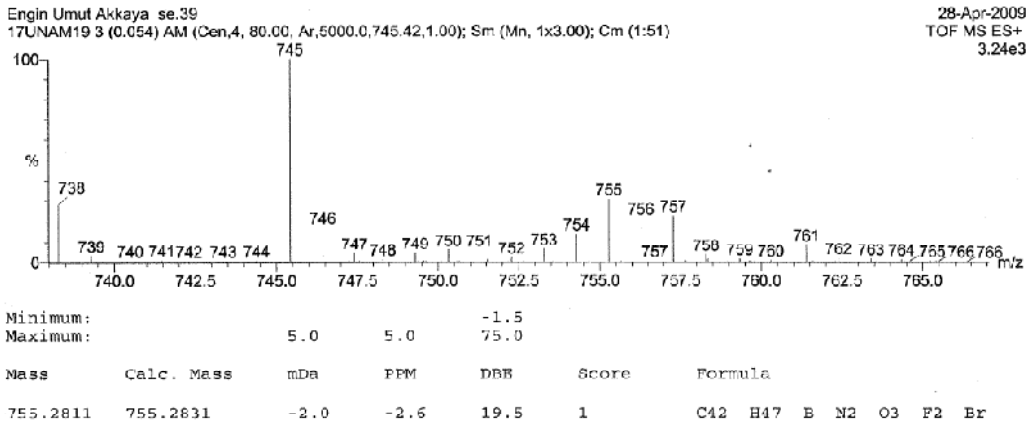

Minimum:				-1.5		
Maximum:		5.0	5.0	75.0		
Mass	Calc. Mass	mDa	PPM	DBE	Score	Formula
755.2811	755.2831	-2.0	-2.6	19.5	1	C42 H47 B N2 O3 F2 Br

Figure 125. ESI-HRMS of compound **15**.

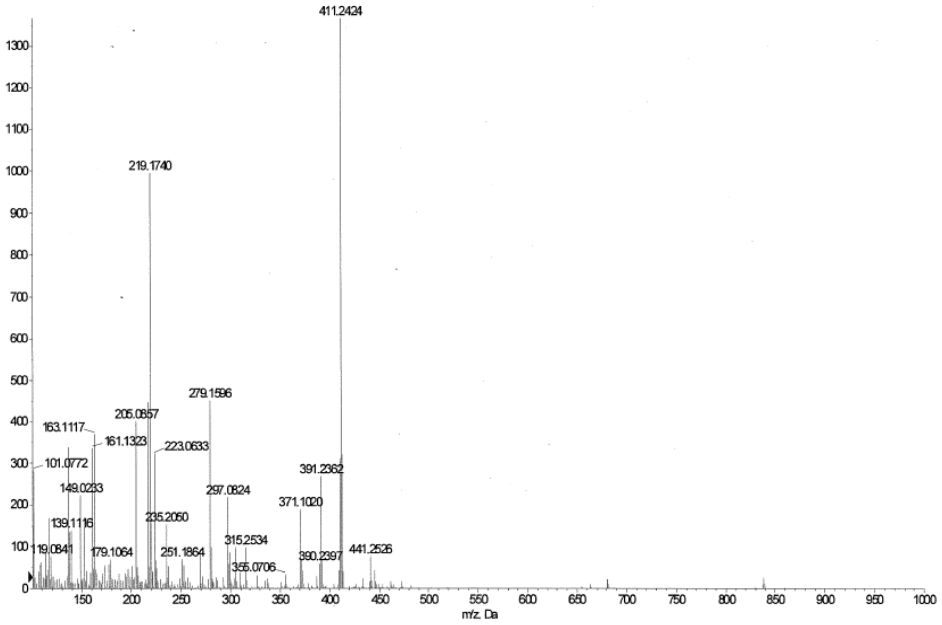

Figure 126. ESI-HRMS of compound **17**.

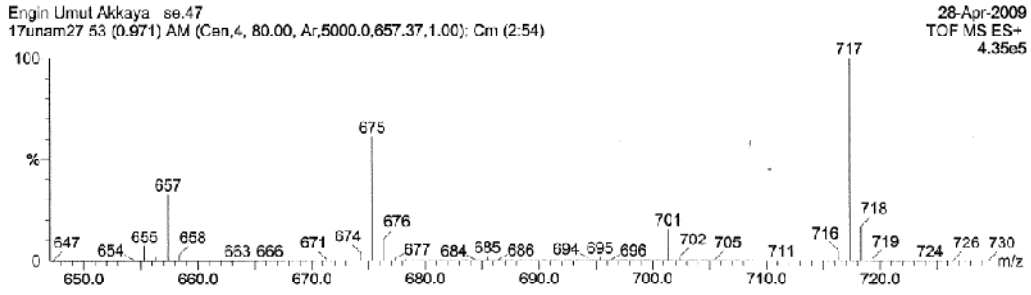

Minimum:		5.0	5.0	-1.5		
Maximum:				75.0		
Mass	Calc. Mass	mDa	PPM	DBE	Score	Formula
717.3060	717.3076	-1.6	-2.2	24.5	1	C44 H41 B N2 O3 F2 Na

Figure 127. ESI-HRMS of compound **18**

.

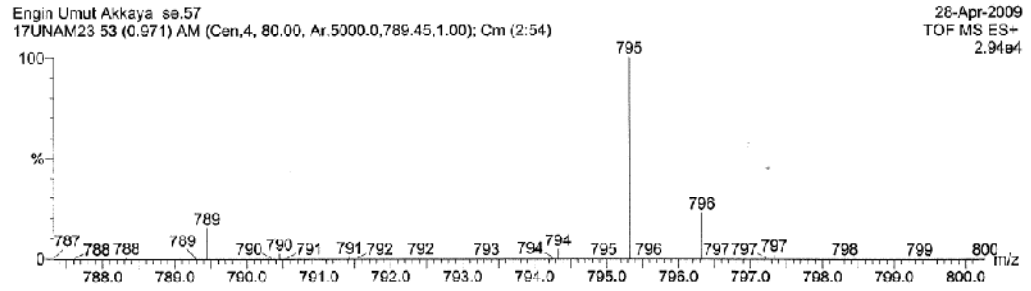

Minimum:		5.0	5.0	-1.5		
Maximum:				75.0		
Mass	Calc. Mass	mDa	PPM	DBE	Score	Formula
795.3199	795.3182	1.7	2.2	28.5	1	C49 H43 B N2 O4 F2 Na

Figure 128. ESI-HRMS of compound **19.**

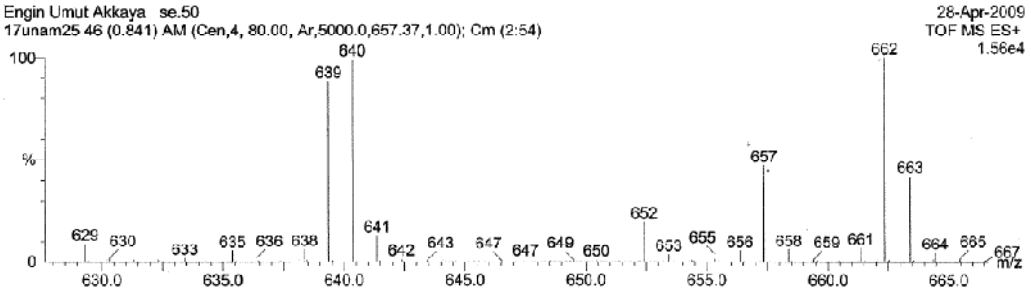

Minimum:		5.0	5.0	-1.5		
Maximum:				75.0		
Mass	Calc. Mass	mDa	PPM	DBE	Score	Formula
640.3604	640.3634	-3.1	-4.8	17.5	1	C37 H45 B N5 O2 F2

Figure 129. ESI-HRMS of compound **20.**

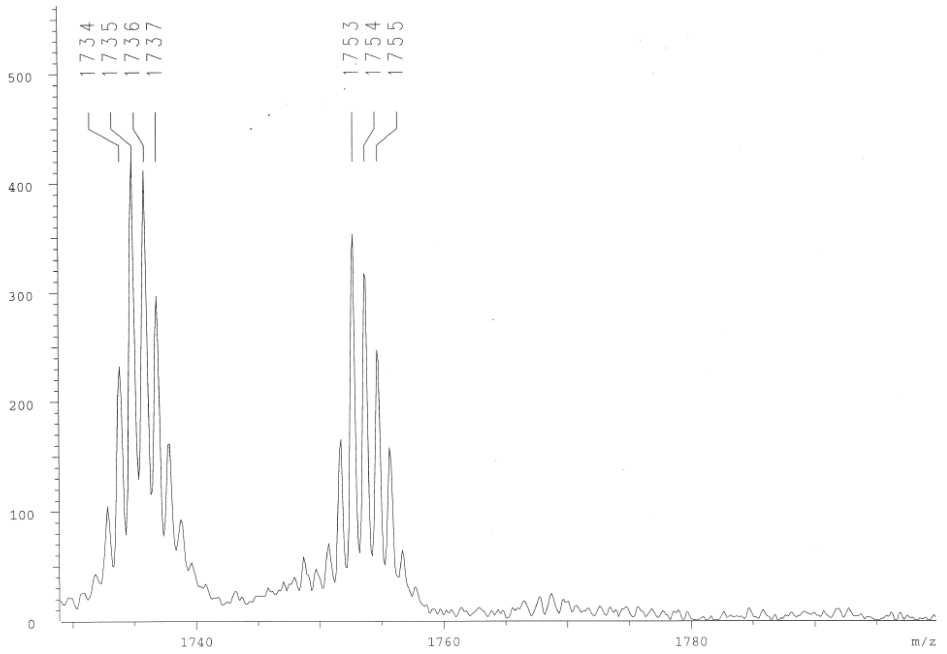

Figure 130. MALDI-MS of compound **21.**

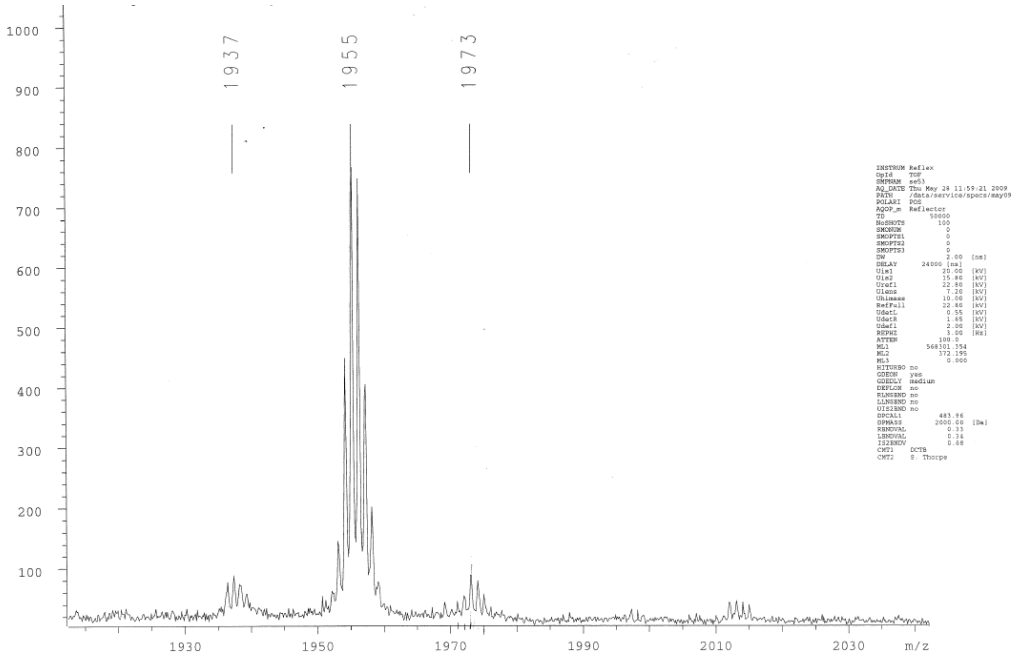

Figure 131. MALDI-MS of compound **23.**

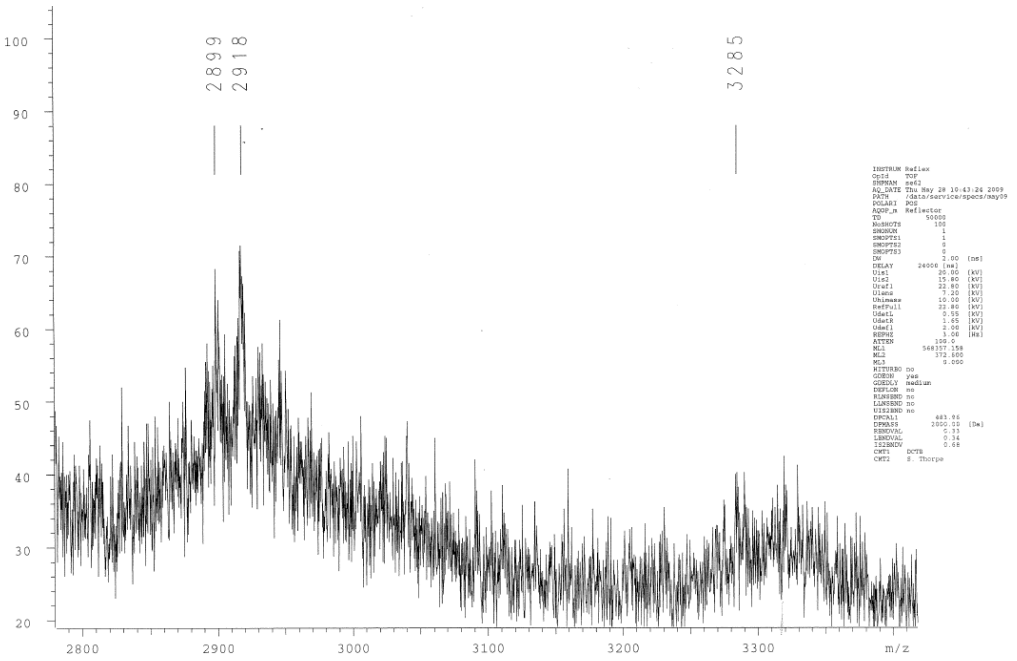

Figure 132. MALDI-MS of compound **24.**

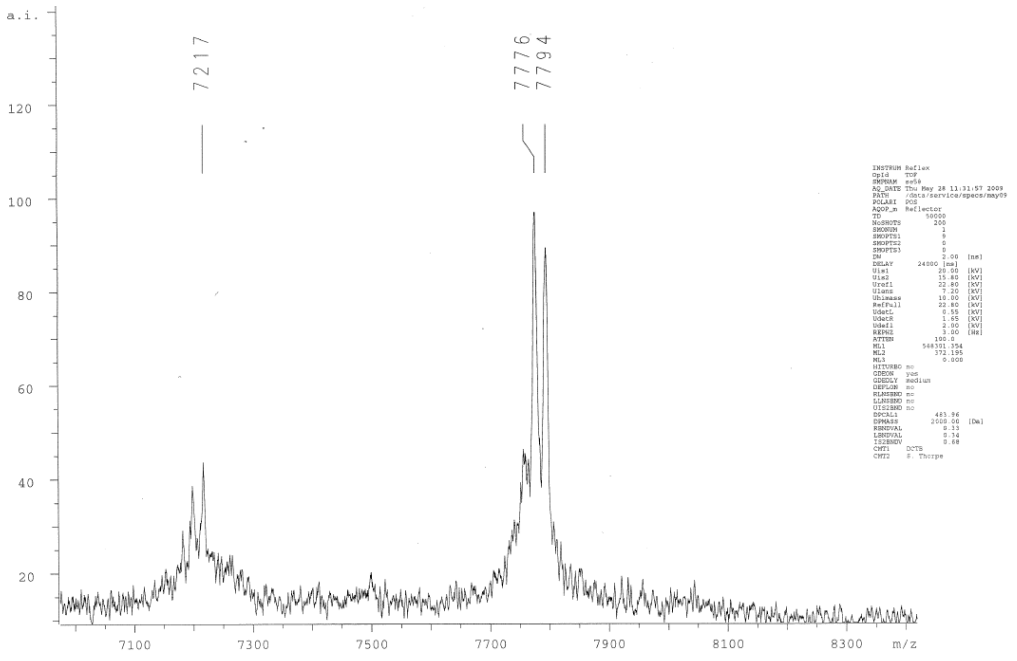

Figure 133. MALDI-MS of compound **25.**

APPENDIX C

FLUORESCENCE DECAY SPECTRA

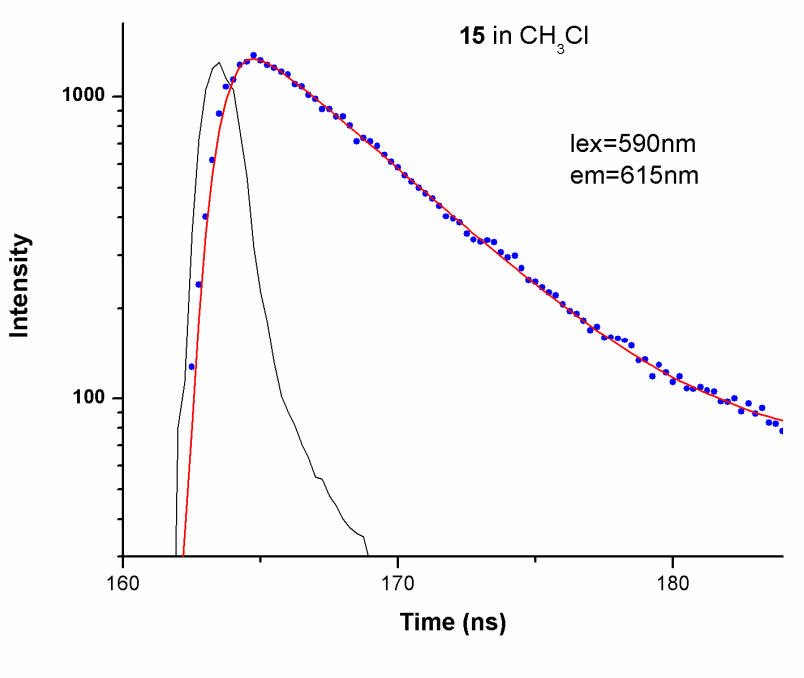

Figure 134. Fluorescence decay spectrum of compound **15**.

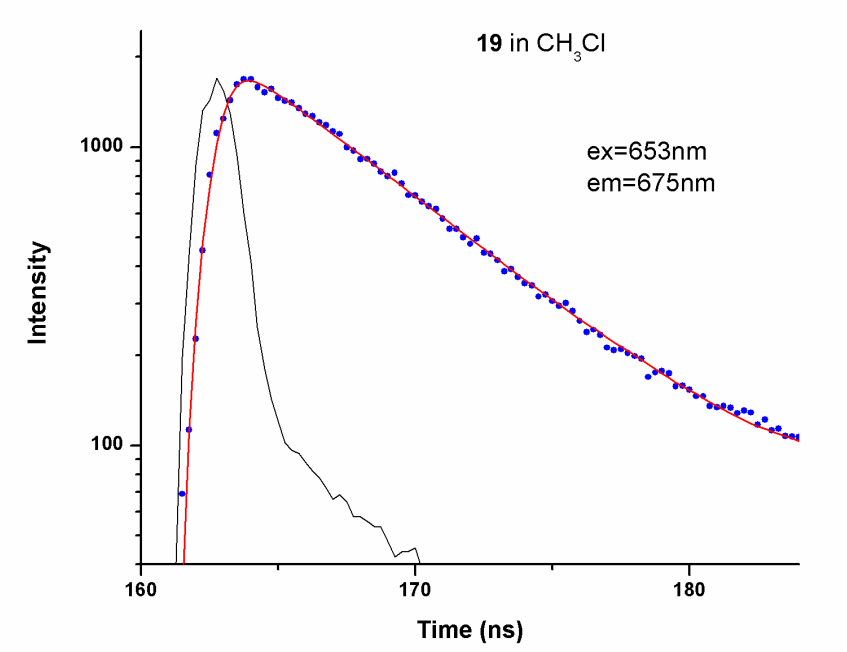

Figure 135. Fluorescence decay spectrum of compound **19**.

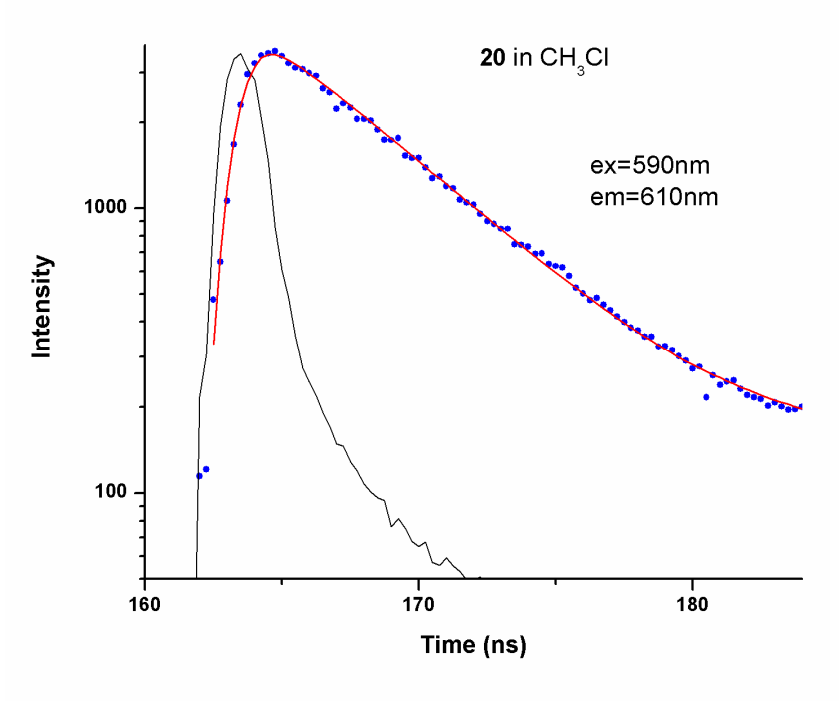

Figure 136. Fluorescence decay spectrum of compound **20**.

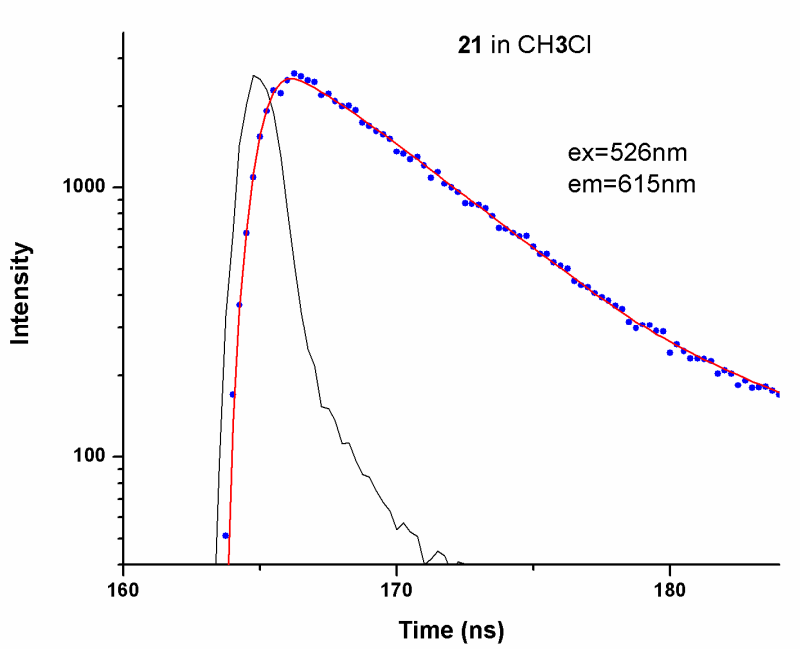

Figure 137. Fluorescence decay spectrum of compound **21**.

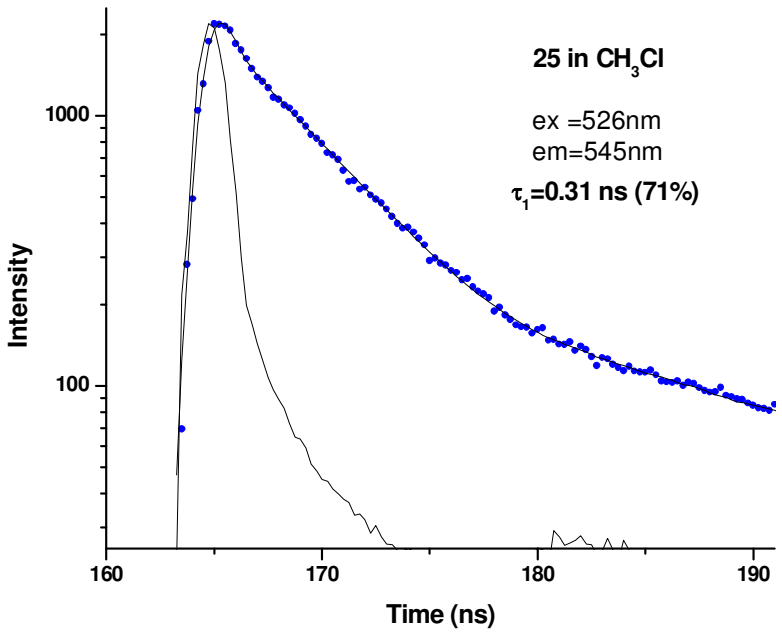

Figure 138. Fluorescence decay spectrum of compound **25,** emission at 545 nm.

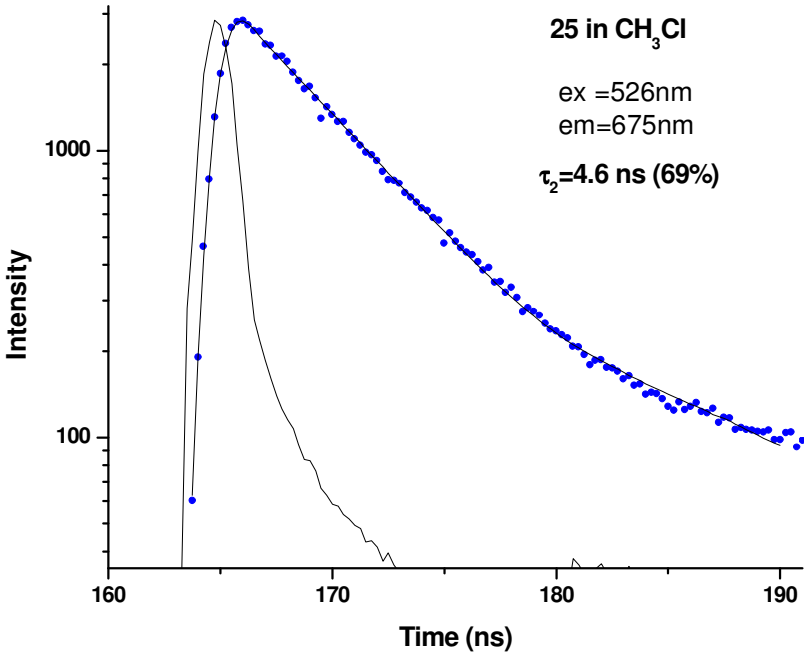

Figure 139. Fluorescence decay spectrum of compound **25**, emission at 675 nm.